THE STABILITY OF THE PLASMA SHEATH WITH SECONDARY EMISSION

Winston E. Han.

Submitted for the degree of Doctor of Philosophy

Department of Physics, City University

To [redacted]

ACKNOWLEDGEMENTS

I am grateful to the Science and Engineering Research Council for providing the funding, and to Theory Division at Culham Laboratory for providing superb facilities and such a stimulating environment in which to carry out the work. My mastery of the computing resources was greatly expedited by the help and advice of [redacted].

My thanks are due to the members of the Department of Engineering Science at the University of Oxford for taking an interest in my work and for allowing me to attend their lectures in plasma science.

I feel fortunate to have had the guidance and support of two inspiring mentors: [redacted], my Culham monitor, and Dr. Raoul Franklin, my academic supervisor at City University. It has been a privilege to work with both of them.

Lastly, I especially want to thank [redacted] who for my benefit became the most over-qualified and underpaid word-processing typist I have yet come across. Most of the equations were typed by her, but any errors that remain are entirely the responsibility of the authors of our bug-ridden word-processing software.

When a plasma is bounded by an electron-emissive wall, the sheath which forms in its vicinity will accelerate any released electrons into the plasma and this will give rise to the beam-plasma instability. The development of this instability has been modelled using a 1-D particle-simulation code developed for this purpose.

When simulating the instability the sheath region is not represented in the code and the parameters for the sheath and associated secondary-electron beam have been obtained from a separate calculation. Equations, generalised to include current flows to the wall under equilibrium conditions, have been derived for this purpose and their solutions obtained. The thermal fluctuation energy of the most unstable mode in the sheath has also been estimated.

The secondary-electron beam-plasma instability develops with initial linear growth of a spectrum of electrostatic waves. The spectrum eventually becomes narrow enough to be considered a single wave which ultimately grows large enough to trap the beam electrons, whereupon the growth saturates. Thereafter the wave amplitude oscillates as the trapped electrons bounce back and forth in the potential well. Neighbouring waves, phase-mixing and particle collisions all have the capability to smear out the beam orbit, thus destroying the wave amplitude oscillations and, depending on the conditions, this can cause the particle distribution to approach that of a BGK mode. When no current is flowing, and assuming the maximum secondary-electron flux, the distance from the sheath to the trapping region is of the order of 100 Debye lengths for all real plasmas; the stability of the sheath itself would appear to remain unaffected by the nonlinear development of the instability. When the sheath carries a current, however, the sheath stability and distance to the trapping region may be modified.

While pursuing the equilibrium calculations a hypothetical plasma system was discovered for which the choice of boundary condition was not clear. The particle-simulation has revealed that such a system adopts the configuration which minimises the wall-potential relative to the midplane. It has also been demonstrated that choosing the equality in the Bohm criterion for sheath formation corresponds to an approximate minimisation of wall-potential relative to the midplane for a plasma bounded by two

Introduction

1.1 Overview

The properties and structure of the sheath which forms adjacent to any surface in contact with a plasma have been investigated for many years. It was originally shown that the sheath forms to prevent the flow of current to the wall [Tonks and Langmuir,1929a, 1929b], and Bohm [1949] has shown that in a collisionless sheath ions must enter it with a minimum energy if the potential distribution is to remain monotonic. Hobbs and Spalding [1966] showed that the sheath acts as a thermal insulator and Hobbs and Wesson [1966] have calculated the heat flow for floating conditions and included the effects of secondary emission. Harbour [1978] has made extensions to the calculation.

Matching of the sheath and plasma solutions for a cold non-emissive boundary has been carried out by Franklin and Ockenden [1964] at low pressure and Blank [1968] at high pressure. The situation for a hot, emissive boundary has been studied by Crawford and Cannara [1965] and Prewett and Allen [1976]. Experimental results have been obtained by Goldan [1970]

The above workers have examined only steady state solutions for the sheath but at around the electron plasma frequency both experimental [Franklin, 1964] and theoretical [Baldwin, 1969, Peratt, 1973] work has indicated that a conventional sheath is stable. At frequencies up to the ion plasma frequency other workers [Weynants et al, 1973] reach similar conclusions.

When secondary emission is included, however, the situation may potentially be unstable since the secondary electrons will be accelerated away from the wall by the sheath potential and into the plasma. A linear analysis of the stability of the sheath in this situation has been undertaken by Franklin

The aim of the present work is to extend existing calculations and to examine the nonlinear development of the secondary electron instability in the plasma with emphasis on its consequences for the stability of the sheath. The existing work which has provided both the foundations of and the starting point for the present investigation will be reviewed in this chapter. These topics are: the Bohm criterion for sheath formation, the effect of secondary emission on sheath parameters, and the linear stability of the plasma sheath.

The following two chapters describe theory which is not specific to the sheath but which nonetheless is directly applicable to the problem being investigated. Chapter two concerns Vlasov theory and discusses both linear and nonlinear effects described by the Vlasov equation which applies to a collisionless plasma. Chapter three considers some theories which have been applied to the development of the instability caused by a small cold beam interacting with a plasma.

Chapter four describes the particle simulation method which has been chosen to model the evolution of the beam-plasma instability resulting from secondary emission and the reasons for selecting this approach are also discussed there. The main features of the computer code developed to perform the simulation are briefly outlined.

In chapter five we deal with calculations which are concerned with equilibrium parameters defining the characteristics of the sheath and associated secondary electron beam. The first two sections cover zero current conditions and the case of a current carrying sheath. The third and last section in this chapter discusses situations where the boundary conditions are not clear; in particular, calculations are carried out for a hypothetical plasma system in which a boundary condition seems to be related to a novel derivation of the Bohm criterion.

more clear cut and straightforward. Also in this chapter we speculate on the nonlinear evolution of the instability beyond the stage represented in the simulations and, finally, we ascertain the stability of the sheath.

A summary of the main results and rationale which led to them is given in chapter seven followed by a discussion of other related work and some implications are drawn for the beam-plasma instability. The last section lists a number of conclusions.

1.2 The Bohm Criterion

Bohm's [1949] model of the sheath assumes a potential variation resembling that shown in Fig. 1.1 and further assumptions required are as follows:

(1) The ion distribution at the plasma-sheath boundary may be approximated by a 'cold' beam.

(2) The electric field and space charge are negligible at the plasma-sheath boundary.

(3) There are no collisions within the sheath.

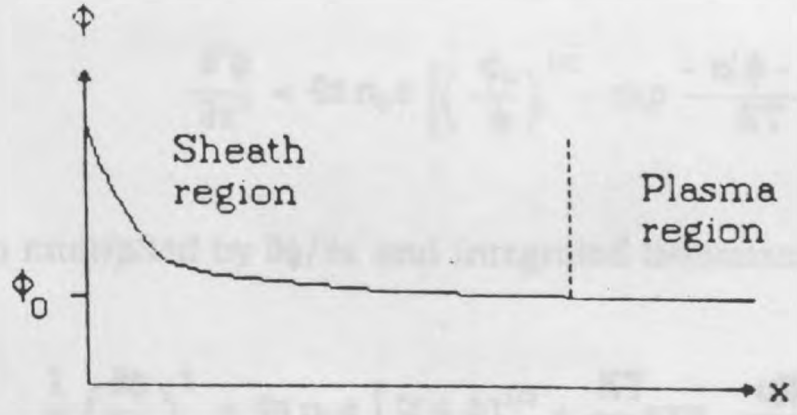

Fig. 1.1 Potential variation near the sheath

these in to the Poisson equation which is:

$$\nabla^2\phi = 4\pi e(n_i - n_e) \tag{1.1}$$

where n_i and n_e are the ion and electron number densities respectively.

Assuming that the electrons have a Maxwellian velocity distribution with temperature T we have:

$$n_e = n_0 \exp \frac{-e(\phi - \phi_0)}{KT} \tag{1.2}$$

where n_0 is the electron density in the sheath edge and ϕ_0 is the potential at the same point.

The ion density is obtained by assuming that the ions fall freely towards the wall through the accelerating potential and by imposing the condition of zero net current to the wall:

$$n_i = n_0 \left(\frac{\phi_0}{\phi}\right)^{1/2} \tag{1.3}$$

Substituting (1.2) and (1.3) into (1.1) gives:

$$\frac{\partial^2\phi}{\partial x^2} = 4\pi n_0 e \left[\left(\frac{\phi_0}{\phi}\right)^{1/2} - \exp \frac{-e(\phi - \phi_0)}{KT}\right] \tag{1.4}$$

which when multiplied by $\partial\phi/\partial x$ and integrated becomes:

$$\frac{1}{2}\left(\frac{\partial\phi}{\partial x}\right)^2 = 4\pi n_0 e \left[2(\phi_0\phi)^{1/2} + \frac{KT}{e}\exp \frac{-e(\phi - \phi_0)}{KT}\right] + C \tag{1.5}$$

$$\left(\frac{\partial\phi}{\partial x}\right)^2 = 8\pi n_0 e\left\{2\phi_0\left[\left(\frac{\phi}{\phi_0}\right)^{1/2} - 1\right] + \frac{KT}{e}\left[\exp\ \frac{-e(\phi-\phi_0)}{KT} - 1\right]\right\} \qquad (1.6)$$

The nature of solutions for ϕ near the plasma-sheath boundary can be investigated by writing $\Delta\phi$ for $\phi - \phi_0$ and expanding equation (1.4) in powers of $\Delta\phi$. Keeping only the first power one obtains:

$$\frac{\partial^2(\Delta\phi)}{\partial x^2} = 4\pi n_0 e\left(\frac{e}{KT} - \frac{1}{2\phi_0}\right)\Delta\phi$$

Clearly if $e\phi_0/KT > 1/2$ then exponential solutions are obtained and if $e\phi_0/KT < 1/2$ then the solutions are oscillatory. Bohm argues qualitatively that in practice one should obtain:

$$\frac{e\phi_0}{KT} = \frac{1}{2} \qquad (1.7)$$

which is the Bohm criterion; this means that ions should enter the sheath with energy equal to the average electron thermal energy. The validity of exponential solutions with $e\phi_0/KT > 1/2$ will be examined next and a different argument from Bohm's will be used to justify taking the equality (1.7).

Returning to the expansion of equation (1.4) in powers of $\Delta\phi$ and continuing the process up to the second power one obtains:

$$\frac{\partial^2(\Delta\phi)}{\partial x^2} = 4\pi n_0 e\left[\left(\frac{e}{KT} - \frac{1}{2\phi_0}\right)\Delta\phi + \left(\frac{3}{8\phi_0^2} - \frac{e^2}{2(KT)^2}\right)(\Delta\phi)^2\right]$$

Considering the case $e\phi_0/KT = 1/2$ this becomes:

$$\frac{\partial^2(\Delta\phi)}{\partial x^2} = \frac{4\pi n_0 e^3}{(KT)^2}(\Delta\phi)^2$$

$$\left(\frac{\partial(\Delta\phi)}{\partial x}\right)^2 = \frac{8}{3}\frac{\pi n_0 e^3}{(KT)^2}(\Delta\phi)^3$$

where the boundary condition $\partial(\Delta\phi)/\partial x = 0$ when $\Delta\phi = 0$ has been used. Integrating again gives:

$$\Delta\phi = \left[\frac{2\sqrt{3}KT}{(8\pi n_0 e^3)^{1/2} x + \sqrt{3}GkT}\right]^2 \qquad (1.8)$$

where G is a constant of integration.

Equation (1.8) shows that $\Delta\phi$ goes to zero at $x = \infty$ and these equations are therefore satisfied if the ions are travelling at the Bohm velocity at $x = \infty$. This means that if the ions reach the Bohm velocity at a sufficient distance from the wall then, provided that the intervening plasma remains collisionless, these equations will accurately describe the sheath potential distribution when we set $e\phi_0/KT = 1/2$.

We now see that solutions with $e\phi_0/KT > 1/2$ cannot be valid because this would imply that ions were entering the sheath at speeds greater than the Bohm velocity which of course means that they must have reached the Bohm velocity at an even greater distance from the wall; if this were the case then, as before, equation (1.6) would accurately describe the sheath potential distribution with $e\phi_0/KT = 1/2$ thus contradicting the original assumption. It is emphasised, again, that this argument remains valid as long as the plasma separating the position where the equality is satisfied from the wall conforms to the three initial assumptions. We can therefore assume its validity for a plasma system which remains entirely collisionless. If we now imagine that collisions are gradually introduced into the system, up to some maximum level constrained by the condition of a collisionless sheath, we wish to know what effect this has on the applicability of the Bohm criterion. This is clearly not

These considerations lead one to conclude that for the purposes of the present investigation Bohm's result (equation (1.7)) is applicable provided that oscillatory solutions do not occur in practice. This will be examined further in Section 5.3.4.

1.3 Secondary Emission and Space Charge Limitation

The approach of the last section has been extended to include the effects of secondary emission of electrons from the wall [Hobbs and Wesson, 1966]. Again the infinite plane wall is situated at $x = 0$, in contact with a plasma filling the half-space $x > 0$. Poisson's equation is now:

$$\frac{d^2\phi}{dx^2} = 4\pi e(n_{ep} + n_{eb} - n_i) \tag{1.9}$$

taking $\phi(\infty) = 0$, where n_{ep} and n_{eb} are the densities of the plasma and emission (or 'beam') electrons respectively and n_i is the density of ions.

The plasma electrons are assumed to have a Maxwellian velocity distributions with temperature T so their density is:

$$n_{ep} = [n_0 - n_{eb}(\infty)] \exp\left(\frac{e\phi}{KT}\right) \tag{1.10}$$

where $n_0 = n_i(\infty)$ and charge neutrality at $x \to \infty$ has been assumed.

If the ions arriving at the sheath edge are monoenergetic with energy $E = \frac{1}{2}Mv_0^2$ and thereupon fall freely to the wall then their density is:

$$n_i = n_0 \left(\frac{E}{E - e\phi}\right)^{1/2} \tag{1.11}$$

current to the wall gives:

$$n_{eb} = n_0 \frac{\Gamma}{1-\Gamma}\left(\frac{m}{M}\,\frac{E}{e(\phi-\phi_0)}\right)^{1/2} \tag{1.12}$$

where Γ is the ratio of emission to primary electron fluxes, m is the electron mass and $\phi_0 = \phi(0)$.

Substituting these densities into the Poisson equation now gives:

$$\frac{d^2\phi}{dx^2} = 4\pi n_0 e \left\{\left[1 - \frac{\Gamma}{1-\Gamma}\left(\frac{m}{M}\,\frac{E}{e\phi_0}\right)^{1/2}\right]\exp\left(\frac{e\phi}{KT}\right)\right.$$

$$\left. + \frac{\Gamma}{1-\Gamma}\left[\frac{m}{M}\frac{E}{e(\phi-\phi_0)}\right]^{1/2} - \left(\frac{E}{E-e\phi}\right)^{1/2}\right\} \tag{1.13}$$

After multiplication by $\partial\phi/\partial x$ and integration from ∞ to x this becomes:

$$\frac{1}{8\pi n_0 KT} KT\left(\frac{d\phi}{dx}\right)^2 = \frac{2E}{KT}\left[\left(1 - \frac{e\phi}{E}\right)^{1/2} - 1\right] + \frac{2\Gamma}{1-\Gamma}\left(\frac{m}{M}\frac{E}{KT}\frac{e\phi_0}{KT}\right)^{1/2}\left[\left(1 - \frac{\phi}{\phi_0}\right)^{1/2} - 1\right]$$

$$+ \left[1 - \frac{\Gamma}{1-\Gamma}\left(\frac{m}{M}\,\frac{E}{e\phi_0}\right)^{1/2}\right]\left[\exp\left(\frac{e\phi}{KT}\right) - 1\right] \tag{1.14}$$

where the boundary condition $d\phi/dx = 0$, $\phi = 0$ has been used. This provides a way of calculating the sheath potential distribution once Γ has been chosen and E and ϕ_0 are known.

Two more equations are required to determine E and ϕ_0: one is the condition which must be satisfied for the total current to the wall to be zero, and the other, the monotonicity criterion for small ϕ, is analogous to the Bohm criterion for conventional sheaths.

$$F_{ep} = \frac{n_{ep}}{4}\left(\frac{8KT}{\pi m}\right)^{1/2}$$

and equating the net ion and electron fluxes thereupon gives:

$$\frac{1}{4}\left[1 - \frac{\Gamma}{1-\Gamma}\left(-\frac{m}{M}\frac{E}{e\phi_0}\right)^{1/2}\right]\exp\left(\frac{e\phi_0}{KT}\right)\left(\frac{8KT}{\pi m}\right)^{1/2} = \frac{1}{1-\Gamma}\left(\frac{2E}{M}\right)^{1/2} \qquad (1.15)$$

for the zero current condition.

By expanding equation (1.13) about $\phi = 0$ the monotonicity condition becomes:

$$E = \frac{KT}{2} + \frac{\Gamma}{1-\Gamma}\left(\frac{m}{M}\right)^{1/2}\left(-\frac{E}{e\phi_0}\right)^{3/2}\left(\frac{KT}{2} - e\phi_0\right) \qquad (1.16)$$

As $(m/M)^{1/2}$ is a small quantity one can obtain the following approproximate solutions to equations (1.15) and (1.16) :

$$-e\phi_0 \approx KT \ln\left[\frac{1-\Gamma}{(2\pi m/M)^{1/2}}\right] \qquad (1.17)$$

and

$$E \approx KT/2 \qquad (1.18)$$

One can see that increasing Γ reduces the potential drop across the sheath but it will be shown that a space charge limitation process prevents the value of Γ from rising above a certain critical value since a reduction in the potential drop will be seen to lead to a reduction in the accelerating electric field at the wall until it goes to zero.

To obtain an equation for the electric field at the wall we eliminate $(m/M)^{1/2}\Gamma/(1-\Gamma)$ from equations (1.14) and (1.16) to give:

$$+\frac{e\phi_0 - E}{2e\phi_0 - KT}\left(\frac{KT}{E}\right)\left[\exp\left(\frac{e\phi_0}{KT}\right) - 1\right] \qquad (1.19)$$

and a simpler, more approximate form can be obtained with the aid of equations (1.17) and (1.18):

$$\frac{1}{8\pi n_0 KT}\left(\frac{d\phi_0}{dx}\right)^2 \approx \left(1 - 2\frac{e\phi_0}{KT}\right)^{1/2} - 2$$

This equation shows that as the magnitude of the (negative) sheath potential is reduced the electric field at the wall decreases until it becomes zero for $e\phi_0 \approx -\frac{3}{2}KT$. At this point no further secondary electrons can be accelerated away from the wall and the critical ratio of secondary to primary electron fluxes corresponding to this state is Γ_c. If the rate of liberation of secondary electrons were increased to a level corresponding to $\Gamma > \Gamma_c$, then a fraction of them would in practice be re-absorbed by the wall to maintain Γ at the value Γ_c.

Thus it is seen that there will be a critical value of Γ which cannot be exceeded irrespective of the precise physical mechanism of production of the secondary electrons.

The equations given in this section have been used in the present work as a basis for calculating the equilibrium distribution function of the plasma in and beyond a sheath for the purpose of investigating the behaviour of the streaming instability. A linear analysis [Franklin, 1980] of this instability is described in the following section.

A similar model to that described in the last section has been used in a linear analysis of sheath stability [Franklin, 1980]. In the following equations η is the potential normalised to KT/e, u is ion velocity normalised to ion sound speed $c_s = (KT/M)^{1/2}$ and ζ is distance normalised to the Debye length λ_D.

$$n_{ep} = n_0 \exp(-\eta) \qquad \text{for the plasma electrons}$$

$$n_i = n_0(1+\alpha)\left(1+\frac{2\eta}{u_{i0}^2}\right)^{-1/2} \qquad \text{for the ions}$$

$$n_{eb} = \alpha\, n_0 \left(\frac{\eta_0}{\eta_c-\eta}\right)^{1/2} \qquad \text{for the secondary electrons}$$

where n_0 is the density of plasma electrons, $\alpha\, n_0$ the density of secondary electrons, u_{i0} the ion speed on entry to the sheath, and η_c is the potential drop across the sheath.

Poisson's equation now becomes:

$$\frac{d^2n}{d\zeta^2} = \frac{1+\alpha}{\left(1+\frac{2\eta}{u_{i0}^2}\right)^{1/2}} - \exp-\eta - \alpha\left(\frac{\eta_c}{\eta_c-\eta}\right)^{1/2}$$

with boundary conditions $\eta = 0$ and $dn/d\zeta = 0$ as $\zeta \rightarrow \infty$.

The corresponding monotonicity condition is:

$$u_{i0}^2 = \frac{1+\alpha}{1-\frac{\alpha}{2\eta_c}}$$

Now η_0 corresponds to the wall potential and α is the relative density of the 'beam' of secondary electrons;

$$1 - \sum_j \frac{\omega_j^2}{(\omega - kv_j)^2 - k^2 c_j^2} = 0$$

where ω_j is the plasma frequency of the jth species, v_j the drift velocity, and c_j the thermal velocity. The three terms for plasma electrons, beam electrons and ions were included and solutions were obtained for the case of spatial growth (complex k and real ω). The results indicated that the sheath would be stable and that significant instability would only be encountered beyond the sheath under floating conditions. For large positive currents to the wall, however, the sheath can be unstable.

In this chapter the Vlasov theory of plasma waves is outlined for the linear case and a quasilinear treatment is also given which may be appropriate for the nonlinear description of certain cases of the beam-plasma instability (see section 7.2.6).

2.1 Basic Linear Theory

Since much of the phenomena we shall be considering is effectively collisionless the appropriate equation to employ is the Vlasov equation:

$$\frac{\partial f}{\partial t} + \mathbf{v} \cdot \nabla f + \frac{q}{m} \mathbf{E} \cdot \nabla_{\mathbf{v}} f = 0 \qquad (2.1)$$

where $f(\mathbf{r}, \mathbf{v}, t)$ is the particle distribution function, m and q are the particle mass and charge respectively. We restrict the problem to one dimension so that all vectors are in the x direction and consider a perturbation f_1 by writing $f = f_0 + f_1$ where $f_0(\mathbf{v})$ is an equilibrium distribution function which we shall take to be a Maxwellian. Substituting for f in equation (2.1) and after linearising we get:

$$\frac{\partial f_1}{\partial t} + v \frac{\partial f_1}{\partial x} + \frac{qE}{m} \frac{\partial f_0}{\partial v} = 0 \qquad (2.2)$$

where it should be noted that the electric field E is a first order quantity. We now assume plane-wave solutions for f_1 and E of the form $\exp i(kx - \omega t)$, so we get the following operator transformations: $\partial/\partial t \rightarrow -i\omega$ and $\partial/\partial x = \rightarrow ik$, which when applied to equation (2.2) gives:

$$f_1 = \frac{iq/m}{\omega - kv} E \frac{\partial f_0}{\partial v} \qquad (2.3)$$

$$\nabla \cdot E = 4\pi e (n_i - n_e)$$

which becomes on substituting the above operators:

$$ikE = 4\pi e \int dv\, (f_{i1} - f_{e1}) \tag{2.4}$$

We can now solve equations (2.3) and (2.4) by eliminating either f_1 or E. Choosing the former route we obtain:

$$\varepsilon(k, \omega) = 1 - \frac{\omega_{pe}^2}{k^2} \int_{-\infty}^{\infty} dv \frac{\partial g(v)/\partial v}{v - \omega/k} = 0 \tag{2.5}$$

where $\varepsilon(k, \omega)$ is known as the dielectric function and g(v) is the spatially averaged velocity distribution function which is normalised such that:

$$\int_{-\infty}^{\infty} g\, dv = 1$$

Equation (2.5) is the dispersion relation for the normal modes of the plasma.

The alternative route of eliminating E gives:

$$(v - \frac{\omega}{k}) f_1 = \frac{\omega_{pe}^2}{k^2} \frac{\partial g}{\partial v} = \int_{-\infty}^{\infty} dv\, f_1 \tag{2.6}$$

and noting that $f_1 = \bar{f}_1(v) \exp i(kx - \omega t)$ we obtain the following solution to equation (2.6):

$$\bar{f}_1(v) = P\left[\frac{\frac{\omega_{pe}^2}{k} \frac{\partial g}{\partial v}}{v - \omega/k}\right] + \delta (v - \omega/k) \left[1 - P \int_{-\infty}^{\infty} \frac{\frac{\omega_{pe}^2}{k^2} \frac{\partial g}{\partial v'}}{v' - \omega/k} dv'\right] \tag{2.7}$$

These are known as Case-Van Kampen modes [Van Kampen, 1955; Case, 1959].

initial value problem which would require the use of the Laplace transform. Such a treatment shows that, in the case of the dispersion relation, the integral in equation (2.5) should be evaluated using the Landau [1946] contour. This is represented in Fig. 2.1. For weak damping and large phase-velocity ($\omega/k >> v_T$) the pole in the integrand at $v = \omega/k$ will be very close to the real v axis since we would then have $\omega_i << \omega_r$; this is because for late times the pole with the largest imaginary (or least damped part) corresponds to the dominant set of modes (the normal modes) for the plasma. Equation (2.5) thus becomes:

$$1 = \frac{\omega_{pe}^2}{k^2}\left[P \int_{-\infty}^{\infty} \frac{\partial g/\partial v}{v - \omega/k}\, dv + i\pi \left.\frac{\partial g}{\partial v}\right|_{v=\omega/k} \right] \qquad (2.8)$$

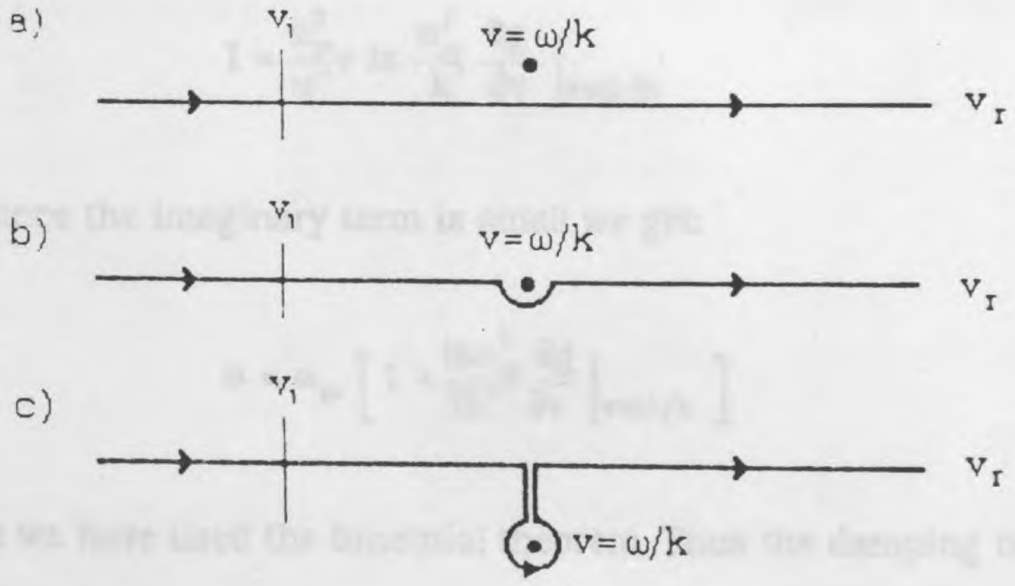

Fig. 2.1. Landau contour for the evaluation of the integral in equation (2.5).

Integrating the first term of equation (2.8) by parts we get:

$$P \int_{-\infty}^{\infty} \frac{\partial g}{\partial v} \frac{dv}{v-\omega/k} = \int_{-\infty}^{\infty} \frac{g\,dv}{(v-\omega/k)^2} \qquad (2.9)$$

the binomial theorem to obtain:

$$\int_{-\infty}^{\infty} \frac{g\,dv}{(v-\omega/k)^2} \approx \frac{k^2}{\omega^2}\left(1+\frac{3k^2\,\bar{v}^2}{\omega^2}\right) \tag{2.10}$$

and the real part of the dispersion relation thus becomes:

$$\omega^2 = \omega_{pe}^2 + \frac{3KT}{m}k^2 \tag{2.11}$$

where we have used $\bar{v}^2 = v_T = (KT/m)^{1/2}$ and assumed that the thermal correction is small. Equation (2.11) is the Langmuir wave dispersion relation.

Now returning to the imaginary part of equation (2.8) and neglecting the thermal correction to ω entirely we have:

$$1 = \frac{\omega_{pe}^2}{\omega^2} + i\pi\,\frac{\omega_{pe}^2}{k^2}\,\frac{\partial g}{\partial v}\bigg|_{v=\omega/k} \tag{2.12}$$

And since the imaginary term is small we get:

$$\omega = \omega_{pe}\left[1+\frac{i\pi\omega_{pe}^2}{2k^2}\,\frac{\partial g}{\partial v}\bigg|_{v=\omega/k}\right] \tag{2.13}$$

where we have used the binomial theorem. Thus the damping rate is given by:

$$\omega_i = \frac{\pi\omega_{pe}^3}{2k^2}\,\frac{\partial g}{\partial v}\bigg|_{v=\omega/k} \tag{2.14}$$

and this is the Landau damping rate.

Quasilinear theory is so called because much of it depends on linear theory but the nonlinearities are assumed to be small corrections to linear theory. The theory does not take into account any interaction between resonant modes, e.g. the possibility of excited electron waves coupling with ion waves through nonlinear wave-wave or wave-particle interactions cannot be included.

The treatment given will be one-dimensional and assumes that the excited wave vectors **k** are aligned in the direction of v_b the beam velocity. The result obtained cannot be extended to a three-dimensional spectrum but in any case the problem at hand is assumed to be one-dimensional. The ions will be treated as a uniform background as it will be assumed that the frequencies will be high enough to prevent the ions from becoming significantly polarised. It should be noted that the applicability of this theory to the beam-plasma instability is discussed in section 7.2.6.

It is required to solve the Vlasov and Poisson equations which are as follows:

$$\frac{\partial f}{\partial t} + v \cdot \nabla f - \frac{eE}{m_e} \nabla_v f = 0 \qquad (2.15)$$

$$\nabla \cdot E = 4\pi n_0 e(1 - \int_{-\infty}^{\infty} f dv) \qquad (2.16)$$

where f is the electron distribution function.

We proceed by writing:

$$f = f_0 + f_1$$

$$E = E_1$$

perturbation E_1. It is convenient to work in terms of Fourier transforms f_k and E_k hence:

$$f_1 = \int_{-\infty}^{\infty} f_k\,(v, t)\, e^{ikx} dk$$

$$E_1 = \int_{-\infty}^{\infty} E_k(t)\, e^{ikx} dk$$

Now the intention is to find an equation for the time evolution of f_0 and this is accomplished by spatially averaging the Vlasov equation:

$$\frac{\partial}{\partial t} \langle f \rangle + v \left\langle \frac{\partial f}{\partial x} \right\rangle - \frac{e}{m_e} \left\langle E_1 \frac{\partial f}{\partial v} \right\rangle = 0$$

where $\langle y \rangle = \lim_{L \to \infty} \frac{1}{L} \int_{-L/2}^{L/2} y\,dx$. The second term thus becomes zero and the third term becomes:

$$\frac{e}{m_e} \left\langle E_1 \frac{\partial f}{\partial v} \right\rangle = \frac{e}{m_e} \left\langle E_1 \frac{\partial f_0}{\partial v} \right\rangle + \frac{e}{m_e} \left\langle E_1 \frac{\partial f_1}{\partial v} \right\rangle$$

$$= \frac{e}{m_e} \left\langle E_1 \frac{\partial f_1}{\partial v} \right\rangle$$

since the first term on the right averages to zero.

$$\therefore \frac{\partial f_0}{\partial t} = \frac{e}{m_e} \left\langle E_1 \frac{\partial f_1}{\partial v} \right\rangle = \frac{e}{m_e} \frac{\partial}{\partial v} \langle E_1 f_1 \rangle \qquad (2.17)$$

So the rate of change of f_0 is a second order quantity and is the only nonlinear part of quasilinear theory.

If one now substitutes $f = f_0 + f_1$ into the Vlasov equation one obtains:

and after eliminating $\partial f_0/\partial t$ with the aid of equation (2.17) we have:

$$\therefore \quad \frac{\partial f_1}{\partial t} + v\frac{\partial f_1}{\partial k} - \frac{eE_1}{m_e}\frac{\partial f_0}{\partial v} - \frac{e}{m_e}\frac{\partial}{\partial v}(E_1 f_1 - \langle E_1 f_1 \rangle) = 0$$

Dropping second order terms and Fourier transforming produces:

$$\frac{\partial f_k}{\partial t} + ikvf_k - \frac{e}{m_e}E_k\frac{\partial f_0}{\partial v} = 0$$

and assuming further that $f_k = \bar{f}_k(v)\, e^{-i\omega t}$ we have $\partial f_k/\partial t = -i\omega f_k$ so that:

$$f_k = \frac{e}{m_e}\frac{E_k\, \partial f_0/\partial v}{i(kv - \omega)} \tag{2.18}$$

This expression for the Fourier mode f_k will be used in evaluating the second order quantity $\langle E_1 f_1 \rangle$ which is required in equation (2.17).

Now:
$$\langle E_1 f_1 \rangle = \lim_{L\to\infty} \frac{1}{L}\int_{-L/2}^{L/2} E_1 f_1\, dx$$

$$= \lim_{L\to\infty} \frac{1}{L}\int_{-L/2}^{L/2} dx \int dk_1\, f_{k_1} e^{ik_1 x} \int dk_2\, E_{k_2} e^{ik_2 x}$$

$$= \lim_{L\to\infty} \frac{1}{L}\int dk_1\, f_{k_1} \int dk_2\, E_{k_2} \int_{-L/2}^{L/2} dx\, e^{i(k_1+k_2)x}$$

$$= \lim_{L\to\infty} \frac{1}{L}\int dk_1\, f_{k_1} \int dk_2\, E_{k_2}\, 2\pi\delta(k_1+k_2)$$

$$= \lim_{L\to\infty} \frac{2\pi}{L}\int dk_1\, f_{k_1} E_{-k_1}$$

Using equation (2.18) to substitute for f_k :

$$\langle E_1 f_1 \rangle = \lim_{L\to\infty} \frac{2\pi}{L} \frac{e}{m_e} \int \frac{E_k E_{-k} \partial f_0/\partial v}{i(kv - \omega)} dk$$

Since $E_k = E_{-k}^*$ then this becomes:

$$\langle E_1 f_1 \rangle = \lim_{L\to\infty} \frac{2\pi}{L} \frac{e}{m_e} \int \frac{|E_k|^2 \partial f_0/\partial v}{i(kv - \omega)} dk \qquad (2.19)$$

Now we define the spectral density $\varepsilon(k)$ as:

$$\varepsilon_k \equiv \lim_{L\to\infty} \frac{1}{4L} |E_k|^2$$

To see what this means we note that the average electric field energy density is given by:

$$\left\langle \frac{E^2}{8\pi} \right\rangle = \lim_{L\to\infty} \frac{1}{8\pi L} \int_{-L/2}^{L/2} E^2 dx$$

$$= \lim_{L\to\infty} \frac{1}{8\pi L} \int_{-L/2}^{L/2} dx \int dk_1 E_{k_1} e^{ik_1 x} \int dk_2 Ek_2 e^{ik_2 x}$$

$$= \lim_{L\to\infty} \frac{1}{8\pi L} \int dk_1 E_{k_1} \int dk_2 E_{k_2} \int_{-L/2}^{L/2} dx e^{i(k_1+k_2)x}$$

$$= \lim_{L\to\infty} \frac{1}{4L} \int E_{k_1} E_{-k_1} dk_1$$

$$\left\langle \frac{E^2}{8\pi} \right\rangle = \lim_{L\to\infty} \frac{1}{4L} \int |E_k|^2 dk$$

So the spectral density corresponds to the average electric field energy density per unit wavenumber interval.

Using the spectral density in equation (2.19) gives:

$$\langle E_1 f_1 \rangle = \frac{8\pi e}{m_e} \int_{-\infty}^{\infty} \frac{\varepsilon_k \, \partial f_0/\partial v}{i(kv - \omega)} \, dk$$

and inserting this into equation (2.17) gives:

$$\frac{\partial f_0}{\partial t} = \frac{8\pi e^2}{m_e^2} \frac{\partial}{\partial v} \left\{ \int_{-\infty}^{\infty} \frac{\varepsilon_k \, \partial f_0/\partial v}{i(kv - \omega)} \, dk \right\}$$

which can be written as:

$$\frac{\partial f_0}{\partial t} = \frac{\partial}{\partial v} \left(D \frac{\partial f_0}{\partial v} \right) \tag{2.20}$$

which is a diffusion equation and the diffusion coefficient is given by

$$D = \frac{8\pi e^2}{m_e^2} \int_{-\infty}^{\infty} \frac{\varepsilon_k}{i(kv - \omega)} \, dk$$

Splitting ω into real and imaginary parts so that $\omega = \omega_r + i\omega_i$ we can obtain:

$$D = \frac{8\pi e^2}{m_e^2} \int_{-\infty}^{\infty} \frac{\omega_i \varepsilon_k}{(kv - \omega_r)^2 + \omega_i^2} \, dk$$

where the k integration passes under the pole.

$$D = \frac{16\pi^2 e^2}{m_e^2} \frac{\varepsilon_{k=\omega_r/v}}{v}$$

and equation (2.20) becomes:

$$\frac{\partial f_0}{\partial t} = \frac{16\pi^2 e^2}{m_e^2} \frac{\partial}{\partial v} \left\{ \frac{1}{v} \varepsilon_{k=\omega_r/v} \frac{\partial}{\partial v} f_0 \left(v = \frac{\omega_r}{|k|}\right) \right\}$$

In the literature an error has been perpetuated as the factor 16 is mistakenly replaced by 8 in both Drummond and Pines [1962] and Krall and Trivelpiece [1973a].

3.1 Single-Wave Theory

3.1.1 Single-Wave Model

Single-wave theory is clearly the opposite extreme to quasilinear theory which is a many wave theory. The single-wave theory was proposed by Drummond, Malmberg, O'Neil and Thompson [1970] to explain the interaction of a small cold beam and cold plasma. In this section we describe the treatment of a cold beam with warm plasma by O'Neil, Winfrey and Malmberg [1971].

The theory is based on the fact that after several e-foldings of the dominant mode in the beam-plasma instability the spectrum of waves should develop a very narrow bandwidth; it can therefore be represented by a single sine wave. Thus, the most unstable mode grows until the electrons are trapped and as the electrons oscillate in the potential well the wave amplitude oscillates at the same frequency, the bounce frequency. The electrons trapped near the bottom of the potential well see an approximately parabolic potential and are governed by a linear equation of motion which produces a linear but time-dependent transformation in phasespace. This effectively amounts to a rotation of a string of beam electrons in phasespace and this approximate picture remains appropriate for several amplitude oscillations since the neighbouring waves will take some time to catch up with the main wave assuming that they never grow faster than the linear rate for the dominant mode. Because a small beam produces a dominant wave with velocity close to the beam velocity it has been possible to treat the background plasma as a linear dielectric and the evolution of the single wave is determined using Poisson's equation while representing the beam as sheets of charge. The calculation was carried out using a computer.

The frequency and wavenumber of the fastest growing mode is obtained by manipulating the dispersion relation and if $\varepsilon_0(k, \omega)$ is the plasma dielectric function this can be written as

$$\varepsilon_0(k, \omega) = (n_B/n_0)[\omega_{pe}^2/(\omega - ku)^2]$$

where n_B and n_0 are the beam and plasma densities respectively, ω_{pe} is the electron plasma frequency and u is the beam drift velocity. The root corresponding to the slow beam wave is unstable and has a growth rate function peaked near the point (ω_0, k_0) which is defined by $\omega_0 = k_0 u$ and $\varepsilon_0(k_0, \omega_0) = 0$. We can Taylor expand the dispersion relation about this point to obtain:

$$\left(\frac{\partial \varepsilon_0}{\partial \omega}\Big|_{\omega_0, k_0} \omega' + \frac{\partial \varepsilon_0}{\partial k}\Big|_{\omega_0, k_0} k'\right)(\omega' - uk')^2 = \omega_{pe}^2 \frac{n_B}{n_0}$$

where $\omega' \equiv \omega - \omega_0$ and $k' \equiv k - k_0$. The maximum growth rate is now derived by differentiating this with respect to k' and setting $\mathrm{Im}(d\omega'/dk') = 0$. This gives the result that the most strongly growing mode has wavenumber k_0, frequency and growth rate given by:

$$\omega \equiv \omega_0 + \mathrm{Re}(\omega') = \omega_0 (1 - \eta^{1/3}/2^{4/3})$$

$$\gamma_{max} \equiv \mathrm{Im}(\omega') = (3^{1/2}/2^{4/3})\, \eta^{1/3} \omega_0$$

where $\eta \equiv (n_B/n_0)(\omega_{pe}^2/\omega_0^2)\, [(\omega_0/2)(\partial \varepsilon_0/\partial \omega)_{\omega_0, k_0}]^{-1}$. Making the approximations $\omega_0 \sim \omega_{pe}$ and $\eta \sim n_B/n_0$ we obtain the group velocity and the half-width of the peaked growth rate function:

$$\frac{d\omega}{dk} = \frac{2}{3} u$$

Since the wavenumber spread of the growing waves just prior to trapping will be seen to be small, it can be assumed that the initial spectrum is effectively flat in this region, and on this basis the shape of the spectrum at time t is given by:

$$|E(k,t)|^2 = |E_0|^2 \exp |2\gamma(k)t|$$

The resulting spectrum half-width becomes:

$$\delta k = (\ln 2)^{1/2} N^{-1/2} \Delta k$$

$$= [3(\ln 2)^{1/2} 2^{-5/6}] \eta^{1/3} N^{-1/2} k_0 \qquad (3.2)$$

where $N = \gamma_{max} t$ is the number of e-foldings. It can therefore be seen that if $\eta^{1/3} N^{-1/2} << 1$, then the spectrum will be very narrow.

The net effect of such a spread is to produce an approximate sine wave, but with some frequency and amplitude modulation. The modulation wavelength is approximately $\lambda_m = 2\pi/\delta k$. We now have to assess whether an electron can detect this modulation during the evolution of the instability. Since nonlinear effects only become important in the last one or two e-foldings it is only necessary to consider the accumulating phase difference within a time of about $2\gamma_{max}^{-1}$ in order to assess whether an electron sees an essentially pure sine wave during the trapping process. It is possible to show [O'Neil, Winfrey and Malmberg, 1971] that in this time an electron travels a distance (relative to the wave) which is an insignificant fraction of the modulation wavelength provided the following condition is satisfied:

$$N^{1/2} >> [8 \ \ln(2)/3]^{1/2}$$

wave.

If the above condition does not hold then we may still be able to use a single-wave model if the wave spectrum is very narrow. Hence, $\delta k << k_0$ is a suitable criterion in this case.

3.1.2 Computer Calculations Using the Single-Wave Model

The assumed conditions of the single-wave model lead to the emergence of a sine wave with velocity v_ϕ given by:

$$\frac{\omega}{k_0} = \frac{\omega_0}{k_0}\left(1 - \frac{\eta^{1/3}}{2^{4/3}}\right) \approx \frac{\omega_0}{k_0} = u$$

and since the wave velocity is so close to the beam velocity it can be assumed that the plasma is non-resonant even during the nonlinear stage of the instability and can thus continue to be treated as a linear dielectric. Using this approximation together with Poisson's equation and representing the beam by discrete charge sheets, it has been possible to obtain equations determining the motion of the individual charge sheets [O'Neil, Winfrey and Malmberg, 1971].

The analysis is carried out in the frame of the initial beam velocity and the single-wave potential can be written:

$$\phi(x,t) = \phi_{k_0}(t) \exp(ik_0 x) + \text{c.c.}$$

and $\phi_{k_0}(t)$ can be expressed as:

$$\phi_{k_0}(t) = \phi_0 \exp\left(-i \int_0^t dt' \omega'(t')\right)$$

are:

$$\frac{d^2x_j}{dt^2} = - ik_0 \frac{e}{m} \phi_{k_0} \exp[ik_0 x_j(t)] + c.c. \qquad (3.3)$$

where $j = 1, ..., M$ and x_j is the position of the jth charge sheet. It will be possible to determine the complete time development of the system if we can obtain an equation for the time evolution of the potential and to this end Poisson's equation is invoked:

$$k_0^2 \phi_{k_0}(t) = 4\pi [\rho_{k_0}^{(P)} + \rho_{k_0}^{(B)}(t)]$$

and it remains to find expressions for $\rho_{k_0}^{(p)}(t)$ and $\rho_{k_0}^{(B)}(t)$ which are the Fourier transformed charge densities for the plasma and beam respectively. If the beam charge density per sheet is $(2en_B\pi)/(Mk_0)$, then we have:

$$\rho_{k_0}^{(B)}(t) = \left(\frac{k_0}{2\pi}\right) \int_0^{2\pi/k_0} dx \exp(-ik_0 x) \left(\frac{2en_B\pi}{Mk_0}\right) \sum_j \delta[x - x_j(t)]$$

$$= \frac{en_B}{M} \sum_j \exp[-ik_0 x_j(t)]$$

Instead of using the plasma charge density we can include the plasma dielectric function which we are assuming to be linear, and so Poisson's equation now becomes:

$$k_0^2 \varepsilon_0(k_0, \omega) \phi_{k_0}(t) = (4\pi en_B/M) \sum_j \exp[- ik_0 x_j(t)] \qquad (3.4)$$

As before we can Taylor expand the dielectric function but this time the wavenumber is assumed constant at k_0:

$$\phi_{k_0}(t) = \frac{4\pi e n_B}{\omega'(t) k_0^2 M} \left(\frac{\partial \varepsilon_0}{\partial \omega} \right)^{-1}_{\omega_0, k_0} \sum_j \exp [- i k_0 x_j(t)]$$

And we thus obtain the following equation for the rate of change of the potential:

$$\frac{d\phi_{k_0}}{dt} = - i\omega'(t) \phi_{k_0}(t) = \frac{- i4\pi e n_B}{k_0^2 M} \left(\frac{\partial \varepsilon_0}{\partial \omega} \right)^{-1}_{\omega_0, k_0} \sum_j \exp [- i k_0 x_j(t)] \qquad (3.5)$$

Now equations (3.3) and (3.5) can be solved by computer but it is possible to scale them in terms of variables which depend on all the significant parameters of the system [O'Neil, Winfrey and Malmberg, 1971]. The new variables are:

$$\left.\begin{aligned} \xi &= k_0 x, & \tau &= t\omega_0 (1/2\eta)^{1/3}, \\ \Omega &= \omega'/\omega_0 (1/2\eta)^{1/3}, & \Phi(\tau) &= e\phi_{k_0}(t)/mu^2 (1/2\eta)^{2/3} \end{aligned}\right\} \qquad (3.6)$$

where $$\Phi(\tau) = \Phi(0) \exp \left[- i \int_0^\tau \Omega(\tau)\, d\tau' \right]$$

and we can rewrite equations (3.3) and (3.5) as:

$$\frac{d^2 \xi_j(\tau)}{d\tau^2} = - i\Phi(\tau) \exp[i\xi_j(\tau)] \qquad (3.7)$$

$$\frac{d^2 \Phi_j(\tau)}{d\tau} = - \frac{i}{M} \sum_j \exp[i\xi_j(\tau)] \qquad (3.8)$$

Computer solutions of these equations have been obtained [O'Neil, Winfrey and Malmberg, 1971].

The numerical solutions of equations (3.7) and (3.8) obtained by O'Neil et al [1971] were carried out using a computer with 60 and 500 beam sheets in various runs. The spatial variable was confined to a one-dimensional "box" one wavelength long and with periodic boundary conditions imposed at the ends. Varying the number of beam sheets was found to produce no significant differences.

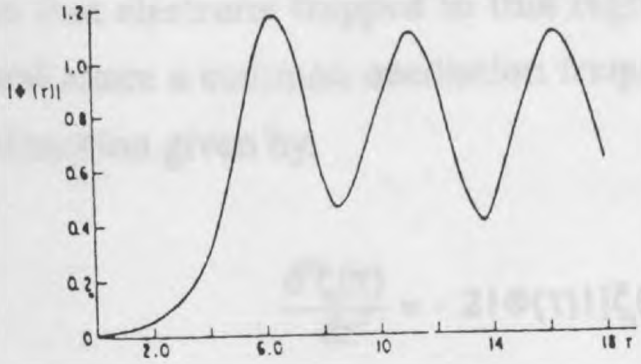

Fig. 3.1 Wave amplitude as a function of time. The wave amplitude and time are scaled according to equation (3.6).

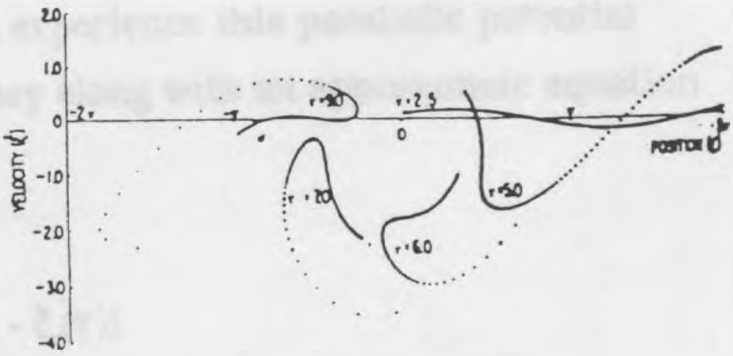

Fig. 3.2 The phasespace loci for the 500 beam sheets are plotted for various times. Each point gives the scaled velocity and coordinate for one of the beam sheets at the particular time denoted; i.e., $\tau = 2.5$, 5, 6, 7 or 9. For clarity, only every third particle is plotted, and the filamentary tails have been truncated to avoid confusing overlap.

Fig. 3.1 depicts the evolution of the wave potential, while Fig. 3.2 summarises the evolution of the beam dynamics. The interpretation is that the wave grows linearly until trapping causes saturation and the wave potential subsequently oscillates in response to the oscillation of the trapped electrons in the potential well. This is because the trapped electrons alternately speed up and slow down in the course of oscillating, and this change in kinetic energy has to be balanced by an equal and opposite change in the potential or field energy. Hence the wave amplitude is synchronised to the beam

One can see that at $\tau = 6.0$ the trapped electrons have reached their lowest position in phasespace and have therefore transferred a maximum amount of energy to the wave. Consequently, Fig. 3.1 shows that the wave potential has reached its first maximum at this time.

The high degree of regularity of this behaviour can be explained in the following way. The potential well is approximately parabolic near the bottom so that electrons trapped in this region experience this parabolic potential and share a common oscillation frequency along with an approximate equation of motion given by:

$$\frac{d^2\xi_j(\tau)}{d\tau^2} = -\,2|\Phi(\tau)|[\xi_j(\tau) - \xi_c(\tau)]$$

where $\xi_c(\tau)$ is the instantaneous bottom of the well. The solution to this equation is:

$$\xi_j(\tau) = A(\tau)\xi_j(0) + B(\tau)\dot{\xi}_j(0) + g(\tau)$$

where $[\xi_j(0),\ \dot{\xi}_j(0)]$ are the initial coordinates in phasespace, and this implies the following transformation for the particle coordinates in phasespace:

$$\begin{pmatrix} \xi_j(\tau) \\ \dot{\xi}_j(\tau) \end{pmatrix} = \begin{pmatrix} A(\tau) & B(\tau) \\ \dot{A}(\tau) & \dot{B}(\tau) \end{pmatrix} \begin{pmatrix} \xi_j(0) \\ \dot{\xi}_j(0) \end{pmatrix} + \begin{pmatrix} g(\tau) \\ \dot{g}(\tau) \end{pmatrix} \qquad (3.9)$$

The first term on the right hand side of equation (3.9) causes a rotation while the second is responsible for the translation and, since the beam electrons are initially arranged in a straight line, the trapped electrons continue to be positioned in an approximate straight line during the course of the trapping process, just as depicted in Fig. 3.2.

from 2 upwards, since the system was periodic. These harmonics were found and also observed to grow, but they made a negligible contribution to the field energy throughout the calculation. O'Neil et al [1971] ascribed their existence to spatial bunching of the beam electrons (see section 7.2.3 and 7.2.4).

3.2.1 General Considerations

To ascertain the ultimate state of a beam-plasma system after the instability has developed is extremely difficult, but one possibility is a BGK mode; these are named after Bernstein, Greene and Kruskal [1957] who first studied this kind of nonlinear wave. A BGK mode is a wave which is in equilibrium when viewed in the wave frame; in other words, assuming that the state is a stable one, the solution remains time independent. One approach for obtaining BGK solutions begins by prescribing an arbitrary periodic potential, a distribution of untrapped electrons and a distribution of untrapped ions. One then substitutes these quantities into the Poisson equation which is inverted to obtain the corresponding distribution function for trapped electrons. In principle there is always a solution for the trapped particles which satisfies the Poisson equation

We are specifically interested in beam-plasma systems and an analysis of such a system has been carried out [Thompson, 1971]. Although the system considered consists of a cold beam and plasma (in contrast to the warm plasma instability we have been considering) it may afford a qualitative understanding of beam-plasma systems generally, since it describes a limiting case of the more general situation. For such a system with a small beam, the background plasma electrons can be described by linear theory. However, in this discussion the principle of adiabatic invariance is used to describe them. This principle depends on the fact that in a system with a coordinate q and conjugate momentum p, a quantity called the action, defined by:

$$J = \oint p dq$$

is often conserved when there is a slow change in a certain parameter. That is, the quantity, also called an adiabatic invariant, is a constant of the motion.

3.2.2 BGK Modes in a Beam-Plasma System

Thompson [1971] considers a cold, one dimensional beam-plasma system in which the density of the beam electrons is much less than that of the background electrons so that $\eta = (\omega_{pb}^2/\omega_{pe}^2) << 1$ is a small parameter, where ω_{pb} is the beam electron plasma frequency. The basic equations describing this system are the Vlasov equation for the distribution function of each species and Poisson's equation for the electric field.

It will be assumed that the ultimate BGK state of this system is accompanied by an electric field consisting of a single sinusoidal mode and that the beam electrons are completely trapped. Now, it can be shown that any distribution function constructed from the constants of the motion of the individual particle orbits must be an equilibrium solution of the Vlasov equation. For the case considered, the Hamiltonian $H(x,v) = \frac{1}{2}mv^2 - (eE_\alpha/k_\alpha)\cos k_\alpha x$ (where the electric field is given by $E(x) = E_\alpha \sin k_\alpha x = -d\phi/dx$ and the potential $\phi(x) = (E_\alpha/k_\alpha)\cos k_\alpha x$) is a constant of the motion and therefore solutions to the time-independent Vlasov equation must be a function of the Hamiltonian. The adiabatic invariant that we shall be using for the background electrons is the spatially averaged velocity:

$$J = \langle | v(H,x,t) | \rangle$$

$$= \frac{4}{\pi}\left(\frac{eE(t)}{mk}\right)^{1/2}\{S(\kappa - 1)\kappa E_2(\kappa^{-1}) + S(1 - \kappa)[E_2(\kappa) - (1 - \kappa^2)K(\kappa)]\} \qquad (3.10)$$

where $\kappa = \{\frac{1}{2}[1 + kH/eE(t)]\}^{1/2}$, K and E_2 are complete elliptic integrals of the first and second kind, and $S(\rho) = \frac{1}{2} + \frac{1}{2}\,\mathrm{sign}\rho$ is the unit step function.

$$F_e(x,v) = F_e[H(x,v)] = \pi n_e \left(\frac{meE_\alpha}{\kappa_\alpha}\right)^{1/2} \kappa_e K^{-1}(\kappa_e^{-1})\delta(H - H_e)$$

where H_e and κ_e are related by $\kappa_e = [\frac{1}{2}(1 + k_\alpha H_e/eE_\alpha)]^{1/2}$. Now the density of the trapped beam electrons is given by:

$$n_b(\kappa) = g(e\phi) = \int_{-e\phi}^{-e\phi_{min}} dH_b F_b(H_b)[2m(H_b + e\phi)]^{-1/2}$$

and this equation can be inverted to obtain the following equation for $F_b(H_b)$:

$$F_b(H_b) = \frac{(2m)^{1/2}}{\pi} \int_{e\phi_{min}}^{-H_b} dV \frac{dg(V)}{dV}(- H_b - V)^{-1/2} \qquad (3.11)$$

The required expression for g(V) or $n_b(x)$ is obtained by invoking Poisson's equation :

$$n_b(x) = g(V) = \frac{1}{4\pi e}\frac{d^2\phi}{dx^2} + n_e + n_b - \int_{-e\phi_{min}}^{\infty} dH\, F_e(H)[2m(H + e\phi)]^{-1/2}$$

$$= -(k_\alpha^2/4\pi e^2)V + n_e + n_b - \pi n_e(eE_\alpha/2k_\alpha)^{1/2} \kappa_e K^{-1}(\kappa_e^{-1})(H_e + V)^{-1/2}$$

where n_b and n_e are the initial uniform beam and background electron densities respectively. Here the ion denstity (equal to $n_e + n_b$) remains constant as the ion mass is assumed to be infinite.

Thus after substituting g(V) into equation (3.11) we are now able to integrate the latter to obtain:

$$F_b(H_b) = -(\tfrac{1}{2} m)^{1/2} \frac{k_\alpha^2}{\pi^2 e^2}\left(\frac{eE_\alpha}{k_\alpha} - H_b\right)^{1/2}$$

determined from four more equations. One of these is the equation for J for the background electrons. Since these remain untrapped, the trapping parameter $\kappa > 1$. Hence equation (3.10) reduces to:

$$J_e = u - v_{\phi b} = \frac{4}{\pi}\left(\frac{eE_\alpha}{mk_\alpha}\right)^{1/2}\kappa_e E_2(\kappa_e^{-1})$$

where u is the initial beam velocity relative to the plasma and $v_{\phi b}$ is the initial beam velocity in the wave frame. The next equation expresses the fact that the beam particle density must vanish at the nodes of the trapping separatrix (i.e., at the points $x = \pm (\pi/k_\alpha) \times$ odd integer):

$$g(e\phi_{min}) = (k_\alpha E_\alpha/4\pi e) + n_e + n_b - \tfrac{1}{2}\pi n_e(1 - \kappa_e^{-2})^{-1/2}K^{-1}(\kappa_e^{-1}) = 0$$

Momentum conservation is expressed by:

$$-\pi n_e\left(\frac{meE_\alpha}{\kappa_\alpha}\right)^{1/2}\kappa_e K^{-1}(\kappa_e^{-1}) + mn_e(u - v_{\phi b}) - mn_b v_{\phi b} = 0$$

and for energy conservation we have:

$$-\frac{E_\alpha^{\,2}}{32\pi} + \frac{\pi n_e eE_\alpha}{\kappa_\alpha}(\kappa_e^{\,2} - \tfrac{3}{4})(1 - \kappa_e^{-2})^{-1/2}K^{-1}(\kappa_e^{-1}) - \tfrac{1}{2}mn_e(n - v_{\phi b})^2 - \tfrac{1}{2}mn_b v_{\phi b}^{\,2} = 0$$

From these four equations the four unknowns are found to be:

$$\kappa_e^{-1} = 2\eta^{1/3}(1 + \tfrac{1}{2}\tfrac{3}{4}\eta^{1/3} + \dots)$$

$$k_\alpha = (\omega_{pe}/u)(1 + \tfrac{13}{8}\eta^{2/3} + \dots)$$

$$v_{\phi b} = u - v_{\phi\alpha} = \tfrac{1}{2}\eta^{1/3}u(1 + \tfrac{5}{8}\eta^{1/3} + \dots)$$

where $T_b(0)$ is the initial beam kinetic energy density. These quantities are close to those obtained from a linear theory projection but the BGK wave velocity is slightly smaller. One should therefore expect the wave to be slowed down by nonlinear effects as the BGK state is approached.

From the discussion so far it is clear that the influence of many waves is important in the development of the beam-plasma instability and there is another point of view that can deal with some aspects of such a situation. If one models the spectrum as a main wave with the addition of small amplitude neighbouring waves to provide a perturbation, one finds that the original separatrix in phasespace no longer clearly separates the trapped electrons from the untrapped ones. Instead, a region is formed near the separatrix where the electrons move stochastically; this has the effect of flattening the distribution function in this region and therefore smoothing out the clump.

The chaotic motion of an electron is due to the fact that it is influenced by more than one wave. Two waves can influence an electron when their trapping regions overlap in velocity space. The size of the trapping region for a given wave is given by:

$$\delta v = \frac{4}{\pi} \left(\frac{A}{k} \right)^{1/2}$$

where A is the wave amplitude and the "Chirikov stochasticity parameter" [Dimonte, 1982] is given by:

$$P = \frac{\delta v_1 + \delta v_2}{2\Delta v}$$

where the subscripts refer to two specific waves. If $P > 1$ then the trapping regions of the two waves overlap, forming a stochastic region for electrons (see section 7.2.5).

A narrow spectrum of waves will produce the result shown in Fig. 3.3 where the shaded area is the stochastic region. In the beam-plasma instability one certainly expects a spectrum of waves but, initially, the wave amplitude

al, 1982] (see section7.2.5).

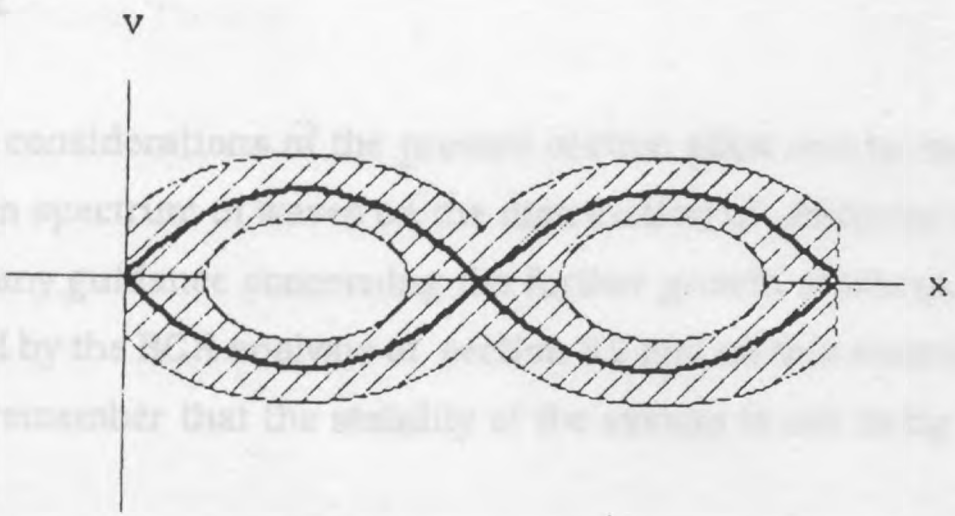

Fig. 3.3 Phasespace showing the stochastic region (shaded) resulting from a narrow spectrum of waves. The bold curve represents the separatrix.

The existence of the stochastic region implies that electrons are constantly being detrapped and then trapped again in a neighbouring potential trough. In time the distribution function should eventually become constant throughout the stochastic region and there would be no further amplitude oscillations. Such a state would resemble a BGK state (see section 3.2) since the distribution function would appear to be time independent in the wave frame and would clearly exhibit constant periodicity. However, as we have invoked a spectrum of neighbouring waves we cannot satisfy the condition of monochromaticity. Even so, it would still be possible to interpret the state as one which conforms macroscopically to a BGK state, but which also encompasses a noise spectrum on the microscopic scale. It might seem more reasonable to expect, in practice, a BGK state with some amplitude and frequency modulation but it is not clear how to justify such a supposition given that we have assumed that a spatially periodic distribution function is the result of this finite spectral spread.

filled in as required in the calculation of section 3.2 but it will be recalled that the distribution function was assumed there to go to zero at the nodes of the separatrix in contrast to the present case. Some disparity is therefore to be expected.

The considerations of the present section allow one to examine the effect of a given spectrum of waves on the distribution of electrons but they do not provide any guidance concerning the further growth of waves. This restriction is shared by the BGK analysis of section 3.2 and on this occasion we again have to remember that the stability of the system is not being considered.

4.1 Simulation Theory

The main purpose of this study has been to investigate the behaviour of the sheath and plasma in conditions where secondary emission is present. The primary approach used has been a computer particle-simulation method and the reasons for making such a choice are discussed in this section.

4.1.1 Finite Difference Approximation and Finite Element Method

There are many methods of tranforming the differential equations of physics to discrete forms suitable for numerical compution. Among the most widely used are finite difference methods, finite element methods, and particle methods.

The finite difference approximation (FDA) [Richtmyer and Morton, 1967] uses a mesh of points distributed in variable space and functions of the continuous variable only possess values at each mesh point. Derivatives of the functions are approximated at each mesh point in terms of differences between values assigned to neighbouring mesh points; this results in difference equations which only apply at mesh points and which replace the original differential equations.

In the finite element method (FEM) [Strang and Fix, 1973] functions are replaced by sets of simpler functions, for example, the piecewise union of simple polynomials or the sum of orthogonal global polynomials; the latter is also known as the spectral method. The FEM provides greater accuracy and flexibility than the FDA.

is the simplest it can run into numerical difficulties in dealing with advection terms (such as in the Vlasov equation): on the other hand a Lagrangian scheme may result in very complex mesh topology or even mesh shearing problems. An example of a Lagrangian scheme is the waterbag model [Berk and Roberts, 1970] which has been applied to the study of two-stream instabilities.

4.1.2 Particle Methods

At present, particle methods provide the most efficient way of combining the advantages of Eulerian and Lagrangian approaches. Using the particle-mesh (PM) scheme a series of sample points is distributed throughout the fluid continuum. Each point (particle) carries attributes (e.g. charge, mass) which are, ideally, conserved quantities so that time advancement is simply a matter of moving the particles; this constitutes the Lagrangian part of the method. The Eulerian part of the calculation solves the remaining equations using the FDA or the FEM. The Lagrangian and Eulerian parts of the scheme are linked together at each timestep by interpolating from the mesh to the particles and performing inverse interpolation from the particles to the mesh.

From now on we consider only the one-dimensional problem and the 'particles' then become infinite plane two-dimensional sheets. For simplicity we assume a 1- D collisionless plasma consisting of an electron gas in a fixed neutralising background of ions, and such a system is described by the following equations:

$$\frac{\partial f}{\partial t} + v\frac{\partial f}{\partial x} + \frac{qE}{m}\frac{\partial f}{\partial v} = 0 \qquad (4.1)$$

$$E = -\frac{d\phi}{dx} \qquad (4.2)$$

$$\rho = \rho_0 + q \int f dv \qquad (4.4)$$

where f(x,v,t) is the electron distribution function. In the PM model equation (4.1) is replaced by:

$$\frac{dx_i}{dt} = v_i , \qquad m_i \frac{dv_i}{dt} = q_i E(x_i) \qquad (4.5)$$

which are the equations of motion of the particles i. m_i and q_i are now mass per unit area and charge per unit area respectively. The particles are in essence a device for transforming the awkward advective equation (4.1) into the set of ordinary differential equations (4.5). Here the electric fields $E(x_i)$ are interpolated from the mesh values.

The PM model also requires the discretisation of equations (4.2) and (4.3) using the FDA and the integral in equation (4.4) is evaluated using some inverse interpolation scheme.

4.1.3 Charge Assignment

The way in which the distribution function f is approximated deserves deeper consideration. One can construct samples $\bar{f}$ of the smooth distribution function f in the following way:

$$\bar{f} = \sum_{i=1}^{N_p} \delta(x - x_i)\, \delta(v - v_i)$$

where N_p is the total number of particles. Now a smooth approximate distribution function f is obtained as follows:

where S is a scaling factor, W is a weighting or 'shape' factor and h is the range of x over which averaging is performed.

The integral in equation (4.4) now becomes:

$$\int f dv = \frac{S}{h_i} \Sigma W(x - x_i)$$

and the scheme can be classified into further categories according to the nature of the shape factor W, the two most common being Nearest Grid Point (NGP) and Cloud In Cell (CIC).

Consider a mesh with interval H; if we set h = H then the shape factors are as follows:

$$W(x) = \begin{cases} \dfrac{H - |x|}{H} & \text{when } |x| \le H \\ 0 & \text{when } |x| > H \end{cases} \quad \text{for CIC}$$

$$W(x) = \begin{cases} 1 & \text{when } -H/2 < x \le H/2 \\ 0 & \text{otherwise} \end{cases} \quad \text{for NGP}$$

The NGP scheme merely amounts to assigning a particle to its nearest grid point, hence its name. To visualise the CIC scheme, however, the mesh can be considered to be composed of equally spaced grid points each occupying the centre of a string of similar cells; the particles can now be considered to be rectangular clouds of length equal to the grid interval and a fraction of any particle equal to the fraction of cloud overlapping a cell is assigned to the grid point occupying that cell.

be seen the charge density variation for NGP is stepwise whilst for CIC it is piecewise continuous linear. The smoother representation resulting from CIC leads to reduced field noise compared to NGP and it therefore allows the use of fewer particles and a coarser grid.

The depicted incremental charge density profile indicates that in both of these schemes the particles have an effective width, which gives the schemes improved noise characteristics compared to those using point particles.

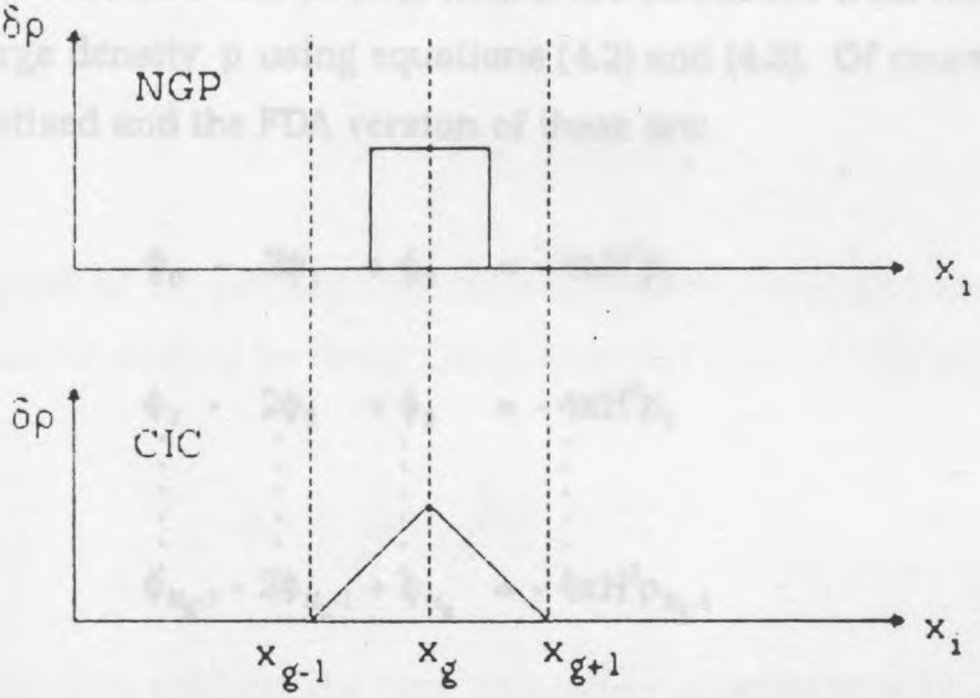

Fig. 4.1 The incremental charge density δρ assigned to a grid point at x_g due to a particle at x_i.

Care must be taken during the inverse process, that is when interpolating from the fields on the mesh to the fields acting on the particles. The reason is that if the interpolation scheme is not the exact inverse of the charge assignment scheme then particle self-forces will arise and produce non-physical behaviour of the simulation.

$$E(x_i) = \left(\frac{x_{g+1} - x_i}{H} \right) E_g + \left(\frac{x_i - x_g}{H} \right) E_{g+1}$$

where $x_g < x_i < x_{g+1}$. This ensures that the two components of self-force experienced by a particle at x_i (due to its own charge contribution to the two grid points at x_g and x_{g+1}) will cancel each other out.

4.1.4 Determining the Electric Field

The mesh values for the electric field E are calculated from the mesh values for the charge density ρ using equations (4.2) and (4.3). Of course these have to be discretised and the FDA version of these are:

$$\begin{aligned}
\phi_0 - 2\phi_1 + \phi_2 &= -4\pi H^2 \rho_1 \\
\phi_1 - 2\phi_2 + \phi_3 &= -4\pi H^2 \rho_2 \\
&\vdots \\
\phi_{N_g-2} - 2\phi_{N_g-1} + \phi_{N_g} &= -4\pi H^2 \rho_{N_g-1} \\
\phi_{N_g-1} - 2\phi_{N_g} + \phi_{N_g+1} &= -4\pi H^2 \rho_{N_g}
\end{aligned}$$

where mesh point zero is at $x = 0$ and mesh point N_g is at x_{max}. Now this is a system of N_g equations in $N_g + 2$ unknowns and we therefore require two boundary conditions to determine all the variables.

There are several methods for solving such a set of equations including Gaussian elimination and tridiagonal matrix inversion but in this particular case a simple method is to multiply the first equation by one, the second by two, the third by three, and so on, then summing them. The result is:

If one now choses periodic boundary conditions, for example, this implies:

$$\phi_0 = \phi_{N_g} = 0, \quad \phi_{N_g+1} = \phi_1$$

so that:

$$N_g\phi_1 = -4\pi H^2 \sum_{p=1}^{N_g} p\rho_p$$

then:

$$\phi_2 = 2\phi_1 - 4\pi H^2\rho_1$$

and:

$$\phi_n = 2\phi_{n-1} - \phi_{n-2} - 4\pi H^2\rho_{n-1}$$

Thus the values of the potential are obtained on the mesh and the electric field can then be derived by using the discretised form of equation (4.2):

$$E_p = \frac{\phi_{p-1} - \phi_{p+1}}{2H}$$

The next step is to perform the time integration of equations (4.5).

4.1.5 Time Integration

If we merely used:

$$x_{new} = x_{old} + v_{old}\,\Delta t$$

and

$$v_{new} = v_{old} + \frac{q_i}{m_i} E(x_{old})\,\Delta t$$

where the new values of position and velocity are explicitly formulated in

used way of overcoming this problem is to use a time-centred method known as the "leapfrog" scheme.

For this scheme the new positions and velocities are given by:

$$x_i^{n+1} = x_i^n + v_i^{n+1/2}\,\Delta t$$

and

$$v_i^{n+1/2} = v_i^{n-1/2} + \frac{q_i}{m_i} E(x_i^n)\;\Delta t$$

The interpretation of the timestep index n is illustrated in Fig. 4.2. It can be seen that in each case the increment is calculated from values which apply at a time which is midway between the preceding and current timesteps. Such a scheme is described as time-centred.

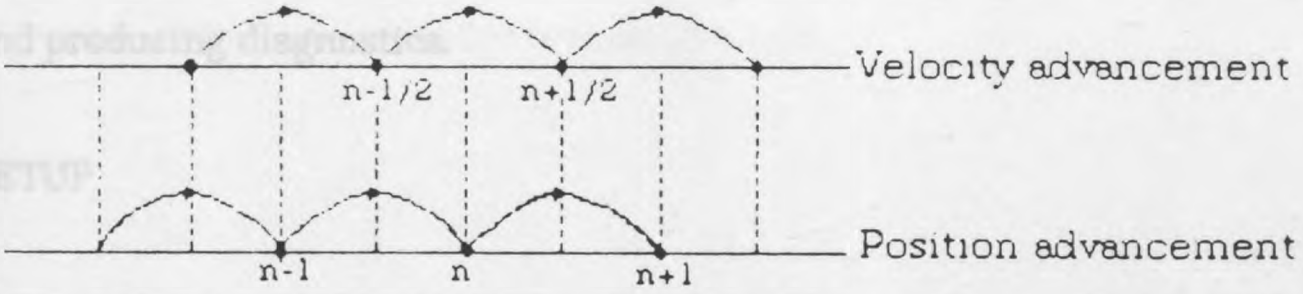

Fig. 4.2 Velocity and position advancement at a series of timesteps n for the leapfrog time-integration scheme.

It should be noted that at time t = 0 we have to obtain v(- Δt/2) from v(0) by using the force F(0) in order to set the leapfrog scheme going. The benefit of introducing the leapfrog modification is that the phase errors are now only proportional to $(\Delta t)^2$.

As we saw in the last section a particle-mesh simulation inherits considerable advantages from its ability to combine Eulerian and Lagrangian features and this was therefore the method, along with the CIC scheme and leapfrog time-integration, which was chosen to investigate the evolution of the beam-plasma instability due to secondary emission. A computer code was developed for this purpose and the functions of its main routines are outlined below.

MAIN

This module initialises the main arrays and variables and creates a plasma with stipulated characteristics at time t = 0. It interprets commands which can either be supplied interactively by the user at a terminal or by a "command" data file when the programme is run in batch mode. Appropriate routines are called when MAIN is required to carry out its other functions which include advancing the simulation by a specified number of timesteps and producing diagnostics.

SETUP

This routine is called by MAIN to set up the plasma with specified initial conditions. The length of the "box" containing the plasma is given and ion-electron pairs are assigned to random positions within this domain. The particle velocities, however, are assigned in accordance with the required initial velocity distribution functions for each species.

MAX

This routine is called by SETUP once for each particle to obtain an initial particle velocity with probability distribution given by a truncated Maxwellian

Each time this routine is called by MAIN it moves the simulation forward by one timestep. It proceeds by assigning charge density to the mesh, solving the field equations using the finite difference approximation and then performing leapfrog time-integration on the particle positions and velocities. The specified boundary conditions are then applied at this point.

IONISE

This routine, which is called by STEP, provides ionisation if necessary by introducing ion-electron pairs to random positions within the "box" at a specified rate.

FOURIE

This routine is called by MAIN and performs a Fourier analysis of the potential field distribution across the box at the conclusion of each timestep. The time evolution of the Fourier modes is thus obtained.

COEFF

This routine is called by FOURIE and calculates the Fourier coefficient for the mode selected by FOURIE.

GRAPH

This routine produces phasespace plots of the ions and electrons and is called by MAIN.

FIELD

This routine produces graphs of the electric field and potential distributions

This routine, called by MAIN, produces graphs of the particle space-averaged velocity distribution functions.

Equilibrium Sheath Calculations

Calculations of parameters defining the equilibrium characteristics of sheaths and associated secondary electron beams have been carried out and are reported in this chapter. Cases with and without current are dealt with in sections 5.2 and 5.1 respectively. A hypothetical system is also investigated in section 5.3 because it provides an example in which the boundary conditions are not clear.

5.1 Zero Current Conditions.

5.1.1 The Effect of Secondary Emission on Wall Potential and Ion Energy

In the equations which follow, all units are normalised to the following quantities:

Mass : m_e Length : λ_D Time : $1/\omega_{pe}$

Velocity : v_{Te} Electric Charge : e Electric Field : $m_e v_{Te} \omega_{pe}$ or $KT_e/e\lambda_D$

Electric Potential : $m_e v_{Te}^2/e$ or KT_e/e

where m_e is the electron mass, λ_D the Debye length, ω_{pe} the electron plasma freqency, v_{Te} the electron thermal velocity, e the electronic charge, K Boltzmann's constant, and T_e is the electron temperature. Note that the normalised ion mass will either be written as M/m or μ and will usually be referred to as the mass ratio.

The zero-current condition and monotonicity criterion (equations (1.15) and (1.16)) are a pair of simultaneous equations which determine the values of

and

$$I = \frac{1}{2} + \frac{\Gamma}{1-\Gamma}\left(\frac{m}{M}\right)^{1/2}\left(-\frac{I}{\Phi_0}\right)^{3/2}\left(\frac{1}{2} - \Phi_0\right) \qquad (5.2)$$

where Φ_0 is the wall potential and I is the ion energy on entry to the sheath. A simple computer code was written to solve these iteratively, giving I and Φ_0 as a function of Γ for three mass ratios. The results are displayed in Fig. 5.1. All the curves exhibit a rising gradient with increasing Γ but, shortly before the slopes become infinite, Γ will have exceeded the critical value and solutions in this region will have no physical significance. Critical values of Γ (signified by Γ_c), which correspond to zero electric field at the wall, along with curves of I and Φ_0, are displayed as a function of mass ratio in Fig. 5.2. In addition, Fig. 5.3 depicts curves of Φ_0, v_b (beam-velocity given by $\sqrt{2e\Phi_0/m}$) and n_b/n_0 (relative beam-density given by equation (1.12)) as a function of mass ratio for the condition of critical Γ.

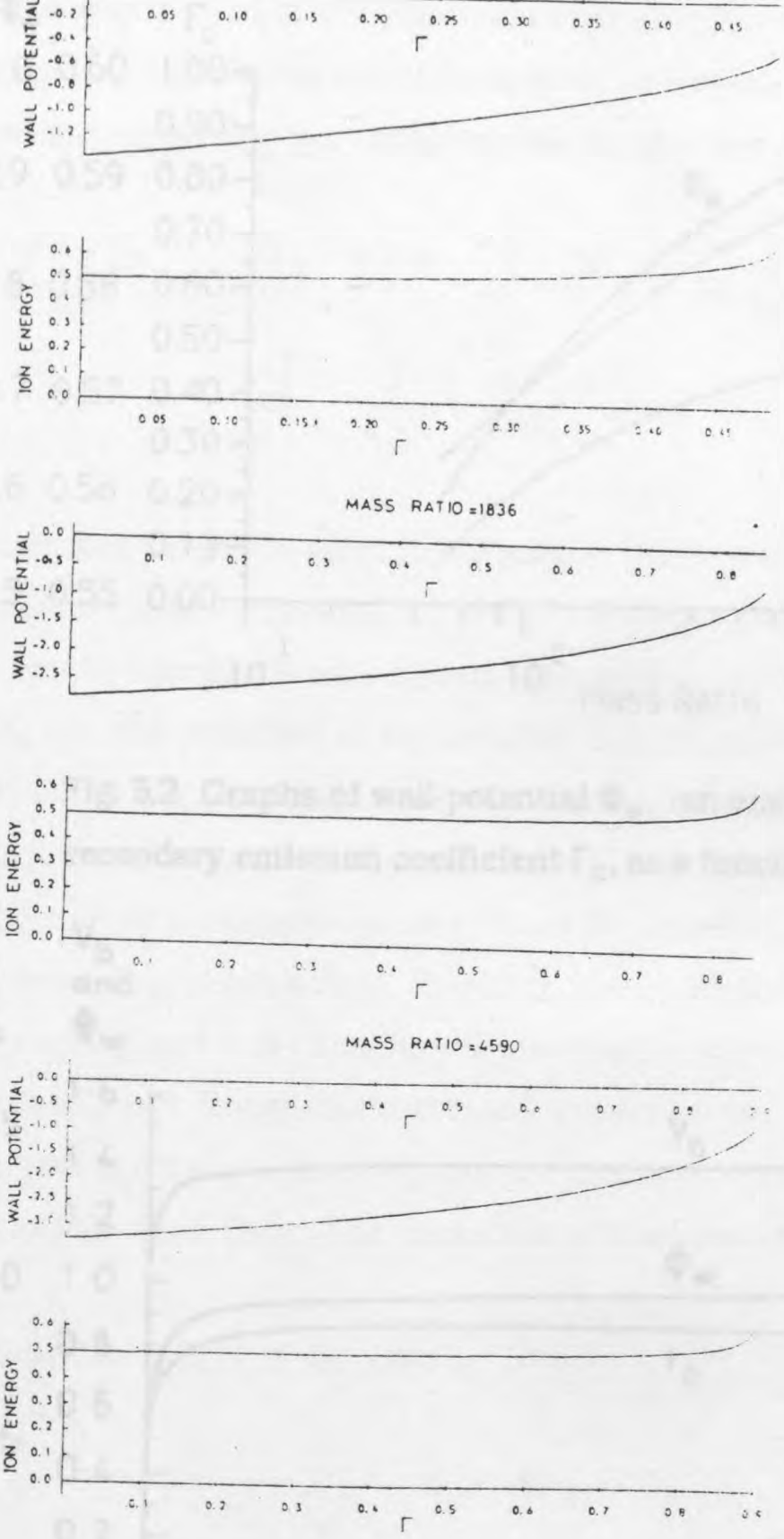

Fig. 5.1 Ion energy and wall potential as a function of the secondary

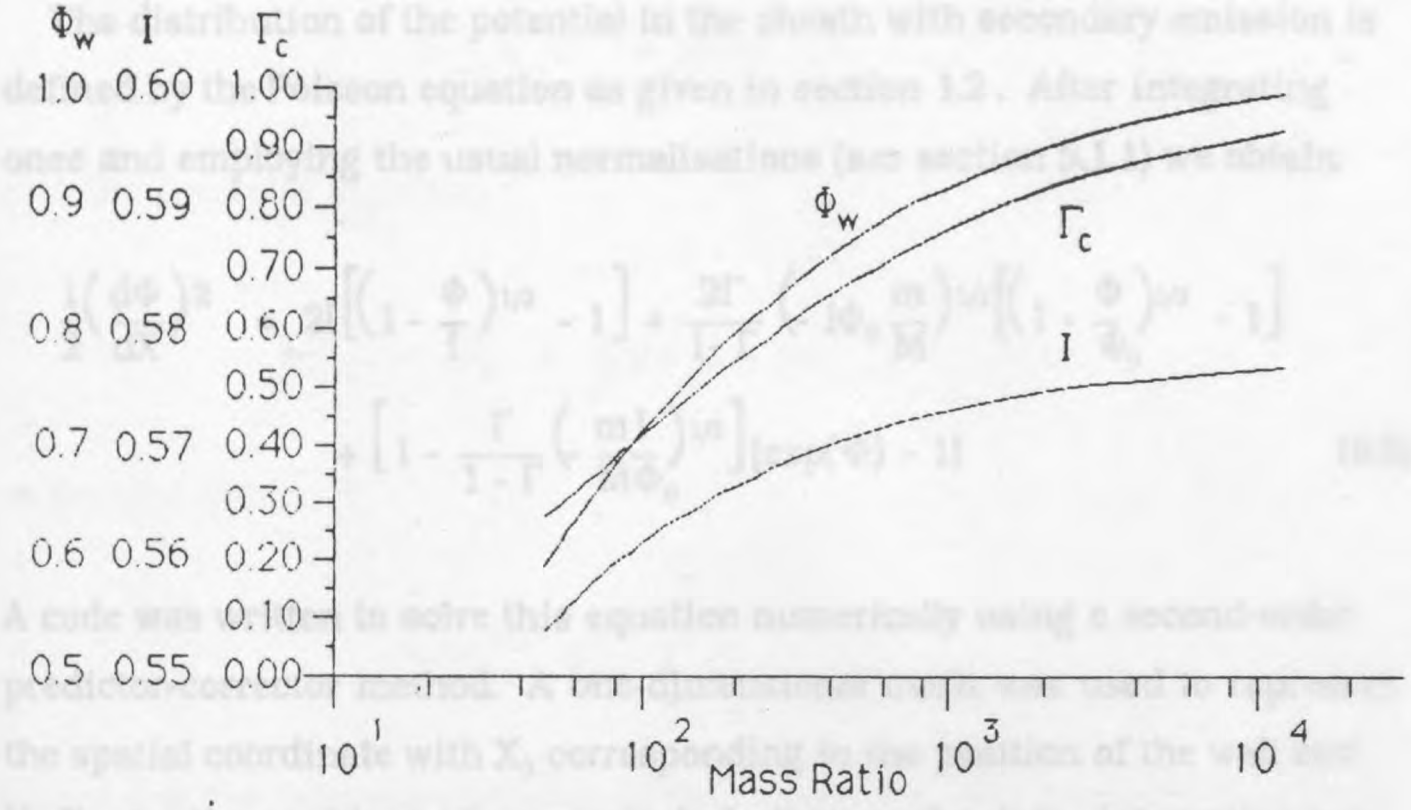

Fig. 5.2 Graphs of wall-potential Φ_w, ion energy I, and critical value of secondary emission coefficient Γ_c, as a function of mass-ratio.

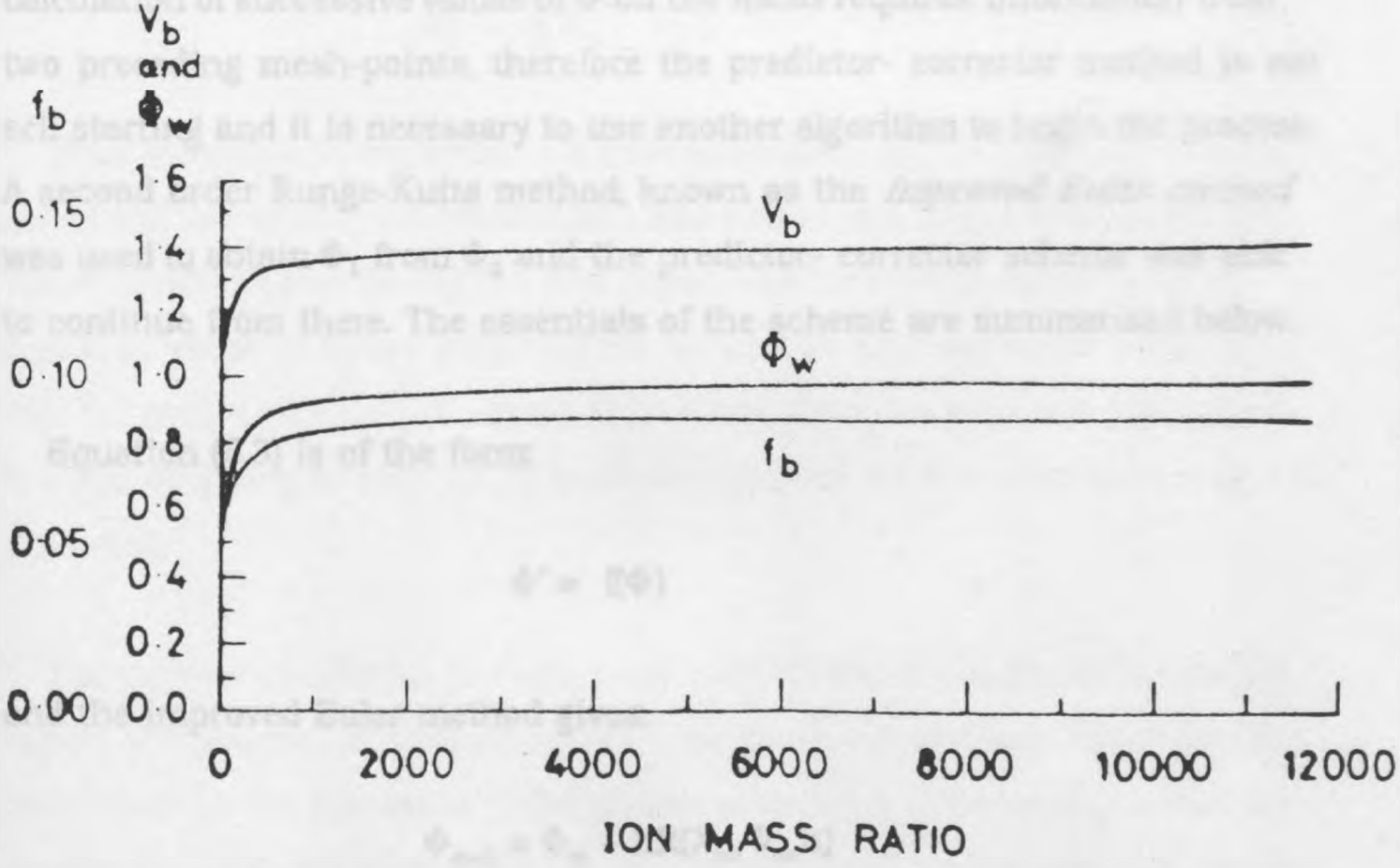

Fig. 5.3 Graphs of wall-potential Φ_w, beam-velocity v_b, and relative beam-density $f_b = n_b/n_i$ as a function of mass-ratio.

The distribution of the potential in the sheath with secondary emission is defined by the Poisson equation as given in section 1.2. After integrating once and employing the usual normalisations (see section 5.1.1) we obtain:

$$\frac{1}{2}\left(\frac{d\Phi}{dX}\right)^2 = 2I\left[\left(1 - \frac{\Phi}{I}\right)^{1/2} - 1\right] + \frac{2\Gamma}{1-\Gamma}\left(-I\Phi_0\frac{m}{M}\right)^{1/2}\left[\left(1 - \frac{\Phi}{\Phi_0}\right)^{1/2} - 1\right]$$
$$+ \left[1 - \frac{\Gamma}{1-\Gamma}\left(-\frac{mI}{M\Phi_0}\right)^{1/2}\right][\exp(\Phi) - 1] \qquad (5.3)$$

A code was written to solve this equation numerically using a second-order predictor-corrector method. A one-dimensional mesh was used to represent the spatial coordinate with X_0 corresponding to the position of the wall and X_1, X_2 etc., the positions of successively further meshpoints. Integration was carried out from the wall into the plasma using the boundary condition at the wall: $X = 0$, $\Phi = \Phi_0$ where Φ_0 was obtained from previous calculations. The calculation of successive values of Φ on the mesh requires information from two preceding mesh-points, therefore the predictor- corrector method is not self starting and it is necessary to use another algorithm to begin the process. A second order Runge-Kutta method, known as the *improved Euler method* was used to obtain Φ_1 from Φ_0 and the predictor- corrector scheme was able to continue from there. The essentials of the scheme are summarised below.

Equation (5.3) is of the form:

$$\Phi' = f(\Phi)$$

and the improved Euler method gives:

$$\Phi_{m+1} = \Phi_m + hR(X_m, \Phi_m, h)$$

where: $R(X, \Phi, h) = \frac{1}{2}[f(X, \Phi) + f(X + h, \Phi + h\Phi')]$

$$\Phi_{m+1}^{(0)} = \Phi_{m-1} + 2hf(\Phi_m)$$

and the corrector equation :

$$\Phi_{m+1}^{(i)} = \Phi_m + \frac{h}{2}[f(\Phi_m) + f(\Phi_{m+1}^{(i-1)})]$$

is iterated until:

$$|\Phi_{m+}^{(i-1)} - \Phi_{m+1}^{(i)}| < \varepsilon$$

where ε is the required precision of the calculation. The truncation error for this method is given by:

$$E_T = \frac{1}{5}(\Phi_m^{(0)} - \Phi_m^{(i)})$$

Thus solutions for equation (5.3) have been obtained for a number of mass ratios and values of Γ; the truncation error was always found to be negligible. These results appear in Fig. 5.4 The sheath can be seen to extend over a region of about 10 Debye lengths from the wall for all mass ratios used. Note that the profiles for critical values of Γ clearly show the potential gradient at the wall dropping to zero which indicates that the electric field here is zero as predicted.

The particle simulation has also been used to obtain results for the sheath region of a plasma for comparison with the above calculations. Since the ions participate in the formation of the sheath potential it is necessary to run the simulation long enough to allow the ions to take up an equilibrium distribution in space. Since the equilibrium state of ions at any position in the sheath depends on the state of ions everywhere else in the sheath the ion distribution

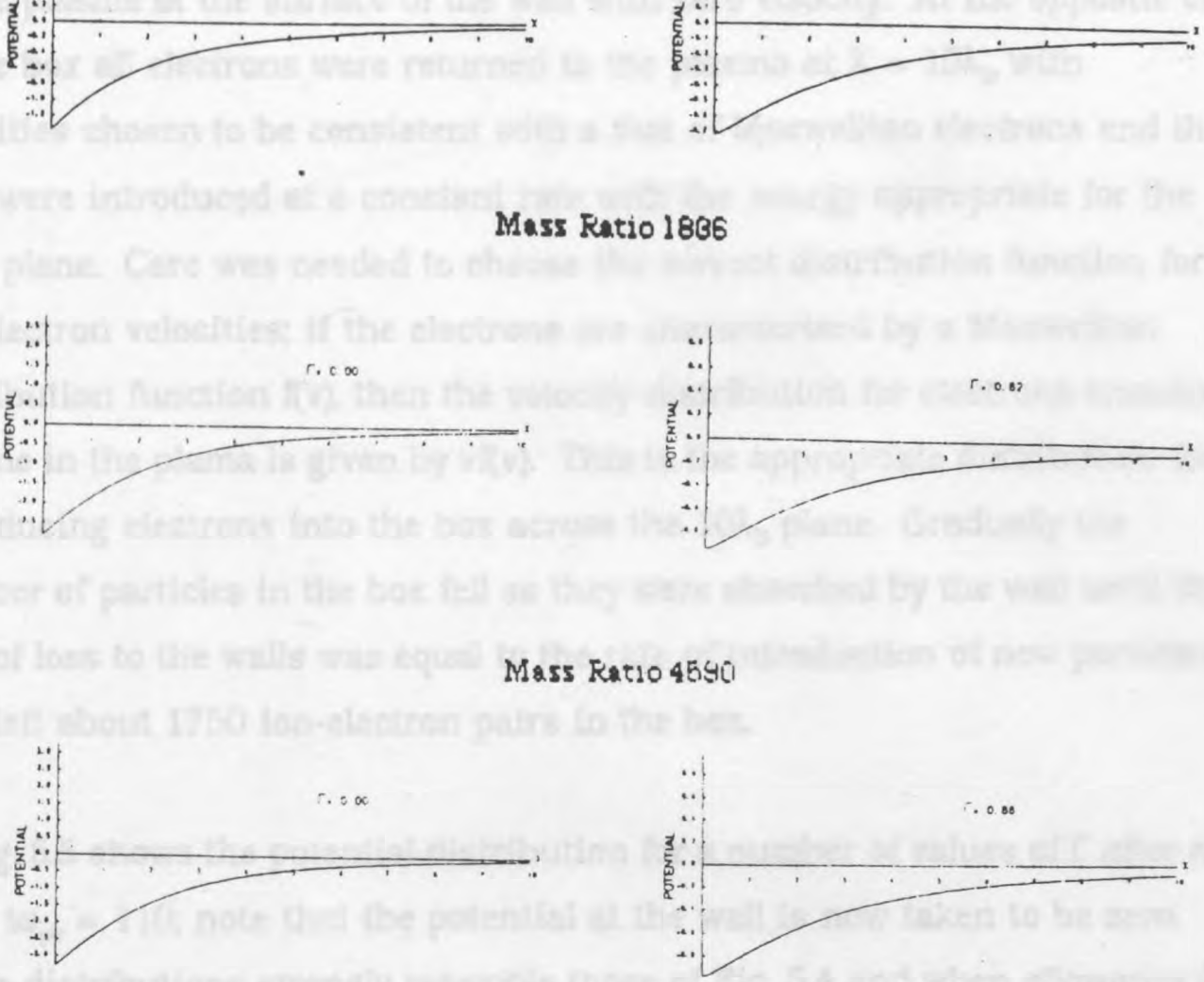

Fig. 5.4 Potential distributions in the sheath for $\Gamma = 0$ and Γ_c for three different mass ratios.

information from all parts of the sheath to propagate to all other parts. We are therefore led to conclude that it is necessary to run the simulation for at least an ion-sound time which is the time for an ion sound wave to travel the length of the simulated region of plasma - in this case 10 Debye lengths. The ion-sound speed is $(m/M)^{1/2}$ when normalised to the electron thermal velocity and the normalised ion-sound time therefore becomes $10(M/m)^{1/2}$. Thus it was decided to restrict the sheath simulations to a mass ratio of 100 in order to minimise computer time.

The simulations were started with 2000 pairs of ions and electrons in a one-dimensional box of length $10\lambda_D$ with the wall at X = 0. The electrons were Maxwellian and the ions monoenergetic with energy equal to that calculated in

of the box all electrons were returned to the plasma at $X = 10\lambda_D$ with velocities chosen to be consistent with a flux of Maxwellian electrons and the ions were introduced at a constant rate with the energy appropriate for the $10\lambda_D$ plane. Care was needed to choose the correct distribution function for the electron velocities; if the electrons are characterised by a Maxwellian distribution function f(v), then the velocity distribution for electrons crossing a plane in the plama is given by vf(v). This is the appropriate distribution for introducing electrons into the box across the $10\lambda_D$ plane. Gradually the number of particles in the box fell as they were absorbed by the wall until the rate of loss to the walls was equal to the rate of introduction of new particles; this left about 1750 ion-electron pairs in the box.

Fig. 5.5 shows the potential distribution for a number of values of Γ after a time $t\omega_{pe} = 110$; note that the potential at the wall is now taken to be zero. These distributions strongly resemble those of Fig. 5.4 and when allowance is made for the large thermal fluctuations of the simulation the agreement is good. Two simulations have values of Γ which are above the critical value of 0.42 for the chosen mass ratio; these are $\Gamma = 0.5$ and 0.8 respectively and the corresponding results are expected to agree with those for $\Gamma = 0.42$. This is because, although a fraction greater than Γ of incident electrons may be emitted from the wall, only a fraction Γ_c will be allowed to flow away from the wall back into the plasma. The rest will form a layer at the surface of the wall and have the same influence on the plasma as if they were absorbed by the wall.

Since the fluctuations are quite large it is necessary to study the time evolution of the simulation. We are interested in the potential drop across the sheath and we therefore consider the time evolution curves for the potential drop across the one- dimensional simulation box; these are plotted in Fig. 5.6.

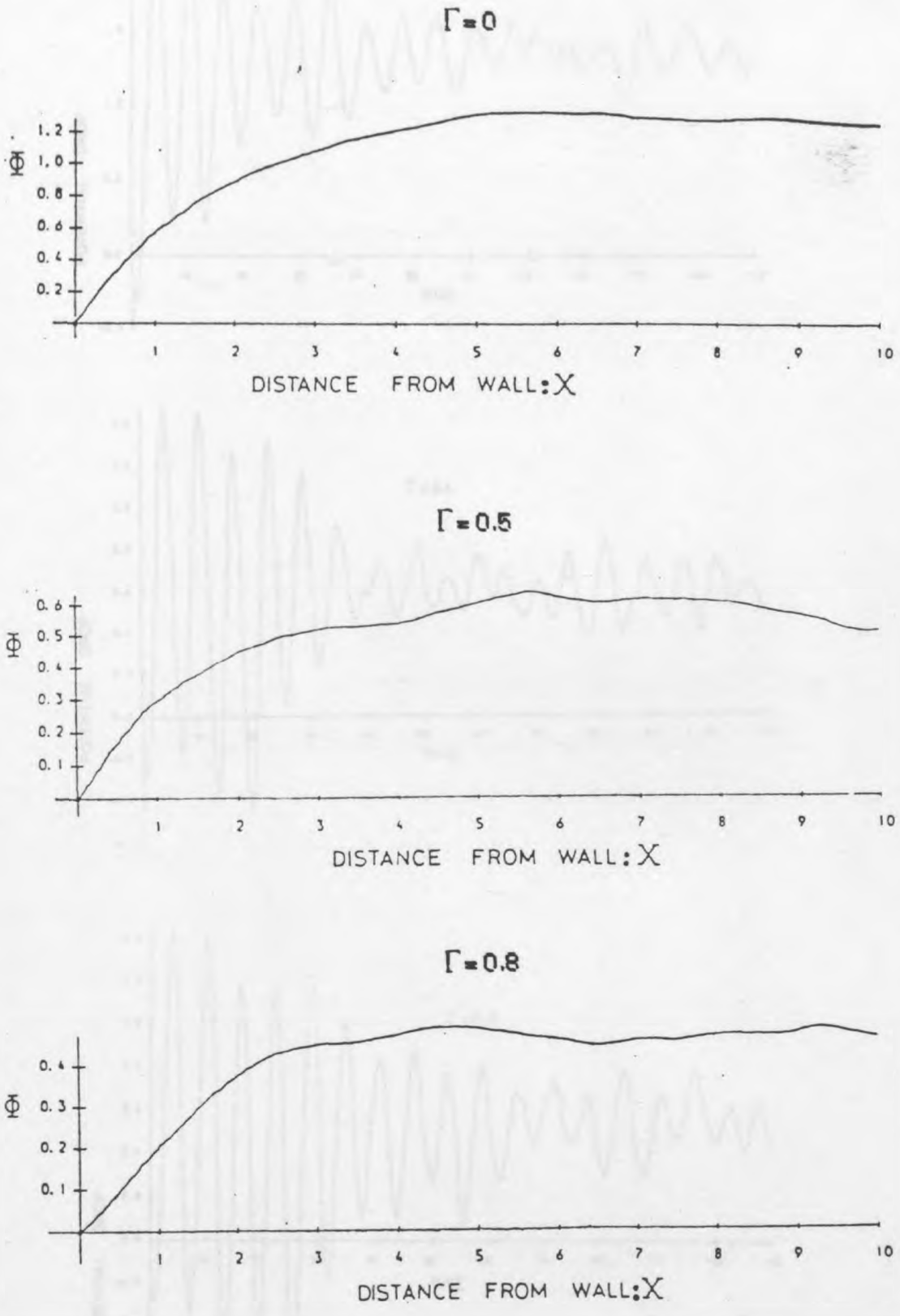

Fig. 5.5 Instantaneous potential distributions after a time $t\omega_{pe} = 110$ during a particle simulation of the sheath for three values of the secondary emission coefficient Γ.

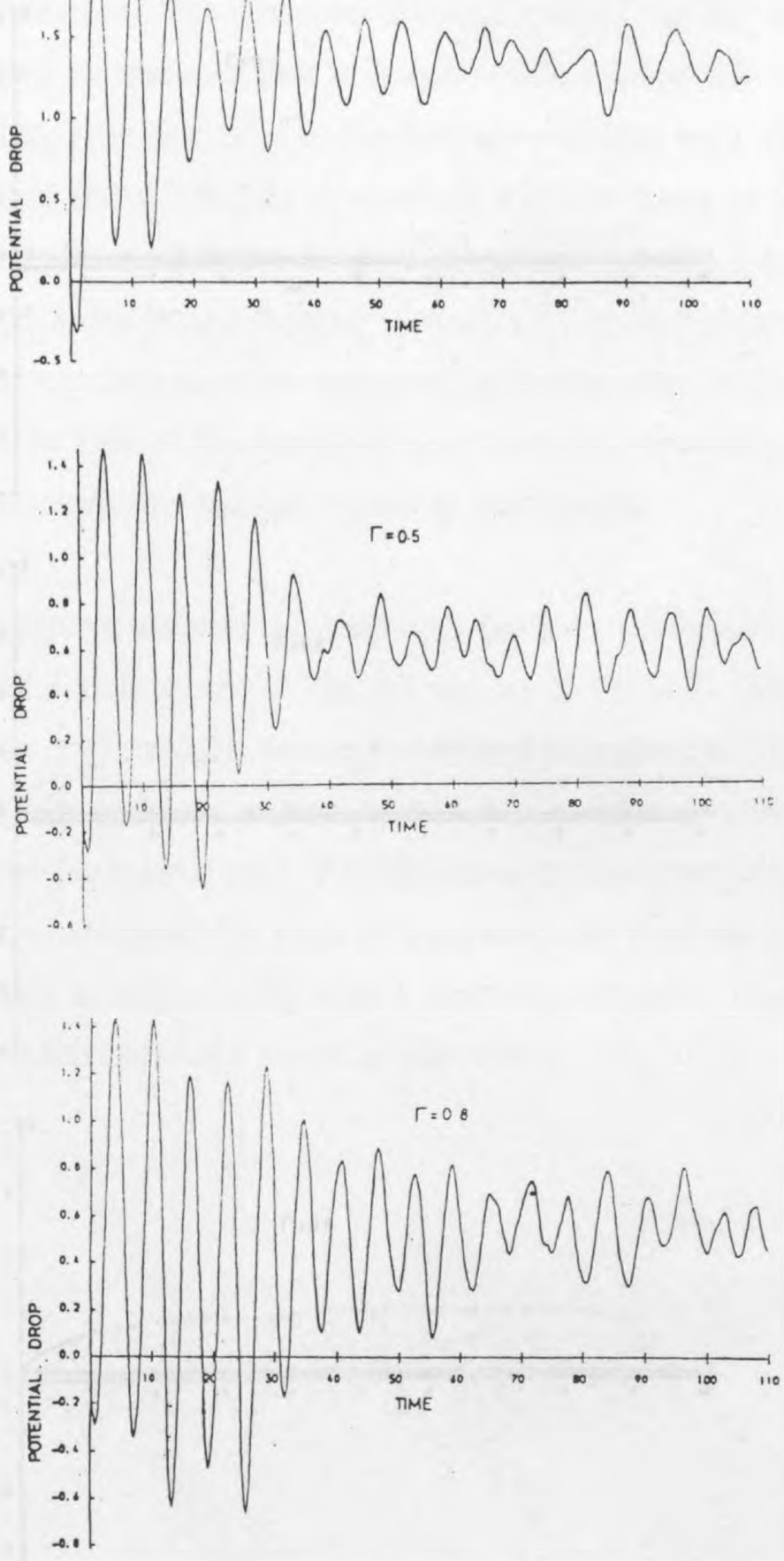

Fig. 5.6 Time evolution of the potential drop across the simulated sheath region for three values of the secondary emission coefficient Γ.

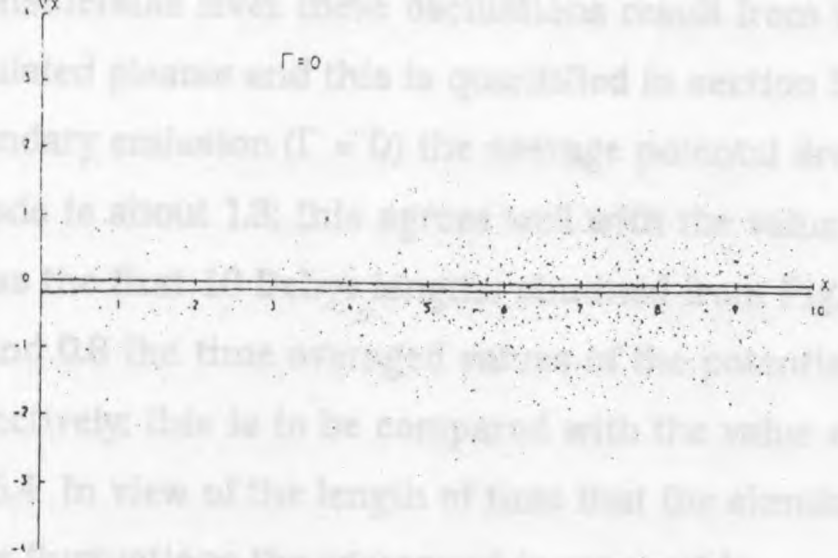

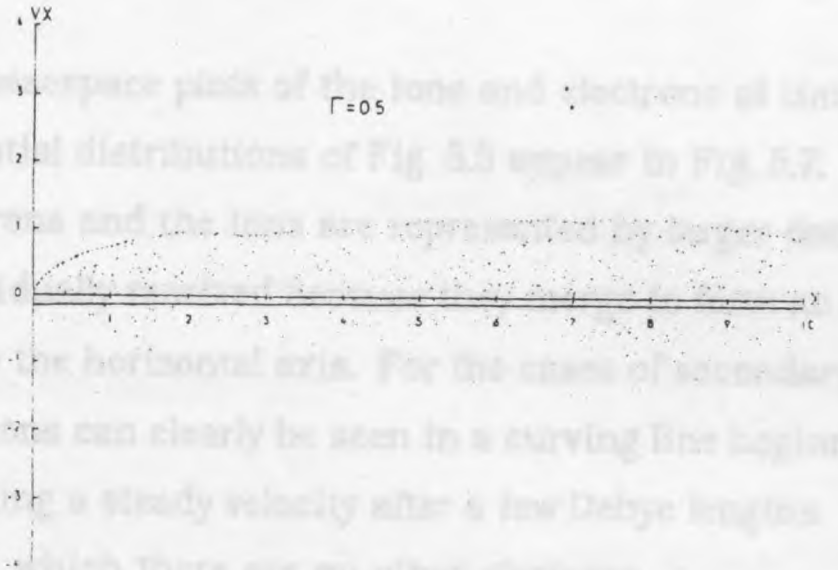

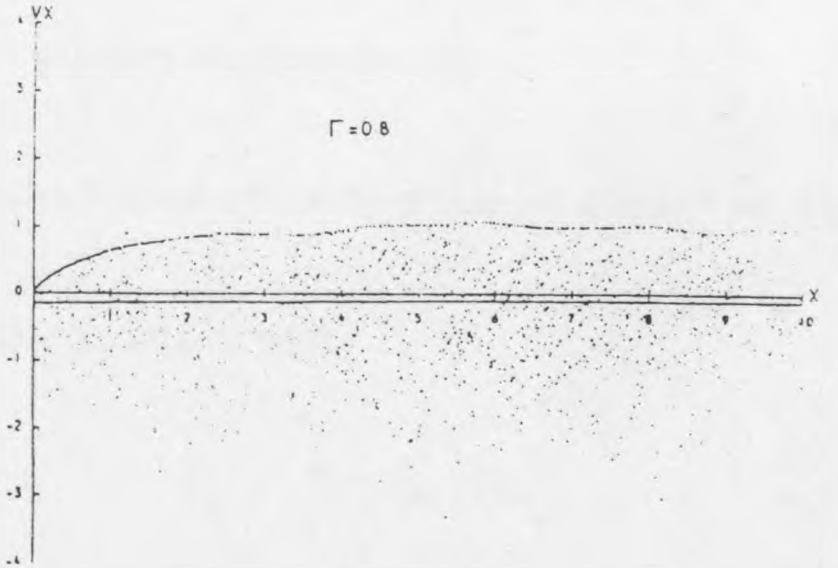

Fig. 5.7 Phasespace plots of ions and electrons for th

inconsiderable level; these oscillations result from thermal fluctuations in the simulated plasma and this is quantified in section 5.2. For the case of no secondary emission ($\Gamma = 0$) the average potental drop over the last ten plasma periods is about 1.3; this agrees well with the value of 1.33 for the potential across the first 10 Debye lengths obtained from Fig. 5.4. For the cases of $\Gamma =$ 0.5 and 0.8 the time averaged values of the potential drop are 0.6 and 0.57 respectively; this is to be compared with the value of 0.64 obtained from Fig. 5.4 In view of the length of time that the simulation was run and the size of the fluctuations the agreement is reasonable.

Phasespace plots of the ions and electrons at times corresponding to the potential distributions of Fig. 5.5 appear in Fig. 5.7. The small dots are electrons and the ions are represented by larger dots but these cannot be individually resolved because they merge to form an almost straight line just below the horizontal axis. For the cases of secondary emission the beam electrons can clearly be seen in a curving line beginning at the origin and reaching a steady velocity after a few Debye lengths. They form a boundary above which there are no other electrons.

5.2.1 Modifying the Equilibrium Equations to Include Current

The sheath calculations described so far have been for floating wall conditions, but we shall now consider how the sheath is modified when a positive current to the wall is allowed. It is also of interest to examine what effect the sheath has on the heat flow to the wall under these conditions. The approach is similar to the one used in the first chapter, so the first task is to obtain expressions for the number densities in order to solve the Poisson equation. The ion and primary electron densities are unaltered and, as before, we obtain:

$$n_i = n_0 \left(\frac{E}{E - e\phi} \right)^{1/2} \tag{5.4}$$

for the ion density, and:

$$n_{e1} = [n_0 - n_{e2}(\infty)] \ \exp(e\phi/KT) \tag{5.5}$$

for the primary electron density.

For the secondary electron flux we proceed as follows.

Net electron flux to wall:

$$F_e = F_{ep} - F_{es}$$

where F_{ep} and F_{es} are the primary and secondary electron fluxes respectively.

Net positive current to wall:

where F_i is the ion flux.

$$J/e = F_i - F_{es}(1 - \Gamma)/\Gamma$$

where $\Gamma = F_{es}/F_{ep}$ is the secondary emission coefficient.

$$J/e = n_0\left(\frac{2E}{M}\right)^{1/2} - \left(\frac{1-\Gamma}{\Gamma}\right)n_{e2}\left[\frac{2e}{m}(\phi - \phi_0)\right]^{1/2}$$

$$\therefore\ n_{e2} = \frac{\Gamma}{1-\Gamma}\left[\frac{m}{2e(\phi - \phi_0)}\right]^{1/2}\left[n_0\left(\frac{2E}{M}\right)^{1/2} - J/e\right]$$

$$\therefore\ n_{e2} = pn_0\frac{\Gamma}{1-\Gamma}\left[\frac{m}{M}\frac{E}{e(\phi - \phi_0)}\right]^{1/2} \qquad (5.7)$$

where we define:

$$p = F_e/F_i = (j_i - J)/j_i \qquad (5.8)$$

and j_i is the ion current. So p is the ratio of electron and ion fluxes.

Thus the Poisson equation for the sheath potential becomes:

$$d^2\phi/dx^2 = 4\pi n_0 e\left\{\left[1 - \frac{\Gamma p}{1-\Gamma}\left(-\frac{m}{M}\frac{E}{e\phi_0}\right)^{1/2}\right]\exp\left(\frac{e\phi}{KT}\right)\right.$$

$$\left. + \frac{\Gamma p}{1-\Gamma}\left[\frac{m}{M}\frac{E}{e(\phi - \phi_0)}\right]^{1/2} - \left(\frac{E}{E - e\phi}\right)^{1/2}\right\}$$

Now we need two conditions to determine the wall potential and the ion energy E on entry to the sheath. These are a) the current relation (which

a) Current Relation:

We manipulate equation (5.6) and substitute expressions for the fluxes:

$$J/e = F_i - F_e = F_i - F_{ep}(1 - \Gamma) \tag{5.9}$$

$$\therefore J/e = n_0 \left(\frac{2E}{M}\right)^{1/2} - n_{e1}(0)\,\frac{\bar{c}}{4}(1 - \Gamma) \quad \text{where } \bar{c} = \left(\frac{8KT}{\pi m}\right)^{1/2}$$

$$\therefore n_{e1}(0)\,\frac{\bar{c}}{4} = n_0 \left(\frac{2E}{M}\right)^{1/2} \frac{p}{1 - \Gamma} \qquad \text{using (5.8)}$$

and after substituting for $n_{e1}(0)$ we have:

$$\frac{1}{4}\left[1 - \frac{p\Gamma}{1 - \Gamma}\left(-\frac{mE}{Me\phi_0}\right)^{1/2}\right]\exp\left(\frac{e\phi_0}{KT}\right)\left(\frac{8KT}{\pi m}\right)^{1/2} = \frac{p}{1 - \Gamma}\left(\frac{2E}{M}\right)^{1/2} \tag{5.10}$$

b) Monotonicity Condition:

The condition for marginal monotonicity of the solutions for small values of ϕ is obtained by expanding the new Poisson equation about $\phi = 0$ and setting the coefficient A to zero in the resulting equation which is of the form:

$$d^2\phi/dx^2 = A\,\phi$$

The condition $A = 0$ becomes:

$$E = \frac{KT}{2} + \frac{p\Gamma}{1 - \Gamma}\left(\frac{m}{M}\right)^{1/2}\left(-\frac{E}{e\phi_0}\right)^{3/2}\left(\frac{KT}{2} - e\phi_0\right) \tag{5.11}$$

To calculate the heat flow through the sheath we need to obtain an expression for the primary electron flux. Equations (5.8) and (5.9) give:

$$F_i(1 - p) = F_i - F_{ep}(1 - \Gamma)$$

$$\therefore\ pF_i = F_{ep}(1 - \Gamma)$$

$$\therefore\ F_{ep} = \frac{n_0 v_0 p}{1 - \Gamma} \tag{5.12}$$

Now each electron hitting the wall carries on average an energy 2KT, while each ion carries its initial energy E plus the energy $-e\phi_0$ gained by falling through the sheath potential. So the heat flux to the wall is given by:

$$Q = 2KTF_{ep} + (E - e\phi_0)F_i$$

$$\therefore\ Q = n_0 v_0 \left(\frac{2KTp}{1 - \Gamma} + E - e\phi_0\right) \tag{5.13}$$

on making use of equation (5.12).

To see whether or not the sheath should be considered as an insulating layer we can rewrite equation (5.13) as:

$$Q = \frac{n_0 \bar{c}}{4} .\ 2KT.\ F(\Gamma)$$

where $$\frac{\bar{c}}{4} = \left(\frac{KT}{2\pi m}\right)^{1/2}$$

and $$F = \left(\pi \frac{m}{M} \frac{E}{KT}\right)^{1/2} \left(\frac{E - e\phi_0}{KT} + \frac{2p}{1 - \Gamma}\right)$$

In the following section the heat flux is calculated for M/m = 4590.

5.2.3 Solutions of the Equations

Thus one can see that the modification required to include current in the equilibrium equations is to replace $1 - \Gamma$ by $(1 - \Gamma)/p$. However, for all quantities which were originally functions of the mass ratio M/m, this is equivalent to altering the dependence on $(m/M)^{1/2}$ to a dependence on $p(m/M)^{1/2}$. So Figs. 5.1 to 5.4 remain valid if we use this substitution. The substitution is defined in this way rather than using $p^2(m/M)$ because the results are sensitive to the sign of p and up to now have been valid for positive p which corresponds to values of Γ less than one. As Γ approaches one the net electron current to the wall approaches zero hence p also approaches zero. The factor $(1 - \Gamma)/p$ thus remains finite and as Γ becomes larger than one p becomes negative, corresponding to negative net electron flux to the wall. These are the conditions that we are most interested in when the wall potential is not floating as the corresponding parameters allow the most dramatic beam-plasma behaviour.

The heat flux (equation (5.13)), on the other hand, does not depend on the factor $p(m/M)^{1/2}$, but it does depend on $p/(1 - \Gamma)$. For the specific case of a mass ratio of 4590 it was decided to express the information in the form of Fig. 5.8 which depicts the Γ – p plane with constant heat flux contours and also the line representing the zero- wall- field condition. The shaded region is physically inaccessible due to space charge limitation. These contours have been calculated assuming that the dominant term in equation (5.13) is the ion energy term; the contours are then simply straight lines passing, along with the zero wall-field line, through the point $p = 0$, $\Gamma = 1$. Note that the normalised heat flow in this approximation is identical to the normalised wall-potential. Also shown on the diagram is a line representing equality of the ion

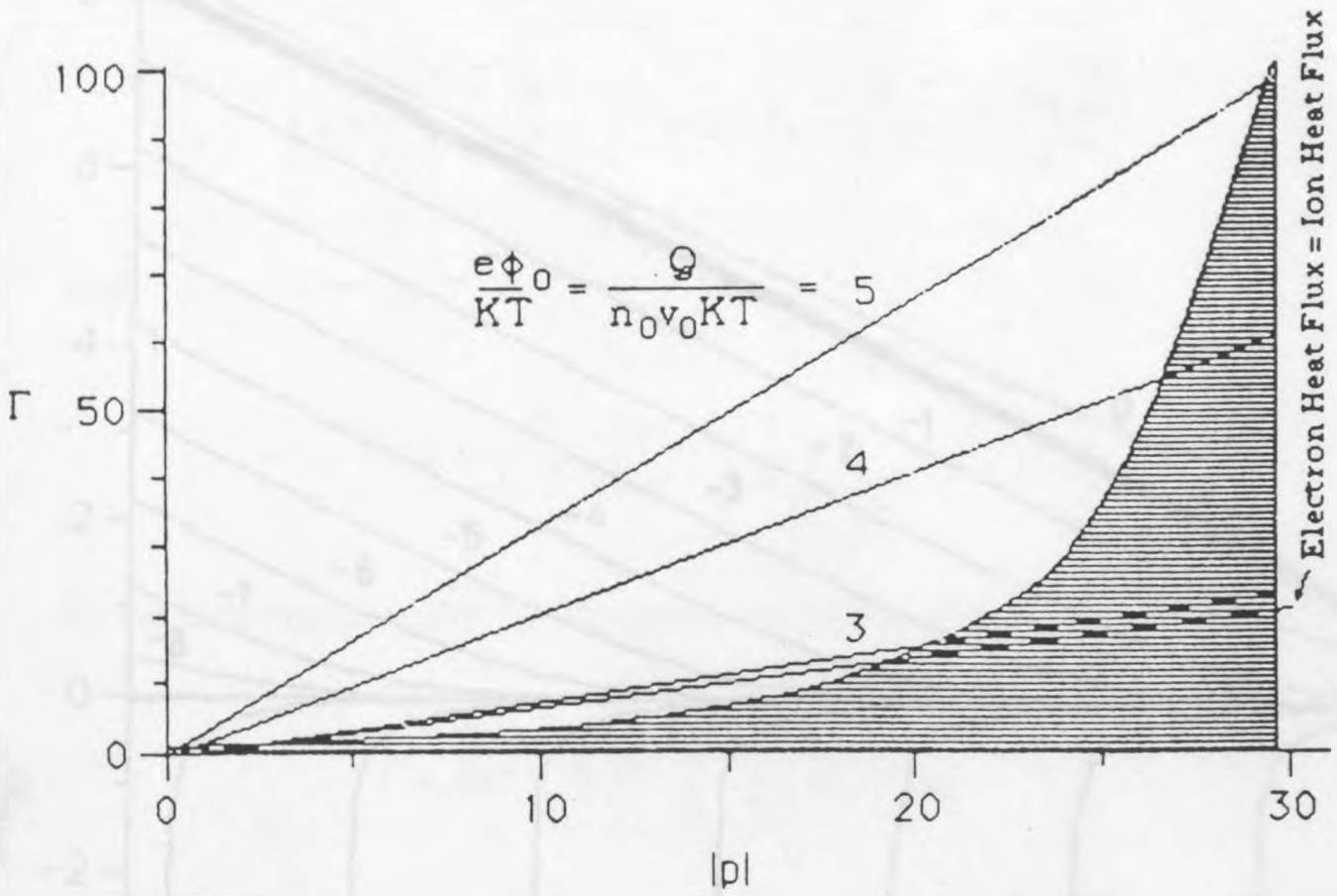

Fig. 5.8 Heat-flow contours for mass ratio 4590 in the plane of Γ, the secondary emission coefficient, and p, the ratio of ion and electron fluxes. Here the sign of p is negative.

In order to graphically illustrate the interrelation of the various quantities, the Γ - Φ_0 plane is displayed in Fig. 5.9 with constant $p(m/M)^{1/2}$ and beam-density contours. Again, the shaded region above the zero wall-field line is physically inaccessible. The equations used to plot these curves are given below.

Equation (1.19) gives the electric field at the wall, and when normalised this becomes:

$$\frac{1}{2}\left(\frac{d\Phi}{dX}\right)_w^2 = 2I\left[\left(1 - \frac{\Phi_0}{I}\right)^{1/2} - 1\right] + 2\frac{\Phi_0^2}{I}\left(\frac{2I-1}{2\Phi_0 - 1}\right) + \frac{1}{I}\left(\frac{\Phi_0 - I}{2\Phi_0 - 1}\right)\left[\exp \Phi_0 - 1\right] \qquad (5.14)$$

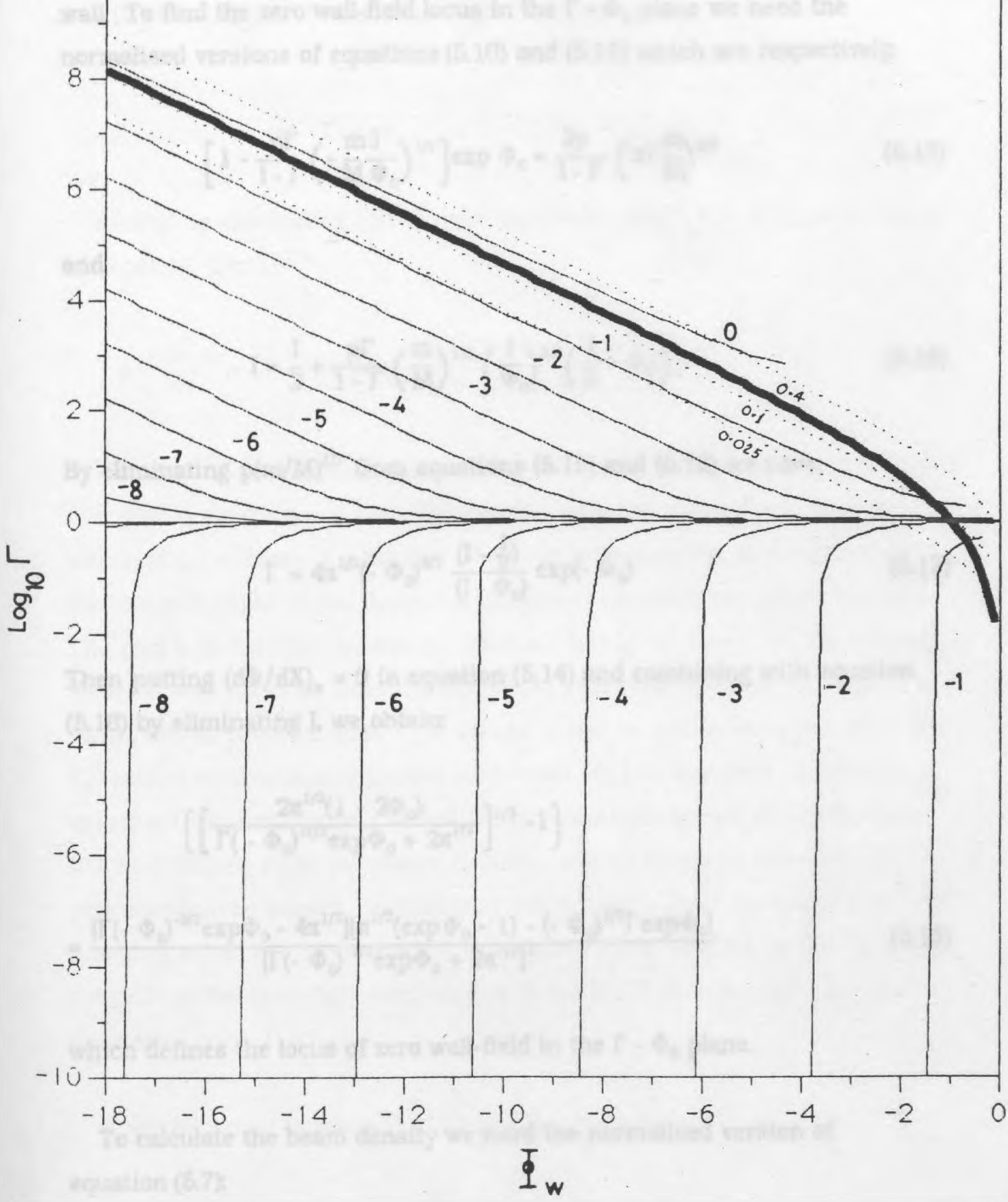

Fig. 5.9 Contours of $p(m/M)^{1/2}$ (solid lines) labelled with values of $\mathrm{Log}_{10}|p(m/M)^{1/2}|$. Note that p is actually negative in the upper half-plane and positive in the lower. The bold line represents the zero wall-field condition, the region above which is physically inaccessible. The three dotted lines are contours of relative beam density labelled with values of n_r/n_0.

wall. To find the zero wall-field locus in the $\Gamma - \Phi_0$ plane we need the normalised versions of equations (5.10) and (5.11) which are respectively:

$$\left[1 - \frac{p\Gamma}{1-\Gamma}\left(-\frac{m}{M}\frac{I}{\Phi_0}\right)^{1/2}\right]\exp\Phi_0 = \frac{2p}{1-\Gamma}\left(\pi I\frac{m}{M}\right)^{1/2} \tag{5.15}$$

and

$$I = \frac{1}{2} + \frac{p\Gamma}{1-\Gamma}\left(\frac{m}{M}\right)^{1/2}\left(\frac{I}{\Phi_0}\right)^{3/2}\left(\frac{1}{2} - \Phi_0\right) \tag{5.16}$$

By eliminating $p(m/M)^{1/2}$ from equations (5.15) and (5.16) we have:

$$\Gamma = 4\pi^{1/2}(-\Phi_0)^{3/2}\frac{(I - \frac{1}{2})}{(I - \Phi_0)}\exp(-\Phi_0) \tag{5.17}$$

Then putting $(d\Phi/dX)_w = 0$ in equation (5.14) and combining with equation (5.16) by eliminating I, we obtain:

$$\left\{\left[\frac{2\pi^{1/2}(1 - 2\Phi_0)}{\Gamma(-\Phi_0)^{-1/2}\exp\Phi_0 + 2\pi^{1/2}}\right]^{1/2} - 1\right\}$$

$$= \frac{[\Gamma(-\Phi_0)^{-3/2}\exp\Phi_0 - 4\pi^{1/2}][\pi^{1/2}(\exp\Phi_0 - 1) - (-\Phi_0)^{1/2}\Gamma\exp\Phi_0]}{[\Gamma(-\Phi_0)^{-1/2}\exp\Phi_0 + 2\pi^{1/2}]^2} \tag{5.18}$$

which defines the locus of zero wall-field in the $\Gamma - \Phi_0$ plane.

To calculate the beam density we need the normalised version of equation (5.7):

$$\frac{n_b}{n_0} = \frac{p\Gamma}{1-\Gamma}\left[\frac{m}{M}\frac{I}{(-\Phi_0)}\right]^{1/2} \tag{5.19}$$

and (5.18) we obtain the locus of constant beam-density:

$$\frac{n_b}{n_0} = \frac{\Gamma \exp\Phi_0}{\Gamma \exp\Phi_0 + 2\pi^{1/2}(-\Phi_0)^{1/2}} \tag{5.20}$$

Finally, by eliminating I from equations (5.16) and (5.17) we have the locus of constant $p(m/M)^{1/2}$:

$$p\left(\frac{m}{M}\right)^{1/2} = (1 - \Gamma)\exp\Phi_0 \frac{[4\pi^{1/2} - \Gamma(-\Phi_0)^{-3/2}\exp\Phi_0]^{1/2}}{[\Gamma(-\Phi_0)^{-1/2}\exp\Phi_0 + 2\pi^{1/2}]^{3/2}} \tag{5.21}$$

We now consider some features of Fig. 5.9. It will be observed that the $\Gamma = 1$ line also forms the $p = 0$ line. The region below this line covers positive values of p, i.e., there is a net flux of electrons towards the wall, while above the line p is negative, i.e., there is a net flux of electrons away from the wall. The zero wall-field line intersects the $\Gamma = 1$ line at $|\Phi_0| = 1$. So, for smaller values of wall potential than this, values of Γ_c must be less than 1. Larger values of wall potential allow Γ_c to exceed 1, and as can be seen, the value of Γ_c reaches enormous magnitudes even when $|\Phi_0|$ is less than 10. If these values of Γ can actually be attained, the physical significance of this quantity will be devalued since secondary electrons will no longer be released by primary electron impact. Instead they will originate from ion impact; for this reason it would be more appropriate to define a new coefficient $\Gamma_i = F_{es}/F_i$, i.e., the ratio of the secondary electron flux to the ion flux at the wall. This is to be contrasted with $\Gamma = F_{es}/F_{ep}$.

It will be useful to relate Γ_i to Γ so we begin by noting:

$$\frac{\Gamma_i}{\Gamma} = \frac{F_{ep}}{F_i} = \frac{pF_{ep}}{F_e} = \frac{p}{1 - \Gamma} \tag{5.22}$$

Hence using equation (5.21) we obtain:

This enables Γ_i to be calculated from a knowledge of Γ, Φ_0 and m/M. Making use of the zero wall-field relation and taking the limit $\Phi_0 \to \infty$ it can be shown that the critical value of Γ_i for large wall-potential is given by:

$$\Gamma_{ic} = \left(\frac{M}{m}\right)^{1/2} \tag{5.24}$$

For the same limit we note that the net electron flux F_e must have a negligible component of primary electrons, so that $p = F_e/F_i$ becomes approximately $p = -F_{es}/F_i$. Therefore, in this limit we have:

$$p = -\Gamma_i \tag{5.25}$$

Thus it also follows from equations (5.24) and (5.25) that in this limit:

$$p(m/M)^{1/2} = -1 \tag{5.26}$$

It is of interest to investigate the behaviour of the incident ion energy for the extreme conditions of maximum or critical Γ and very large wall potential. To do this we set $(d\Phi/dX)_w = 0$ in equation (5.14) and assume that I remains of the order of 1/2 even when Φ_0 is large. Thus we have approximately:

$$\frac{E}{KT} = \frac{1}{2}\left[1 - \left(\frac{E}{KT}\right)^{1/2}\left(-\frac{KT}{e\phi_0}\right)^{1/2}\right]^{-1} \tag{5.27}$$

or since the rightmost term is small:

$$\frac{E}{KT} \approx \frac{1}{2}\left[1 + \left(\frac{E}{KT}\right)^{1/2}\left(-\frac{KT}{e\phi_0}\right)^{1/2}\right] \tag{5.28}$$

the incident ion energy in the limit of infinite wall-potential is 1/2. It is remarkable that a prediction given by Bohm for a sheath in the vicinity of a non- emissive wall at floating potential is equally applicable for the extreme conditions dealt with here: namely, intense secondary emission of electrons and currents induced by very large wall potentials.

Although p is related to the total current, it is not a direct measure, therefore it will be useful to define a normalised current given by:

$$J_N = J/j_{if} \tag{5.29}$$

where j_{if} is the ion current for floating conditions. We then have:

$$J_N = (F_i - F_e)/F_{if} = \frac{n_0(2E/M)^{1/2} + n_{e2}(\infty)(-2\,e\phi_0)^{1/2}}{n_0(2E_f/M)^{1/2}} \tag{5.30}$$

where we have made use of the simplifying approximation $\Gamma >> 1$ and $E_f = KT/2$ is the ion energy for floating conditions. Eliminating n_{e2}/n_0 from equations (5.7) and (5.30) after applying the large Γ approximation again gives:

$$J_N = \left(\frac{2E}{KT}\right)^{1/2}(1 - p) \tag{5.31}$$

Since $E/KT \approx 1/2$ we can write for $-p >> 1$:

$$J_N \approx - p \tag{5.52}$$

Thus for intense secondary emission and large currents and wall-potentials, the parameters J_N, Γ_i and - p can be taken to be equivalent.

The simulation results, as reported in section 5.1, appear to be consistent with the calculations of Hobbs and Wesson, [1966]. It was felt, however, that the basis for one of the assumptions needed further investigation. The assumed condition of marginal monotonicity at the sheath boundary, first suggested by Bohm [1949], seemed to be an arbitrary choice and further justification for this was sought by examining the equations describing the potential distribution in the whole plasma.

Further exploration led to the discovery of a hypothetical plasma system in which the usual condition E = KT/2 (where E is the ion energy on entry to the sheath) did not apply. Even more surprising was the fact that there did not seem to be any way of predicting the boundary condition appropriate to the system as a whole. This motivated a search for some principle which would enable one to do this and which, hopefully, would apply to plasma systems generally.

5.3.1 An Equation Defining the Potential Distribution Throughout a Plasma

Consider a plasma contained in a one-dimensional box. We shall deal with one half of the plasma which is bounded by the mid-plane at x = 0 and one wall at x = L. The ions at position x are assumed to be formed by ionisation at positions z, where $0 < z < x$, falling to x (and of course beyond) under the influence of the potential. The potential ϕ, the ionisation rate per unit volume N and the ion and electron densities n_i and n_e are all functions of position x with $\phi(0)=0$. The ion density is therefore given by:

$$n_i = \int_0^x N(z)[M/2e\{\phi(z) - \phi\}]^{1/2}dz$$

where we have made use of the fact that $v_e = [2e\{\phi(z) - \phi\}/M]^{1/2}$ (assuming long mean free paths). Assuming the electrons have a Maxwellian velocity distribution we have:

Now Poisson's equation is:

$$\nabla^2\phi = -4\pi e(n_i - n_e)$$

and substitution of the densities into this produces:

$$-\frac{\nabla^2\phi}{4\pi e} = \int_0^x N(z)[M/2e\{\phi(z) - \phi\}]^{1/2}dz - n_\infty \exp\left(\frac{e\phi}{KT}\right)$$

which is the 'plasma-sheath equation'. We are interested in the solution appropriate for the plasma region where quasineutrality prevails because when it breaks down it will give us some idea where the sheath region begins. We can therefore make the approximation $|n_i - n_e << n_e$ which means that we can drop the first term to obtain:

$$LN'\int_0^y g(l)[M/2e\{\phi(l) - \phi(y)\}]^{1/2}dl - n_\infty \exp\left(\frac{e\phi(y)}{KT}\right) = 0 \qquad (5.33)$$

where we have made the substitutions:

$$\left.\begin{aligned} z/L &= l \\ x/L &= y \\ N(z) \rightarrow N(l) &= N'g(l) \end{aligned}\right\} \qquad (5.34)$$

N' is a constant and $g(l)$ defines the profile of ionisation. This is the 'plasma equation' and, in the region where quasineutrality no longer holds, the electric field predicted by this equation becomes infinite. The potential ϕ_* at this point can be taken to be the approximate potential at which the sheath begins.

We now explore the dependence of ϕ_* on box length L and M/m the ratio of

N' by noting that the rate of production of plasma particles must equal their rate of loss to the walls. The flux of electrons to the walls is given approximately by:

$$n_{ew}\frac{\bar{c}}{4}$$

where n_{ew} is the electron density and $\bar{c} = (8KT/\pi m)^{1/2}$, so by equating the production and loss fluxes we get:

$$LN' \int_0^1 g(y)dy = n_{eo} \exp\left(\frac{e\phi_w}{KT}\right)\left(\frac{8KT}{\pi m}\right)^{1/2} \qquad (5.35)$$

where we have employed substitutions (5.34). Recall that the potential drop across a sheath is given by $\frac{1}{2}\ln(4\pi Em/KTM)$ setting $\Gamma = 0$ in equation (1.17)), so that the wall potential ϕ_w (equal to the potential between mid-plane and wall) becomes:

$$\frac{e\phi_w}{KT} = \frac{e\phi_s}{KT} - \frac{1}{2}\ln\left(\frac{M}{4\pi m}\frac{KT}{E}\right) \qquad (5.36)$$

Substituting in (5.35) produces:

$$LN' = n_{eo}\left(\frac{E}{2MKT}\right)^{1/2} \exp\left(\frac{e\phi_s}{KT}\right) \Big/ \int_0^1 g(y)dy$$

and when this in turn is substituted into (5.33) we obtain:

$$\frac{1}{\int_0^1 g(y)dy} \exp\left(\frac{e\phi_s}{KT}\right)\left(\frac{KT}{E}\right)^{1/2} \int_0^y g(l)\left(\frac{KT}{e\phi(l)}\right)dl - \exp\left(\frac{e\phi(y)}{KT}\right) = 0 \qquad (5.37)$$

which is an equation defining ϕ as a function of y (=x/L) that is independent of mass ratio. Now if we choose ionisation profiles g(y) which are independent of L, then we can see that equation (5.37) is also independent of L. This confirms

several different geometries for the cases of uniform ionisation rate and ionisation rate proportional to n_e. Both these cases conform to the condition that g(y) is independent of L and therefore their results do not depend on either L or mass ratio. The values of $e\phi_*/KT$ (where ϕ_* is the potential at which the electric field is predicted by equation (5.37) to become infinite) calculated by Tonks and Langmuir are given in Table 5.1 and the corresponding values of E, the ion energy on entry to the sheath, appear in Table 5.2.

TABLE 5.1

Values of $e\phi_*/KT$ for three plasma geometries

	Planar	Cylindrical	Spherical
$N \propto n_e$	0.854	1.155	1.418
N uniform	0.854	1.054	1.195

TABLE 5.2

Values of E/KT for three plasma geometries

	Planar	Cylindrical	Spherical
$N \propto n_e$	0.654	0.736	--
N uniform	0.654	0.695	0.719

The above calculation confirms the approximate validity of the Bohm criterion E = KT/2 and demonstrates how to derive the potential distribution in the plasma. This procedure is straightforward as we know that the appropriate boundary condition for the plasma is zero electric field at the mid-plane, but in section 5.3.3 we discuss a plasma system for which the choice of boundary condition seems arbitrary.

5.3.2 An Alternative Derivation of the Bohm Criterion

It was hoped that some principle could be found which applied to plasma systems generally and which in particular could be used to derive the appropriate boundary conditions in unresolved situations. The adoption of this objective at first led to an interesting observation which was thought to be relevant.

energy on entry to the sheath I= E/KT and the potential $\Phi = e\phi/KT$. In practice there is a spread of ion energies since the ions are created in different positions throughout the plasma but we continue to use a monoenergetic model, attributing ions with the average kinetic energy at a given position. Now on entry to the sheath the ions have fallen through an average potential equal in magnitude to I and it will be taken to be equal to the potential drop between the mid-plane and sheath although this is not strictly accurate. Equation (5.36) with normalisations thus becomes:

$$\Phi_w = -I - \frac{1}{2}\ln\left(\frac{\mu}{4\pi I}\right)$$

and differentiating with respect to I produces:

$$\frac{d\Phi_w}{dI} = -1 + \frac{1}{2I}$$

Setting $d\Phi_w/dI = 0$ gives I = 1/2, which is the Bohm criterion! So perhaps the plasma, in effect, chooses the boundary condition which minimises the wall potential.

5.3.3 A Hypothetical Plasma System

This system was originally devised by the author to test the computer code and explore the sheath formation process. (It was later discovered that this paralleled a model treated earlier [Langmuir, 1929].) Again the plasma is contained in a one-dimensional box but new plasma is only introduced at the mid-plane where the ionisation is deemed to take place. Here the electrons enter the box with a Maxwellian velocity distribution but the ions are positioned at the mid-plane with zero velocity. We shall later refer to this system as the 'single-point ionisation' case. We assume the potential distribution is monotonic and we again obtain expressions for the electron and

approximately Maxwellian velocity distribution everywhere we have:

$$n_e = n_0 \exp\left(\frac{e\phi}{KT}\right)$$

and using the usual approximate expression for the flux of particles to an absorbing wall along with the fact that the ion and electron fluxes are equal we obtain for the ions:

$$n_i = \frac{n_0}{2}\left(\frac{M}{m\pi}\frac{KT}{(-e\phi)}\right)^{1/2} \exp\left(\frac{e\phi_w}{KT}\right)$$

As before these expressions are substituted into the Poisson equation to give:

$$\nabla^2\phi = 4\pi e\left[n_0 \exp\left(\frac{e\phi}{KT}\right) - \frac{n_0}{2}\left(\frac{M}{m\pi}\frac{KT}{(-e\phi)}\right)^{1/2} \exp\left(\frac{e\phi_w}{KT}\right)\right]$$

After integrating once we arrive at:

$$\left(\frac{d\phi}{dx}\right)^2 = 8\pi n_0 KT\left[\exp\left(\frac{e\phi}{KT}\right) + \left(\frac{M}{m\pi}\frac{(-e\phi)}{KT}\right)^{1/2} \exp\left(\frac{e\phi_w}{KT}\right)\right] + C$$

On using the normalisations described in section 5.1.1 this becomes:

$$\left(\frac{d\Phi}{dX}\right)^2 = 2\left[\exp(\Phi) + \left(-\Phi\frac{M}{m\pi}\right)^{1/2} \exp(\Phi_w) - A\right] \qquad (5.38)$$

where the maximum permissible value of the constant A is +1, which corresponds to zero electric field at the mid-plane. Other values of A correspond to finite values of electric field.

Equation (5.38) can be integrated to find the potential profile if the value of the electric field at the mid-plane is known. Unfortunately, there does not seem to be an obvious principle which can be used to determine this value of

system within a box of length $100\lambda_D$ using a mass ratio M/m of 100 and a phasespace plot of the electron and ion trajectories for steady state conditions appears in Fig. 5.10 The electric field fluctuations are so large as a result of the relatively small number of particles used that the potential profile is difficult to determine, so an alternative method was used to analyse the results.

Fig. 5.10 reveals that the ions maintain a constant velocity except for small regions near the wall and mid-plane. This indicates that the potential has formed a plateau throughout most of the box and we shall assume that small sheath regions have been created at either end.

Setting $\Gamma = 0$ in equation (1.17) we obtain:

$$\Phi_w - \Phi_p = \frac{1}{2} \ln \left(\frac{4\pi\, m(-\Phi_p)}{M} \right) \tag{5.39}$$

where Φ_w is the wall potential, Φ_p is the plateau potential and the usual normalisations have been performed.

We will now assume that the electric field at the mid-plane is zero and therefore set A = 1 in equation (5.38), then noting that the electric field in the plateau is zero we have:

$$\exp(\Phi_p) + \left(- \Phi_p \frac{M}{\pi m} \right)^{1/2} \exp(\Phi_w) - 1 = 0 \tag{5.40}$$

Eliminating Φ_w from equations (5.39) and (5.40) we have:

$$\exp(\Phi_p)(1 - 2\Phi_p) = 1 \tag{5.41}$$

and solving numerically we obtain $\Phi_p = -1.26$ (c.f. Langmuir [1929]). This

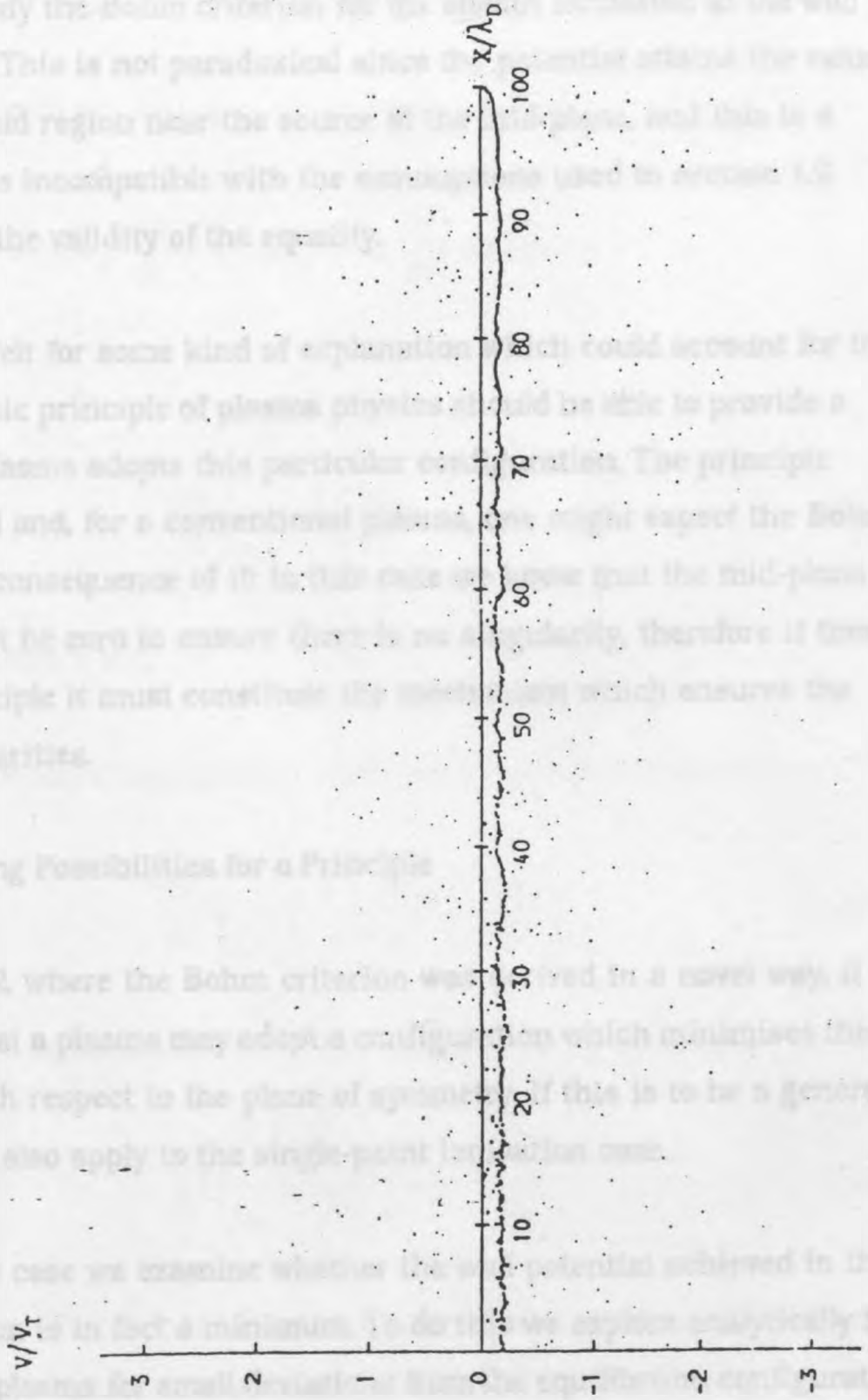

Fig. 5.10 Phasespace plot of the particles using a mass ratio M/m of 100. Small dots are electrons, large dots are ions.

confirm the original assumption that the electric field at the mid-plane is zero. Note that the magnitude of the plateau potential exceeds the value of 0.5 demanded to satisfy the Bohm criterion for the sheath formation at the wall (see section 1.2). This is not paradoxical since the potential attains the value 0.5 in the high-field region near the source at the mid-plane, and this is a condition which is incompatible with the assumptions used in section 1.2 which argues for the validity of the equality.

The need was felt for some kind of explanation which could account for this finding. Some basic principle of plasma physics should be able to provide a reason why the plasma adopts this particular configuration. The principle should be general and, for a conventional plasma, one might expect the Bohm criterion to be a consequence of it; in this case we know that the mid-plane electric field must be zero to ensure there is no singularity, therefore if there is a general principle it must constitute the mechanism which ensures the absence of singularities.

5.3.4 Investigating Possibilities for a Principle

In section 5.3.2, where the Bohm criterion was derived in a novel way, it was suggested that a plasma may adopt a configuration which minimises the wall potential with respect to the plane of symmetry. If this is to be a general principle it must also apply to the single-point ionisation case.

To analyse this case we examine whether the wall potential achieved in the particle simulation is in fact a minimum. To do this we explore analytically the behaviour of the plasma for small deviations from the equilibrium configuration maintained in the simulation. The deviation is expressed by replacing the value of 1 for the constant A in equation (5.38) by $1 - \varepsilon$ where ε is a small positive quantity, so that $\varepsilon = 0$ corresponds to zero electric field at the mid-plane. Corresponding to equations (5.38) and (5.41) we now have respectively:

$$(1 - 2\Phi_p)\exp(\Phi_p) = 1 - \varepsilon \tag{5.43}$$

And differentiating (5.43) with respect to ε we obtain:

$$\exp(\Phi_p)\frac{d\Phi_p}{d\varepsilon}\left(1 - 2\Phi_p\right) - 2\frac{d\Phi_p}{d\varepsilon}\exp(\Phi_p) = -1$$

So that:

$$\left.\frac{d\Phi_p}{d\varepsilon}\right|_{\varepsilon=0} = \frac{1 - 2\Phi_{p0}}{1 + 2\Phi_{p0}} \tag{5.44}$$

where $\Phi_{p0} = \Phi_p$ when $\varepsilon = 0$.

Now, after differentiating equation (5.39) with respect to ε we arrive at:

$$\left.\frac{d\Phi_w}{d\varepsilon}\right|_{\varepsilon=0} = \left(\frac{1 + 2\Phi_{p0}}{2\Phi_{p0}}\right)\left.\frac{d\Phi_p}{d\varepsilon}\right|_{\varepsilon=0} \tag{5.45}$$

and after substituting equation (5.44) into equation (5.45) we obtain:

$$\left.\frac{d\Phi_w}{d\varepsilon}\right|_{\varepsilon=0} = \frac{1 - 2\Phi_{p0}}{2\Phi_{p0}} \tag{5.46}$$

We have previously calculated the numerical value of plateau potential for the case of zero electric field at the mid-plane and after substituting this into equation (5.46) we obtain the increment in wall potential:

$$\Delta\Phi_w \approx -1.4\varepsilon \tag{5.47}$$

(corresponding to non-zero electric field at the mid-plane) produces an increase in the magnitude of the wall potential. The magnitude of the wall-potential maintained by the plasma is therefore the smallest value which can be achieved whilst still preserving monotonicity of the potential profile. It would appear that the adopted wall-potential is not stationary with respect to ε. However, it will now be shown that the adopted wall-potential is stationary with respect to the electric field at the mid-plane.

From equation (5.42) we have:

$$\left.\frac{d\Phi}{dX}\right|_{\Phi_{-0}} = \sqrt{2\varepsilon}$$

$$\therefore \frac{d}{d\varepsilon}\left(\frac{d\Phi}{dX}\right)_{\Phi_{-0}} = (2\varepsilon)^{-1/2}$$

$$\therefore \frac{d\Phi_w}{dE_0} = (2\varepsilon)^{1/2}\,\frac{d\Phi_w}{d\varepsilon}$$

where $E_0 = (d\Phi/dX)_{\Phi_{-0},\varepsilon_{-0}}$

$$\therefore \left(\frac{d\Phi_w}{dE_0}\right)_{\varepsilon_{-0}} = 0$$

It is suggested that 'stationarity' is only relevant with respect to some local value of a real plasma parameter. After all, some purely mathematical quantity can always be defined with resect to which one can achieve stationarity or otherwise at will.

A second candidate for a general principle which has been reviewed is the possibility that a plasma settles into a configuration which minimises the total electric field energy. The pusuit of this idea was originally motivated by a line of reasoning which ultimately proved to be flawed. However, the validity of the

both conventional plasmas and the single-point ionisation case was investigated.

We first examine single-point ionisation and we now need to specify a coordinate system. We take the wall to be at X = 0 and the mid-plane is situated in the positive half space. The total field energy for the zero source-field case is then given by:

$$E = \int_0^L \left(\frac{d\Phi}{dX}\right)^2 dX = \int_{\Phi_w}^0 \frac{d\Phi}{dX}\, d\Phi \qquad (5.48)$$

and after differentiating with respect to ε we obtain:

$$\left.\frac{dE}{d\varepsilon}\right|_{\varepsilon=0} = \int_{\Phi_w}^0 \left.\frac{d}{d\varepsilon}\left(\frac{d\Phi}{dX}\right)\right|_{\varepsilon=0} d\Phi \; - \left.\left(\frac{d\Phi}{dX}\right)\right|_{\substack{\varepsilon=0 \\ \Phi=\Phi_w}} \left.\frac{d\Phi_w}{d\varepsilon}\right|_{\varepsilon=0}$$

By setting ε = 0 and I = Φ_w in equation (5.42) and making use of equation (5.46) we are able to derive an expression for the rightmost term:

$$-\left.\left(\frac{d\Phi}{dX}\right)\right|_{\substack{\varepsilon=0 \\ \Phi=\Phi_w}} \left.\frac{d\Phi_w}{d\varepsilon}\right|_{\varepsilon=0} = 1.4\left\{2\left[\exp(\Phi_w) + \left(-\Phi_w \frac{M}{\pi m}\right)^{1/2} \exp(\Phi_w) - 1\right]\right\}^{1/2}$$

An expression for the integrand is obtained by differentiating equation (5.42) with respect to ε and making use of equations (5.46) and (5.43), so that:

$$\int_{\Phi_w}^0 \left.\frac{d}{d\varepsilon}\left(\frac{d\Phi}{dX}\right)\right|_{\varepsilon=0} d\Phi = \int_{\Phi_{w0}}^0 \frac{1 - (\Phi/\Phi_{p0})^{1/2}}{\{\exp(\Phi) + 2(\Phi\Phi_{p0})^{1/2}\exp(\Phi_{p0}) - 1\}^{1/2}}\, d\Phi \qquad (5.49)$$

where Φ_{w0} is the wall potential when ε = 0. This integrand has singularities at Φ = 0 and Φ_{p0}. The nature of the one at $\Phi = \Phi_{p0}$ is elucidated by substituting $\Phi = \Phi_{p0} + \Delta\Phi$ into equation (5.49). ΔΦ is a small quantity and enables an approximate expression for the integrand to be obtained through simplifying expansions:

$$\frac{d}{d\varepsilon}\left(\frac{d\Phi}{dX}\right)\Big|_{\varepsilon=0} \approx \frac{1}{(-\Phi)^{1/4}\,\{2(-\Phi_{p0})^{1/2}\exp(\Phi_{p0})\}^{1/2}}$$

Thus at $\Phi = \Phi_{p0}$ the integrand is just a step function which does not usually cause problems for numerical integration schemes.

The singularity at $\Phi = 0$ is treated by an approximate expansion of equation (5.49) valid for small Φ :

So integrating over a small range Φ' to 0 we obtain:

$$\int_{\Phi'}^{0} \frac{d}{d\varepsilon}\left(\frac{d\Phi}{dX}\right)\Big|_{\varepsilon=0} d\Phi = \frac{\frac{4}{3}(-\Phi')^{3/4}}{\{2(-\Phi_{p0})^{1/2}\exp(\Phi_{p0})\}^{1/2}}$$

which is finite. The shape of the integrand is depicted in Fig. 5.11. Hence the integration can be performed numerically and this has been done.

The result for $(dE/d\varepsilon)_{\varepsilon=0}$ varies with mass ratio M/m and this also affects the integration by determining the wall-potential which forms one extreme of the range of integration. The consequence of this is that the result is positive for mass ratios below 1000 and negative above this value, as can be seen in Fig. 5.12. Hence the field energy too is found not to be stationary with respect to ε. However, as in the case of the wall-potential, it is found to be stationary with respect to $\mathbf{E}_0$ since $d\mathbf{E}_0/d\varepsilon = (2\varepsilon)^{-1/2}$. The interesting point is that, for zero-field at the mid-plane, field energy is at its maximum value when the mass ratio is above 1000 and at its minimum value for mass ratios below this. So minimisation of the field energy as a principle would have greater corroboration if it were confirmed for mass ratios above 1000.

It was still of interest to know whether the principle might apply to a conventional plasma-in-box system. Hence, we recall the expression for the

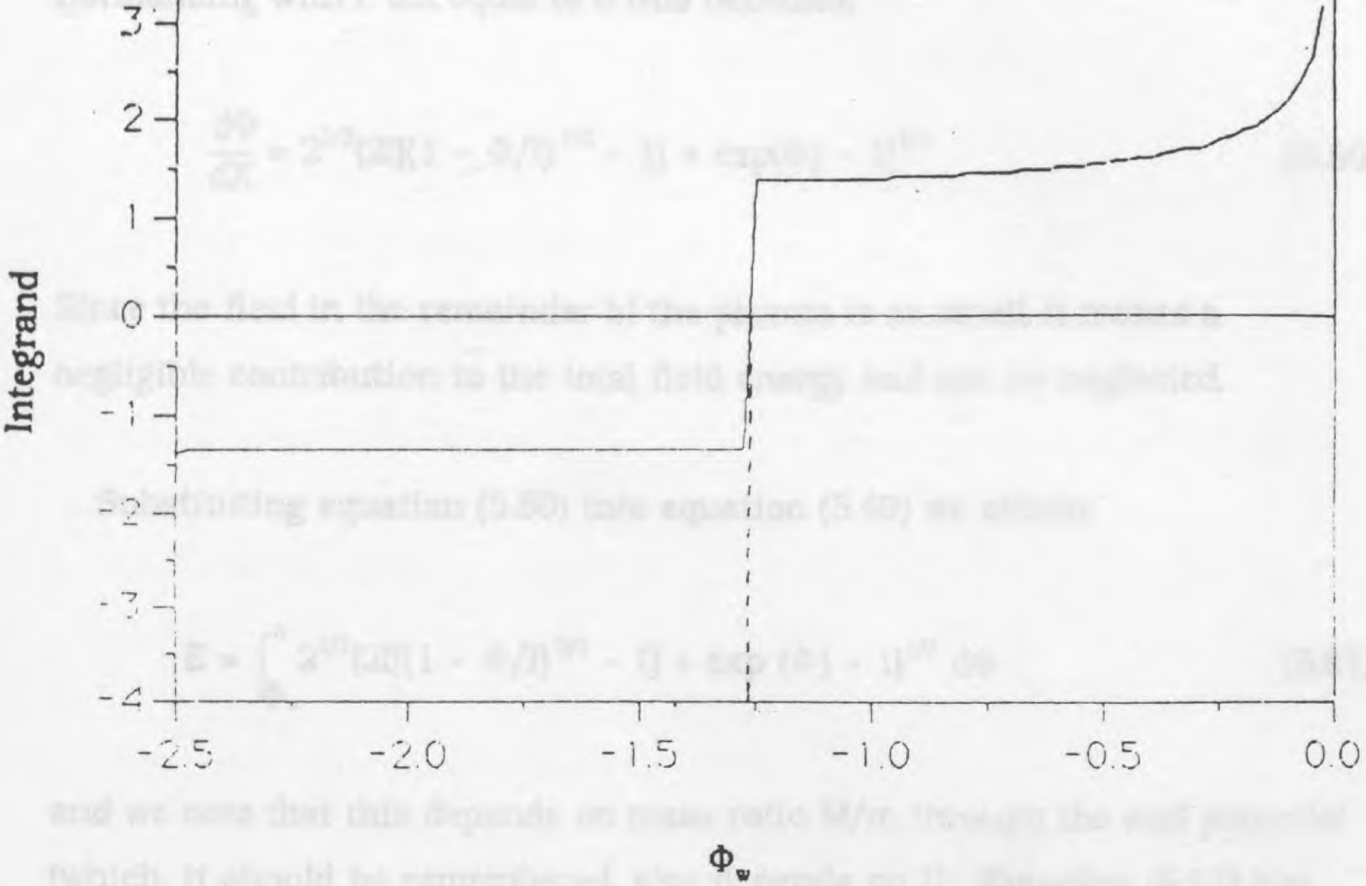

Fig. 5.11 Integrand in equation (5.49).

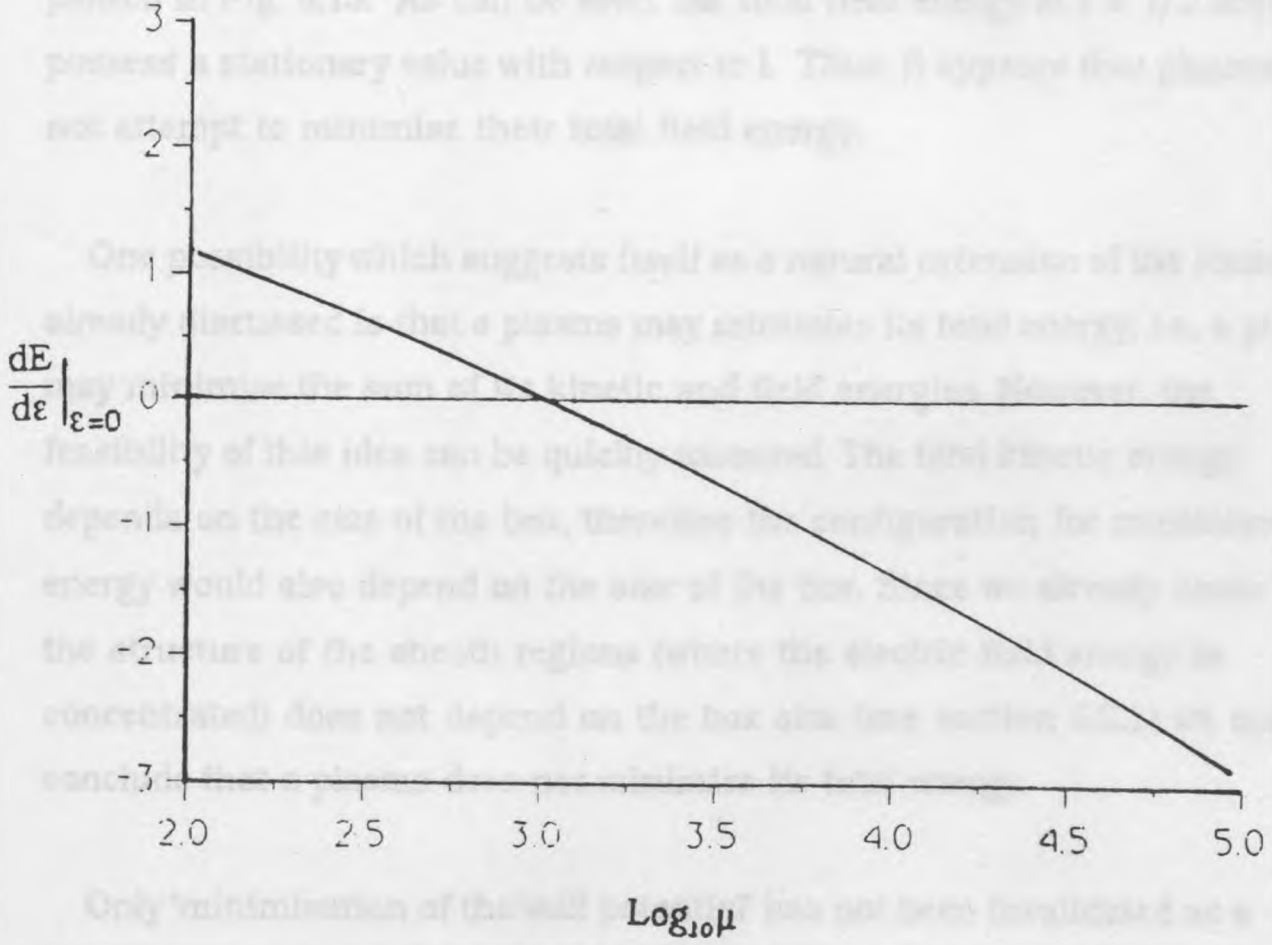

Fig. 5.12 The derivitive of the total field energy ($dE/d\varepsilon|_{\varepsilon=0}$) as a function of mass ratio M/m.

normalising with Γ set equal to 0 this becomes:

$$\frac{d\Phi}{dX} = 2^{1/2}\{2I[(1 - \Phi/I)^{1/2} - 1] + \exp(\Phi) - 1\}^{1/2} \qquad (5.50)$$

Since the field in the remainder of the plasma is so small, it makes a negligible contribution to the total field energy and can be neglected.

Substituting equation (5.50) into equation (5.49) we obtain:

$$E = \int_{\Phi_w}^{0} 2^{1/2}\{2I[(1 - \Phi/I)^{1/2} - 1] + \exp(\Phi) - 1\}^{1/2}\, d\Phi \qquad (5.51)$$

and we note that this depends on mass ratio M/m through the wall potential (which, it should be remembered, also depends on I). Equation (5.51) has been integrated for a range of mass ratios and ion energies; the results are plotted in Fig. 5.13. As can be seen, the total field energy at I = 1/2 does not possess a stationary value with respect to I. Thus, it appears that plasmas do not attempt to minimise their total field energy.

One possibility which suggests itself as a natural extension of the ideas already discussed is that a plasma may minimise its total energy, i.e., a plasma may minimise the sum of its kinetic and field energies. However, the feasibility of this idea can be quickly assessed. The total kinetic energy depends on the size of the box, therefore the configuration for minimised total energy would also depend on the size of the box. Since we already know that the structure of the sheath regions (where the electric field energy is concentrated) does not depend on the box size (see section 5.3.1) we may conclude that a plasma does not minimise its total energy.

Only 'minimisation of the wall potential' has not been invalidated as a principle. Clearly, it would be preferable if this result were shown to follow

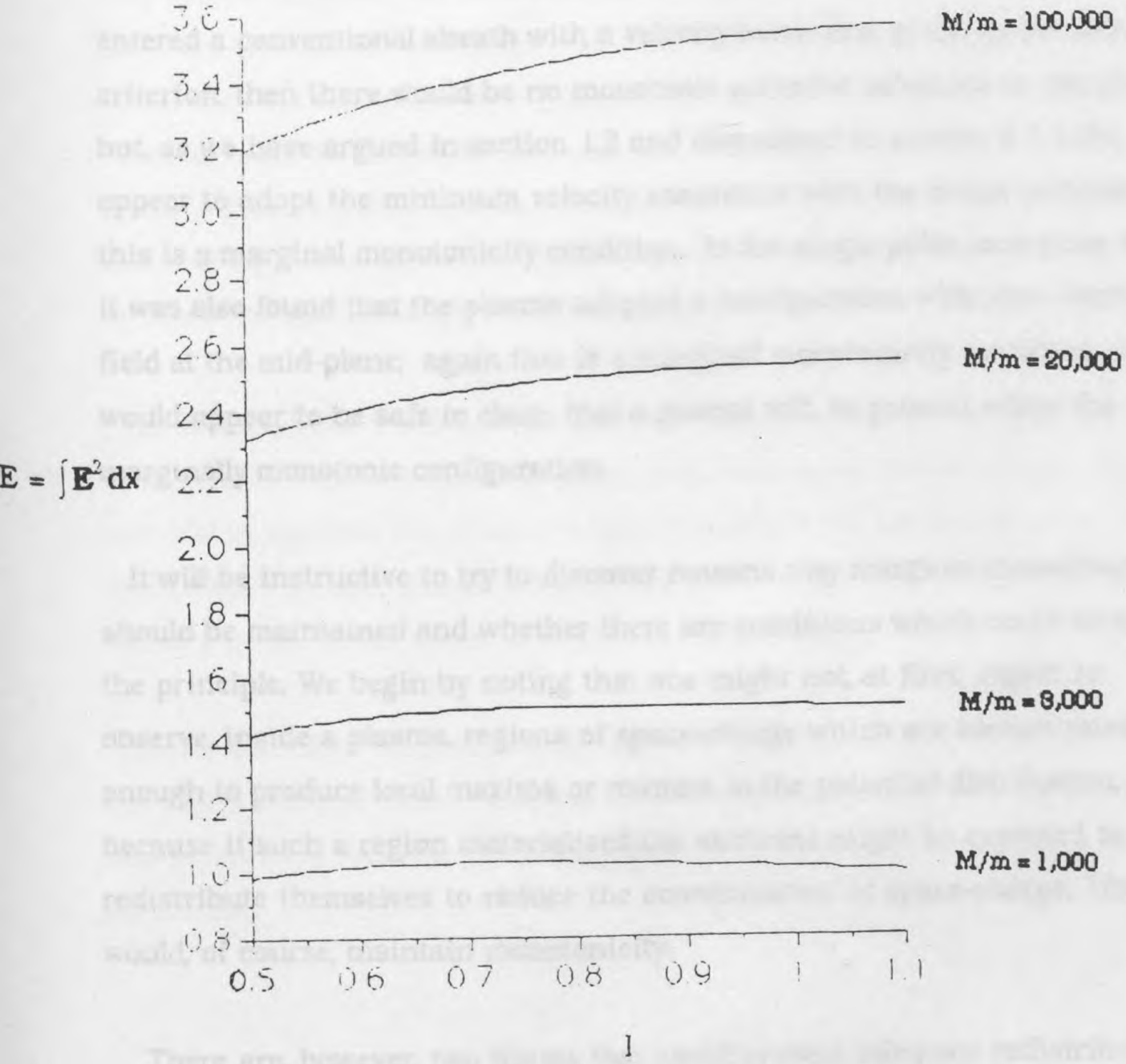

Fig. 5.13 Total field energy in a plasma as a function of I,

following observation.

It was noticed that there was one characteristic which was common to both of the plasma systems analysed above. In each case the plasma seems to adopt a configuration which can be described as marginally monotonic. If ions entered a conventional sheath with a velocity below that given by the Bohm criterion, then there would be no monotonic potential solutions in the sheath but, as we have argued in section 1.2 and discovered in section 5.3.1, the ions appear to adopt the minimum velocity consistent with the Bohm criterion; this is a marginal monotonicity condition. In the single-point ionisation case it was also found that the plasma adopted a configuration with zero electric field at the mid-plane; again this is a marginal monotonicity condition. It would appear to be safe to claim that a plasma will, in general, adopt the marginally monotonic configuration.

It will be instructive to try to discover reasons why marginal monotonicity should be maintained and whether there are conditions which could invalidate the principle. We begin by noting that one might not, at first, expect to observe, inside a plasma, regions of space-charge which are concentrated enough to produce local maxima or minima in the potential distribution, because if such a region materialised the electrons might be expected to redistribute themselves to reduce the concentration of space-charge. This would, of course, maintain monotonicity.

There are, however, two things that could prevent adequate redistribution. Firstly, if by some means a steady stream of electrons can be directed towards a negative space-charge region at a rate equalling that at which electrons are being repelled by the negative potential then a local minimum in potential can be maintained. Secondary electrons from a hot, emissive boundary is one mechanism which may provide sufficient energy to electrons to enable them to produce such a minimum. Secondly, a maximum in potential can occur if

of the one-dimensional box, in which case the maximum is situated at the mid-plane; but of course our previous remarks concerning monotonicity refer to each separate half of such a system.

The above considerations ensure that in both of the cases discussed so far only monotonic potential distributions can occur, thus supporting the observed features of the calculations. The other half of the principle, which states that the monotonicity is marginal, has not to date been explained in terms of more fundamental concepts, but it is suggested that the principle remains generally true in circumstances where the profile is not influenced by either of the two mechanisms which interfere with the ability of the electrons to moderate space-charge concentration.

In summary then, the principle of a minimum ion energy for sheath formation is shown to follow from the requirement for monotonicity; the conclusion that this should also represent a maximum ion energy for a conventional sheath follows from the argument of section 1.2. The use of the equality in the Bohm criterion (equation (1.7)) is thus justified.

It has also been verified that the above criterion corresponds to the minimum wall-potential consistent with monotonicity, and that the adopted wall-potential is stationary with respect to the boundary value of a real plasma parameter.

Simulation of the Instability and Interpretation

Results for zero current conditions and current carrying conditions will be dealt with separately. We will begin with those for the current case (section 6.1) since the behaviour is more clear-cut and straightforward. The zero current case with parameters more likely to be relevant to tokamaks will be discussed in section 6.2. In section 6.3 we investigate the evolution of the instability beyond the stage represented in the simultation and assess the stability of the sheath.

6.1 Beam-Plasma Results With Current.

In this section we investigate the development of the beam-plasma instability when large currents are allowed to flow through the sheath to the wall under space-charge limited conditions. This choice was made to ensure maximum beam-density, thus enhancing the strength of the instability.

Two cases have been chosen corresponding to values of normalised wall potential of -10 and -100. For $\Phi_0 = -10$ the corresponding values of beam velocity and density are:

$$v_b/v_T = 4.47, \qquad n_b/n_0 = 0.149$$

In the case of $\Phi_0 = -100$ these values become:

$$v_b/v_T = 14.14, \qquad n_b/n_0 = 0.0632$$

The system we are concerned with is one where the instability is expected to grow spatially in the beam as it moves out from the sheath into the plasma. The evolution of the instability would therefore be affected by a very large region of plasma which would be difficult to simulate because of finite

relationship between the temporal growth simulation and the spatial growth case is dealt with in section 6.2 where the importance of other unnatural effects, such as exaggerated thermal fluctuations, are also discussed.

The particle simulation code was employed with box length equal to one wavelength of the fastest growing wave. This mode was determined by solving a linear dispersion relation for the appropriate electron distribution function, the ion interaction being neglected since their large mass is expected to prevent them from playing a significant role in the evolution of the instability. The dispersion relation is given [Wesson, 1974] by:

$$k^2 + \sum_j \frac{\omega_{pj}^2}{v_{Tj}^2}\left[1 + \gamma_j Z(\gamma_j)\right] = 0$$

where:

$$Z(\xi) = \pi^{-1/2} \int_C \frac{\exp(-x^2)}{x - \xi}\, dx$$

is the plasma dispersion function – evaluated using the Landau contour (see fig. 2.1),

$$\gamma_j = \frac{(\omega/k - v_{jd})}{\sqrt{2}\, v_{Tj}} \quad , \quad \omega_{pj}^2 = \frac{4\pi n_j e_j^2}{m_j} \quad ,$$

$v_{Tj}^2 = KT_j/m_j$ and v_{jd} is the drift velocity of the j^{th} species. For a beam of electrons passing through Maxwellian plasma electrons the dispersion relation, when normalised (see section 5.1.1), becomes:

$$1 - \frac{f_b}{(\Omega - KV_d)^2} + \frac{f_p}{K^2}\left[1 + \frac{\Omega}{\sqrt{2}K} Z\left(\frac{\Omega}{\sqrt{2}K}\right)\right] = 0$$

appeared in the definition of v_{Tj}, $f_p = n_p/n_0$ and $f_b = n_b/n_0$.

The solution to the dispersion relation for $\Phi_0 = -100$ is shown in Fig. 6.1. The parameters discussed so far are applicable to arbitrary mass ratio, but once this is selected then it fixes the current and associated variables such as p and Γ_i. For the two cases considered, the appropriate quantities for a number of mass ratios have been calculated and are given in Table 6.1. The actual mass ratio used in the simulation was 100 but since we are assuming ion motion is negligible we also assume that the results are applicable to all mass ratios for which $(M/m)^{1/2} >> 1$.

Phasespace plots of the particle motion are displayed in Figs. 6.2 and 6.3. In both cases the beam of electrons is initially clearly visible as a horizontal line separated in velocity space from the main plasma. The velocity perturbation of the beam begins with wavelength equal to the box size and it continues to grow until the beam is trapped by the growing wave. This happens after $t\omega_{pe} = 15$ and 20 for the lower and higher wall-potential cases respectively. After trapping, the beam and plasma continue to orbit in phasespace but the varying amplitude of the trapping potential allows electrons to be periodically spilled across the separatrix near the nodes, where the local potential is small. The resulting filamentary spikes can clearly be seen at intervals corresponding to the bounce frequency. Smaller spikes can also be seen at other times due to the considerable thermal fluctuations experienced by this kind of simulation. This 'detrapping' of the electrons prevents them from following a constant orbit, thus ensuring that they all have slightly different bounce frequencies. This has the effect of smearing out the electron distribution function along orbits, which would, in turn, gradually diminish the size of the amplitude of the oscillations of the trapping potential. The $\Phi_0 = -10$ case still retains at the end of the simulation a void at the centre of the particle orbits, while, in the $\Phi_0 = -100$ case, stochasticity theory (see section 3.3 and 7.2.5) may be applicable since electron orbits are rather chaotically scattered throughout the region enclosed by the separatrix; at this stage the spatially averaged electron

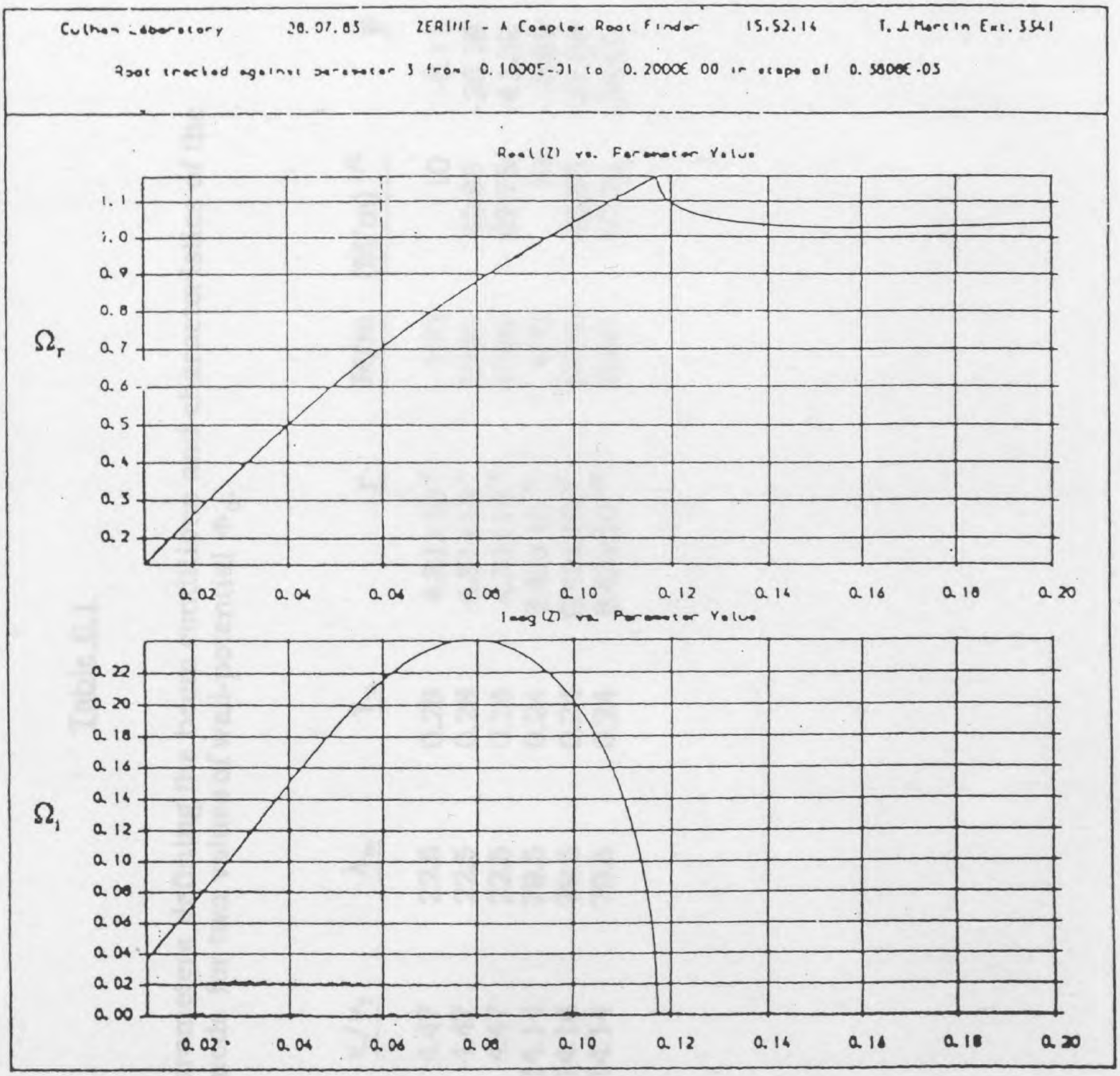

Fig. 6.1 Solution to the dispersion relation for $\Phi_0 = -100$ case

Table 6.1

Relevant parameters defining the beam conditions and characteristics of the dominant mode for two values of wall-potential Φ_0.

Φ_0	n_b/n_0	v_b/v_T	λ_m	γ_m	Γ	M/m	$(M/m)^{1/2}$	P	Γ_1
10	0.149	4.47	22.5	0.28	4.31×10^{4}	100	10	-6.11	6.11
10	0.149	4.47	22.5	0.28	4.31×10^{4}	1836	42.85	-26.18	26.8
10	0.149	4.47	22.5	0.28	4.31×10^{4}	4590	67.75	-41.39	41.39
100	0.0632	14.14	79.5	0.24	6.43×10^{43}	100	10	-8.65	8.65
100	0.0632	14.14	79.5	0.24	6.43×10^{43}	1836	42.85	-37.08	37.08
100	0.0632	14.14	79.5	0.24	6.43×10^{43}	4590	67.75	-58.63	58.63

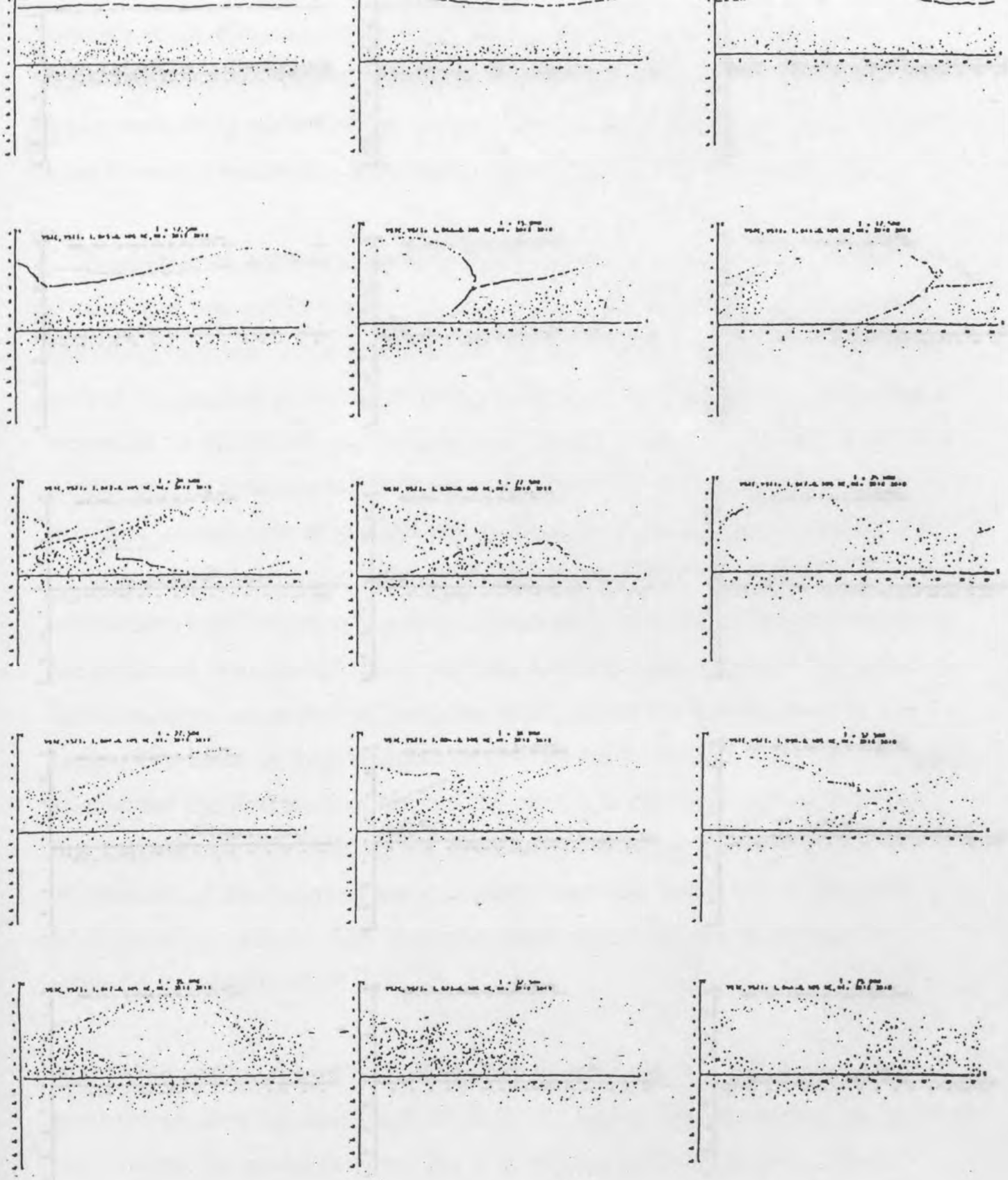

Fig. 6.2 Electron phasespace corresponding to the $\Phi_0 = -10$ case (see also Appendix A for an enlarged version). The times correspond to those given for the distribution functions of Fig. 6.4.

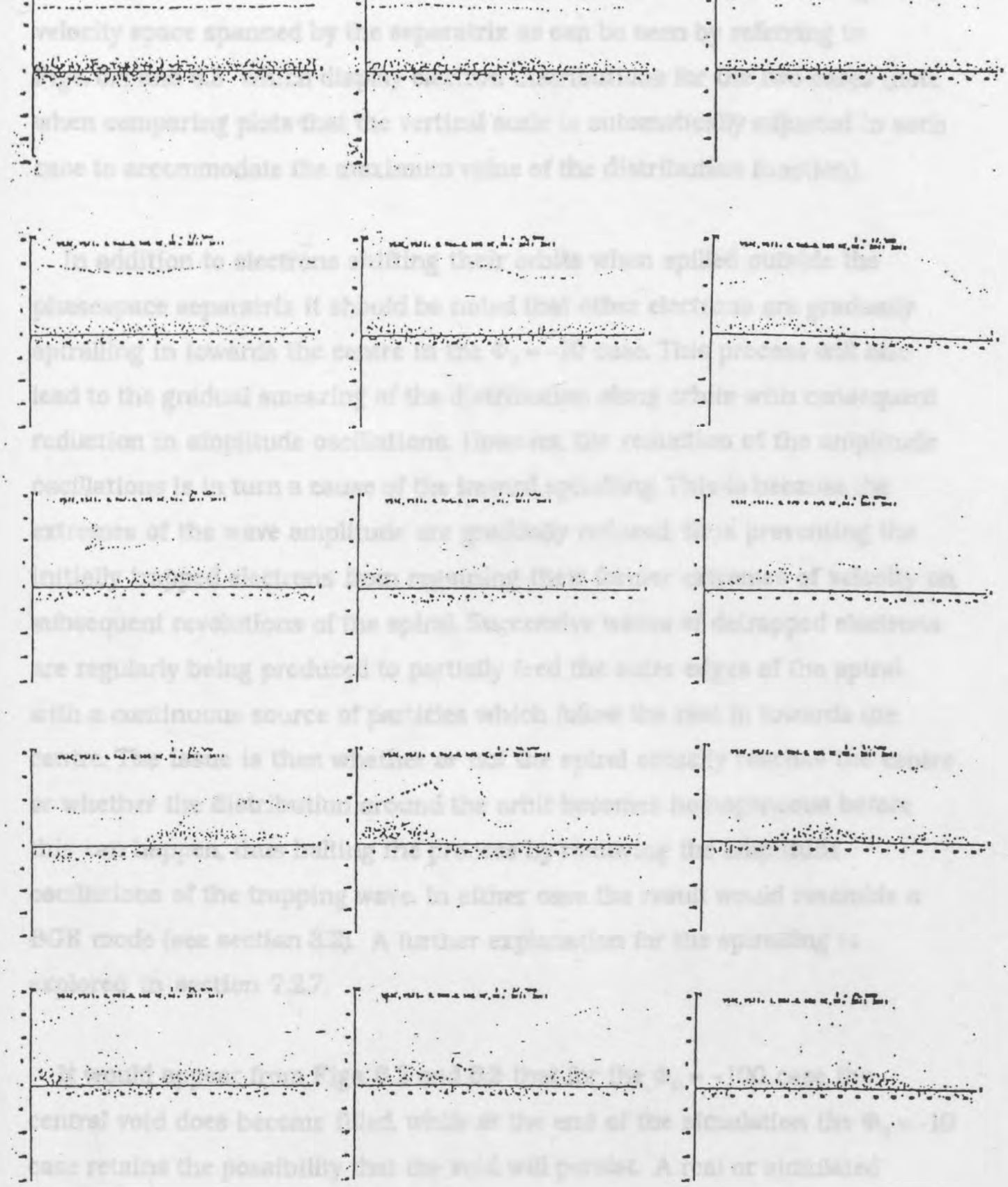

Fig. 6.3 Electron phasespace corresponding to the $\Phi_0 = -100$ case (see also Appendix B for an enlarged version). The times correspond to those given for the distribution functions of Fig. 6.5.

velocity space spanned by the separatrix as can be seen by referring to Figs. 6.4 and 6.5 which display electron distributions for the two cases (note when comparing plots that the vertical scale is automatically adjusted in each case to accommodate the maximum value of the distribution function).

In addition to electrons shifting their orbits when spilled outside the phasespace separatrix it should be noted that other electrons are gradually spiralling in towards the centre in the $\Phi_0 = -10$ case. This process will also lead to the gradual smearing of the distribution along orbits with consequent reduction in amplitude oscillations. However, the reduction of the amplitude oscillations is in turn a cause of the inward spiralling. This is because the extremes of the wave amplitude are gradually reduced, thus preventing the initially trapped electrons from regaining their former extremes of velocity on subsequent revolutions of the spiral. Successive waves of detrapped electrons are regularly being produced to partially feed the outer edges of the spiral with a continuous source of particles which follow the rest in towards the centre. The issue is then whether or not the spiral actually reaches the centre or whether the distribution around the orbit becomes homogeneous before this can happen, thus halting the process by removing the amplitude oscillations of the trapping wave. In either case the result would resemble a BGK mode (see section 3.2). A further explanation for the spiralling is explored in section 7.2.7.

It would appear from Figs. 6.2 and 6.3 that for the $\Phi_0 = -100$ case the central void does become filled, while at the end of the simulation the $\Phi_0 = -10$ case retains the possibility that the void will persist. A real or simulated plasma, however, is not restricted to the idealised behaviour determined by the Vlasov equation; there are thermal fluctuations, which in the simulation are especially large, and these must continue to spread out the orbits to fill in the voids. There is also the fact that, strictly speaking, there is never only a single mode involved in the instability, although there is the possibility that for a period of time the plasma may appear to behave as if there were a single

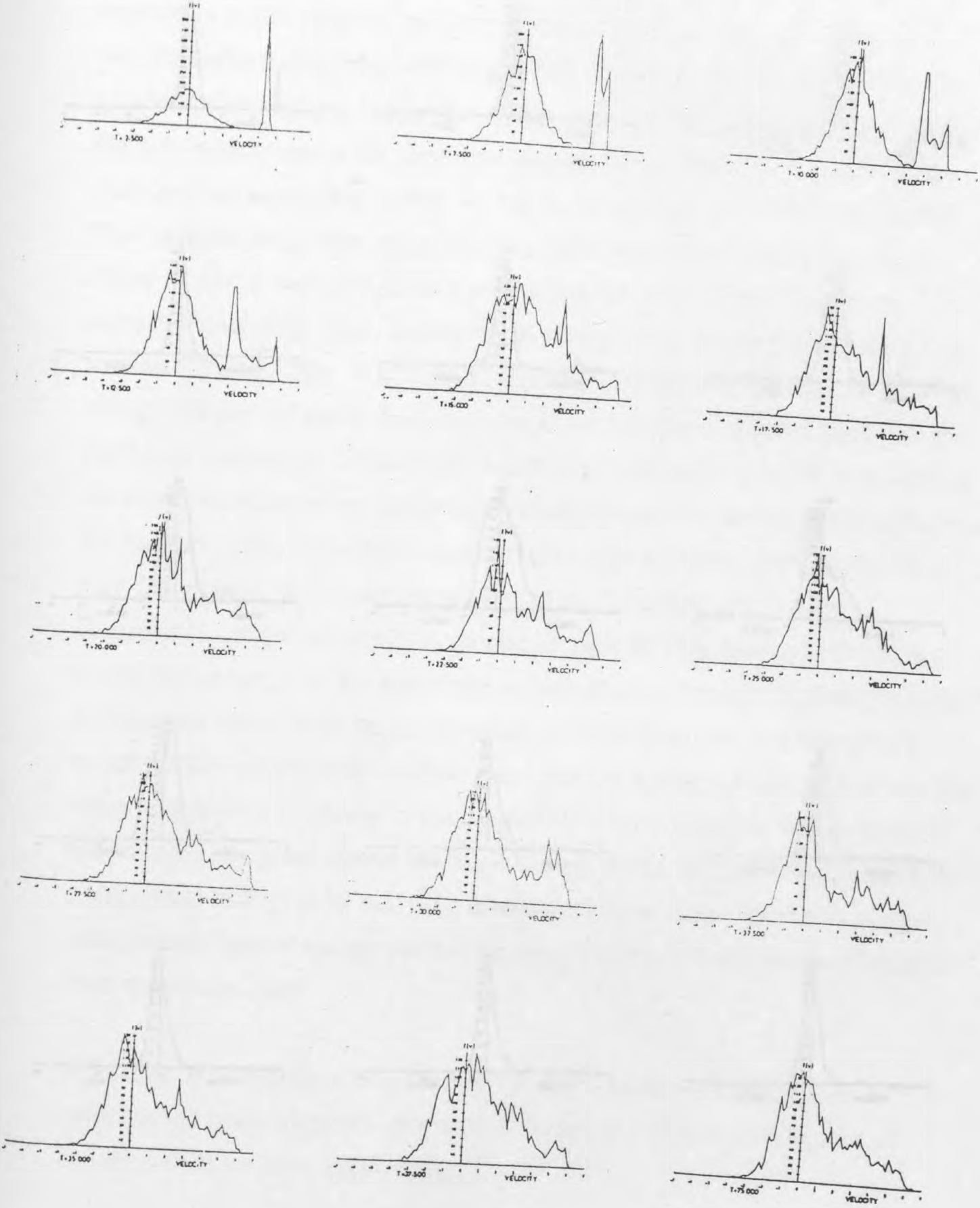

Fig. 6.4 Electron distribution functions for $|\Phi_0| = 10$

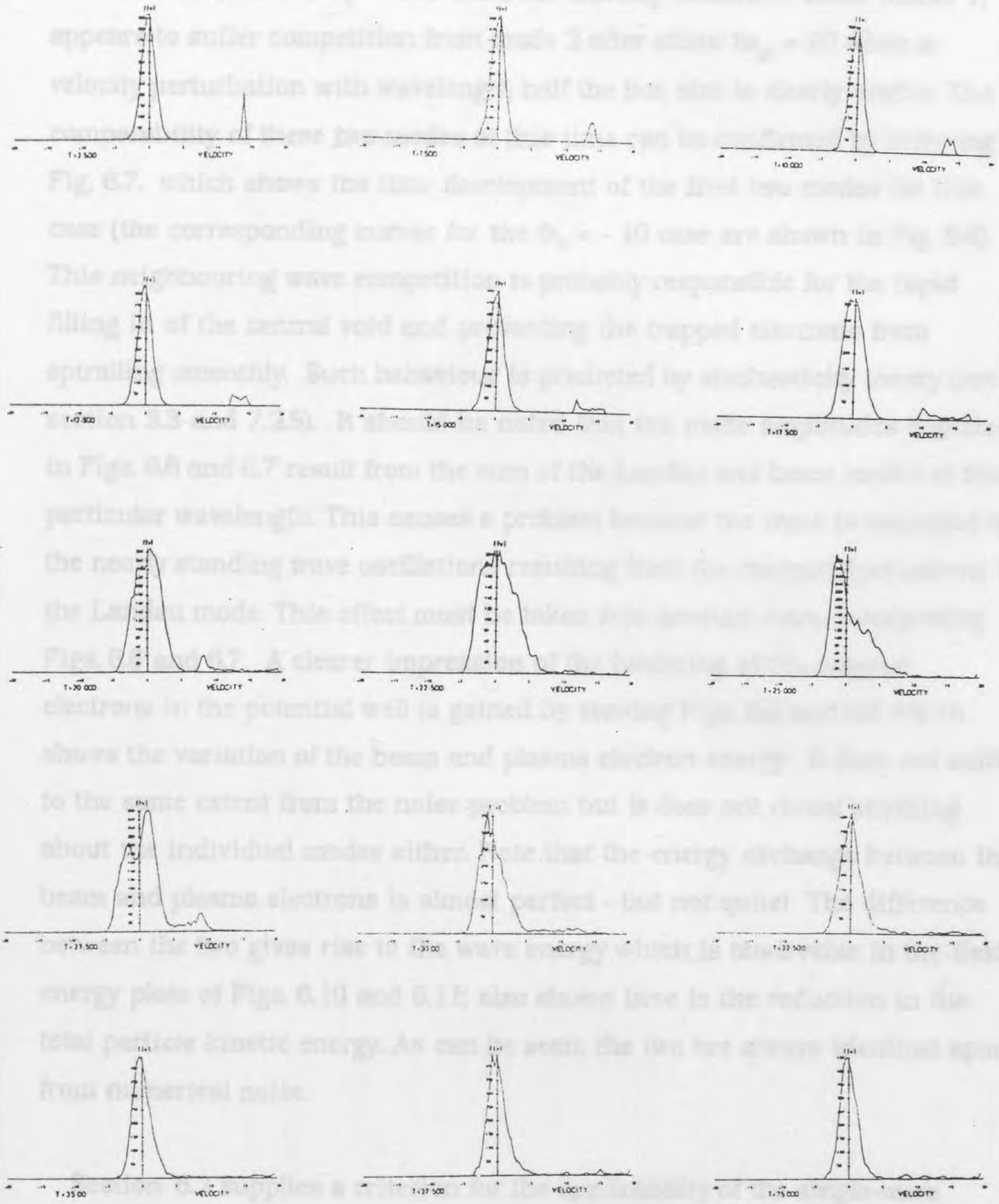

Fig. 6.5 Electron distribution functions for $|\Phi_0| = 100$

wave, provided that the appropriate criterion is met (see section 6.2). As a matter of fact, for the $\Phi_0 = -100$ case, the initially dominant mode (mode 1) appears to suffer competition from mode 2 after about $t\omega_{pe} = 30$ when a velocity perturbation with wavelength half the box size is clearly visible. The comparability of these two modes at this time can be confirmed by referring to Fig. 6.7. which shows the time development of the first two modes for this case (the corresponding curves for the $\Phi_0 = -10$ case are shown in Fig. 6.6). This neighbouring wave competition is probably responsible for the rapid filling in of the central void and preventing the trapped electrons from spiralling smoothly. Such behaviour is predicted by stochasticity theory (see section 3.3 and 7.2.5). It should be noted that the mode amplitudes depicted in Figs. 6.6 and 6.7 result from the sum of the Landau and beam modes at that particular wavelength. This causes a problem because the trace is swamped by the nearly standing wave oscillations resulting from the thermal fluctuations in the Landau mode. This effect must be taken into account when interpreting Figs. 6.6 and 6.7. A clearer impression of the bouncing of the trapped electrons in the potential well is gained by viewing Figs. 6.8 and 6.9 which shows the variation of the beam and plasma electron energy. It does not suffer to the same extent from the noise problem but it does not reveal anything about the individual modes either. Note that the energy exchange between the beam and plasma electrons is almost perfect - but not quite! The difference between the two gives rise to the wave energy which is observable in the field energy plots of Figs. 6.10 and 6.11; also shown here is the reduction in the total particle kinetic energy. As can be seen, the two are always identical apart from numerical noise.

Section 6.2 supplies a criterion for the applicability of the single-wave model of the beam-plasma instability (equation (6.11)) and making use of equation (3.1) we have approximately:

$$\frac{2^{5/6}}{3(\ln 2)^{1/2}} \quad \frac{(\gamma_m t_r)^{1/2}}{\eta^{1/3}} >> 1 \qquad (6.1)$$

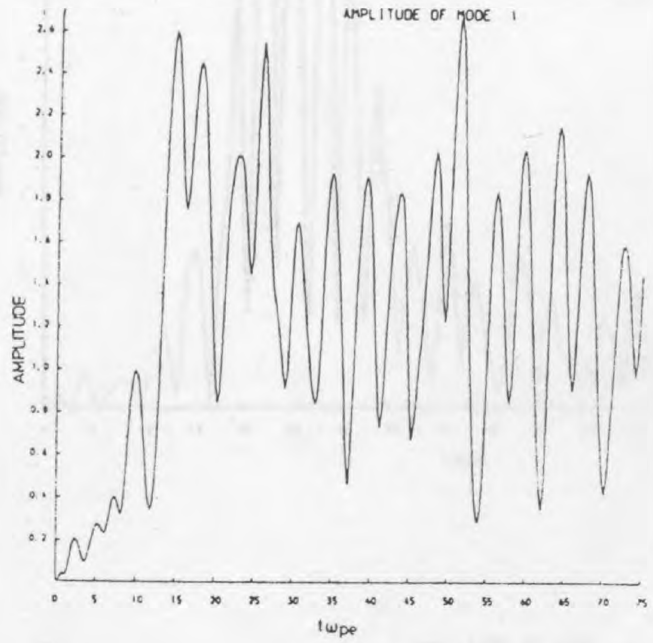

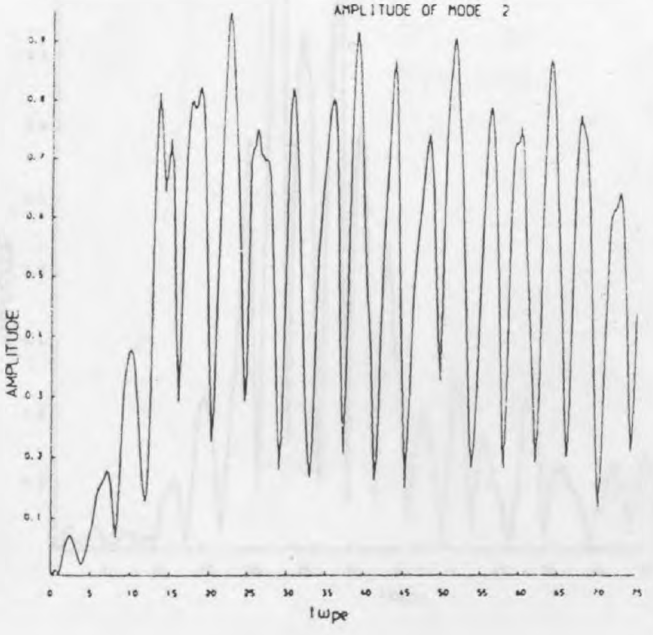

Fig. 6.6 Mode amplitudes v time for $|\Phi_0| = 10$

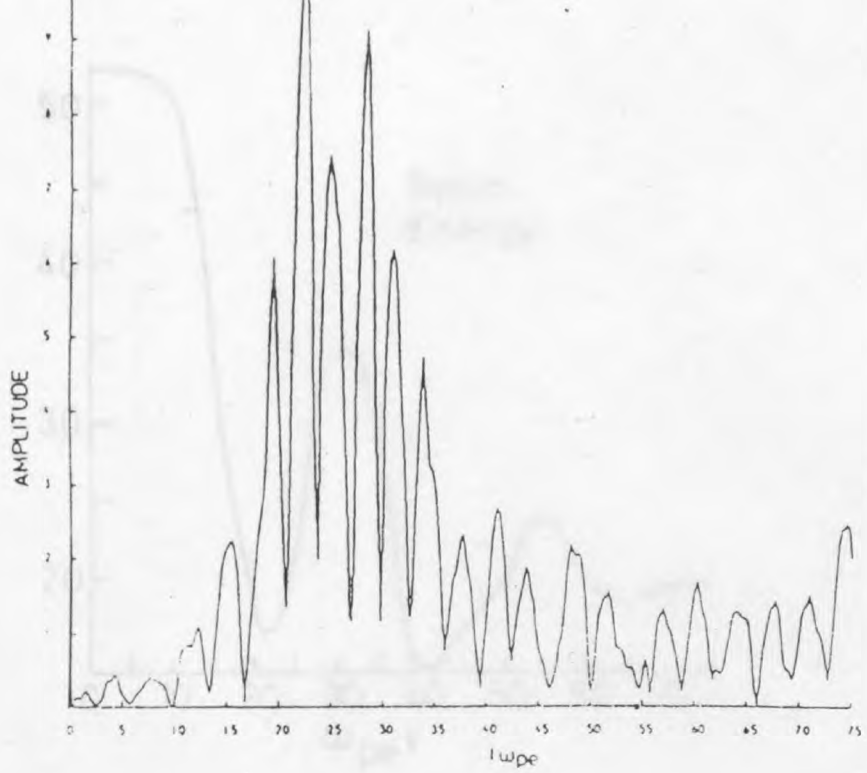

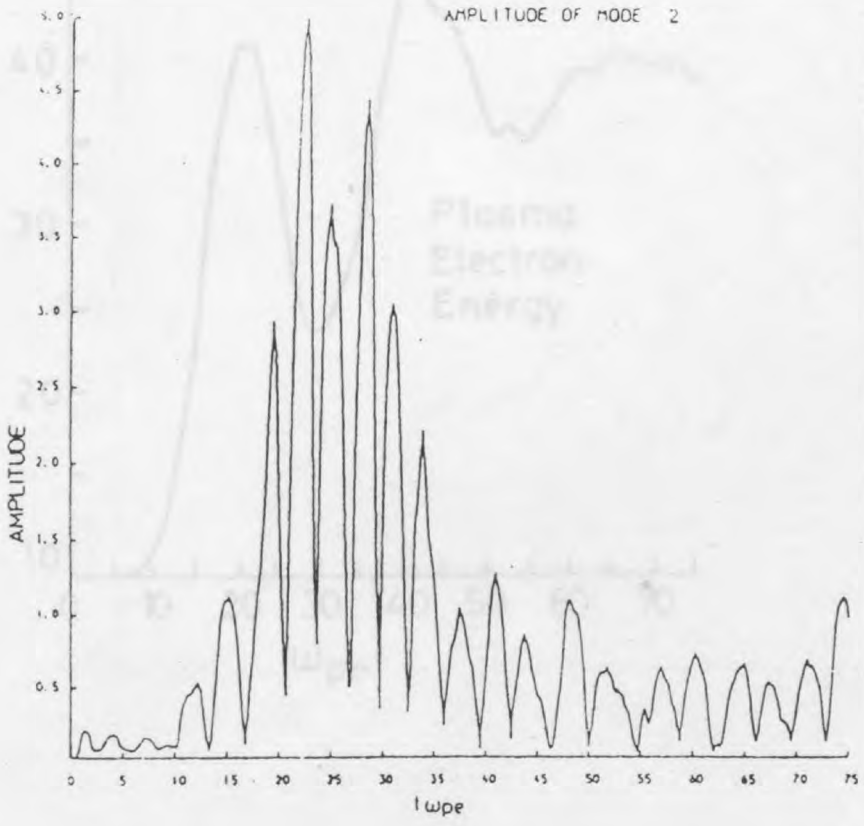

Fig 6.7 Mode amplitudes v time for $|\Phi_1| = 100$

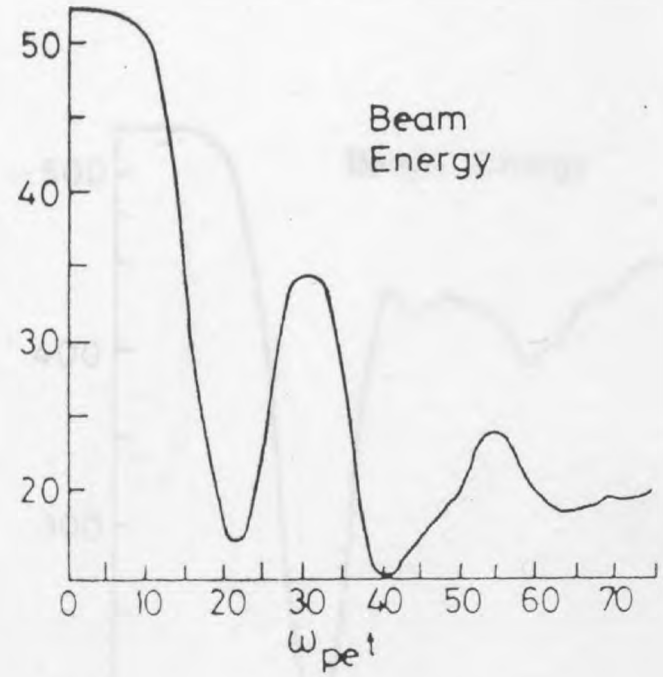

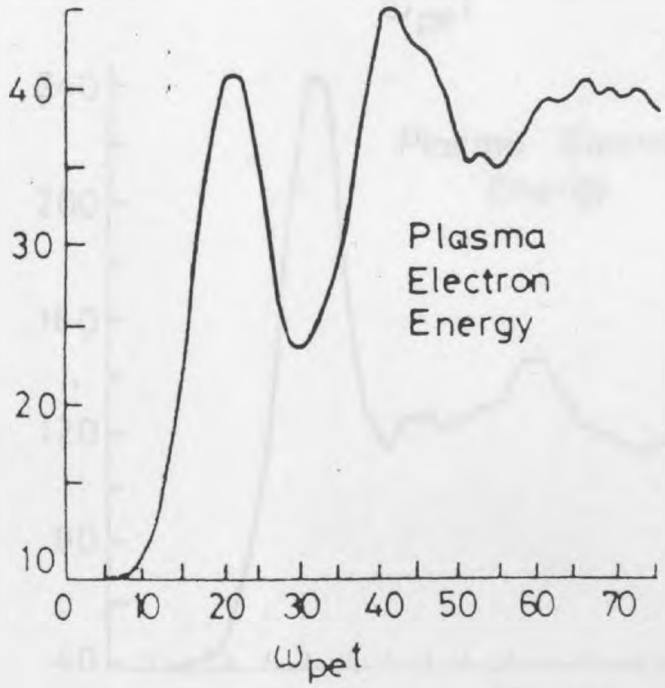

Fig. 6.8 Beam and plasma electron energy v time for $|\Phi_0| = 10$

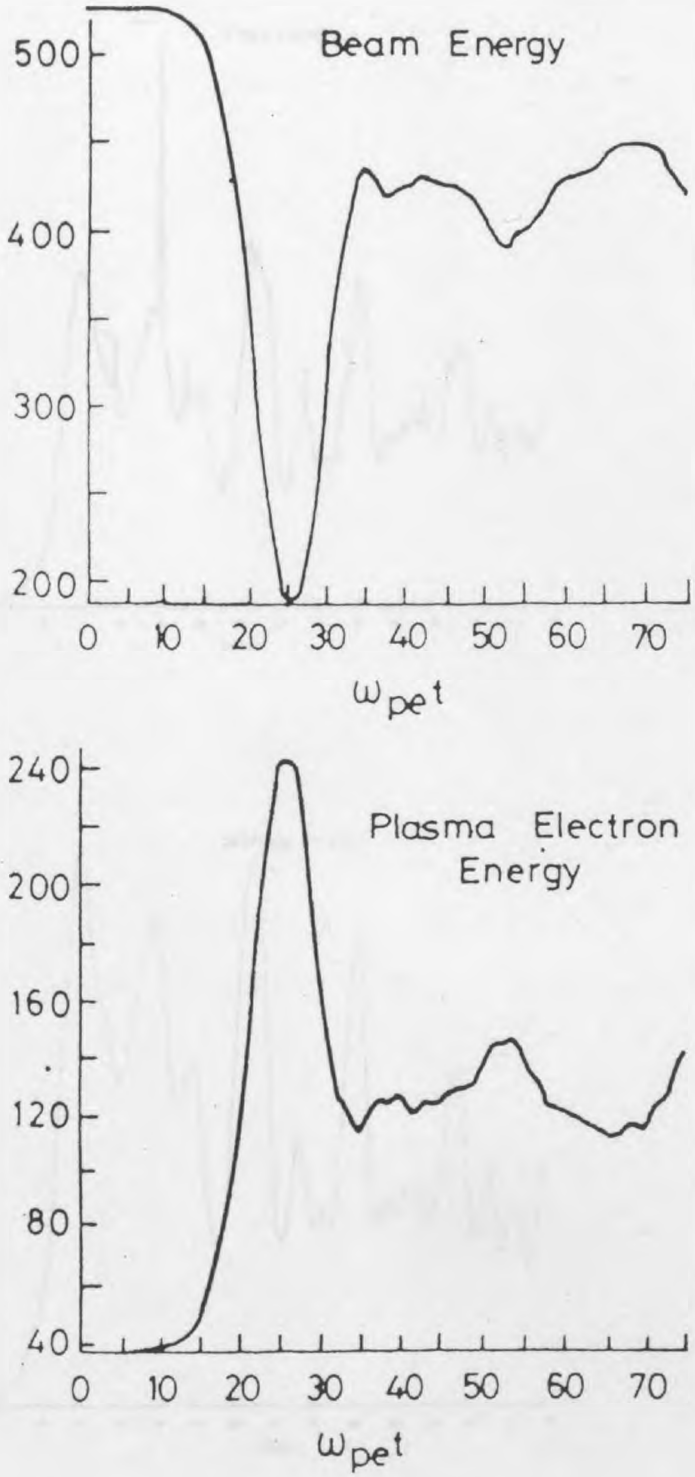

Fig. 6.9 Beam and plasma electron energy v time for $|\Phi_0| = 100$

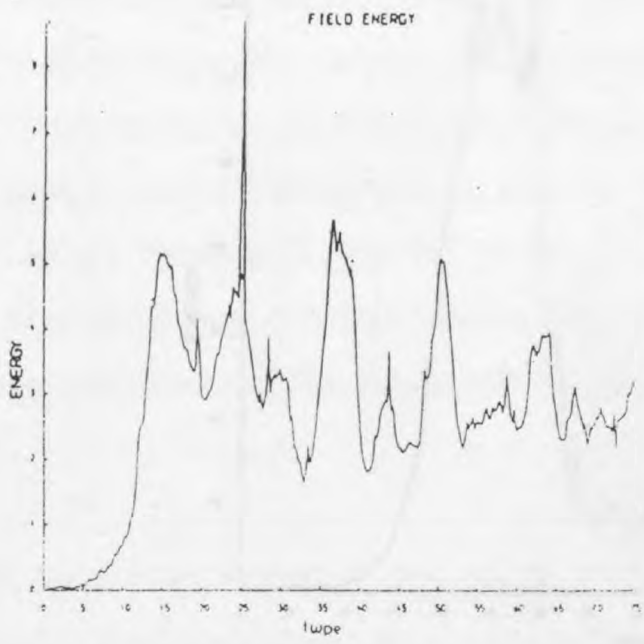

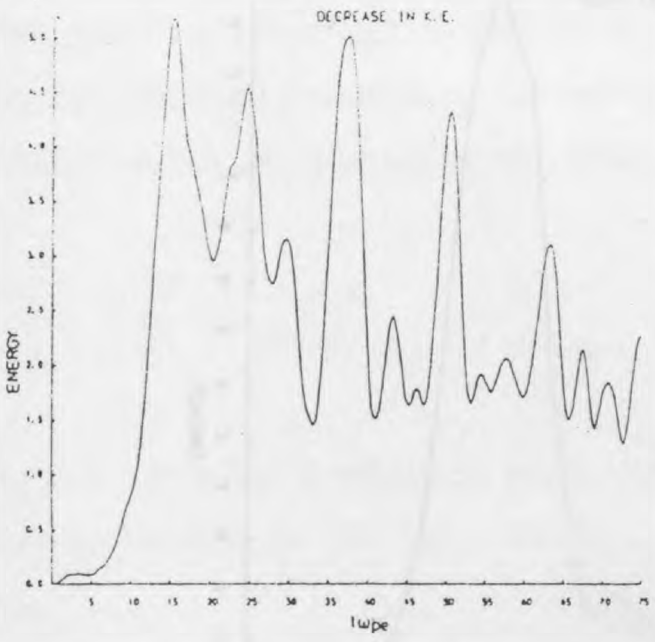

Fig. 6.10 Field energy v time and loss of

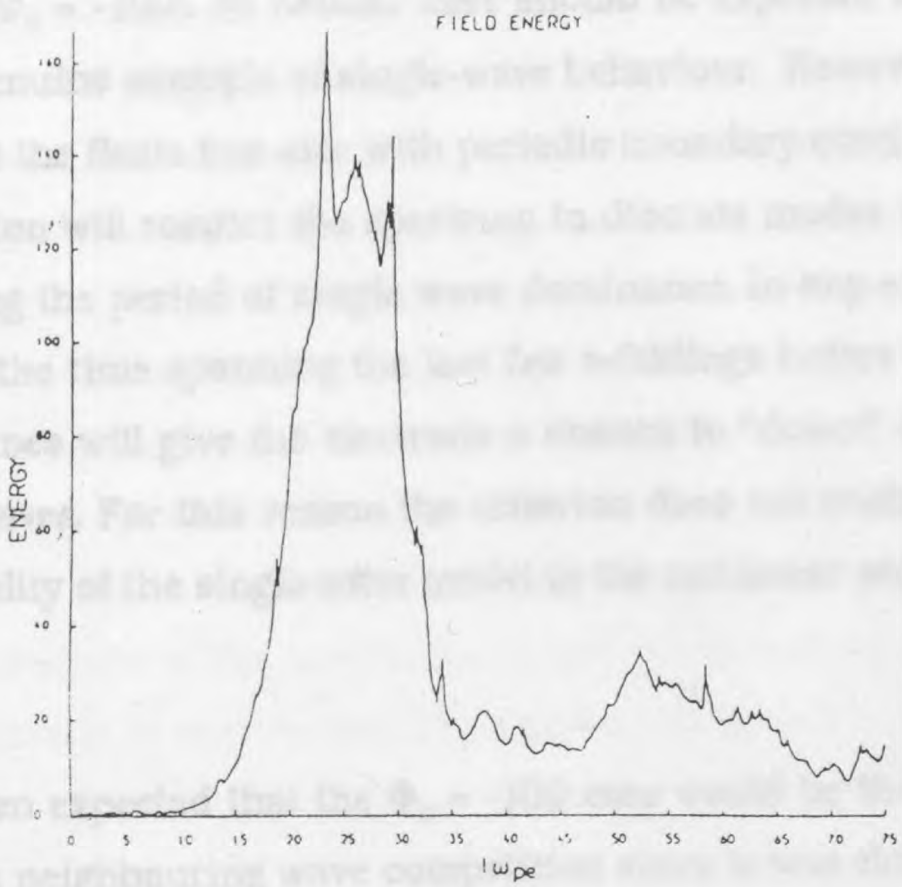
FIELD ENERGY
ENERGY
0
20
40
60
80
100
120
140
0
5
10
15
20
25
30
35
40
45
50
55
60
65
70
75
ωpe

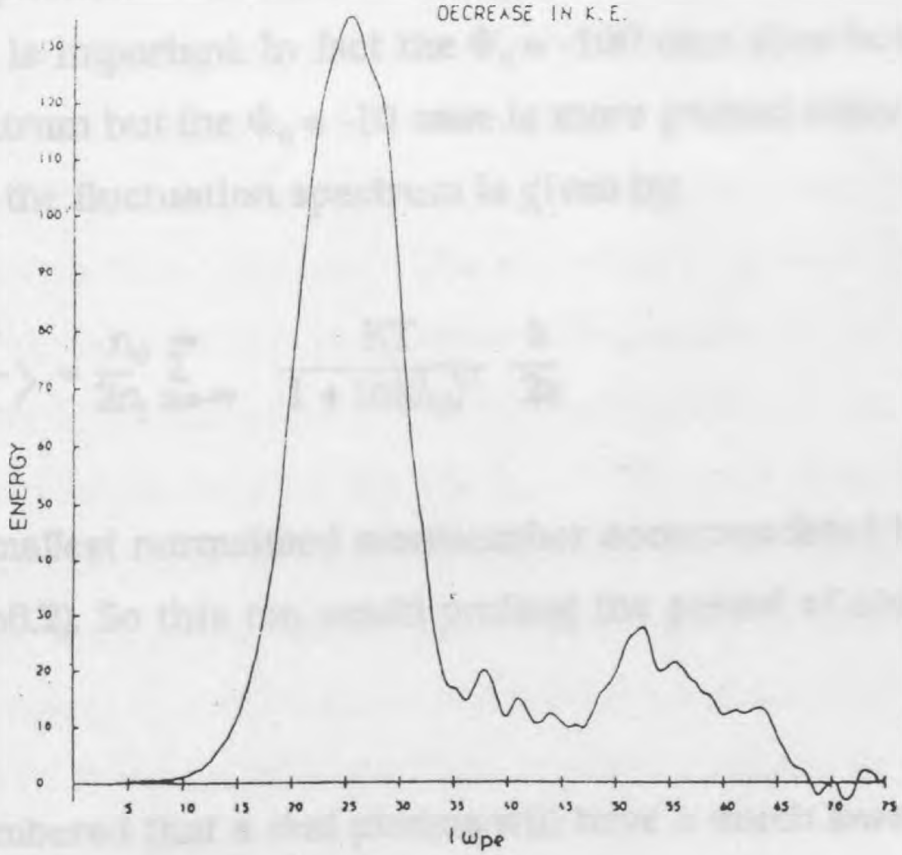
DECREASE IN K.E.
ENERGY
0
10
20
30
40
50
60
70
80
90
100
110
120
130
5
10
15
20
25
30
35
40
45
50
55
60
65
70
75
ωpe

obtain 2.76 in the lower wall-potential case ($\Phi_0 = -10$) and 4.12 in the higher wall-potential case ($\Phi_0 = -100$). So neither case should be expected on this basis to provide a genuine example of single-wave behaviour. However, it should be noted that the finite box size with periodic boundary conditions used in the simulation will restrict the spectrum to discrete modes thus somewhat prolonging the period of single wave dominance. In any event the criterion applies to the time spanning the last few e-foldings before trapping occurs, so longer times will give the electrons a chance to "detect" the presence of other waves. For this reason the criterion does not enable one to assess the applicability of the single-wave model to the nonlinear stage of the instability.

It might have been expected that the $\Phi_0 = -100$ case would be the least likely to suffer from neighbouring wave competition since it was closer to satisfying criterion (6.1) than the $\Phi_0 = -10$ case. However, the criterion is based on an assumption that the initial wave spectrum is flat in the region where wave growth is important. In fact the $\Phi_0 = -100$ case does have a reasonably flat spectrum but the $\Phi_0 = -10$ case is more peaked since the box size is smaller and the fluctuation spectrum is given by:

$$\left\langle \frac{E^2}{8\pi} \right\rangle = \frac{n_0}{2n_1} \sum_{n=-\infty}^{\infty} \frac{KT}{1 + (nk\lambda_D)^2} \frac{k}{2\pi} \qquad (6.2)$$

where $k\lambda_D$ is the smallest normalised wavenumber accommodated by the system (see section6.2). So this too would prolong the period of single wave dominance.

It must be remembered that a real plasma will have a much lower level of thermal fluctuations initially than the artificial plasma of these simulations, so that by the time that nonlinear behaviour begins the wave spectrum will be much more peaked in reality. The single-wave dominance will therefore continue much longer and the oscillations in the amplitude of the trapping

should exhibit more broadband behaviour than observed in temporal growth during the nonlinear phase.

Some computer beam-plasma experiments (see section 3.1.3) effectively restrict the spectrum of growing waves to a single mode. In these cases it is observed that "clumps" of trapped electrons maintain their rotation indefinitely while the amplitude of the trapping potential continues to oscillate between fixed maximum and minimum values. This indicates that there can be no detrapping of electrons here otherwise this would gradually erode the magnitude of the oscillations of the trapping potential amplitude. The time variation in shape of the potential well and the motion of the electrons must be such as to ensure that they all have the same bounce frequency.

It would seem therefore that the long timescale evolution of the beam-plasma instability in a collisionless plasma depends on the nature of the wave spectrum. Electron detrapping and attendant reduction of amplitude oscillations would seem to require neighbouring wave growth to enable the process to take place; these and already existing waves ensuring further smoothing of the distribution function. The evolution is difficult to calculate exactly but the speed with which it progresses will undoubtedly be related to the width of the wave spectrum when trapping begins (witness the rapid flattening of the distribution function for the $\Phi_0 = -100$ case). This will be more important than the noise spectrum at more distant wavelengths. Note that another possible mechanism causing the spiralling of electrons in phasespace and damping of amplitude oscillations of the main wave is, however, discussed in sections 7.2.2 and 7.2.7 and even applies to a single-wave situation.

If there are significant collisions these will of course play a similar role in hastening the flattening of the distribution function and they will ultimately lead to the restoration of a Maxwellian velocity distribution function. The

then collisions will be the dominant mechanism. This is a difficult issue to resolve without unlimited computer resources as the many wave problem is a complex one.

Thus, depending on the relative importance of the above mechanisms, the instability may or may not penetrate deep into the plasma, but even if the structure exists over a large distance it does not make sense to expect a true BGK mode to be created since such an entity can only survive by virtue of the artificial requirement for an absolutely monochromatic single wave (see section 3.2).

The computer simulation of the beam-plasma instability is difficult as it would require a prohibitively large number of particles to model all the attributes of a real plasma for the conditions of interest. Since computer resources are limited it is necessary to invoke as many simplifications as theoretical assessments will allow.

The simplest way of representing a plasma is to model a small segment of it and use periodic boundary conditions; this heavily restricts the spectrum of waves which can propagate by only allowing discrete modes. The adequacy of such a reduced spectrum will be discussed later but for the moment we simply note that these restrictions will have to be borne because there is no possibility of including sufficient particles to be able to fully represent the entire region of interest. This immediately presents a problem because the conditions we are interested in do not relate to a spatially homogeneous situation. The beam-plasma instability is expected to grow spatially in the direction of the plasma centre and away from the sheath, whereas use of periodic boundary conditions will only permit the simulation of temporal growth, starting from spatially homogeneous conditions. It is, however, possible to relate some aspects of a temporally evolving simulation to those for the case of spatial evolution. This has been done analytically for the linear dispersion relation [O'Neil and Malmberg, 1968] and for the evolution of the instability [O'Neil and Winfrey, 1972; Winfrey and Dunlop, 1977].

A linear analysis of the beam-plasma instability was carried out by O'Neil and Malmberg [1968] in connection with the transition from beam type to gentle bump type roots of the dispersion relation (see section 7.2.6). For temporal growth (i.e., choosing k to be real and ω complex) near the intersection of the beam and Landau roots they have derived the following equation in transformed coordinates:

$$y(y - x + is)^2 = 1 \qquad (6.3)$$

$$\frac{k - k_0}{k_0} = \left(\frac{RP}{P+Q}\right)x, \quad \frac{\omega - \omega_0}{\omega_0} = Ry - \left(\frac{RQ}{P+Q}\right)x \tag{6.4a}$$

The constants P, Q and R are defined by:

$$P = 2\left[1 + 3\left(\frac{v_T}{v_D}\right)^2\right]$$

$$Q = -6\left(\frac{v_T}{v_D}\right)^2\left[1 - 7\left(\frac{v_T}{v_D}\right)^2\right] \tag{6.4b}$$

$$R = \left(\frac{n_B}{n}\,\frac{\omega_{pe}^2}{\omega_0^2}\,\frac{1}{P}\right)^{1/3}, \quad Rs = \frac{\bar{v}_B}{v_D}$$

Note that the point (ω_0, k_0) is defined by $\omega_0 = k_0 v_D$ and Re $\varepsilon(k_0, \omega_0) = 0$ (there is a small imaginary part of order $\exp(v_D^2/v_T^2)$).

O'Neil and Malmberg [1968] have also examined the case of spatial growth by choosing ω to be real and k to be complex. The equation which they derive to describe the dispersion relation near the intersection of the beam and Landau roots is identical to equation (6.3) if transformation (6.4) is replaced with the following transformation:

$$\frac{\omega - \omega_0}{\omega_0} = -\left(\frac{R'Q}{P+Q}\right)x$$

$$\frac{k - k_0}{k_0} = -R'y + \left(\frac{R'P}{P+Q}\right)x$$

$$R' = \left(-\frac{n_B}{n}\,\frac{\omega_{pe}^2}{\omega_0^2}\,\frac{1}{Q}\right)^{1/3}, \quad R's = \frac{\bar{v}_B}{v_D}$$

It turns out that k_0 is the wavelength of maximum temporal growth rate while ω_0 is the frequency of maximum spatial growth rate and this offers some hope that a temporal simulation using the mode at wavelength k_0 may provide information about the mode at frequency ω_0 in the spatial problem. However, the important point to note is that the terms in the dispersion relation have been expanded about the point (ω_0, k_0). Maximum growth rate for both the temporal and spatial cases therefore occurs close to this point; thus it would seem unlikely that failure to properly distinguish between these two modes would lead to significant deviations of detail if the single-wave model is applicable to this situation.

We also need to be more clear about whether the nonlinear stage of the temporal simulation can be considered relevant to the spatial problem. However, further discussion will be better comprehended after some simulation results have been examined. Fig. 6.12 is a series of phasespace plots of the plasma particles during a simulation carried out for illustrative purposes. The region spanned by the calculation has a length of $40\lambda_D$ and the emissive wall is taken to be located at the left-hand edge ($x = 0$). The boundary conditions chosen here are that all impinging ions and electrons are absorbed but a fraction Γ_c (the critical value of the secondary emission coefficient) of the electrons are returned at $x = 0$ with zero velocity. The boundary conditions at the right-hand edge are that the ions are introduced monoenergetically at a constant rate while the introduction of electrons across the entry plane is arranged to exactly parallel those electrons crossing another plane which is a distance $10\lambda_D$ from the entry plane or $30\lambda_D$ from the wall. This is done to enforce periodicity with a wavelength of $10\lambda_D$ which is about the wavelength of the most strongly growing mode for the case of a deuterium/tritium mixture. Clearly, it does not greatly influence the wavelength of the mode that actually materialises in this case where the mass ratio is 100. The actual wavelength appears to be $\approx 5\lambda_D$. The energy of the injected ions was chosen to be that calculated for entry to the sheath for such a mixture with Γ at the critical value. The beam of electrons can be clearly seen accelerating away from the wall and after approaching a limiting velocity

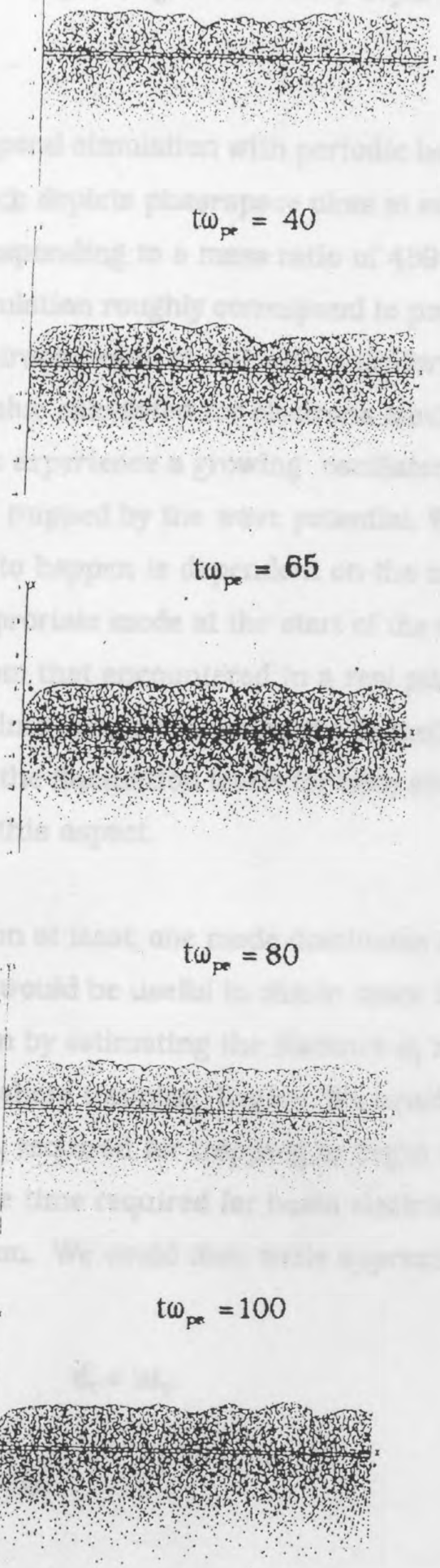

Fig. 6.12 Phasespace showing spatial development of instability

box.

The results of a temporal simulation with periodic boundary conditions are shown in Fig. 6.13 which depicts phasespace plots at successive times for beam parameters corresponding to a mass ratio of 4590 with no current. Later times in this simulation roughly correspond to positions further from the wall. The beam electrons began at t=0 with a uniform velocity corresponding to the value calculated for electrons leaving the sheath region and they can be seen to experience a growing oscillatory perturbation until they eventually become trapped by the wave potential. We must remember that the time taken for this to happen is dependent on the natural level of the perturbations in the approriate mode at the start of the simulation and that this will be different from that encountered in a real plasma. However, it will be possible to take this into account by using the formulae described later in this section to estimate the fluctuation levels for both situations and for the moment we will ignore this aspect.

Thus, in the simulation at least, one mode dominates and grows until the electrons are trapped. It would be useful to obtain some idea of the physical scale of this phenomenon by estimating the distance d_T between the wall and the approximate region where trapping begins. We could approach this by assuming that the time t_T required for trapping to begin in the temporal simulation is equal to the time required for beam electrons to travel from the wall to the trapping region. We could then write approximately:

$$d_T = ut_T \tag{6.5}$$

where u is the beam velocity.

We shall now try to examine the relation between the temporal and spatial problems with a little more precision. The paper by O'Neil and Winfrey [1972]

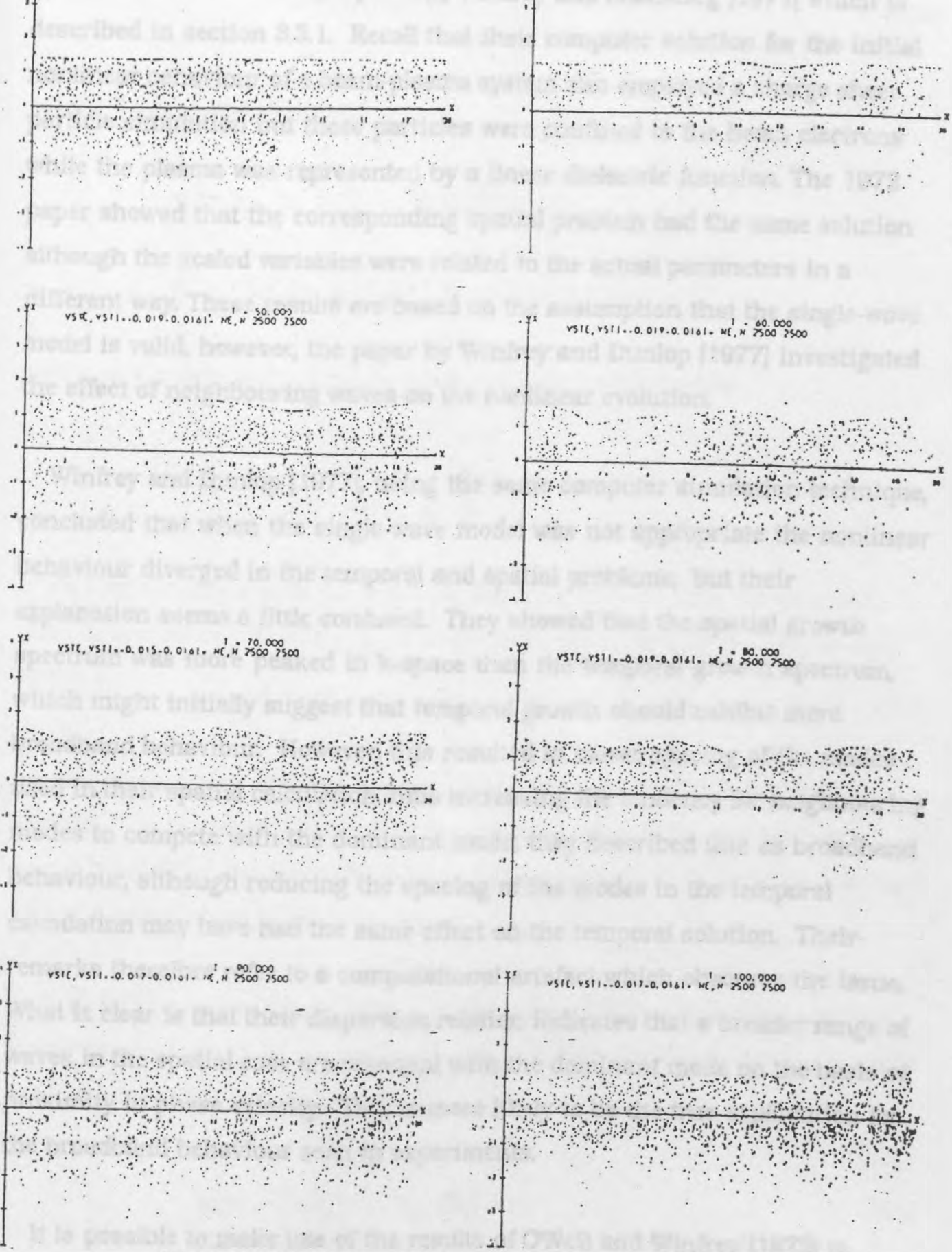

Fig. 6.13 Electron phasespace at successive times for zero current conditions with mass ratio 4590 (see also Appendix C for an enlarged version).

is an extension to the one by O'Neil, Winfrey and Malmberg [1971] which is described in section 3.3.1. Recall that their computer solution for the initial nonlinear behaviour of a beam-plasma system also employed a charge sheet particle simulation but these particles were confined to the beam electrons while the plasma was represented by a linear dielectric function. The 1972 paper showed that the corresponding spatial problem had the same solution although the scaled variables were related to the actual parameters in a different way. These results are based on the assumption that the single-wave model is valid, however, the paper by Winfrey and Dunlop [1977] investigated the effect of neighbouring waves on the nonlinear evolution.

Winfrey and Dunlop [1977], using the same computer simulation technique, concluded that when the single-wave model was not appropriate the nonlinear behaviour diverged in the temporal and spatial problems, but their explanation seems a little confused. They showed that the spatial growth spectrum was more peaked in k-space than the temporal growth spectrum, which might initially suggest that temporal growth should exhibit more broadband behaviour. However, this resulted in closer spacing of the modes used in their spatial calculation, thus increasing the tendency for neighbouring modes to compete with the dominant mode; they described this as broadband behaviour, although reducing the spacing of the modes in the temporal calculation may have had the same effect on the temporal solution. Their remarks therefore refer to a computational artefact which obscures the issue. What is clear is that their dispersion relation indicates that a broader range of waves in the spatial case are resonant with the dominant mode on the basis of proximity in phase velocity. This is more likely to be the true explanation for the broadband behaviour seen in experiments.

It is possible to make use of the results of O'Neil and Winfrey [1972] to relate the trapping time t_T of the temporal simulation to the trapping distance d_T of the spatial problem. In terms of unscaled variables they give the following transformation between the temporal and spatial coordinate:

$$t = (x/u)(\eta'/\eta)^{1/3} \tag{6.6}$$

where η and η' are given by:

$$\eta = (n_B/n_0)(\omega_{pe}^2/\omega_0^2)[(\omega_0/2)(\partial\varepsilon/\partial\omega)_{\omega_0,k_0}]^{-1}$$

$$\eta' = -(n_B/n_0)(\omega_{pe}^2/\omega_0^2)[(\omega_0/2u)(\partial\varepsilon/k)_{k_0,\omega_0}]^{-1}$$

and $\omega_0 = k_0 u$ (see section 3.1.1). Equation (6.6) thus becomes:

$$x = ut\left[\frac{1}{u}\left(\frac{\partial\omega}{\partial k}\right)_{\omega_0,k_0}\right]^{1/3}$$

If we now identify x with the trapping distance d_T and t with the trapping time t_T, and since $(\partial\omega/\partial k)_{\omega_0,k_0}$ is of the same order as u in general, we can write:

$$d_T \approx ut_T \tag{6.7}$$

which is consistent with the estimate given by equation (6.5). Actually, $(\partial\omega/\partial k)_{\omega_0,k_0}$ is always less than u, therefore equation (6.7) represents an upper limit. Thus the heuristic estimate of equation (6.5) is confirmed, at least in the context of single-wave theory.

It should be emphasised that the above workers have been able to employ simplifying approximations on the assumption that the electron beam is small, cold and fast. This requires:

$$\exp(-u^2/2v_T^2) << (n_B/n_0) << 1 \tag{6.8}$$

and

$$(\bar{v}_B/u) << (n_B/n_0)^{1/3} \tag{6.9}$$

where $\bar{v}_B$ is the thermal velocity of the beam electrons. Since $\bar{v}_B$ is zero for

$\Phi_T = 1.356$ (since $\Phi_W = -0.976$), so that $\exp(-u^2/2v_T^2) = 0.377$ and $(n_B/n_0)^{1/3} = 0.557$. The beam is therefore neither sufficiently small nor sufficiently fast for the instability to be accurately described by the analyses of this section. Of course, this is one reason why it is important to perform the particle simulation.

We next examine the applicability of the single-wave model in the case we are considering. The simulation produces nonlinearity in smaller times or distances than a real plasma since the instability grows from an artificially boosted level of energy in the mode of interest; this is because the simulation contains a restricted number of particles. The derived trapping distance will be adjusted to take this effect into account but we need to estimate the width of the wave spectrum in the simulation just before the evolution becomes nonlinear. Actually, a simulation which uses periodic boundary conditions can only allow the growth of certain discrete modes so that, depending on the spacing of the neighbouring modes, the spectrum may effectively remain artificially narrow over an extended period of time. However, we will ignore this aspect for the moment.

We need to assess whether an electron can detect the spread of wavelengths in the spectrum. Recall from section 3.1.1 that one criterion is obtained by considering whether an electron detects the modulation in wavenumber. The condition for the modulation to remain undetected over a period spanning the last few e–foldings prior to the onset of nonlinearity is therefore given by:

$$\delta k\,|(v_e - v_\phi)|\,t_2 << 2\pi$$

where t_2 is the time over which there are two e-foldings of the dominant wave, v_e is the electron velocity and v_ϕ is the phase velocity of the wave. This can be written:

$$\delta k\,|(v_e - v_\phi)| << \pi\gamma_m$$

γ_m is the linear growth rate of the dominant mode. The choice of v_e depends on which electrons have the most important role. We note that the dominant contribution to the wave potential is supplied by the plasma electrons as opposed to the beam electrons since there are many more of the former. Hence for simplicity we take v_e to be zero (the most probable velocity). The above inequality thus becomes:

$$\delta k \frac{\omega}{k} << \pi\gamma_m \tag{6.10}$$

Now recall from section 3.1.1 (equation 3.2) that after N e-foldings the width of the spectrum of waves is given by:

$$\delta k = (\ln 2)^{1/2} N^{-1/2} \Delta k$$

where Δk is the width of the linear growth spectrum and we shall assume the equivalence of this δk with that appearing in equation (6.10). Substituting this equation into condition (6.10) now gives:

$$N^{-1/2}(\ln 2)^{1/2} \Delta k \frac{\omega}{k} << \pi\gamma_m$$

Examination of the dispersion relation for the conditions of our simulation provides the following approximate values:

$$\gamma_m = 0.095$$

$$\omega/k = 1.0$$

$$\Delta k = 1.0$$

so that $N^{1/2} >> 2.79$.

Another condition can be obtained by simply requiring the spectrum width to be small. So for the single-wave model to be applicable we require $\delta k << k$ or:

$$N^{-1/2} << (\ln 2)^{-1/2}\ k/\Delta k \qquad (6.11)$$

which gives $N^{1/2} >> 1.23$.

The two assessments give different requirements but we only need to employ the least restrictive condition which is (6.11). Therefore the wavenumber spread seen by the electrons is just that of the wave spectrum itself. Thus the number of e-foldings required depends on the purity of the spectrum demanded. For example, to obtain $\delta k/k < 0.2$ requires $N^{1/2} > 5 \times 1.23$ or $N > 37.8$. To obtain $\delta k/k < 0.1$ requires $N > 151$; this cannot be satisfied by either a real or simulated plasma. Clearly, one will get an approximation to single-wave behaviour in a real plasma which is quantifiable in the fashion just outlined, but the conditions assumed here do not define perfect single-wave behaviour. However, we return to the consideration of the mode restricting nature of the periodic boundary conditions employed in the simulation.

The wavelength of the most strongly growing mode was $10\lambda_D$ for the conditions of interest and the length L of the box enclosing the simulated plasma was chosen to be twice this value. Thus the wavelengths of the only modes which were allowed are given by $\Lambda_n = 20\lambda_D/n$, $n=1,2,...$ etc. and the strongest growing mode therefore has mode number $n = 2$. The potential distribution across the box was Fourier analysed throughout the simulation and the amplitudes of the separate modes were recorded as a function of time; the development of the first three modes is plotted in Fig. 6.14 It will be noticed that, at first, mode 2 dominates until shortly after it reaches a peak at about $t\omega_{pe} = 65$ whereupon its amplitude begins to fall and is comparable with the steadily increasing amplitude of mode 1 at about $t\omega_{pe} = 85$. The peak signifies that trapping of the beam electrons has begun and

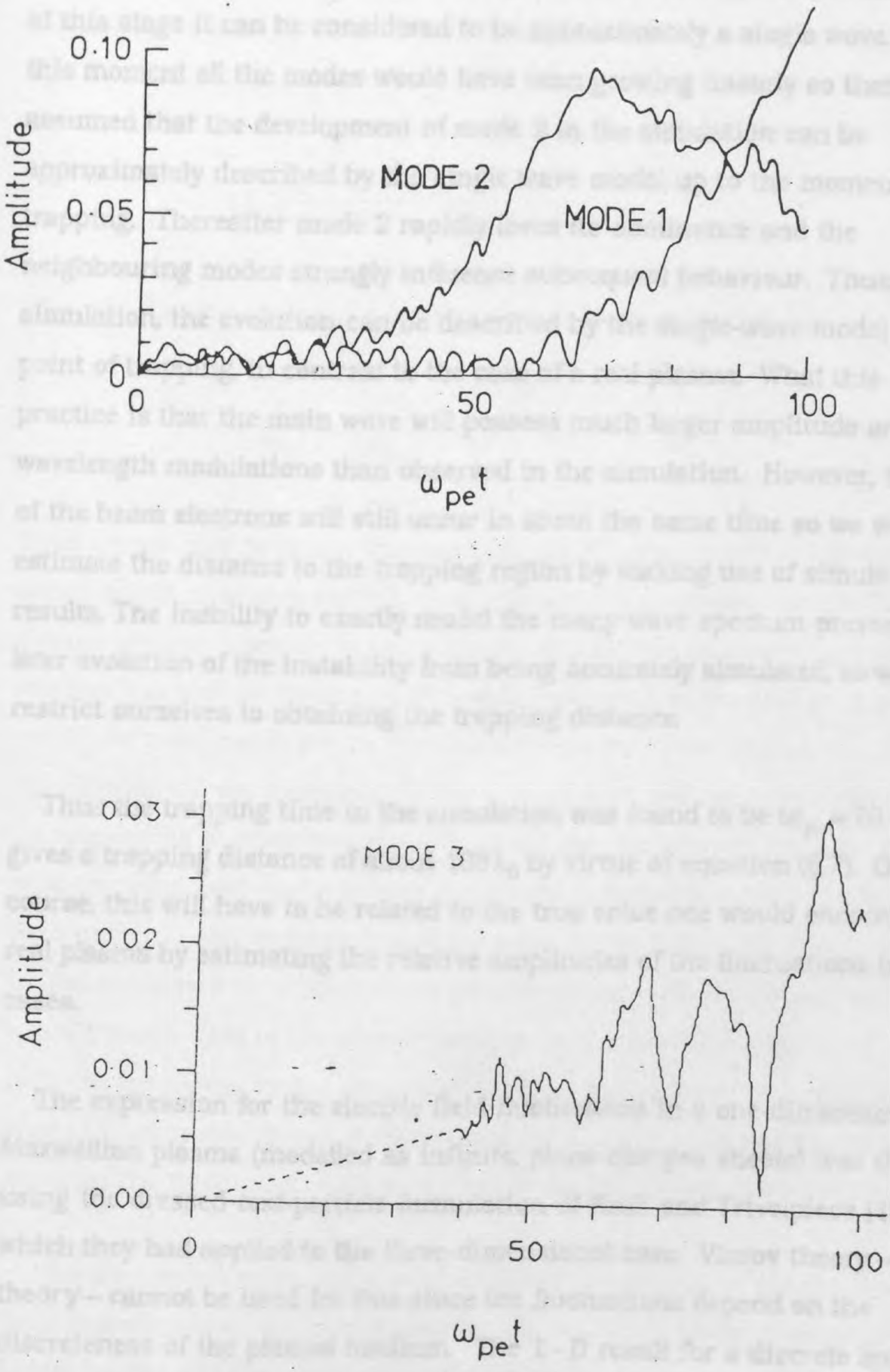

Fig. 6.14 Amplitudes of the first three modes v time.

greater than either of its neighbouring modes 1 and 3 by about a factor of 5, so at this stage it can be considered to be approximately a single wave. Prior to this moment all the modes would have been growing linearly so that it can be assumed that the development of mode 2 in the simulation can be approximately described by the single wave model up to the moment of trapping. Thereafter mode 2 rapidly loses its dominance and the neighbouring modes strongly influence subsequent behaviour. Thus, in the simulation, the evolution can be described by the single-wave model up to the point of trapping, in contrast to the case of a real plasma. What this means in practice is that the main wave will possess much larger amplitude and wavelength modulations than observed in the simulation. However, trapping of the beam electrons will still occur in about the same time so we will estimate the distance to the trapping region by making use of simulation results. The inability to exactly model the many wave spectum prevents the later evolution of the instability from being accurately simulated, so we shall restrict ourselves to obtaining the trapping distance.

Thus the trapping time in the simulation was found to be $t\omega_{pe} = 70$ which gives a trapping distance of about $103\lambda_D$ by virtue of equation (6.7). Of course, this will have to be related to the true value one would encounter in a real plasma by estimating the relative amplitudes of the fluctuations in the two cases.

The expression for the electric field fluctuations in a one-dimensional Maxwellian plasma (modelled as infinite, plane charged sheets) was derived using the dressed test-particle formulation of Krall and Trivelpiece [1973b] which they had applied to the three-dimensional case. Vlasov theory – a fluid theory – cannot be used for this since the fluctuations depend on the discreteness of the plasma medium. The 1 - D result for a discrete spectrum is:

$$\left\langle \frac{E^2}{8\pi} \right\rangle = \frac{n_0}{2n} \sum_{n=-\infty}^{\infty} \frac{KT}{1+(nk\lambda_D)^2} \frac{k}{2\pi} \qquad (6.12)$$

length and k is the smallest wavenumber accommodated by the system. So the energy in a single mode (after transformation to normalised units) is given by:

$$\langle \varepsilon_n^2 \rangle = \frac{1}{2\pi(n_i \lambda_D)} \frac{k\lambda_D}{1+(nk\lambda_D)^2} \qquad (6.13)$$

Also, the electric field and potential amplitudes are related by:

$$\langle \Phi_n^2 \rangle = \frac{1}{(nk\lambda_D)^2} \langle \varepsilon_n^2 \rangle \ , \quad \bar{\Phi}_n = \sqrt{2 \langle \Phi_n^2 \rangle} \qquad (6.14)$$

Thus we are able to obtain the potential amplitudes for any of the modes which would arise in a particle simulation of a Maxwellian plasma. The beam-plasma system, however, is not a simple Maxwellian and the dispersion relation has both beam-like and Landau type roots, so the energy at a particular wavelength will be divided between the beam and Landau modes. Specifically, we are interested in the beam mode and the amplitude of the corresponding fluctuations at $t = 0$ which can be inferred from the growth rate, trapping time and trapping amplitude of the appropriate mode. We will then make the assumption that S, the ratio of the amplitude of the beam mode to that calculated for a Maxwellian plasma, is the same for the simulation as for a real plasma. This is reasonable because we expect the energy to be divided between the modes in the same way for both cases. Since we can calculate the level of fluctuations in a real Maxwellian plasma this ratio will enable us to estimate the fluctuation level in the beam mode of a real beam-plasma system.

The simulation employed a total of 999,852 particles or charge sheets (both ions and electrons) or, approximately, $n_i \lambda_D = 25{,}000$ electron particles per Debye length, and the dispersion relation indicates that the wavenumber of the most strongly growing mode is $k\lambda_D = 0.667$. For a Maxwellian plasma, these values taken with equations (6.13) and (6.14) predict a value of 2.528×10^{-3} for the initial potential amplitude $\bar{\Phi}_{...}$ of mode 2 in either the

positive or negative wavenumber case. For the beam-plasma system we now wish to estimate the initial amplitude of the beam mode.

We can write approximately:

$$\bar{\Phi}_{sat} = \bar{\Phi}_{B0}\, e^{\gamma_n t_T}$$

where $\bar{\Phi}_{sat}$ is the saturation amplitude of the unstable wave and $\bar{\Phi}_{B0}$ is the initial amplitude of the wave. Using $\bar{\Phi}_{sat} = 0.09$, $t_T = 70$ and $\gamma_n = 0.095$ we obtain $\bar{\Phi}_{B0} = 1.165 \times 10^{-4}$. We therefore arrive at:

$$S = \bar{\Phi}_{B0} / \bar{\Phi}_{M0} = 0.046 \qquad (6.15)$$

We now turn our attention to the task of calculating the initial amplitude of the fastest growing beam mode in a real plasma. In a real plasma we have point particles instead of sheets of charge. Any magnetic field along the direction of the beam will, to a greater or lesser extent, restrict the perpendicular motion of the plasma particles but will leave the parallel motion unconstrained. Since the fluctuation spectrum for wave-vectors parallel to the field depends only on the parallel motion it might be assumed that adding the magnetic field makes no difference to the fluctuation spectrum. This will hold true for some conditions but when $\omega_{ce} >> \omega_{pe}$ (where ω_{ce} is the electron gyrofrequency) the electrons will interact more strongly (when oscillating in a Langmuir wave) if the gyroradius becomes larger than the mean inter-particle distance; this will change the results.

To find out if this combination of events can happen we characterise the inter-particle separation as $l = 1/n_0^{1/3}$ and note that the electron gyroradius is given by:

$$\rho_e = \omega_{ce}^{-1} \left(\frac{KT_e}{m_e} \right)^{1/2}$$

two distances are comparable we have:

$$n_0^{-1/3} = \omega_{ce}^{-1} \left(\frac{KT_e}{m_e} \right)^{1/2} \qquad (6.15)$$

and this can be rewritten as:

$$\omega_{ce} = \omega_{pe} (n_0 \lambda_D^3)^{1/3}$$

where $\lambda_D = (KT/4\pi ne^2)^{1/3}$. Since $n_0 \lambda_D^3$ is the number of particles per Debye sphere (usually a very large number) we can conclude that $\omega_{ce} >> \omega_{pe}$ when the gyroradius is comparable to the particle separation and the behaviour of the electrons is then much more like that of two-dimensional charge sheets moving in one dimension – as in the 1-D particle simulation code.

In order to obtain plasmas with comparable electron gyroradius and particle separation we need a specific magnetic field which is calculated by substituting $\omega_{ce} = eB/m_e c$ (where e/m_e is the electronic ratio of charge to mass and c is the velocity of light) into equation (6.15) which is rearranged to give:

$$B = \frac{c}{e} (m_e KT_e)^{1/2} n_0^{1/3}$$

$$\text{or} \quad B = 2.38 T^{1/2} n_0^{1/3}$$

in Gaussian units. This value of magnetic field would have to be greatly exceeded if the electrons were to be constrained to behave like point particles in the context of fluctuation theory.

Of course if $\omega_{pe} \geq \omega_{ce}$ then the magnetic field is too weak to influence the electrostatic fluctuations and again the electrons will behave like point particles. For this to be the case we find that:

$$\text{or } B \leq 3.2 \times 10^{-8}\, n_0^{1/2}$$

in Gaussian units. For example, we see that for a density of 10^{14}cm^{-3} the magnetic field should not exceed about 3 Tesla if the electrons are to behave like point particles. Thus, depending on the conditions, the electrons can behave like either point particles or sheet particles and we now estimate the fluctuation level for the two cases.

Consider first the sheet particle model. In order to infer the parameters relevant to a sheet model we turn to the following heuristic argument. Fig. 6.15 depicts a cylinder of radius equal to the electron gyroradius passing through a plasma with axis along a field line. The electrons enclosed by the cylindrical surface are constrained by the magnetic field to remain approximately within the volume of the cylinder and thus effectively play the role of individual charge sheets of area roughly equal to the cross-sectional area of the cylinder. The fluctuations in such a system depend on the average number of charge sheets per unit length which, in this case, is effectively given by:

$$n_l = \pi \rho_e^2 n_0$$

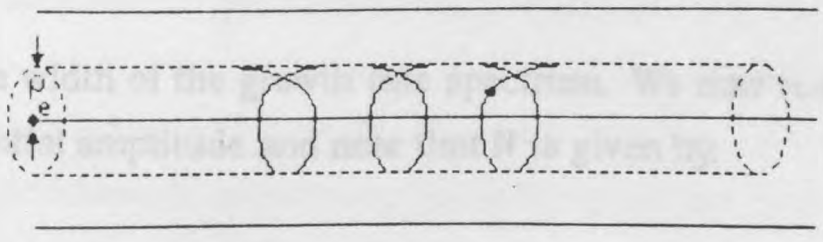

Fig. 6.15 Charge sheet model for gyrating electrons.
The solid parallel lines are magnetic field lines.

dimensional Maxwellian plasma are now assessed using the continuous spectrum version of equation (6.12):

$$\left\langle \frac{E^2}{8\pi} \right\rangle = \frac{n_0}{2n_i} \int_{-\infty}^{\infty} \frac{KT}{1+(k\lambda_D)^2} \frac{dk}{2\pi}$$

which becomes in normalised units:

$$\langle \varepsilon^2 \rangle = \frac{1}{2\pi(n_i\lambda_D)} \int_{-\infty}^{\infty} \frac{d\kappa}{1+\kappa^2}$$

where $\kappa \equiv k\lambda_D$. We are interested in the initial energy distributed over the final spread of wavelengths contained in the wave spectrum when the growth has saturated due to electron trapping. Since the wavenumber of strongest growth is 0.667 we obtain approximately:

$$\langle \varepsilon^2 \rangle = \frac{0.11\delta\kappa}{n_i\lambda_D}$$

where $\delta\kappa$ is the width of the saturated spectrum and by making use of equation (3.2) this becomes:

$$\langle \varepsilon^2 \rangle = \frac{0.11(\ln 2)^{1/2} N^{-1/2} \Delta\kappa}{n_i\lambda_D} \qquad (6.17)$$

and $\Delta\kappa$ is now the width of the growth rate spectrum. We now rewrite in terms of the potential amplitude and note that N is given by:

$$\bar{\Phi}_{sat} = \bar{\Phi}_{B0}\, e^N$$

where $\bar{\Phi}_{sat}$ is the saturation potential amplitude and $\bar{\Phi}_{B0}$ is the initial potential amplitude of the beam mode, so that equation (6.17) becomes:

$$\bar{\Phi}_{B0} = \frac{S}{(n_i\lambda_D)^{1/2}[\ln(\Phi_{sat}/\Phi_{B0})]^{1/4}} \qquad (6.18)$$

where S is given by equation(6.16). Equation(6.18) is an implicit equation for $\bar{\Phi}_{B0}$ which is easily soluble by iteration and solutions have been obtained for a wide range of the parameter $n_i\lambda_D$. The results are shown in Table 6.2.

Table 6.2

$n_i\lambda_D$	$\bar{\Phi}_{B0}$	d_T
10^5	5.69×10^{-5}	110
10^6	1.73×10^{-5}	127
10^7	5.30×10^{-6}	145
10^8	1.63×10^{-6}	162
10^9	5.02×10^{-7}	180

The range in $n_i\lambda_D$ was chosen to span the extremes corresponding to the following ranges of density and magnetic field strength:

n_0: 10^{19} - 2 x 10^{20} m^{-3}

T : 500 - 10^4 eV

B : 4 - 1T

These ranges encompass the typical operating conditions of present day tokamaks. Also shown in Table 6.2 are the corresponding trapping distances, in units of the Debye length, obtained from $\gamma_n t_T = N$ and $d_T = ut_T$. As can be seen, the trapping distance is rather insensitive to variations in the conditions and is always of the order of $100\lambda_D$.

We now consider the second case, i.e., conditions where the magnetic field is sufficiently weak to allow three-dimensional behaviour of the plasma or, alternatively, sufficiently strong to force the electrons to play the role of point

and Trivelpeice, 1973b] by:

$$\left\langle \frac{E^2}{8\pi} \right\rangle = \frac{1}{2} \int_{-\infty}^{\infty} \frac{KT}{1+(k\lambda_D)^2} \frac{dk}{(2\pi)^3}$$

where $k^2 = k_1^2 + k_2^2 + k_3^2$. As usual we transform to normalised units:

$$\left\langle \varepsilon^2 \right\rangle = \frac{1}{(2\pi)^3 (n_0 \lambda_D^3)} \int_{-\infty}^{\infty} \frac{d\kappa}{1+\kappa^2}$$

where $d\kappa = d\kappa_1\, d\kappa_2\, d\kappa_3$. We choose κ_3 to be perpendicular to the emissive wall and since we need this component we need to integrate out κ_1 and κ_2. This is accomplished by transforming to:

$$\langle \varepsilon^2 \rangle = \frac{1}{(2\pi)^3 (n_0 \lambda_0^3)} \int_{-\infty}^{\infty} d\kappa_3 \int_0^{r_c} \frac{2\pi r}{1+(r^2+\kappa_3^2)}\, dr$$

where $r^2 = k_1^2 + \kappa_2^2$ and we have introduced a cutoff r_c in the integration as the integral diverges for $r_c \to \infty$; this is an acceptable procedure because the spectrum of fluctuations does not extend to infinitesimally small wavelengths and we must assume that fluctuations with wavelengths smaller than the average inter-particle distance cannot exist. On this basis we take $r_c = 2\pi n_0^{1/3} \lambda_D$.

Thus we obtain:

$$\langle \varepsilon^2 \rangle = \int_{-\infty}^{\infty} \frac{\pi \left[\ln\{1+(r^2+\kappa_3^2)\} \right]_0^{r_c}}{(2\pi)^3 (n_0 \lambda_D^3)} d\kappa_3$$

$$\approx \int_{-\infty}^{\infty} \frac{\pi \ln \left[2\pi n_0^{1/3} \lambda_D / (1+\kappa_3^2) \right]}{(2\pi)^3 (n_0 \lambda_D^3)} d\kappa_3$$

The integrand is a very slowly varying function of κ_3 in the region of

$$\langle \varepsilon^2 \rangle \approx \frac{}{(2\pi)^3 (n_0 \lambda_D^3)}$$

Following the procedure used for the 1-D case we again obtain an implicit equation for $\bar{\Phi}_{B0}$:

$$\bar{\Phi}_{B0} = \frac{S(\ln 2)^{1/4} (\Delta\kappa)^{1/2}}{2\pi\kappa_m [\ln(\Phi_{sat}/\Phi_{B0})]^{1/4}} \left\{ \frac{\ln [2\pi n_0^{1/3} \lambda_D/(1+\kappa_m^2)]}{n_0 \lambda_D^3} \right\}^{1/2}$$

where $\Delta\kappa$ is the width of the growth rate spectrum and κ_m is the wavenumber of the dominant mode. Resulting values of $\bar{\Phi}_{B0}$ and d_T (in units of the Debye length) appear in Table 6.3. The range in $n_0\lambda_D^3$ covers all plasmas which can be physically realised. Again it is clear that the trapping distance is rather insensitive to the plasma conditions and, as before, it is of the order of $100\lambda_D$.

Table 6.3

$n_0 \lambda_D^3$	$\bar{\Phi}_{B0}$	d_T
10^9	5.71×10^{-7}	176
10^8	1.79×10^{-6}	159
10^7	5.60×10^{-6}	142
10^6	1.75×10^{-5}	126
10^5	5.49×10^{-5}	109
10^4	5.43×10^{-4}	92
10^3	1.72×10^{-4}	75
10^2	5.54×10^{-3}	58
10	6.23×10^{-3}	41

Confidence in the formulae derived for calculating the fluctuation levels can be gained by comparing their predictions with the simulation results. We assume the fluctuation level at t = 0 is approximately like that in a Maxwellian plasma and note that any mode would then be composed of positive and negative k components of equal magnitude. The result is a standing wave of amplitude equal to twice that of each component. The Fourier analysis of the simulation simply finds the resultant wave for each wavenumber and the measured amplitude of a given mode will therefore fluctuate approximately between zero and twice the amplitude of one of its

when it ceases to be an insignificant contribution to the total signal at that wavelength. This can be confirmed by examining the evolution of the amplitudes of the first four modes; the peak to peak magnitude of the fluctuations remains approximately constant with time. Table 6.4 lists the calculated and measured fluctuation energies and amplitudes of the first four modes for two values of $n_i\lambda_D$. Remember that we are considering one component (e.g. positive k) only. Considering the approximations and the coarseness of the estimation technique the agreement is extremely good.

Table 6.4

mode	$\langle\varepsilon_n^2\rangle$	$\bar{\Phi}_0$	$\bar{\Phi}_0$	$\langle\varepsilon_n^2\rangle$	$\bar{\Phi}_0$	$\bar{\Phi}_0$
No	25000	25000	25000	2500	2500	2500
n	calculated	calculated	observed	calculated	calculated	observed
1	1.82×10^{-6}	28×10^{-4}	24×10^{-4}	1.82×10^{-5}	90×10^{-4}	120×10^{-4}
2	1.43×10^{-6}	25×10^{-4}	20×10^{-4}	1.43×10^{-5}	80×10^{-4}	75×10^{-4}
3	1.06×10^{-6}	22×10^{-4}	14×10^{-4}	1.06×10^{-5}	69×10^{-4}	60×10^{-4}
4	0.78×10^{-6}	19×10^{-4}	12×10^{-4}	0.78×10^{-5}	59×10^{-4}	40×10^{-4}

As a further check we have estimated the total energy of the electric field fluctuations and compared with the simulation results using $n_i\lambda_D = 25000$. The calculated sum of energies of the first 100 modes is found to be:

$$\langle\varepsilon^2\rangle = 1.76 \times 10^{-5}$$

while the initial electric field energy was found to be:

$$\langle\varepsilon^2\rangle = 7.5 \times 10^{-6}$$

using the field energy plot shown in Fig. 6.16. Note that this graph is a plot of $\int E^2 dx$ which must be converted by dividing by the box length. The measured energy is about 50% lower than the predicted level and this is consistent with the measured amplitudes which can be seen to be about 70% of the predicted

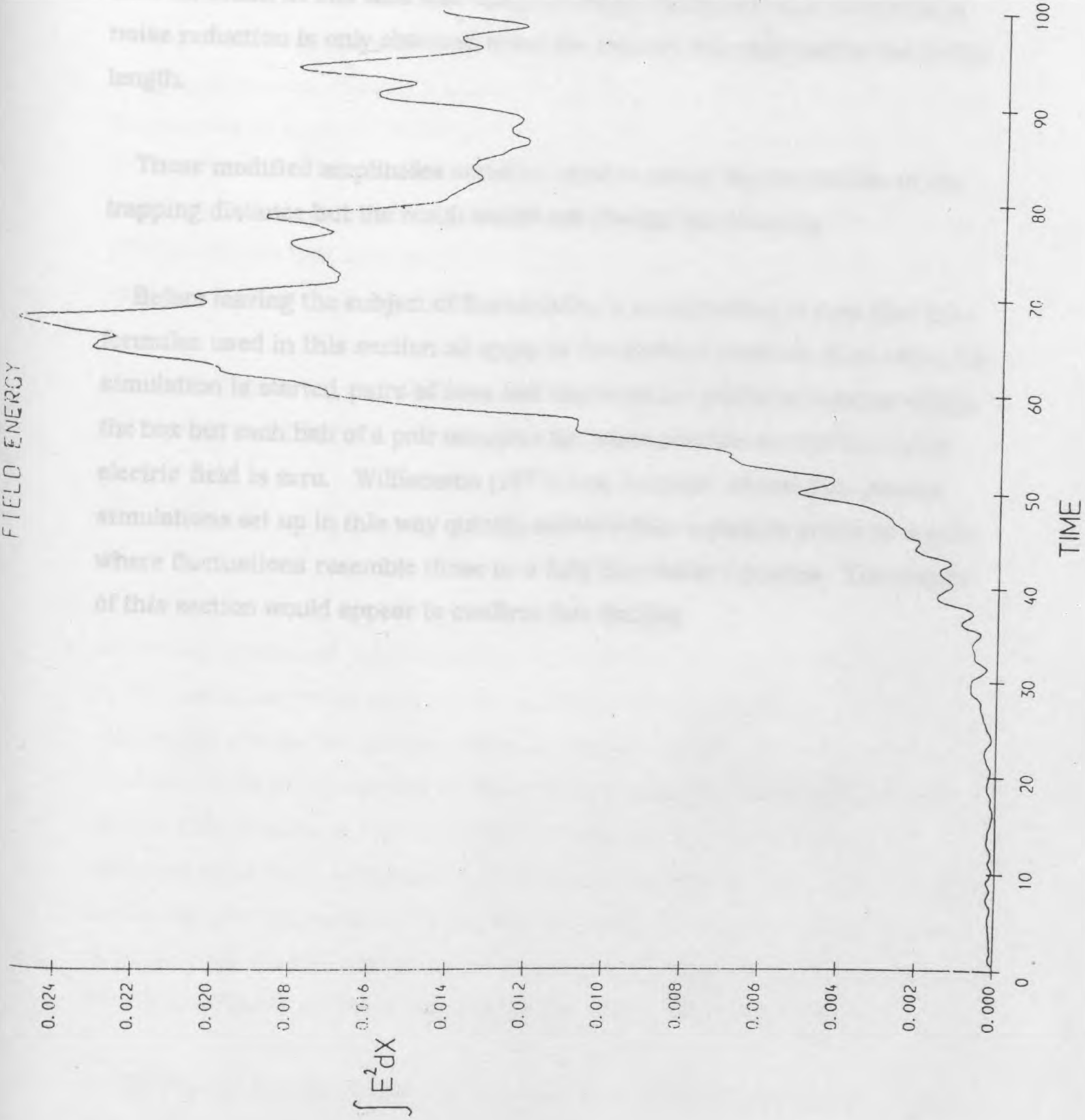

Fig. 6.16 Total field energy v time

particle size induced by using a mesh and employing the CIC charge assignment scheme. The effective particle size is determined by the mesh interval which in this case was $0.2\lambda_D$ but really significant improvements in noise reduction is only obtained when the particle size approaches the Debye length.

These modified amplitudes could be used to revise the calculation of the trapping distance but the result would not change significantly.

Before leaving the subject of fluctuations it is interesting to note that the formulae used in this section all apply to thermalised plasmas. Now, when the simulation is started, pairs of ions and electrons are placed at random within the box but each half of a pair occupies the same position so that the initial electric field is zero. Williamson [1971] has, however, shown that plasma simulations set up in this way quickly evolve within a plasma period to a state where fluctuations resemble those in a fully thermalised plasma. The results of this section would appear to confirm this finding.

6.3.1 The Effect of Collisions on the Distribution Function and Vice Versa

The evolution of the instability would ultimately be affected by collisions in a collisional plasma. However, a tokamak plasma is likely to be collisionles for the timescales involved in this problem. Even so, certain features of the developing distribution function may greatly enhance the collision rate. In a tokamak plasma conventional collisions are treated by Fokker-Planck theory which assumes that large-angle deflections of plasma particles result from very many small-angle scatterings.

The change in the distribution function of a species of particles along paricle orbits is given by:

$$\frac{\partial f}{\partial t} + \mathbf{v} \cdot \nabla f + \frac{q}{m} \mathbf{E} \cdot \nabla_v f = \left(\frac{\partial f}{\partial t} \right)_c \qquad (6.19)$$

where the right-hand side, known as the collision term, is to be determined by the particular model used for the particle interactions. Of course, in a collisionles plasma the collision term is zero and we are left with the Vlasov equation. This is appropriate for describing processes with timescales much shorter than a collision time. In a tokamak plasma individual ions and electrons exert their influences over distances of the order of a Debye length and a charged test particle will therefore be influenced by the sum of a very large number of small perturbations as it passes through the plasma. Hence the Fokker-Planck model is appropriate for sufficiently long timescales.

The Fokker-Planck equation is derivable from kinetic theory but a simpler, less rigorous derivation [Rosenbluth, 1957] is summarised here. We take $\Psi(\mathbf{v}, \Delta\mathbf{v})$ to be the probability that a particle with velocity $\mathbf{v}$ changes its velocity to $\mathbf{v} + \Delta\mathbf{v}$ in a time Δt; this is assumed to be independent of time and therefore

written:

$$f(\mathbf{r},\mathbf{v},t) = \int f(\mathbf{r},\mathbf{v}-\Delta\mathbf{v},t-\Delta t)\,\Psi(\mathbf{v}-\Delta\mathbf{v},\Delta\mathbf{v})\,d(\Delta\mathbf{v}) \tag{6.20}$$

Since the increments $\Delta\mathbf{v}$ are small we can expand equation (6.20) to second order in $\Delta\mathbf{v}$ to obtain:

$$f(\mathbf{r},\mathbf{v},t) = \int d(\Delta\mathbf{v}) \left\{ f(\mathbf{r},\mathbf{v},t-\Delta t)\,\Psi(\mathbf{v},\Delta\mathbf{v}) - \Delta\mathbf{v}\cdot\left[\frac{\partial f}{\partial\mathbf{v}}\Psi + \frac{\partial\Psi}{\partial\mathbf{v}} f\right]\right.$$

$$\left. + \frac{1}{2}\Delta\mathbf{v}\Delta\mathbf{v}:\left[\frac{\partial^2 f}{\partial\mathbf{v}\partial\mathbf{v}}\Psi + 2\frac{\partial f}{\partial\mathbf{v}}\frac{\partial\Psi}{\partial\mathbf{v}} + \frac{\partial^2\Psi}{\partial\mathbf{v}\partial\mathbf{v}} f\right] + \cdots\right\} \tag{6.21}$$

By noting that $\int_{-\infty}^{\infty}\Psi d(\Delta\mathbf{v}) = 1$ and defining the rate of change of f due to collisions as:

$$\left(\frac{\partial f}{\partial t}\right)_c = \frac{f(\mathbf{r},\mathbf{v},t) - f(\mathbf{r},\mathbf{v},t-\Delta t)}{\Delta t} \tag{6.22}$$

we obtain from equation (6.21):

$$\left(\frac{\partial f}{\partial t}\right)_c = \frac{1}{\Delta t}\int\left(-\Delta\mathbf{v}\cdot\frac{\partial}{\partial\mathbf{v}} f\Psi + \frac{1}{2}\Delta\mathbf{v}\Delta\mathbf{v}:\frac{\partial^2}{\partial\mathbf{v}\partial\mathbf{v}} f\Psi\right) d(\Delta\mathbf{v}) \tag{6.23}$$

or:

$$\left(\frac{\partial f}{\partial t}\right)_c = \frac{\partial}{\partial\mathbf{v}}\cdot\left\langle\frac{\Delta\mathbf{v}}{\Delta t}\right\rangle f(\mathbf{r},\mathbf{v},t) + \frac{1}{2}\frac{\partial^2}{\partial\mathbf{v}\partial\mathbf{v}}:\left[\left\langle\frac{\Delta\mathbf{v}\Delta\mathbf{v}}{\Delta t}\right\rangle f(\mathbf{r},\mathbf{v},t)\right] \tag{6.24}$$

where:

$$\left\langle \frac{\Delta \mathbf{v}}{\Delta t} \right\rangle = \frac{1}{\Delta t} \int f(\mathbf{r}, \mathbf{v}, t)\ \Psi(\mathbf{v}, \Delta \mathbf{v}) \Delta \mathbf{v}\, d(\Delta \mathbf{v})$$

$$\left\langle \frac{\Delta \mathbf{v} \Delta \mathbf{v}}{\Delta t} \right\rangle = \frac{1}{\Delta t} \int f(\mathbf{r}, \mathbf{v}, t)\, \Psi(\mathbf{v}, \Delta \mathbf{v}) \Delta \mathbf{v} \Delta \mathbf{v}\, d(\Delta \mathbf{v}) \qquad (6.25)$$

In order to evaluate the quantities (6.25) the function Ψ must be derived from details of the collision model. A diagram representing a small-angle binary collision appears in Fig. 6.17 in which the impact parameter b is defined. The analysis of this encounter leads to the following results:

$$\left\langle \frac{\Delta \mathbf{v}}{\Delta t} \right\rangle = - \frac{4\pi\, \bar{n}_\alpha\, q_T^{\,2} q_\alpha^{\,2}\, \ln\Lambda}{\mu_\alpha m_T} \int f_\alpha(\mathbf{v}') \frac{\mathbf{v} - \mathbf{v}'}{|\mathbf{v} - \mathbf{v}'|^3}\, d\mathbf{v}'$$

$$\left\langle \frac{\Delta \mathbf{v} \Delta \mathbf{v}}{\Delta t} \right\rangle = \frac{4\pi\, \bar{n}_\alpha q_T^{\,2} q_\alpha^{\,2}\, \ln\Lambda}{m_T^{\,2}} \frac{\partial^2}{\partial \mathbf{v} \partial \mathbf{v}} \int f_\alpha(\mathbf{v}') |\mathbf{v} - \mathbf{v}'|\, d\mathbf{v}' \qquad (6.26)$$

The subscript T denotes quantities relating to the test particle in collision with plasma species denoted by α. Note that the quantity ln Λ has replaced $\ln \frac{b_{max}}{b_{min}} = \int_{b_{min}}^{b_{max}} db/b$ which arises in the calculation. The limits 0 and ∞ cannot be used in this integral because it would diverge. So λ_D is chosen for b_{max} as the Coulomb potential is screened beyond this distance and b_{min} is taken as $Ze^2/3KT$ which is a lower limit for the validity of the approximations used for small angles of scatter (large angle scattering is very rare as has already been stated). The integral is not sensitive to the coarseness of these gross approximations and we therefore define:

$$\Lambda = \frac{3}{2} \left(\frac{K^3 T^3}{\pi n_e} \right)^{1/2} \frac{1}{Ze^3}$$

Substituting equations (6.26) into equation (6.24) we finally obtain the Fokker-Planck equation:

$$\left(\frac{\partial f_T}{\partial t} \right)_c = \sum_\alpha \left[- \frac{\partial}{\partial v_i} \left(f_T \frac{\partial h_\alpha}{\partial v_i} \right) + \frac{1}{2} \frac{\partial^2}{\partial v_i \partial v_j} \left(f_T \frac{\partial^2 g_\alpha}{2\, \partial v_i \partial v_j} \right) \right] \frac{4\pi\, \bar{n}_\alpha q_T^{\,2} q_\alpha^{\,2}}{m_T^{\,2}} \ln\Lambda \qquad (6.27)$$

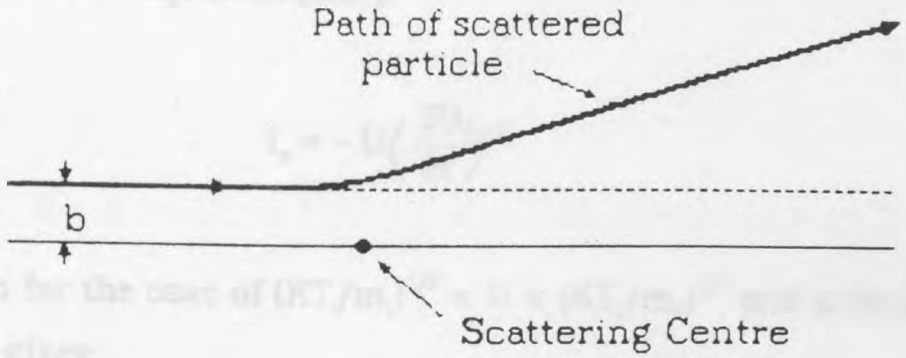

Fig. 6.17 Small-angle binary collision

where the first term is known as the coefficient of dynamical friction and the second the coefficient of diffusion. The functions appearing in this equation are depicted as:

$$\left.\begin{aligned} g_\alpha(\mathbf{v}) &= \int f_\alpha(\mathbf{v}')\,|\mathbf{v}-\mathbf{v}'|\,d\mathbf{v}' \\ h_\alpha(\mathbf{v}) &= \frac{m_T}{\mu_\alpha}\int \frac{f_\alpha(\mathbf{v}')}{|\mathbf{v}-\mathbf{v}'|}\,d\mathbf{v}' \\ \mu_\alpha &= \frac{m_T\, m_\alpha}{m_T + m_\alpha} \end{aligned}\right\} \qquad (6.28)$$

and the Landau contour (see Fig. 2.1) must be used to evaluate the integrals in equations (6.28).

characterstic times for collision processes by taking moments of it. Multiplying equation (6.27) by $\mathbf{v}$ and integrating with respect to $\mathbf{v}$ produces an equation for the time rate of change of the velocity U of a beam of incident particles since we define $U \equiv \int f \mathbf{v} d\mathbf{v}$. We then define the slowing down time for a beam of particles impinging on a plasma with distribution given by the right hand side of equation (6.27):

$$\tau_s \equiv - U\left(\frac{\partial U}{\partial t}\right)^{-1}$$

which for the case of $(KT_i/m_i)^{1/2} < U < (KT_e/m_e)^{1/2}$ and a delta function beam gives:

$$\tau_s \approx \frac{m_T^2}{4\pi n_e e^2 q_T^2 \left[\frac{Z}{U^3}\left(1+\frac{m_T}{m_i}\right)+\frac{4}{3\sqrt{\pi}}\left(1+\frac{m_T}{m_e}\right)\left(\frac{m_e}{2KT_e}\right)^{3/2}\right]\ln\Lambda}$$

These integrations retain only the dynamical friction term which confirms the choice of name.

Measures of the speed with which a beam evolves an isotropic distribution and with which its particles spread in velocity are obtained by multiplying equation (6.27) by $\mathbf{v}^2$ and integrating with respect to $\mathbf{v}$. It is best to separate the components parallel and perpendicular to the initial direction. The result for $\partial(U_{\|}^2)/\partial t$ contains both the friction and diffusion terms while that for $\partial(U_{\perp}^2)/\partial t$ involves only the diffusion term. The characterisitic time for progress towards isotropy is obtained by defining a deflection time:

$$\tau_D \equiv \frac{U^2}{\partial U_{\perp}^2/\partial t}$$

When $U \approx (KT_e/m_e)^{1/2}$ for a beam of electrons this becomes:

$$\tau_D = \frac{}{\sqrt{2}\pi n_e e^4 \ln\Lambda}\left[\phi(1) + \frac{2e^{-1}}{\sqrt{\pi}} + 2\right]$$

where ϕ is the error function given by $\phi(x) = \frac{2}{\pi^{1/2}}\int_0^x \exp(-y^2)\,dy$.

We can also define a time for the exchange of energy:

$$\tau_W = \frac{-W}{\partial W/\partial t}$$

where $W = \frac{1}{2} m_T U^2$. And for a beam of electrons of speed $U = (2KT_e/m_e)^{1/2}$ we get:

$$\tau_W \approx \frac{m_e^{1/2}(2KT_e)^{3/2}}{8\pi n_e e^4[\phi(1) - 4e^{-1}/\sqrt{\pi}]\ln\Lambda}$$

The above collisional times are appropriate for a beam of secondary electrons leaving a wall with Γ at the critical value and streaming into the plasma. This is because under these conditions the beam velocity is of the order of the plasma electron thermal velocity. In the case of a deuterium-tritium plasma we have $m_T = m_e$, $q_T = -e$ and $Z \approx 1\frac{1}{2}$; this gives the result that $\tau_W \approx \frac{5}{4}\tau_s$, $\tau_D \approx 10\tau_s$. We therefore use τ_s as our collision time and note that a typical plasma in the JET Tokamak would have a collision time of $\tau_s\omega_{pe} \approx 5 \times 10^6$ while a plasma capable of supporting thermonuclear reactions would have a collision time of $\tau_s\omega_{pe} \approx 4 \times 10^7$.

The relevance of these collisions to the beam-plasma instability is that they will gradually destroy any system of waves which may survive the nonlinear stages of the evolution. The tendency of collisions is to push the particle distribution function towards a Maxwellian. However, this involves the extension of the negative slope region of the distribution to larger phase velocities and that implies negative wave growth according to the formula for Landau damping (see equation 2.14). Thus, we can expect these processes to be accompanied by the damping of waves which have their phase velocities in this region. It should be noted, however, that the Landau damping formula

perturbation, i.e., that the wave is of small amplitude. So the approximation will be less good for large amplitude waves.

It will be useful to consider the timescale for the collisional destruction of a BGK mode since, as we have seen, the later stages of the beam-plasma instability may strongly resemble such a mode. We will call it a quasi-BGK mode since the finite width of the wave spectrum is also expected to cause the gradual destruction of the mode with consequent broadening and probable flattening of the spectrum. This problem has been analysed by Zakharov and Karpman [1963] and the rate given for the collisional destruction of a BGK mode is:

$$\gamma_{c.d.} = \beta \left(\frac{kv_{th}}{\omega}\right)^2 \frac{\tau_{osc}\gamma_M}{\tau_{coll}} \qquad (6.29)$$

where $\beta \approx 3$, γ_M is the Landau damping rate for a Maxwellian plasma, $\tau_{osc} = (m_e/e\phi k^2)^{1/2}$ is the 'bounce' time of the trapped electrons in the wave trough and τ_{coll} is the collision time. This formula reflects the interaction of two mechanisms: the collisions attempting to change the distribution towards a Maxwellian and the resulting positive slope reducing the wave amplitude by the equivalent of Landau damping. The damping, of course, has a tendency to reduce the slope.

As explained in sections 6.1 and 6.2 the instability is not expected to evolve into a genuine BGK mode but it will probably resemble one at some stage of its development. Taking as an example conditions typical of a JET plasma, one might have a collision time of $\tau_{coll}\omega_{pe} \approx 10^7$ and for the parameters of the instability in a deuterium-tritium plasma which we have been considering we have: $\tau_{osc}\omega_{pe} \approx 3$, $\gamma_M/\omega_{pe} \approx 0.6$, $kv_{th}/\omega \approx 1$, so that the time for the collisional destruction of the BGK mode becomes:

$$\tau_{c.d.}\omega_{pe} \approx 2.10^6$$

velocity, the wave structure would be destroyed within about $2.10^6\lambda_D$ from the wall. However, this would correspond to a distance of about 40m or so since $\lambda_D \approx 2.10^{-5}$m. Thus ordinary collisions probably do not play a role in the development of this instability under conditions such as these.

We must remember that a BGK mode is an ideal which will probably never be reached by the evolving plasma. As we have seen in section 6.1, depending on the conditions, the trapped electrons may gradually spiral in towards the centre of the phasespace voids so that the distribution function in these regions may ultimatlely appear approximately flat on a coarse scale but on a fine scale the spiral pattern constitutes a very jagged distribution. This feature of the distribution function will strongly affect the term containing the ∇^2 operator in the Fokker-Planck equation and on this basis we shall estimate a new slowing down time. The estimate will be very approximate since we shall assume that, after the initially trapped electrons have performed ten spirals, the collision time will be reduced by a factor of 100, and so on. One spiral is executed in a bounce time so after a time t the effective collision *time* is given by:

$$\tau_{c_{eff}} = \left(\frac{\tau_{osc}}{t}\right)^2 \tau_c$$

Since this parameter is continuously dropping we can obtain a rough value by setting $t = \tau_{c_{eff}}$. Thus we have:

$$\tau_{c_{eff}} \approx (\tau_{osc}\, \tau_c)^{1/3}$$

and using our previous values we obtain $\tau_{c_{eff}}\omega_{pe} \approx 450$. We now replace τ_{coll} in equation (6.26) with $\tau_{c_{eff}}$ and obtain a new rate for the collisional destruction of the wave structure: $\tau_{c.d.}\omega_{pe} \approx 100$. Of course, the multi-wave nature of the problem for these conditions may in the first place prevent the formation of a distribution resembling a BGK mode [Buchelnikova and

phasespace fine-structure can have a large effect on collision rates.

The previous treatment of collisions depended on the fine-grain jaggedness of the distribution function resulting from the spiralling of the trapped electrons. However, electrons do not have to be trapped for the distribution function to develop this kind of fine-grain structure. To see this we recall the Case-Van Kampen modes discussed in section 2.1. These can be represented by $f_1(x,v,t) = \bar{f}_1(v) \exp i(kx - \omega t)$ where $\bar{f}_1$ is given by:

$$\bar{f}_1(v) = P\left[\frac{(\omega_{pe}^2/k^2)\,\partial g/\partial v}{v - \omega/k}\right] + \delta(v - \omega/k)\left[1 - P\int_{-\infty}^{\infty} \frac{(\omega_{pe}^2/k^2)\,\partial g/\partial v'}{v' - \omega/k}\,dv'\right] \quad (6.30)$$

where P is the principal value. Strictly speaking, an individual mode is non-physical because the delta function in equation (6.30) renders f_1 infinite when $v = \omega/k$! However, we are able to recover the normal Fourier components by summing the Case-Van Kampen modes over ω; we then have:

$$f_1(v,k) = e^{ikx}\int_{-\infty}^{\infty} e^{-i\omega t}\,\bar{f}_1(v,\omega)\,c(\omega)\,d\omega \quad (6.31)$$

where the weighting function $c(\omega)$ is chosen to fit a given initial condition $f_1 = f_1(v,k,t=0)$. This process also removes the singularities present in equation (6.30). If we now substitute equation (6.30) into equation (6.31) we obtain:

$$f_1(v,k) = e^{ikx}\,\frac{\omega_{pe}^2}{k^2}\,\frac{\partial g}{\partial v}\,P\int_{-\infty}^{\infty} \frac{e^{-i\omega t}\,c(\omega)}{v - \omega/k}\,d\omega$$

$$+ k\,e^{ik(x - vt)}\,c(\omega = kv)\left[1 - P\int_{-\infty}^{\infty} \frac{(\omega_{pe}^2/k^2)\,\partial g/\partial v'}{v' - v}\,dv'\right] \quad (6.32)$$

It will be noticed that the term $k\,e^{ikx}\,c(\omega=kv)\,e^{-ikvt}$ in equation (6.32) does not damp away at late times but instead its oscillations in velocity space become ever more compressed. Thus a significant perturbation will eventually

modify the friction term of the Fokker-Planck equation and thereby reduce the effective collision time, just as in the case of trapped electrons.

6.3.2 Sheath Stability

The relation between the spatial and temporal growth solutions for the beam-plasma instability, as discussed in section 6.2, strictly depended on an assumption of linearity, i.e., the background plasma was described by linear theory, but after trapping occurs we know that the behaviour of much of the plasma in our simulations is nonlinear. We therefore consider the question of whether this nonlinearity will modify the results for the region of plasma near the wall for which linear theory was originally assumed to be valid and we would like to know, in particular, whether the sheath remains stable as linear theory predicts. Computer simulation cannot answer this question since it is impossible to represent the whole plasma so we resort to a rather heuristic treatment of the problem.

We begin by noting that the nonlinear region of the plasma will only affect or modify the linear region through the action of the plasma moving from the nonlinear to the linear region. If this plasma carries a 'memory' of the nonlinear influences back to the sheath then the original nonlinear treatment of this region may not be adequate. To simplify the discussion we shall assume that at some point beyond the sheath there exists a region of indefinite extent where the solution at some time resembles a BGK mode. We next observe that the plasma in this region travelling towards the wall can be represented by a large number of beams each of which has a different total energy and we consider just one of these beams during this time. We are interested in whether there exists an equilibrium solution for the beam which we shall model using the following fluid equations:

$$\frac{\partial v}{\partial t} + v\frac{\partial v}{\partial x} + \frac{q_T}{m_i}\frac{\partial \phi}{\partial x} = 0 \qquad (6.33)$$

$$\frac{\partial n_T}{\partial t} = -\frac{\partial}{\partial x}(n_T v) \tag{6.34}$$

These constitute the equation of motion and the equation of particle conservation. We now define $x = x_0$ and $v = v_0$ when $\phi = \phi_0 = 0$ and set $\partial v/\partial t = \partial n_T/\partial t = 0$ since we are looking for equilibrium solutions; this implies that we are working in the wave frame. Equations (6.33) and (6.34) are now integrated from x_0 to x giving respectively:

$$v^2 = v_0^2 - \frac{2q_T\phi}{m_T} \tag{6.35}$$

$$n_T v = \Gamma_T \tag{6.36}$$

where Γ_T is the constant particle flux carried by the beam. Eliminating v from equations (6.35) and (6.36) gives:

$$n_T \approx \frac{\Gamma_T}{v_0}\left(1 + \frac{q_T\phi}{m_T v_0^2}\right) \tag{6.37}$$

where we have assumed that $2q_T\phi/m_T v_0^2 \ll 1$ and employed the binomial expansion. So the density perturbation is proportional to the potential and this in turn gives rise to a contribution to the total potential. The magnitude of the contribution can be obtained from the Poisson equation:

$$\nabla^2\phi = -4\pi\rho$$

We consider the charge density ρ to be composed of two components, i.e., the elemental beam charge density ρ_{el} and the charge density ρ_p of the remaining plasma as a whole, so we have:

$$\rho_{el} = \rho_0 + \rho_1$$

$$\rho_p = \rho_{p0} + G(x)$$

where G(x) is a periodic function of x with wavelength equal to that of the potential variation. At the nodes in the potential we have $\rho_1 = \phi = G = 0$ and by assuming quasineutrality ($\rho_{el} + \rho_p \approx 0$) at these points we deduce that $\rho_0 + \rho_{p0} = 0$, hence we have:

$$\rho = \rho_1 + G(x)$$

Thus the Poisson equation becomes:

$$\nabla^2\phi = -4\pi \frac{q_T\Gamma_T}{v_0}\left[\frac{q_T\phi}{m_T v_0^2} + \frac{G(x)v_0}{q_T\Gamma_T}\right]$$

and if we now assume the perturbation to be sinusoidal then $\phi = \bar{\phi}\sin kx$, $G(x) = \bar{G}\sin kx$ which when substituted in the Poisson equation leads to:

$$\bar{\phi} = \frac{\bar{G}v_0}{q_T\Gamma_T\left(\frac{v_0 k^2}{4\pi q_T\Gamma_T} - \frac{q_T}{m_T v_0^2}\right)}$$

which is of course the total wave amplitude in terms of the plasma density variation G and the elemental beam characteristics. We are, however, more interested in the elemental beam contribution separately, and for this purpose we substitute $\rho = \rho_1$ into the Poisson equation giving:

$$\nabla^2\phi_b = -\frac{4\pi n_T q_T^2 \phi}{m_T v_0^2}$$

where ϕ_b is the potential contributed by the elemental beam which is assumed to be given by $\phi_b = \bar{\phi}_b \sin kx$. This leads to:

$$\bar{\phi}_b = \frac{4\pi n_T q_T^2}{m_T v_0^2 k^2}\ \bar{\phi}$$

The plasma streaming towards the wall is of course characterised by a distribution, i.e., it is composed of a set of beams and we can write:

$$\bar{\phi}_w = \int_{-\infty}^{0} \frac{4\pi q_T^2 f(v_0)}{m_T v_0^2 k^2}\, dv_0\ \bar{\phi}$$

where $\bar{\phi}_w$ is the wave amplitude contributed by the wall-directed flux. So the contributed fraction is independent of the wave amplitude. If the solution is valid then the result holds in the nonlinear region and also right down into the thermal fluctuation levels of the sheath region. In that case the nonlinear region has no permanent effect on the plasma moving towards the wall and we would conclude that the original linear theory results still apply to the volume of plasma between the wall and the trapping region. Thus it is now necessary to attend to the problem of what conditions are required for the validity of the equilibrium solution discussed above.

We again consider equations (6.33) and (6.34) and eliminate $\partial v/\partial x$ to obtain:

$$\frac{\partial v}{\partial t} - \frac{v}{n_T}\frac{\partial n_T}{\partial t} = \frac{q_T}{m_T}\frac{\partial \phi}{\partial x} + \frac{v^2}{n_T}\frac{\partial n_T}{\partial x} \qquad (6.38)$$

To be able to neglect the time dependent terms we can see that the right hand side of equation (6.38) must be small compared to either of its terms. Differentiating equation (6.37) and using $\phi = \bar{\phi}\sin kx$ gives us:

$$\frac{\partial \phi}{\partial x} = \bar{\phi}\cos kx$$

and

$$\frac{\partial n_T}{\partial x} = -\frac{\Gamma_T q_T \bar{\phi}}{m_T v_0^3}\cos kx$$

which can be substituted into the right hand side of equation (6.38) to give us the condition that:

$$\frac{q_T \bar{\phi} \cos kx}{m_T} - \frac{\Gamma_T q_T \bar{\phi}}{n_T m_T v_0} \cos kx$$

must be small, or after substituting for n:

$$\frac{\dfrac{q_T \bar{\phi} \cos kx}{m_T} - \dfrac{q_T \bar{\phi} \cos kx}{m_T}\left(1 - \dfrac{q_T \bar{\phi} \sin kx}{m_T v_0^2}\right)}{\dfrac{q_T \bar{\phi} \cos kx}{m_T} + \dfrac{q_T \bar{\phi} \cos kx}{m_T}} \ll 1$$

This finally reduces to:

$$\frac{q_T \bar{\phi}}{2 m_T v_0^2} \ll 1 \qquad (6.39)$$

Since the potential amplitude required to trap the electron beam is given by $2q_T \bar{\phi} \approx m_T v_0^2$ then condition (6.39) can be interpreted to mean that the equilibrium or time-independent solution, given previously, will be valid if the wave amplitude is smaller than that required to trap the beam. For the case of the deuterium-tritium plasma which we have already studied the above condition is satisfied for the plasma flowing towards the wall and we therefore know that when this plasma reaches the sheath it will not carry any influence from the higher field regions where trapping of the secondary electron beam has occurred. We are thus able to conclude that the nonlinear stage of the instability in this case does not destroy the stability of the sheath.

CHAPTER 7

Discussion

This chapter summarises the goals which have been achieved and analyses a number of aspects of the work.

7.1 Summary

7.1.1 The Main Findings

a) Novel derivation of the Bohm Criterion.

The instability with which we have been concerned is made possible by virtue of the sheath, hence the importance of the Bohm criterion. This led to an examination of the validity of this criterion during which a novel derivation was discovered (see section 5.3.2). The criterion was found to follow from minimising the wall potential which, in turn, suggested the possibility of an underlying principle.

b) A suggested principle determining the configuration of a plasma

The need for some principle was felt when a calculation for a hypothetical plasma system with 'single-point ionisation' (section 5.3.3) appeared to lack a clear choice for one of the boundary conditions. It was suggested that plasma systems adopt the minimum wall-potential consistent with monotonicity of the potential profile and that this value of wall-potential is stationary with respect to small changes in the boundary conditions. This was consistent with the conclusions based on the Bohm criterion and the 'plasma equation' analysed in section 5.3.1; the suggestion was also confirmed by the particle-simulation code when applied to the 'single-point' problem.

Equations describing the above system have been derived and solved in section 5.3.3.

d) Solution of the sheath equations with secondary emission.

Since the beam derives from secondary electrons it was necessary to solve the equations for a plasma bounded by an emissive wall (see sections 5.1 and 5.2).

e) Development of a particle-simulation code.

The results from the previous calculations supplied input to the particle simulation code developed especially to determine the evolution of the instability (see section 4.2).

f) Confirmation of the predictions of Hobbs-Wesson equations.

Tests with the simulation confirmed the correctness of the solution to the Hobbs-Wesson equations (see section 5.1.2).

g) Equilibrium for the single-point ionisation case modelled.

The particle simulation was used to model the 'single-point' ionisation plasma system and confirm the equations derived for this case (see section 5.3.3).

h) Beam-plasma instability modelled

The beam-plasma instability was modelled with the particle-simulation using parameters relevant to the secondary emission case. Owing to limitations of computer resources, the simulation could only qualitatively illustrate how the nonlinear phase of the instability

crucial parameter determined from these results was the relative fluctuation energies in the beam and Landau modes which enabled the distance to the trapping region to be calculated (see sections 6.1 and 6.2).

h) Dependence of thermal fluctuation levels on the strength of the magnetic field.

A real physical plasma is three-dimensional and it was necessary to determine when it could be represented by a 1-D charge sheet model in order to estimate the thermal fluctuation levels at the relevant frequencies. When the magnetic field is sufficiently weak the 3-D nature of the plasma must be properly treated and it was necessary to derive the equivalent 1-D fluctuation levels for such conditions see section 6.2).

i) Estimate of collision time for the late evolution of the instability.

The ultimate behaviour of the instability after long times (or large distances from the wall) remains speculative but an effective collision time has been estimated on the basis that the electrons develop a very jagged distribution function (see section 6.3.1). The complete suggested evolution deserves a separate section and is therefore described more fully in section 7.1.2.

j) Stability of the sheath.

A condition for the stability of the sheath is derived and found to indicate stability for the conditions considered (see section 6.3.2).

7.1.2 The Evolution of the Instability

We now describe the picture that has emerged of the development of the instability in the secondary emission problem. Secondary electrons are emitted from a wall confining a plasma and, after being accelerated through the sheath, these electrons pass through the plasma as a monoenergetic beam. Such a system will develop the beam-plasma instability

is peaked in velocity space and has a range of phase velocities in the frame of the plasma lying below the velocity of the beam.

At first, the waves grow linearly until the dominant mode is large enough to trap the beam electrons. At this stage the wave spectrum may be narrow enough to affect the electrons as a single wave and the single-wave model would then be appropriate for describing the behaviour of the system until neighbouring waves were large enough to significantly affect the motion of the electrons.

Typically, the instability develops by causing an initially sinusoidal perturbation of the beam in phasespace at the wavelength of the dominant mode, until the beam electrons are trapped to form a rotating clump; this gives rise to oscillations in the amplitude of the saturated wave. This process does not continue indefinitely, however, as neighbouring waves continue to grow and eventually become significant enough to affect the trapped electrons, smearing them out in phasespace and thus flattening the distribution function in the range of velocities spanned by the beam detectors. Quite apart from neighbouring waves, phase-mixing may also be a significant homogenising factor, depending on the conditions. At this point the electron distribution function may closely resemble that of a BGK mode; this is only a temporary state, however, since there are many waves in the system giving rise to fluctuations in the distribution function and ensuring continued evolution through the process of detrapping. Unless new processes influence the development, the distribution function will ultimately become flat in the region of velocity space spanned by the spectum of waves, and will become spatially homogeneous.

One mechanism which may modify or succeed the flattening process described above is a secondary instability. It is likely that if the spatially averaged distribution function develops or retains a minimum then further instability will arise. Depending on the parameters, the evolution may resemble that of the initial beam-plasma instability with a dominant

homogeneous development. A succession of such instabilities may be described as "cascading" and is considered by other workers Winfrey and Dunlop [1977].

For the parameters used in our simulations the primary instability would not appear to evolve towards a spatially averaged distribution with a minimum in velocity space and secondary beam-plasma instabilities are, presumably, not relevant here. For the case of mass ratio 4590 with floating conditions it was concluded that single wave theory did not accurately describe any part of the evolution because the wave spectrum was not narrow enough to constitute a single mode. In such a case one should perhaps talk of a predominant as opposed to a dominant mode. Modes1 and 2 are shown in Fig. 6.14 and it can be seen that mode1 displaces mode 2 from dominance after $t\omega_{pe} = 85$. It appears to have maintained its linear growth rate during this period. A succession of neighbouring modes is expected to grow and dominate temporarily until the distribution is flattened in this region in a manner reminiscent of the quasilinear theory predictions.

The advanced stages of the instability for other conditions may not be determined solely by the many-wave picture described so far; the continuous shifting of electron orbits observed in the simulations leads to a distribution function with ever more "corrugations" - a new one appearing about every bounce period of the trapped electrons. These features increase the magnitude of the friction term containing ∇^2 in the Fokker-Planck equation and enhance the effective collision rate. If the distribution resembles a BGK mode at this stage, it will therefore be destroyed more quickly than would a real BGK mode expressed in a smooth distribution function. There is also the possibility that phase-mixing is by itself sufficient to cause the amplitude osallations to be destroyed (see section7.2.2).

The 3 sets of conditions which have been simulated can be represented on a diagram depicting the wall-potential — beam-density plane (Fig.7.1). The available region is bounded by two lines representing floating conditions and

the inequality of equation 6.8, one satisfying it by an order of magnitude and the other simply satisfying the equality. This division of parameter space is related to work reported recently by Buchelnikova and Matochkin [1987] (see section 7.2.4).

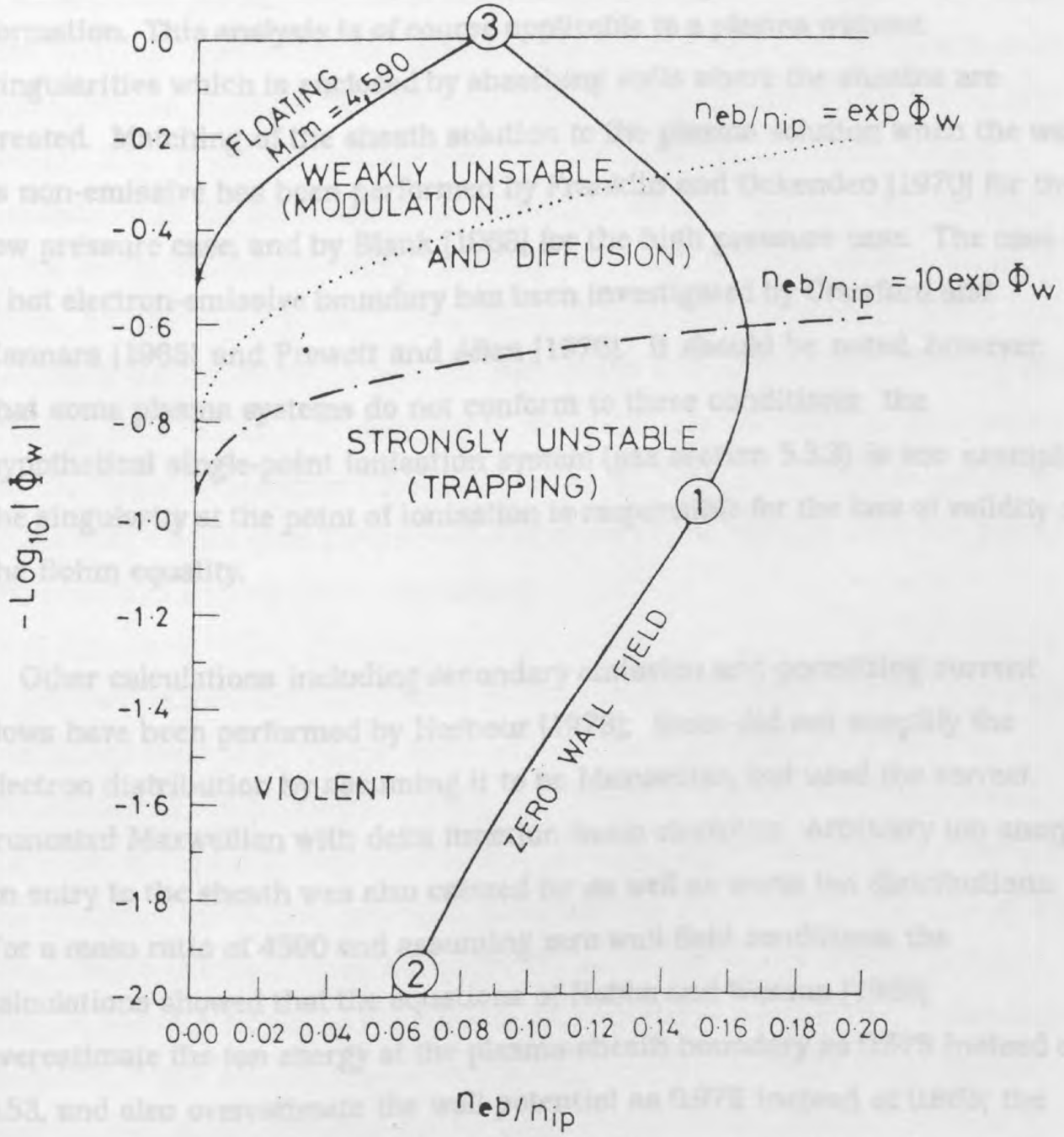

Fig. 7.1 The wall-potential – beam density plane, showing the physically accessible region bounded by lines representing zero wall-field and zero current or 'floating' conditions; the latter is a function of mass ratio. The positions of the three circled numbers indicate the conditions for which results have been reported in chapter six. Cases 1 and 2 represent the conditions corresponding to Φ_w - 10 and Φ_w = - 100 respectively. Case 3 corresponds to mass ratio 4590 with zero current.

7.2.1 Sheath Parameters

It has been shown (see section 5.3.1) that solutions to the plasma equation are consistent with assuming equality in the Bohm criterion for sheath formation. This analysis is of course applicable to a plasma without singularities which is enclosed by absorbing walls where the sheaths are created. Matching of the sheath solution to the plasma solution when the wall is non-emissive has been performed by Franklin and Ockenden [1970] for the low pressure case, and by Blank [1968] for the high pressure case. The case of a hot electron-emissive boundary has been investigated by Crawford and Cannara [1965] and Prewett and Allen [1976]. It should be noted, however, that some plasma systems do not conform to these conditions; the hypothetical single-point ionisation system (see section 5.3.3) is one example; the singularity at the point of ionisation is responsible for the loss of validity of the Bohm equality.

Other calculations including secondary emission and permitting current flows have been performed by Harbour [1978]; these did not simplify the electron distribution by assuming it to be Maxwellian, but used the correct truncated Maxwellian with delta function beam electrons. Arbitrary ion energy on entry to the sheath was also catered for as well as warm ion distributions. For a mass ratio of 4590 and assuming zero wall-field conditions, the calculations showed that the equations of Hobbs and Wesson [1966] overestimate the ion energy at the plasma-sheath boundary as 0.575 instead of 0.53, and also overestimate the wall potential as 0.976 instead of 0.865; the latter error leads to an overestimate of the final beam velocity by only about 6%, and a similar overestimate of the wavelength of the dominant mode. The relative beam density n_b/n_o, on the other hand, is underestimated by Hobbs and Weson as 0.0871 instead of 0.113 which leads to an underestimate of the growth rate of the dominant mode by about 6%. Clearly these small errors do not have important concequences for the results obtained in the present

7.2.2 Beam-Plasma Theory and a Possible New Factor Contributing to the Destruction of Wave Amplitude Oscillations.

The first analysis of the beam-plasma instability was undertaken by Buneman [1959] who dealt with counter-streaming, cold electrons and ions. We have been particularly interested in warm plasmas and single-wave theory and therefore specifically required the characteristics of the dominant mode and spectrum width as derived by O'Neil, Winfrey and Malmberg [1971] (see section 3.1). It will be recalled that their computer simulations showed oscillations in the saturated amplitude of the wave in common with all studies of the beam-plasma instability. These oscillations did not, however, damp away; similar findings were reported by Shapiro and Shevcenko [1976]. This contrasts with more recent studies [Fukumasa et al, 1978, 1982, Winfrey and Dunlop, 1977] which find damping of the amplitude oscillations. The reason for the disparity is claimed to be due to the artificial restriction to one mode in the single wave case, the inclusion of many waves being at least one possible cause of the damping of the oscillations.

The oscillations are reminiscent of those in the nonlinear Landau damping coefficient derived by O'Neil [1965] which similarly result from the oscillations of the trapped electrons. The amplitude of the oscillations and the value of the coefficient tend to zero for long times due to phase-mixing of the electron distribution function. Evidently the amplitude oscillations of the Single-Wave simulations do not suffer the same fate, which implies that a trapped electron endlessly retraces its orbit in these calculations. Al'tshul and Karpman [1965] also derived an oscillating damping coefficient but did not find the oscillations diminishing for long times; this is probably an error resulting from use of a perturbation scheme which was not valid for all parts of the calculation.

Both the single-wave beam-plasma calculations and the nonlinear Landau damping coefficient relate to a monochromatic wave, so one might wonder why phase-mixing does not also occur in the beam-plasma case; if it did then,

the vicinity of the phase velocity of the wave being damped. In the latter case all trapped electron orbits are adjacent to neighbouring electron orbits and this results in phase-mixing.

In some beam-plasma systems, depending on the parameters, the trapped electrons derive from both the beam and the plasma (this does not apply to the single-wave calculations [O'Neil et al already referred to) and therefore begin with an initial spread of phase velocities. This suggests the possibility that time variation of the distribution function may gradually phase-mix away under these circumstances, even if the wave spectrum is restricted to one mode. Of course, any real wave spectrum does have a finite width which contributes to the damping of the amplitude oscillations, but the phase-mixing described here may be an additional mechanism which could prove to be significant. In the case of mass ratio 4590 with floating-wall conditions the trapped plasma electrons derive from a wide range of initial phase velocities and consequential phase-mixing may be at least as important in destroying the amplitude oscillations as competition from neighbouring waves. Trapped electrons which are initially non-monoenergetic may, therefore, lead to significant additional damping of the amplitude oscillations in the nonlinear evolution of the beam-plasma instability. A possible further role played by this mechanism is discussed in section 7.2.7.

7.2.3 Related Experiments

In this section we briefly survey some relevant experiments and the extent to which theoretical predictions have been confirmed.

The earliest experiments which clearly suggest the presence of beam-plasma oscillations are described by Mahaffey [1959] and Emeleus [1964] in which a mercury vapour tube has a current passed through it via an anode and a hot, flat, oxide-coated cathode; Fig. 7.2 shows the geometry. The

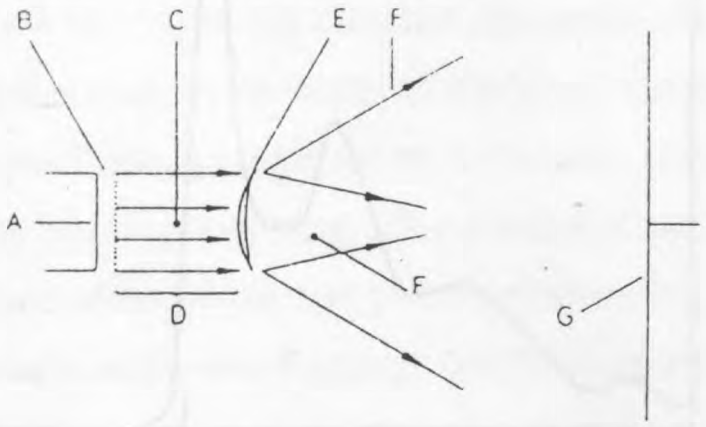

Fig. 7.2 Diagram of sections of single-beam self-oscillating discharge from flat-oxide-coated cathode (after A. Garscadden). A, cathode (usually 8 mm diameter); B, cathode sheath; C, nearly parallel electron beam about same diameter as cathode; D, oscillation dead space; E, oscillation front (meniscus); F, deviated electron beams; G, anode. Most of the space between B and G is nearly equipotential apart from the oscillation fields.

anode by scattering some of them obliquely. This is possible confirmation of a greatly enhanced collision rate due to fine-scale velocity-space perturbations caused by the instability, as suggested in section 6.3.1. Spatial variation in the intensity of oscillation as observed by Mahaffey [1959] is shown in Fig. 7.3 and it is noted that it bears a remarkable resemblance to the temporal variation seen in the plasma electron energy of the simulation corresponding to a wall potential $|\Phi_w| = 10$ shown in Fig. 6.8 – this is, of course, the analogue of the expected spatial variation in energy.

Malmberg and Wharton [1969] launched a very low density beam into a plasma to test linear theory whose predictions regarding growth rate and dispersion relation were confirmed in the appropriate regime. The saturated wave amplitude was approximately in agreement with that expected and it did not depend on the initial wave amplitudes, but only on the parameters of the system. The harmonic content was very low.

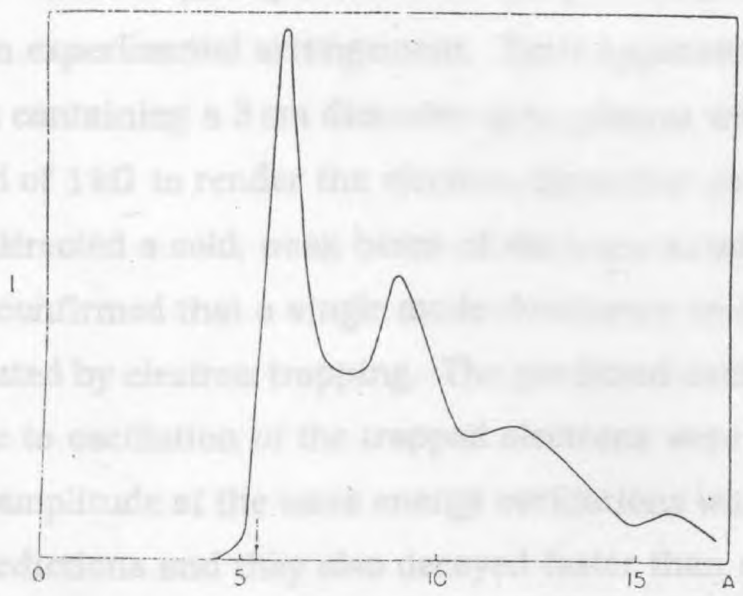

Fig. 7.3 Intensity of oscillation (I) in arbitary units at different distances (cm) from cathode (C) towards anode (A) of discharge of form shown in Fig. 7.2 (after W. Mahaffey). The position of the front (E) seen is shown by an arrow. Gas, mercury; pressure, 1.3μ; current, 4.8 ma; tube voltage, 21 volts. Here $\mu = 10^{-3}$ mm Hg pressure.

In another beam-plasma experiment Apel [1969] observed a power law dependence for the the harmonic spectrum which was given by:

$$P_{k_r} = P_0(k_r/k_0)^{-5}$$

where P_{k_r} is the wavepower of the harmonic, P_0 is that of the dominant mode, k_0 is the wavenumber of the dominant mode and k_r is that of the harmonic. Apel suggests that this is due to turbulence in which Bohm diffusion is the dissipation mechanism causing energy to cascade from small wavenumber modes to larger ones. Indeed, other workers [Chen, 1965; Sagdeev and Galeev, 1966] have derived a negative exponent of 5 with a power law by assuming such theories of turbulence. However, the phase-velocities of the harmonics were measured to be the same as that of the dominant mode moving with the beam and this strongly suggests that the origin of the harmonics is simply the spatial bunching of the beam electrons (see section 3.1.3).

theory with an experimental arrangement. Their apparatus consisted of a two-metre column containing a 3 cm diameter quiet plasma with a longitudinal magnetic field of 1 kG to render the electron dynamics one-dimensional. An electron-gun directed a cold, weak beam of electrons axially into the plasma. Their results confirmed that a single mode dominates and grows until the wave is saturated by electron trapping. The predicted oscillations of the wave amplitude due to oscillation of the trapped electrons were also observed. However, the amplitude of the wave energy oscillations was smaller than theoretical predictions and they also decayed faster than expected.

Sidebands of the main wave were observed in a beam-plasma system by van Wakeren and Hopman [1972] who expected to find them symmetrically displaced from the main wave by $\omega_B/2\pi$ (where ω_B is the bounce frequency of trapped electrons) as observed in experiments with quiescent plasmas. However, they only observed the lower sideband and the displacement was not the predicted value. A possible explanation for the latter feature is given in section 7.2.4 [Winfrey and Dunlop, 1977]. It was concluded that the upper sideband probably existed, but with a very low growth rate. Like others, this study also found that the phase-velocities of the harmonics were equal to that of the main wave, again suggesting spatial bunching origins.

Mizuno and Tanaka [1972] have measured trapped-electron distribution functions in a beam-plasma system using an externally excited wave. Their results confirm the description of the evolution given by O'Neil, Winfrey and Malmberg [1971] (see section 3.1.3) in which the trapped beam electrons roughly form a line in phasespace which rotates to go from a position of bunching in velocity to spatial bunching. At this point in the experiment the harmonic spectrum was seen to conform to a power law given by:

$$E_n^2 = n^{-2.5}$$

where E_n is the electric field amplitude of the n^{th} harmonic. This is further

case of a spatially periodic delta-function [O'Neil, Winfrey and Malmberg, 1971].

These results were extended by Gentle and Lohr [1973] who were able to fully confirm the predictions of single-wave theory up to the point of electron trapping. However, the wave lost its monotonicity and the spectrum broadened more rapidly than sideband theories had predicted, as other studies also discovered. The distribution function and phasespace plots were also obtained. Their harmonic spectrum revealed a power law exponent of between -3.5 and -4.

It is noted that the negative exponent of empirically obtained power-law spectra ranges from about 2.5 to 5. This reflects the degree to which the spatial bunching of beam electrons approaches the periodic delta function. The ideal value of 2 represents the minimum and as shown by O'Neil and Winfrey [1972] the ensemble averaging of the local solution over all possible phases and amplitudes causes the value to increase.

Empirical determinations of electron velocity distribution functions in the presence of secondary emission are very hard to find but recent experiments by Behrndt, Klagge and Leven [1986] with a He glow discharge have produced some interesting results. They found that secondary emission is very efficiently induced by impact from metastable He atoms. By introducing Ar gas into the discharge they were able to destroy the He metastables by:

$$Ar + He^{*} \rightarrow Ar^{+} + e + He$$

with a consequent reduction of the energy and quantity of the emitted electrons as is clear from the change in 'beam' distribution shown in Fig. 7.4.

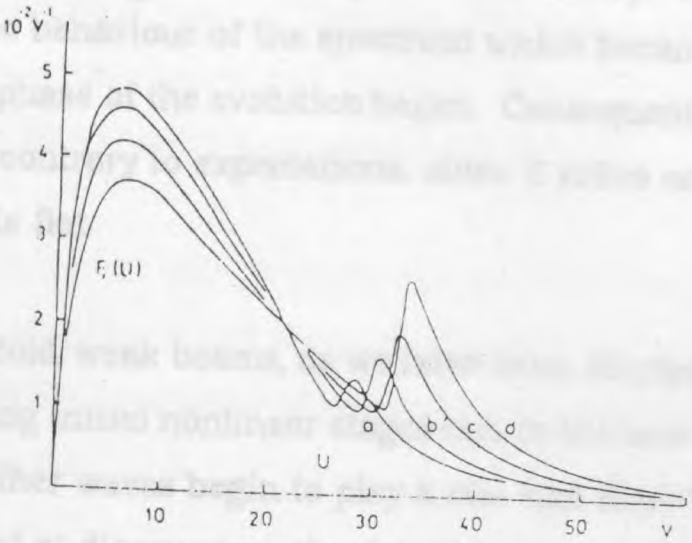

Fig. 7.4 Electron distribution functions for a) 2% Ar, b) 0.1% Ar, c) 0.05% Ar, d) pure He.

7.2.4 The Role of Neighbouring Waves.

Dawson and Shanny [1968] performed numerical simulations using a sheet model for the electrons. They modelled conditions appropriate to the bump on tail instability (see section 7.2.6) and confirmed the theoretical prediction of the flattening of the distribution function.

Morse and Nielson [1969] used a particle-in-cell computation with two unequal warm beams to model a variety of conditions from bump-on-tail to more strongly unstable cases. In the latter situation, single-wave structures in phasespace resembling those obtained for current flow conditions in section 6.1 were produced. The bump-on-tail case confirmed the theoretical predictions of quasilinear theory which are that the spectrum of unstable waves is very broad and leads to the gradual diffusion of the distribution of the bump in velocity space until it forms a plateau.

calculations by numerically integrating the Vlasov equation in 1-D but were surprised to discover that the fastest growing mode dominated the evolution, in conflict with the predictions of quasilinear theory. They attributed this disparity to the behaviour of the spectrum which became very peaked before the nonlinear phase of the evolution began. Consequently quasilinear theory was not valid, contrary to expectations, since it relies on the assumption that the spectrum is flat.

Cases with cold, weak beams, as we have seen, display strongly single-wave behaviour during initial nonlinear stages but, in the later stages of development, other waves begin to play a role and there have been a number of studies aimed at discovering the details of these interactions.

Many studies have shown that, even in plasmas without a beam, a monochromatic wave is unstable to sidebands at nearby frequencies. Wharton, Malmberg and O'Neil [1968] carried out experiments in which they launched a large amplitude wave into a collisionless plasma and measured a continuous spectrum of excited neighbouring waves. However, there was a small separation in frequency between the main wave and the peak in the excited spectrum. The unstable waves were named trapped particle sidebands as they were thought to obtain their energy from the trapped electrons. It was later noticed that the data revealed the existence of these sidebands in a part of the plasma near the source of the launched wave where no plasma electrons had yet become trapped [Morales and Malmberg, 1974].

Morales and Malmberg undertook to further pursue the origin of these sidebands by launching a small amplitude wave into a plasma in order to avert the influence of trapped particle effects. The amplitude of the wave was gradually increased until the more familiar results were obtained. This experiment decisively demonstrated that the trapped particle sidebands evolved from 'linear sidebands' which were themselves a result of the initial interaction between the launched wave and a noise spectrum of streaming

Franklin et al [1978] also performed experiments with large amplitude waves launched into a plasma. They concluded that electrons which became trapped and then later untrapped, behaved like a beam, giving rise to the growth of a sideband via the beam-plasma instability.

Further experiments with large amplitude waves have recently been reported by Buchelnikova and Matochkin [1987] and they also define 3 regions (ie. weak, strong and unstable) of parameter space analogous to those discussed in section 7.1.2.

The above experiments suggest that there is more than one possible mechanism for the generation of sidebands. Their characteristics may therefore depend on precise plasma conditions which could be difficult to replicate in different plasma experiments. Numerical experiments using computers of course allow greater consistency.

Koch and Leven [1983] have performed a computer simulation of the sideband instability by solving the Vlasov equation numerically. The initial conditions consisted of a Maxwellian plasma carrying a large amplitude wave; the closest neighbouring modes in this system were separated in k-space from the main wave by an amount corresponding to about 15% of one wavelength. In order to determine the extent to which the sidebands owe their existence to quasilinear effects, an interrelated calculation was simultaneously performed in which the spatially averaged distribution function from the first calculation was used to calculate the sideband growth from quasilinear theory. The results showed that quasilinear theory almost completely accounted for the development of the upper sideband but did not predict any growth of the lower sideband (see Figs. 7.5 and 7.6). It was therefore apparent that the development of the lower sideband can only be described by the inclusion of the mode coupling terms. Koch and Leven suggested that this may occur through the interaction of the upper sideband with the first harmonic of the

function is, on average, positive, and it would seem reasonable to associate this distortion of the distribution with the 'beam' of untrapped electrons postulated by Franklin et al [1978]; after all, this feature of the distribution appeared to be retained throughout the calculation, which spanned many bounce periods. Koch and Leven, however, believed that the sidebands were caused by trapped particles.

So far we have been considering the various ways in which neighbouring waves can develop when a single monochromatic wave is launched into a plasma. In a beam-plasma system the situation can be similar because the evolution of the instability is dominated by a single mode and there is no reason why the trapped particle sidebands or the 'untrapped electron beam' sidebands should not materialise here. It is also possible that there are other ways in which the spectrum of a beam-plasma system can become broadened. There are a number of numerical studies which have examined this aspect of beam-plasma systems and the consequential damping of the amplitude oscillations of the main wave.

A numerical study of the effect of neighbouring waves on the development of the beam-plasma instability was carried out by Winfrey and Dunlop [1977], some of whose conclusions have been described in section 6.2. Their main discovery was that the evolution of the beam-plasma instability was different in the two cases of spatial and temporal growth because of their different dispersion relations; neighbouring waves were found to more strongly influence the evolution in the spatial case and damp the amplitude oscillations of the main wave more quickly. This accounts very well for the broadband behaviour observed experimentally [Gentle and Lohr, 1973].

Winfrey and Dunlop referred to the growth of the sidebands as a manifestation of the trapped-particle instability. However, it is doubtful that this is literally the same mechanism as that reponsible for the results of Wharton et al [1968] and Morales and Malmberg [1974], where the sidebands

is suggested by Winfrey and Dunlop that the sidebands result from a 'secondary beam-plasma' instability where the distribution of trapped electrons behaves like another beam with smaller velocity than the first, but still capable of causing instability. They also suggest that 'cascading' can occur when there is a succession of such secondary beams. For certain conditions there may be some truth in these suggestions but it might be more accurate to say that the dispersion relation is modified so that, as the beam slows, the peak in growth rate continuously shifts to lower velocity, thus exciting successively slower modes.

Winfrey and Dunlop have defined a parameter known as the 'beam-strength' given approximately by:

$$s = [(n_b v_b^2)/(6 n_p v_T^2)]^{1/3} \quad \text{or} \quad s = (n_b/2n_p)^{1/3}$$

for spatial and temporal modes respectively. As this quantity becomes larger the effects of neighbouring waves are found to become stronger, the damping of the amplitude oscillations occurring much more rapidly. For the spatial case, the beam-strength is related to the parameter η introduced in section 3.1.1 through $\eta = 2s^3$.

Fukumasa et al [1982] have carrried out similar computations for spatial growth and discovered that the effects of neighbouring waves are sensitive to the beam velocity in addition to the beam strength s. They find that as v_b/v_T increases the competition from neighbouring waves decreases. Their explanation is that, after trapping, the frequency shift of the most unstable wave is proportional to $s(v_T^2/v_b^2)$ and the shift is therefore smaller for larger beam velocities, implying that the single-wave ideal is more closely approached under such conditions. Note that, as has already been suggested, the frequency of the most unstable wave must change continuously as the beam progressively slows down. This comment is thought to be worth making since it is felt that some of the literature being reported here manages to

occurs only when trapping has taken place.

An alternative reason for the dependence on beam-velocity observed above seems to have been overlooked. It should be recalled that the widths of the growth-rate spectrum and saturated wave spectrum depend on beam-velocity; for the conditions appropriate to the numerical simulations, this leads to a spectrum width which is comparable to the size of the wavelength shift induced by the slowing and trapping of the beam. The reduced competition from neighbouring waves resulting from increasing the beam velocity may therefore be as much due to the narrowing of the spectrum as to the reduction of the wavelength shift of the most unstable mode. To demonstrate this we begin by recalling equation 3.1b for the spectrum half-width:

$$\delta k = \frac{3(\ln 2)^{1/2}\eta^{1/3}k_0}{2^{5/6}N^{1/2}}$$

where N is the number of e-foldings before trapping and, on substituting $k_0 = \omega_0/u$, the half-width of the spectrum, after trapping, becomes:

$$\delta k = \frac{3(\ln 2)^{1/2}\omega_0\eta^{1/3}}{2^{5/6}N^{1/2}u} \qquad (7.1)$$

Since $\omega_0 \approx \omega_{pe}$ we can write the wavenumber shift as $\Delta k \approx -\Delta u\omega_0/u^2$ and we now require an estimate for the change in velocity of the beam. From section 3.1.1 we have:

$$\omega = \omega_0(1 - \eta^{1/3}/2^{4/3})$$

$$\therefore\ v_\varphi = \omega/k = u(1 - \eta^{1/3}/2^{4/3})$$

$$\therefore\ \Delta u \approx u - v_\varphi = u\eta^{1/3}/2^{4/3}$$

thus the wavenumber shift becomes:

Since $N \approx 7$ in the computer simulations, the numerical factor multiplying the R.H.S. of equation (7.1) evaluates to 0.530, while that in equation (7.2) becomes 0.397. The finite spectral width is therefore a significant factor and cannot be ignored in these calculations.

There is an additional consideration which should theoretically affect the width of the saturated spectrum in a real plasma: the level of thermal fluctuations in a plasma increases with decreasing wavenumber (see section 6.2), which corresponds to increasing beam velocity. Hence, when there is a faster beam the most unstable mode grows from a greater fluctuation level; this factor alone will tend to reduce the number of e-foldings and broaden the saturated spectrum, but it turns out that the effect is small compared to the those considered above.

In addition to the effects of neighbouring waves, Fukumasa et al [1978, 1982] investigated the influence of collisions on the nonlinear evolution of the beam-plasma instability. They found that, with single-wave simulations, collision rates of the order of $\nu/\omega_0 = 10^{-3}$ (where ω_0 is the frequency of the most unstable mode) induced significant damping of the amplitude oscillations during or soon after the first bounce of the trapped particles. Collisions, then, affect the evolution of the instability in a similar way to sidebands.

There is an aspect of many-wave behaviour which may appear paradoxical and deserves some discussion. In computer calculations using the single-wave model [O'Neil et al, 1971] (see section 3.1) it has been observed that the higher harmonics of the main wave grow and during trapping form a power law spectrum given by:

$$|E_{nk_0}|^2 = A n^{-2.5}$$

k_0 is the wavenumber of the main wave; thus the model is not single-wave in the very strictest sense. The power law spectrum is a direct consequence of the periodic spatial bunching of the beam electrons. This may seem a little puzzling when one considers the fact that all waves grow from some initial amplitude and we are therefore used to the idea that the initial conditions determine the evolution of an instability. We have to conclude from the facts that the harmonic spectrum depends only on the amplitude of the dominant mode and is insensitive to the initial amplitudes of the harmonics. Although surprising, an illustration of such insensitivity to initial conditions can be seen in the calculations of Koch and Leven [1983] described earlier in this section. Figs. 7.5 and 7.6 depict two sets of their results showing the development of the main wave with upper and lower sidebands. The only difference between the two calculations is that the upper sideband begins with a finite amplitude in one case and, in the other, it is initially zero. It can be seen that after t = 100 the sidebands are present in both calculations and are evolving in a virtually identical manner. This clearly indicates that plasma behaviour can, in a non-trivial sense, be independent of some of the initial conditions.

7.2.5 Stochasticity Approach

The main wave with its oscillating amplitude may be considered to be the combination of an unperturbed wave plus a small amplitude perturbation. In phasespace there will be a separatrix corresponding to the unperturbed wave; of course, in the absence of a perturbation this would separate the trapped from the untrapped electrons. Perturbations introduce extra resonances which correspond to and microscopically modify specific particle orbits in phasespace. If the perturbation remains small the particle motions within the resonances can remain adiabatic (see section 3.2.1). However, if the perturbation becomes large enough the widths of the resonances will increase to the point at which overlapping will occur. When this happens, some or all of the particles travelling along orbits which reside in the overlapping resonance region, no longer behave adiabatically. Such particles essentially perform a random walk in phasespace through the region spanned by

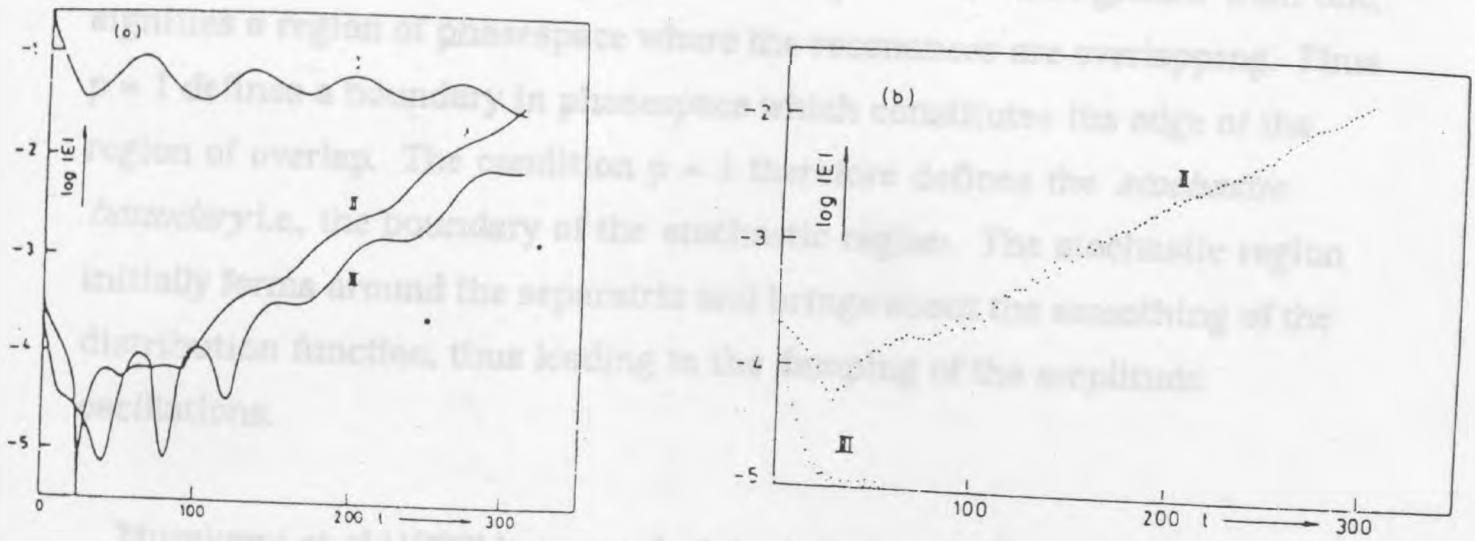

Fig. 7.5 Example (1): (a) Amplitudes of the main wave (I) and of the lower (II) and upper (III) sidebands according to complete calculation. (b) Amplitudes of the lower (II) and Upper (III) sidebands according to quasilinear calculation.

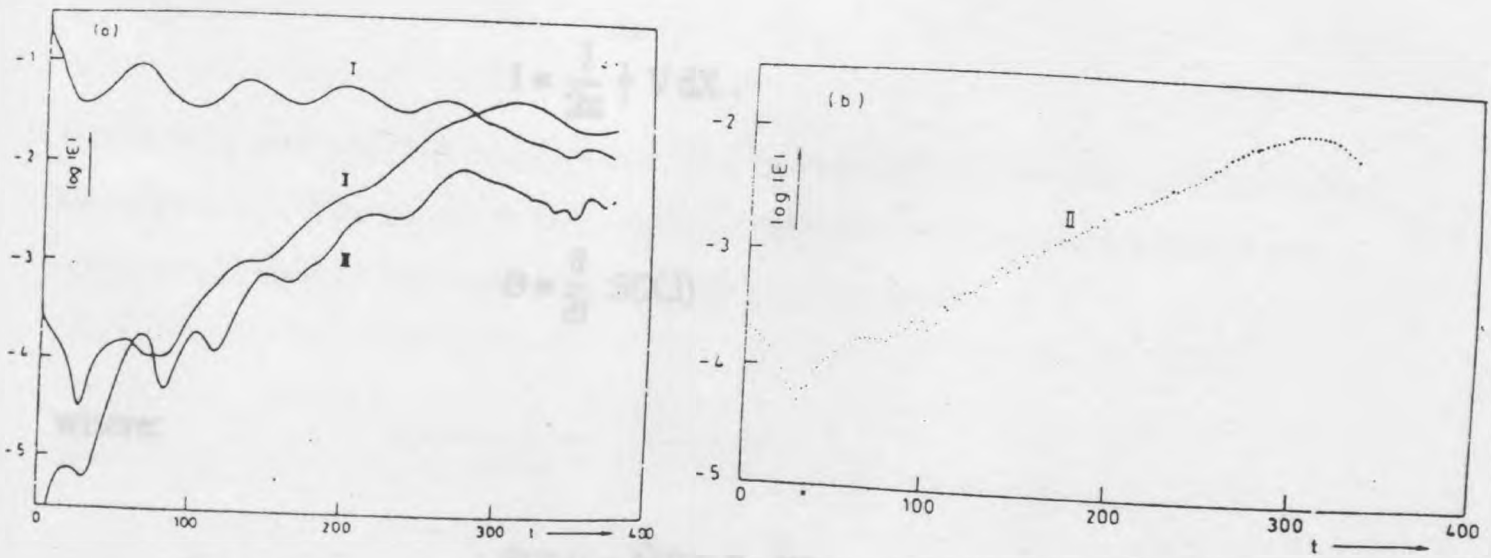

Fig. 7.6 Example (2): (a) Amplitudes of the main wave (I) and of the lower (II) and upper (III) sidebands according to complete calculation. (b) Amplitudes of the lower (II) and Upper (III) sidebands according to quasilinear calculation.

[Zaslavskii and Chirikov, 1972; Chirikov, 1979; Chirikov et al, 1971].

One can define a *stochasticity parameter* p which, when greater than one, signifies a region of phasespace where the resonances are overlapping. Thus p = 1 defines a boundary in phasespace which constitutes the edge of the region of overlap. The condition p = 1 therefore defines the *stochastic boundary* i.e., the boundary of the stochastic region. The stochastic region initially forms around the separatrix and brings about the smoothing of the distribution function, thus leading to the damping of the amplitude oscillations.

Murakami et al [1982] have used a 'single wave with amplitude perturbation' model to analyse the stochastic behaviour of electrons. For this purpose they have taken the perturbation to be a constant oscillation of the amplitude of the main wave; in practice, the oscillations always damp away, so this is only an approximation. The analysis is more easily accomplished if the usual phasespace coordinates are transformed into action-angle coordinates I, Θ given by:

$$I = \frac{1}{2\pi} \oint V\,dX ,$$

$$\Theta = \frac{\partial}{\partial I} S(X,I)$$

where:

$$S(X,I) = \int_0^X V(X',I)\ dX'$$

and where X and V are the particle position and velocity respectively. Units of length and time have been normalised to k^{-1}, the inverse wavenumber of the

main wave, and ω_b^{-1}, the inverse bounce frequency, respectively. Contours of I and Θ in normal phasespace are shown in Fig. 7.7.

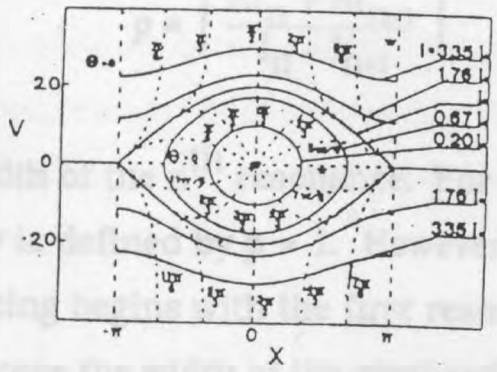

Fig. 7.7 The relation between the coordinates (I, Θ) and (V, X). The line $I = I_0$ is the separatrix.

Resonances are found to lie on specific I contours given by:

$$2n\Omega(I_n) - 1 = 0$$

where n is any positive or negative integer - except zero which identifies the separatrix I_0. The function Ω is defined differently within and without the separatrix. Inside the separatrix ($0 < b_i < 1$) we have:

$$\Omega(I) = \frac{\pi}{2K(b_i)} \qquad b_i^2 = \frac{1+W}{2}$$

while outside ($0 < b_0 < 1$) we have:

$$\Omega(I) = \frac{\pi}{2b_0 K(b_0)} \qquad b_0^2 = \frac{2}{1+W}\,.$$

In both cases K is the complete elliptic integral of the second kind and W is the particle energy eigenvalue corresponding to the time independent unperturbed Hamiltonian; note that W = 1 on the separatrix.

The stochastic parameter is given by:

$$p = \left| \frac{\Delta I_n + \Delta I_{n+1}}{I_n - I_{n+1}} \right|$$

where ΔI_n is the width of the n^{th} resonance. For large values of n the stochastic boundary is defined by p = 1. However, for the problem considered, overlapping begins with the first resonances on each side of the separatrix; in this case the width of the stochastic region is given approximately by $2\Delta I_1$.

If this picture is applied to the amplitude oscillations of the saturated beam-plasma instability we would expect the stochastic behaviour of the trapped beam electrons to smear out the beam along orbits and lead to the damping of the oscillations as is observed in practice. But, it is not clear how this analysis can be reconciled with the observation that simulations using the single-wave model showed negligible damping of the amplitude oscillations [O'Neil et al, 1972; Shapiro and Shevchenko, 1976] (see section 7.2.2). Perhaps the conditions of the simulation simply imply very small damping via the stochasticity mechanism.

Stochastic behaviour can also be predicted by considering the trapping regions in phasespace of neighbouring waves as if they were resonances [Dimonte, 1982; Bodrow, 1985] (see section 3.3). One finds the width in velocity-space of the trapping region of a wave to be

$$\Delta v = \frac{4}{\pi} \left(\frac{E}{2k} \right)^{1/2}$$

where E is the amplitude of the electric field and k is the wavenumber. And the corresponding stochasticity parameter is:

$$p = \frac{\Delta v_1 + \Delta v_2}{2\delta v} \ .$$

where Δv_1 and Δv_2 are the widths of consecutive trapping regions and δv is the distance between their centres. Typically, neighbouring waves of even very small relative amplitude can produce values of p larger than 1 and hence stochasticity. Their influence is greatest near the nodes where the electric field of the main wave is small.

In the beam-plasma instability, stochasticity theory may thus be applicable on the basis of two mechanisms: amplitude oscillations of the main wave and competition from neighbouring waves. Further comments on the applicability of stochasticity theory are given below in section 7.2.7.

7.2.6 The Domain of Quasilinear Theory

Quasilinear theory can describe the complete time evolution of the bump-on-tail instability whereas the single-wave model generally describes only the initial stages of the beam-plasma instability, but it has not been made clear whether the two theories can overlap. We shall see that an examination of this question throws light on the range of validity of quasilinear theory.

We recall that setting k = 0 in the Fourier transform of the perturbed Vlasov equation leads to:

$$\frac{\partial g}{\partial t} = \lim_{L\to\infty} \frac{e}{Lm} \int E_{-k} \cdot \nabla_v f_k \frac{dk}{2\pi} \qquad (7.3)$$

and substituting $d/dt = -i\omega$ in the same equation provides an expression for f_k:

$$\Gamma_k = \frac{\nabla_v g}{i(k\cdot v - \omega)} + \lim_{L\to\infty} \frac{(e/Lm)\int E_{k-q}\cdot\nabla_v f_q \; dq/2\pi}{i(k\cdot v - \omega)} \qquad (7.4)$$

Substituting (7.4) into (7.3) gives:

$$\frac{\partial g}{\partial t} = \lim_{L\to\infty}\left[\frac{e^2}{Lm^2}\int E_{-k}\cdot E_k \nabla_v\left\{\frac{\nabla_v g}{i(k\cdot v - \omega)}\right\}\frac{dk}{2\pi}\right.$$

$$\left. + \frac{e^2}{L^2m^2}\int\int E_{-k}\cdot E_{k-q}\nabla_v\left\{\frac{\nabla_v f_q}{i(k\cdot v-\omega)}\right\}\frac{dq}{2\pi}\frac{dk}{2\pi}\right] \qquad (7.5)$$

and if we drop the second term we obtain:

$$\frac{\partial g}{\partial t} = \frac{16\pi^2e^2}{m^2}\nabla_v\left\{\frac{\varepsilon_k}{v}\nabla_v g\right\}_{k=\pm|\frac{\omega}{v}r|} \qquad (7.6)$$

which is the quasilinear equation for g the space-averaged distribution function. Since this equation should remain valid for arbitrarily small perturbations it might seem natural to expect this equation to predict the same initial behaviour as the single wave model for the same starting conditions. Now, as we know, the single wave model predicts perturbations of the beam velocity and thus a broadening of the space averaged distribution function; this occurs at a velocity faster than the wave phase velocity since the beam is moving faster than the wave. However, on examination of equation (7.6) we note that it can only describe changes to the distribution function at velocities where there are plasma waves. So we have to be able to explain this apparent contradiction.

One of the reasons for this disparity is that dropping the second term in equation (7.5) involved glossing over a rather inconspicuous subtlety. The term which is retained in the quasilinear equation is only the lowest significant order term if all the maxima in the integrand occur in the region of k-space corresponding to the range of phase velocity spanned by the distribution of beam electrons. For beam-like as opposed to gentle bump distributions this is

diffusion of the distribution function faster than the quasilinear rate.

We therefore observe that for distributions which are beam-like we would have to include the mode-coupling terms in equation (7.5). Now one can instantly see that there is not going to be any overlap between the two theories since mode-coupling is not consistent with a single wave view. Examining this point further we note that if we allowed the mode-coupling terms to modify the beam distribution until it developed a large spatial variation, then the condition $f_1 \ll f_0$ would be violated and the perturbation scheme would break down. So we conclude that the perturbed Vlasov equation is not capable of describing single wave behaviour.

We can therefore see that quasilinear theory is only valid when the phase-velocity of waves with the maximum growth rate falls into the region spanned by the beam electrons. This can only happen when the beam has a large enough velocity-spread to be classified as 'warm' according to some appropriate criterion. This question has been investigated by Self et al [1971] who derived a dispersion relation in a similar manner to O'Neil and Malmberg [1968] (see section 6.2) and extended it by including the effects of collisions. They have defined parameters which, when collisions are ignored, reduce to:

$$s_1 = \left[2 \frac{n_p}{n_b} \left(\frac{v_b}{v_0} \right)^3 \right]^{1/3} \qquad \text{and} \qquad s_2 = \left[6 \frac{n_p}{n_b} \left(\frac{v_b}{v_0} \right)^5 \right]^{1/3}$$

for the spatial and temporal cases respectively. These expressions are valid only for small v_b/v_0, which is the ratio of the velocity spread of the beam to its drift velocity, and under these conditions they correspond to the parameter s in the analysis of O'Neil and Malmberg (see section 6.2). The beam is deemed to be cold or hot depending on whether $s \ll 1$ or $s \gg 1$ respectively. Self et al find that the beam is still cold according to this criterion when the phase-velocity for maximum growth-rate initially encounters the positive-slope region of the total distribution function, i.e., when it enters the region of velocity

order 1 in both the temporal and spatial cases.

There is a further consideration which warrants a cautious approach to making quasilinear calculations. As described in section 7.2.4, Armstrong and Montgomery [1969] found considerable discrepancies between the predictions of quasilinear theory and the results of direct numerical integration of the Vlasov equation for a plasma with gentle-bump system. They found that the most unstable mode in the latter calculation dominated the spectrum of waves when trapping occurred, and they traced this to the fact that the spectrum became strongly peaked at the wavelength of strongest growth even before the evolution had entered the nonlinear stage; thus, at the stage in which quasilinear theory was deemed to become applicable, the spectrum did not have the degree of flatness assumed in the derivation of the theory. The applicability of quasilinear theory must, therefore, be judged very carefully when considering the analysis of any given set of physical conditions.

On the other hand it is gratifying to note that, despite the above difficulties, quasilinear theory has been demonstrated to be capable of enabling useful calculations to be performed, even when the perturbation scheme it relies upon has broken down. The calculations of Koch and Leven [1983] described in section 7.2.4 showed that quasilinear theory almost completely accounted for the growth of the upper sideband. However their distribution functions indicate that the large amplitude wave had induced such large spatial variations that the perturbation scheme underpinning quasilinear theory was no longer valid.

7.2.7 Interpreting Simulation Results

We now examine some of the simulation results in the light of theories referred to above. Clear examples of the stong effects of perturbations near the nodes of the separatrix can be seen in Fig. 6.2, which depicts the phasespace during the nonlinear phase of the beam-plasma instability

interest to observe the fact that these detrapping events are not, after all, random as suggested by stochasticity theory. They appear to occur once every bounce period! At the same time it should be noticed that the electrons which were the first to be trapped continue to spiral in towards the centre of the orbit. Thus, the region spanned by non-adiabatic electron orbits gradually widens on each side of the separatrix, in agreement with stochasticity theory, but the motion of the electrons cannot be described as a random-walk. Theory, therefore, does not appear to fully explain the observations.

Pursuing this point further, we note that the beam-plasma behaviour contains two features which have only been tackled separately in theoretical treatments: one feature is the amplitude oscillations and the other is the competition from neighbouring waves. The combination of these two aspects within one single physical problem could lead to unpredicted behaviour but, assuming the theories are correct, it would be surprising if they conspired to produce the rather coherent spiralling observed in the simulations. It seems more likely that the predicted stochasticity is missing either because of invalid assumptions in the analyses or because of some extra feature in the simulation which has not been taken into account.

As explained in section 7.2.2 one mechanism which has not been discussed in the literature as a means of destroying the amplitude oscillations is phase-mixing. It is presumably taken for granted that this will naturally result from the non-adiabaticity caused by other factors; however, it should be stressed that for certain conditions it may, in its own right, turn out to be the dominant cause of non-adiabaticity. Phase-mixing would be expected to play this role if a significant amount of the warm plasma becomes trapped along with the beam electrons. If this happens, the consequent smearing out of the spatial bunching of beam electrons is inescapable and the reduction of the oscillations in amplitude, inevitable. Clearly, the clumps of electrons rotating in phasespace must then experience a reduction of the extremes of velocity within which they are constrained; this is just another way of saying that the trapped electrons must spiral towards the centre of their

simulations. It may be that the cyclic detrapping of electrons at the nodes also depends on this phase-mixing; certainly, the stochasticity theory would merely predict random ejection of particles at these points.

Thus, it is suggested that the inward spiralling of electrons, seen for some conditions, can only be explained by phase-mixing.

7.2.8 A New Approach to the Sheath Formation Criterion

We now return to the subject of the Bohm criterion for the last time. We examine how it is normally interpreted by others (including Bohm) and discover that it has been misunderstood. An alternative approach supplies a clearer criterion.

The standard interpretation of the Bohm criterion ($I = E/KT \geq 1/2$) is that when $I<1/2$ the potential solutions are oscillatory and that solutions with $I>1/2$ are not ruled out by the assumptions on which the model is based. The truth is that the Bohm model is basically overdetermined if one tries to explore solutions with $I \neq 1/2$ while simultaneously stipulating that $n_i = n_e$ at the sheath boundary. Thus the conclusion that oscillatory solutions correspond to $I<1/2$ cannot be drawn. The apparent prediction from the model that solutions with $I<1/2$ will be oscillatory is merely a result of the fact that the proposed value of ion energy will actually generate conditions which violate the Bohm assumptions; hence this prediction is invalid.

The particular assumption which will be violated is that $n_i = n_e$ at the plane of injection of the ions. This assumption should not be made as the relative densities are determined by the dynamics of the model. To show this we return to the 'single-point' ionisation model of section 5.3.3 and generalise it to permit ion injection with any energy $I = E/KT$. The once integrated Poisson equation then becomes:

$$\left(\frac{d\Phi}{dX}\right)^2 = 2\left[\exp(\Phi) + \left[(I - \Phi)\frac{M}{m\pi}\right]^{1/2} \exp(\Phi_w) - A\right]$$

As before, this defines a plateau potential Φ_p with sheath structure at both ends. The plateau potential is thus obtainable from:

$$\exp(\Phi_p) + \left[(I - \Phi_p)\frac{M}{m\pi}\right]^{1/2} \exp(\Phi_w) - A = 0 \qquad (7.7)$$

The potential distribution can represent one monotonic wall-sheath solution if we choose A to give zero-field at the midplane and let $\Phi_p \rightarrow 0$. Setting $p = 1$ and $\Gamma = 0$ in equation 5.10 enables us to obtain a zero current relation for our new system if we replace Φ_w with $\Phi_w - \Phi_p$ and I with $I - \Phi_p$:

$$\Phi_w = \Phi_p + \ln\left[\frac{4\pi m(I - \Phi_p)}{M}\right]^{1/2} \qquad (7.8)$$

Substituting equation (7.8) into equation (7.7) with $A = 1 + I^{1/2} \exp(\Phi_w)(M/m\pi)^{1/2}$ and squaring provides the following equation:

$$4I \exp(2\Phi_p)(I - \Phi_p) = [\exp(\Phi_p) + 2\exp(\Phi_p)(I - \Phi_p) - 1]^2 \qquad (7.9)$$

Thus Φ_p is a monotonic function of I (apart from the trivial solution $\Phi_p = 0$) and it can be shown from equation (7.9) that $I \rightarrow 1/2$ when $\Phi_p \rightarrow 0$. Thus the criterion for sheath formation is:

$$I = 1/2 \qquad (7.10)$$

and there is no ambiguity here. If $I<1/2$ then there is a highly concentrated region of positive space-charge near the input plane leading to acceleration of the ions into the plateau; this violates the assumptions of the Bohm model. Fig. 5.10 shows an example of this for the special case $I = 0$. When $I>1/2$,

prediction because no monotonic distributions obtained by varying I could encompass features which violate the assumptions of this 'single-point' ionisation model.

For a normal sheath, then, we conclude that I = 1/2 since it would be unreasonable to allow the region of concentrated space-charge at the plasma-sheath boundary (with corresponding jump in potential) which is required to violate this criterion.

7.3 Conclusions

Assuming the maximum secondary-electron flux and no current flow, the secondary-electron beam plasma instability grows spatially away from the sheath and into the plasma where, at a distance of about 100 Debye lengths the dominant mode traps the beam electrons. The stability of the sheath itself would appear to remain unaffected by the nonlinear development of the instability. When there is a current flow the growth rate is increased; this may modify the sheath stability and distance to the trapping region.

The wave energy grows linearly until trapping occurs and thereafter it oscillates with the bounce frequency of the trapped electrons. Neighbouring waves, phase-mixing and particle collisions all have the capability to smear out the trapped electron orbits, thus destroying the wave energy oscillations and, depending on the conditions, this can cause the particle distribution to temporarily approach that of a BGK mode.

It has been demonstrated that the plasma in the hypothetical 'single-point ionisation' system adopts the configuration which minimises the wall-potential relative to the midplane, and this corresponds to zero electric field at the midplane; no other general principle to guide the choice of boundary condition has been found for this case. It has also been shown that choosing the equality in the Bohm criterion for sheath formation corresponds to an

plasma bounded by two absorbing walls.

A new criterion for sheath formation has been derived using a model which reveals previously held misconceptions about the dependence on ion energy.

APPENDIX A

Phasespace diagrams for the beam-plasma instability corresponding to a wall potential of $\Phi_0 = -10$.

These diagrams are enlargements of those appearing in Fig. 6.2. The value of $t\omega_{pe}$ is given on each diagram as "T". The monotonic ions are visible as a line parallel to and just below the x-axis. Trapping of beam electrons is observable after $t\omega_{pe} = 15$ and, at the end of the simulation, voids in the centre of the trapped electron orbits appear likely to persist for some time.

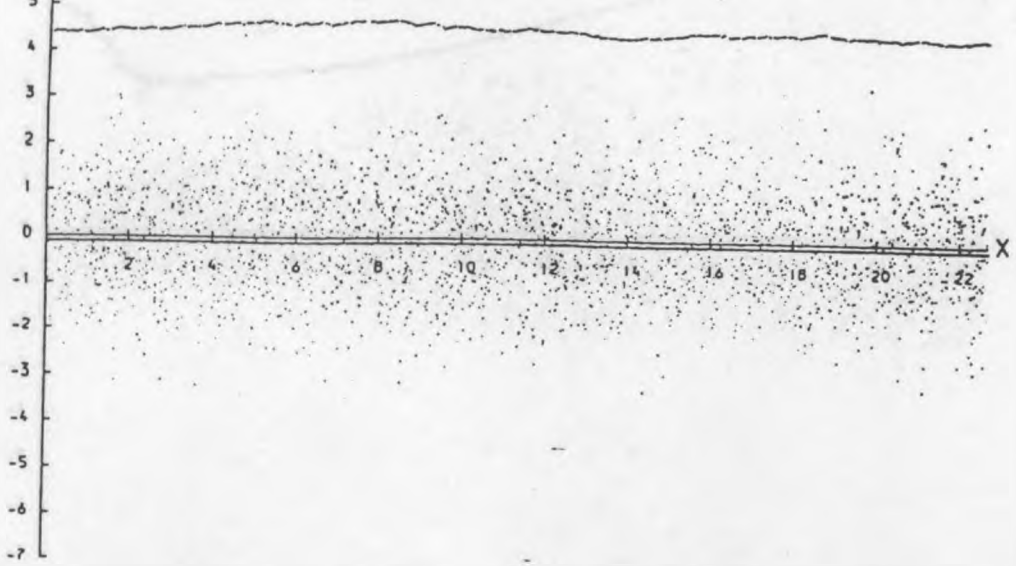
X
2
4
6
8
10
12
14
16
18
20
22
7
6
5
4
3
2
1
0
-1
-2
-3
-4
-5
-6
-7

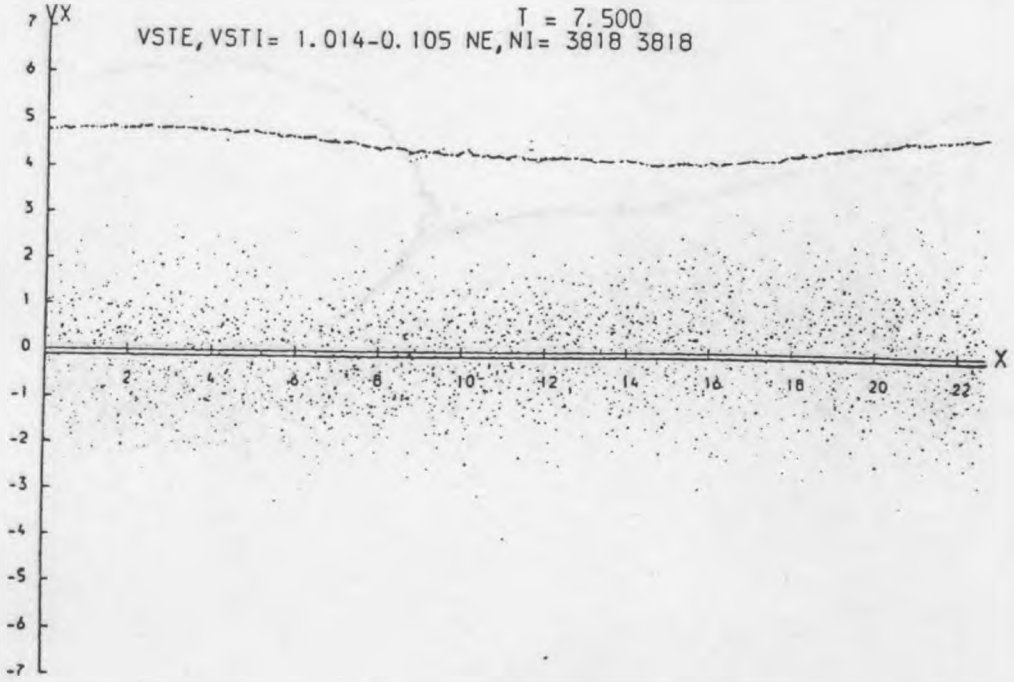
VX
T = 7.500
VSTE, VSTI= 1.014-0.105 NE, NI= 3818 3818
X
2
4
6
8
10
12
14
16
18
20
22
7
6
5
4
3
2
1
0
-1
-2
-3
-4
-5
-6
-7

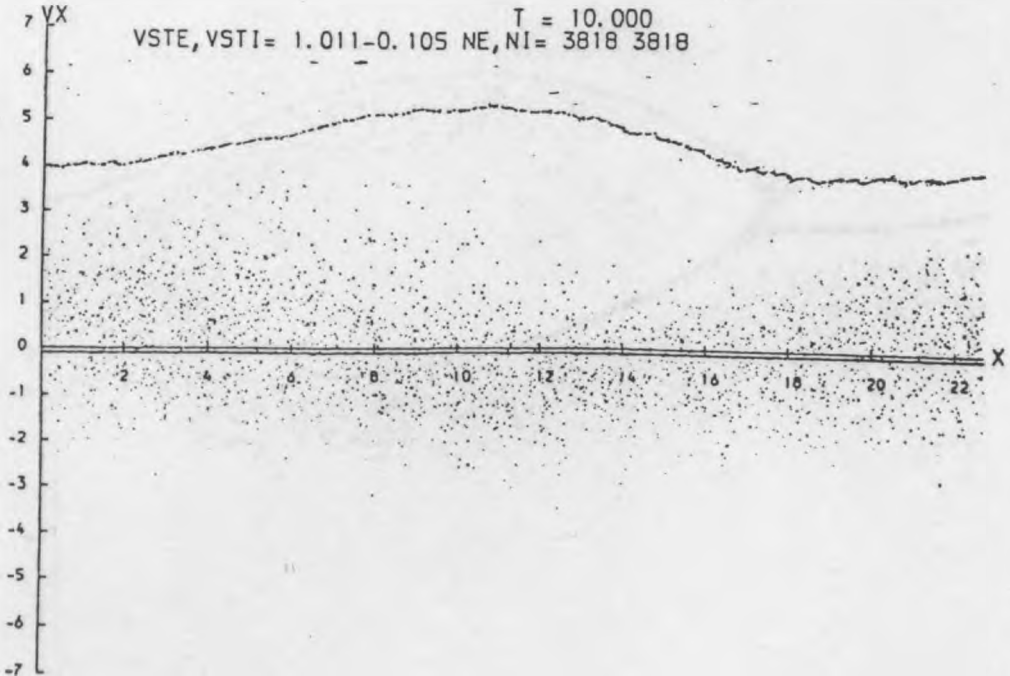
VX
T = 10.000
VSTE, VSTI= 1.011-0.105 NE, NI= 3818 3818
X
2
4
6
8
10
12
14
16
18
20
22
7
6
5
4
3
2
1
0
-1
-2
-3
-4
-5
-6
-7

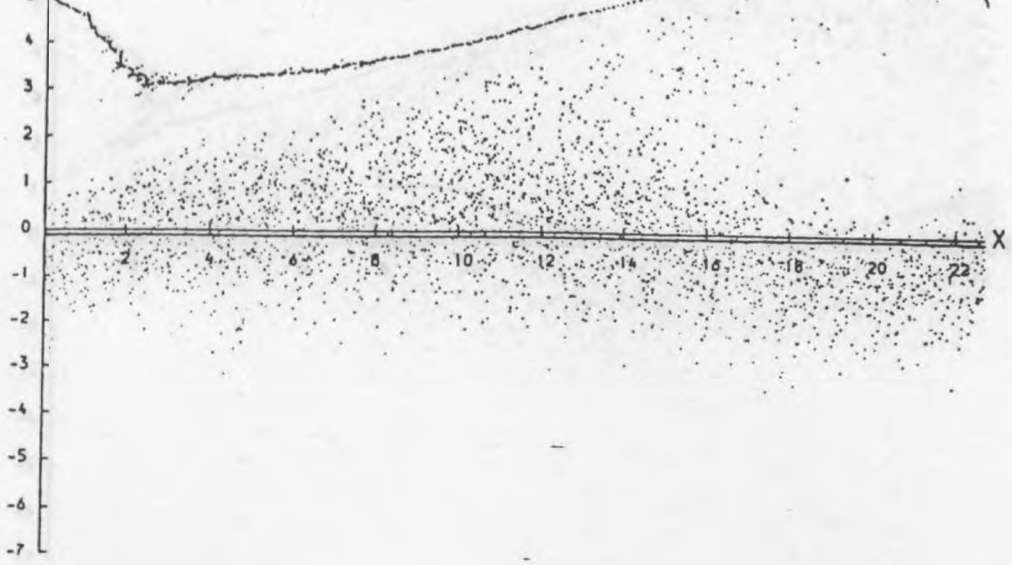
X
2
4
6
8
10
12
14
16
18
20
22
4
3
2
1
0
-1
-2
-3
-4
-5
-6
-7

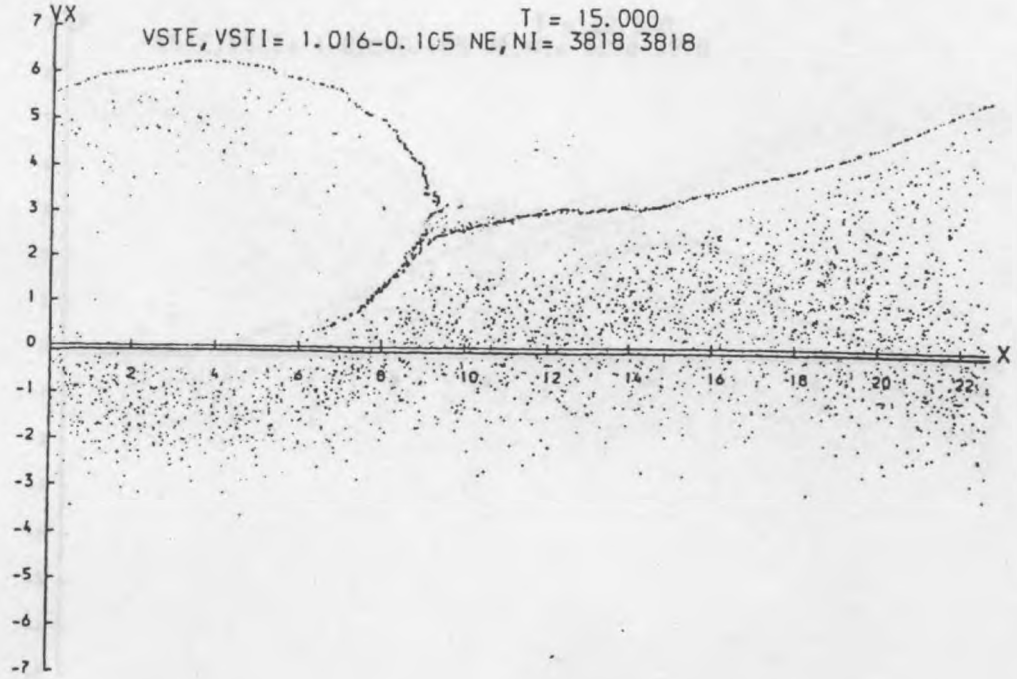
VX
T = 15.000
VSTE, VSTI= 1.016-0.105 NE, NI= 3818 3818
X
2
4
6
8
10
12
14
16
18
20
22
7
6
5
4
3
2
1
0
-1
-2
-3
-4
-5
-6
-7

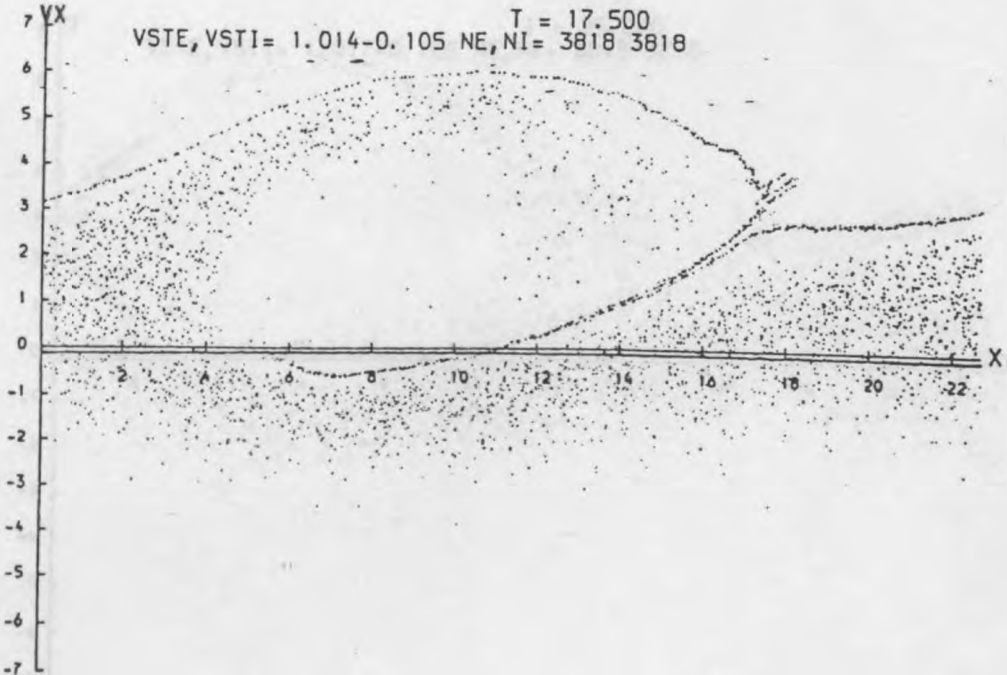
VX
T = 17.500
VSTE, VSTI= 1.014-0.105 NE, NI= 3818 3818
X
2
4
6
8
10
12
14
16
18
20
22
7
6
5
4
3
2
1
0
-1
-2
-3
-4
-5
-6
-7


X
2
4
6
8
10
12
14
16
18
20
22
5
4
3
2
1
0
-1
-2
-3
-4
-5
-6
-7

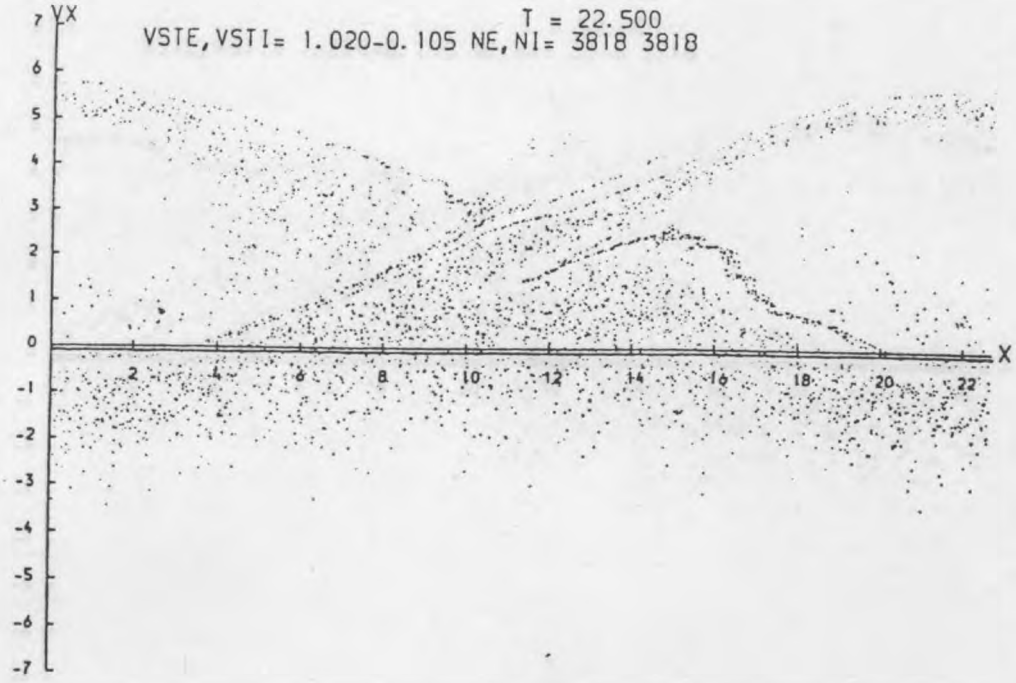
VX
T = 22.500
VSTE, VSTI= 1.020-0.105 NE, NI= 3818 3818
X
2
4
6
8
10
12
14
16
18
20
22
7
6
5
4
3
2
1
0
-1
-2
-3
-4
-5
-6
-7

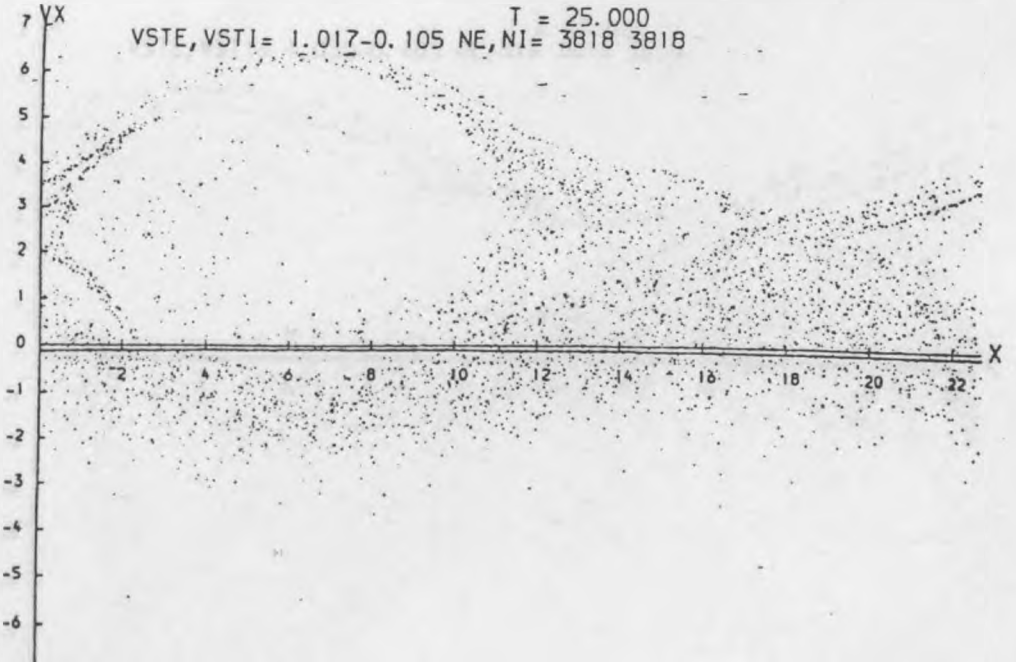
VX
T = 25.000
VSTE, VSTI= 1.017-0.105 NE, NI= 3818 3818
X
2
4
6
8
10
12
14
16
18
20
22
7
6
5
4
3
2
1
0
-1
-2
-3
-4
-5
-6


5
4
3
2
1
0
-1
-2
-3
-4
-5
-6
-7
2
4
6
8
10
12
14
16
18
20
22
X

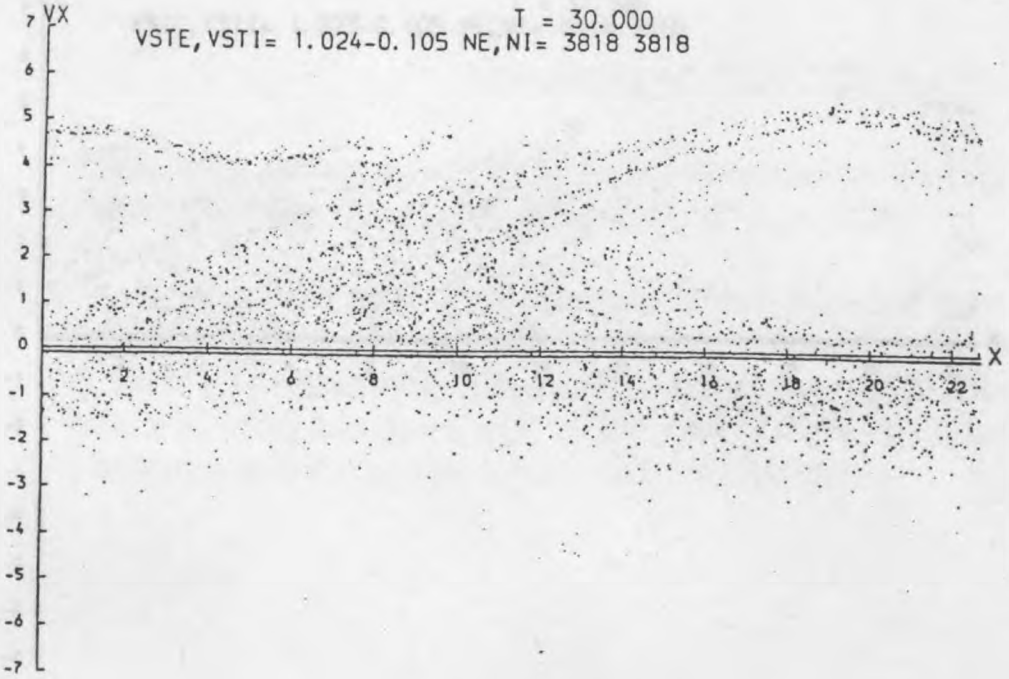
VX
T = 30.000
VSTE, VSTI= 1.024-0.105 NE, NI= 3818 3818
7
6
5
4
3
2
1
0
-1
-2
-3
-4
-5
-6
-7
2
4
6
8
10
12
14
16
18
20
22
X

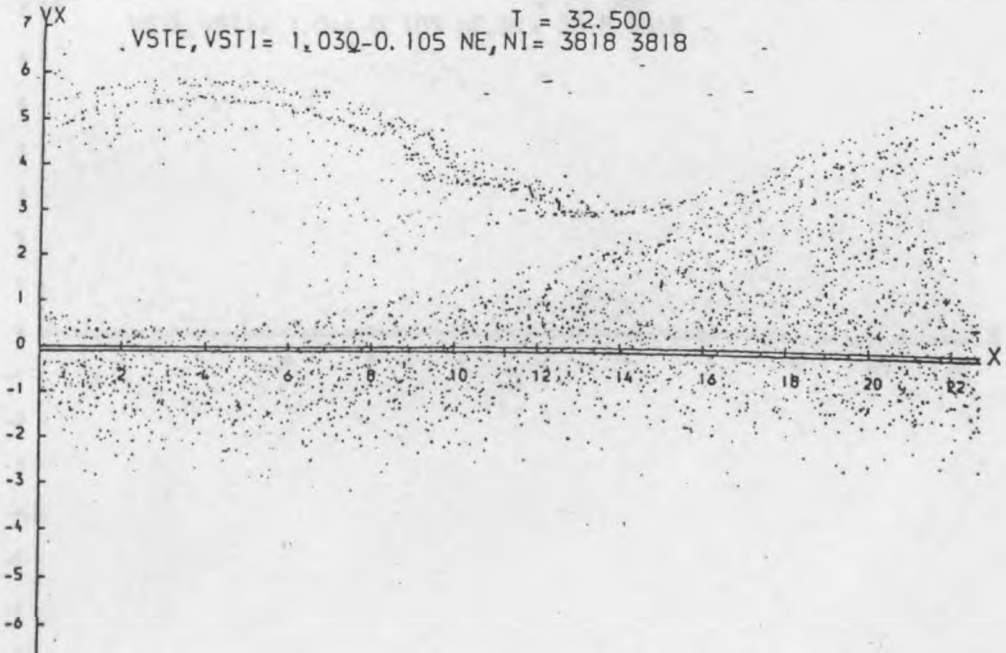
VX
T = 32.500
VSTE, VSTI= 1.030-0.105 NE, NI= 3818 3818
7
6
5
4
3
2
1
0
-1
-2
-3
-4
-5
-6
2
4
6
8
10
12
14
16
18
20
22
X


X
2
4
6
8
10
12
14
16
18
20
22
7
6
5
4
3
2
1
0
-1
-2
-3
-4
-5
-6
-7

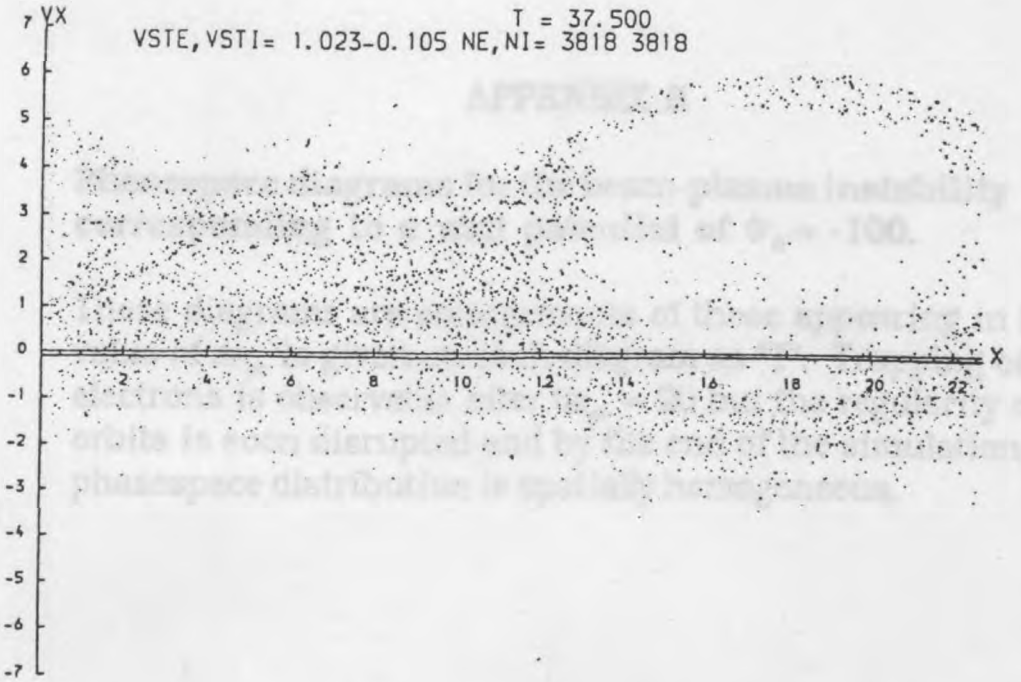
VX
T = 37.500
VSTE, VSTI= 1.023-0.105 NE, NI= 3818 3818
X
2
4
6
8
10
12
14
16
18
20
22
7
6
5
4
3
2
1
0
-1
-2
-3
-4
-5
-6
-7

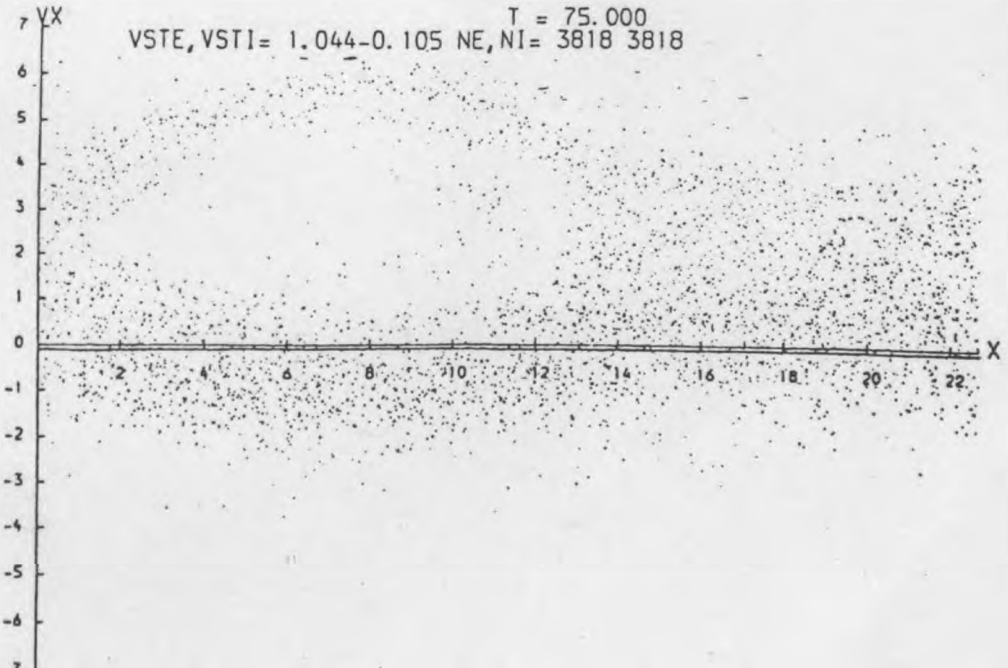
VX
T = 75.000
VSTE, VSTI= 1.044-0.105 NE, NI= 3818 3818
X
2
4
6
8
10
12
14
16
18
20
22
7
6
5
4
3
2
1
0
-1
-2
-3
-4
-5
-6

APPENDIX B

Phasespace diagrams for the beam-plasma instability corresponding to a wall potential of $\Phi_0 = -100$.

These diagrams are enlargements of those appearing in Fig. 6.3. The value of $t\omega_{pe}$ is given on each diagram as "T". Trapping of the beam electrons is observable after $t\omega_{pe} = 20$ but the regularity of their orbits is soon disrupted and by the end of the simulation the phasespace distribution is spatially homogeneous.

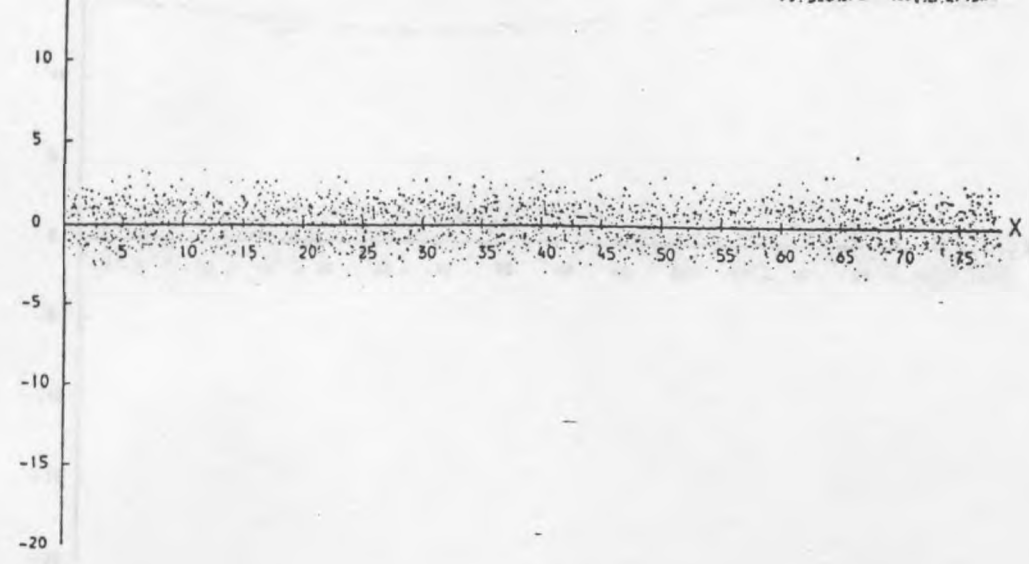
10
5
0
-5
-10
-15
-20
5 10 15 20 25 30 35 40 45 50 55 60 65 70 75
X

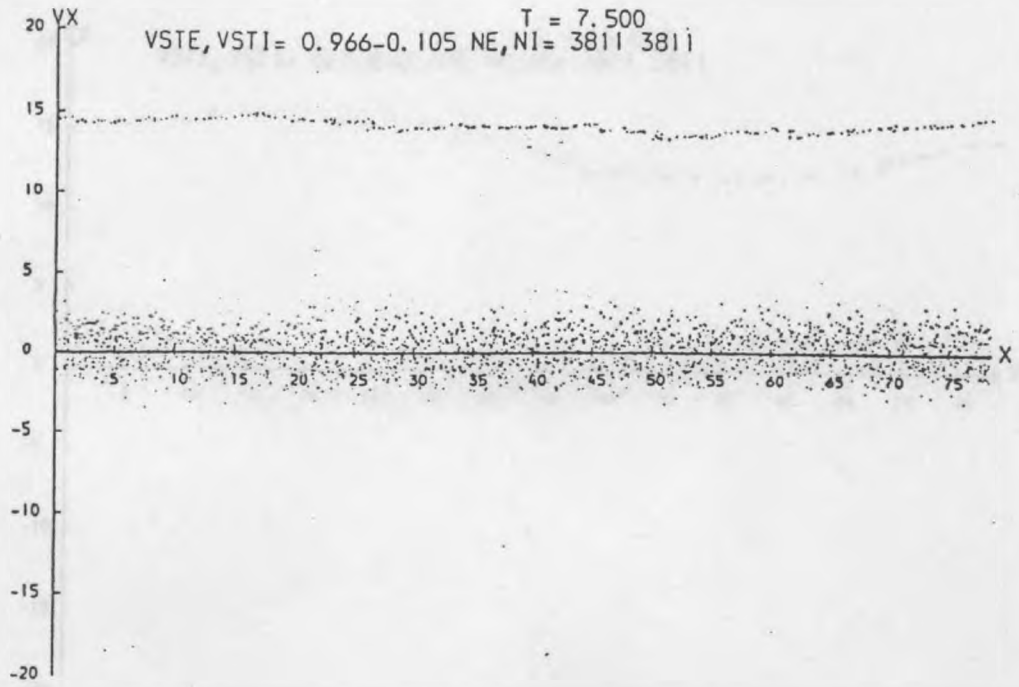
VX
T = 7.500
VSTE, VSTI= 0.966-0.105 NE, NI= 3811 3811
20
15
10
5
0
-5
-10
-15
-20
5 10 15 20 25 30 35 40 45 50 55 60 65 70 75
X

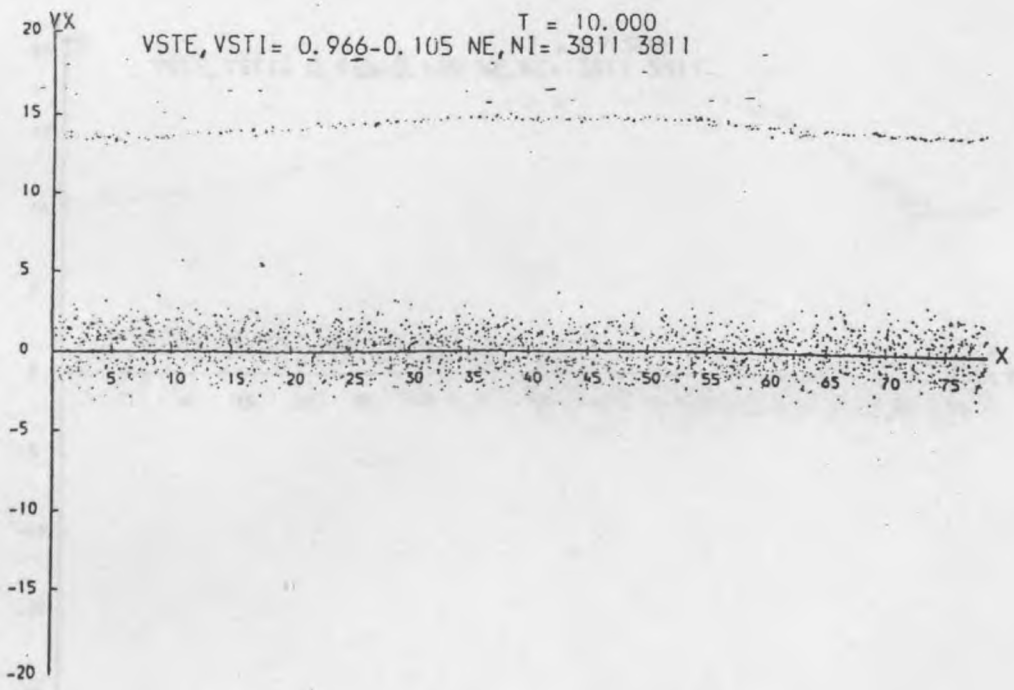
VX
T = 10.000
VSTE, VSTI= 0.966-0.105 NE, NI= 3811 3811
20
15
10
5
0
-5
-10
-15
-20
5 10 15 20 25 30 35 40 45 50 55 60 65 70 75
X


10
5
0
X
5 10 15 20 25 30 35 40 45 50 55 60 65 70 75
-5
-10
-15
-20

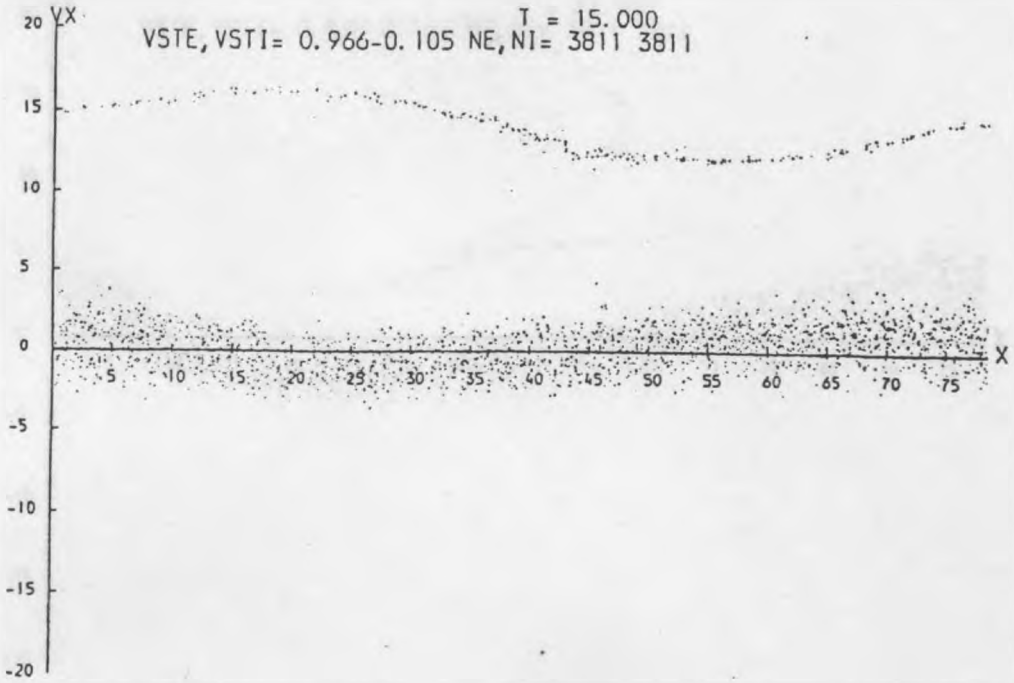
VX
T = 15.000
VSTE, VSTI= 0.966-0.105 NE, NI= 3811 3811
20
15
10
5
0
X
5 10 15 20 25 30 35 40 45 50 55 60 65 70 75
-5
-10
-15
-20

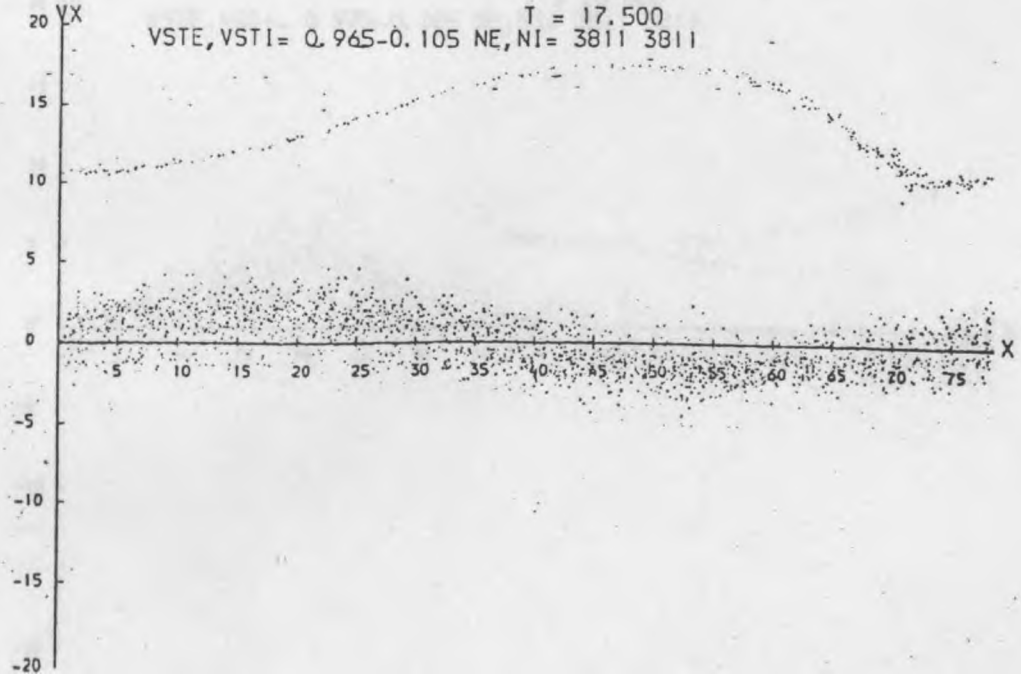
VX
T = 17.500
VSTE, VSTI= 0.965-0.105 NE, NI= 3811 3811
20
15
10
5
0
X
5 10 15 20 25 30 35 40 45 50 55 60 65 70 75
-5
-10
-15
-20

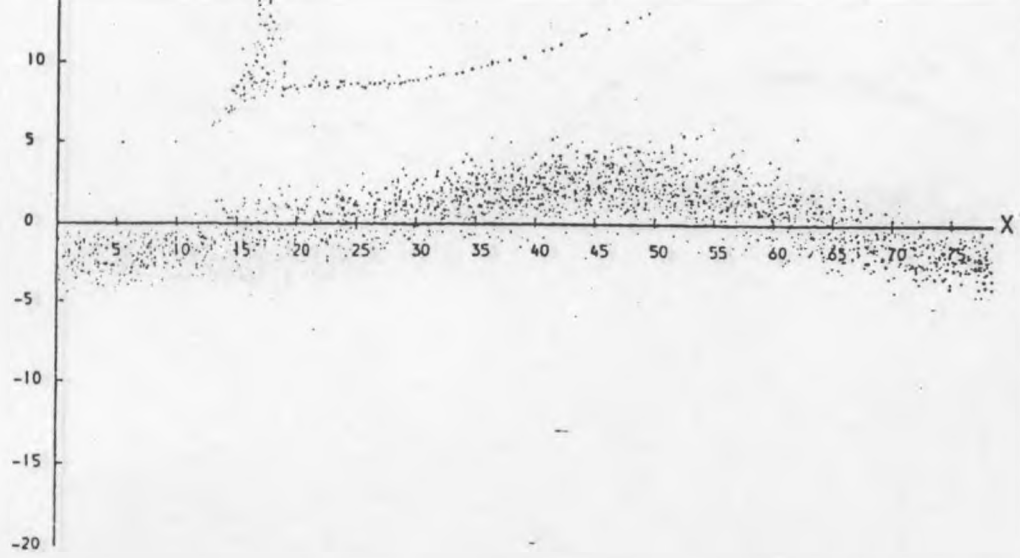
10
5
0
-5
-10
-15
-20
X
5 10 15 20 25 30 35 40 45 50 55 60 65 70 75

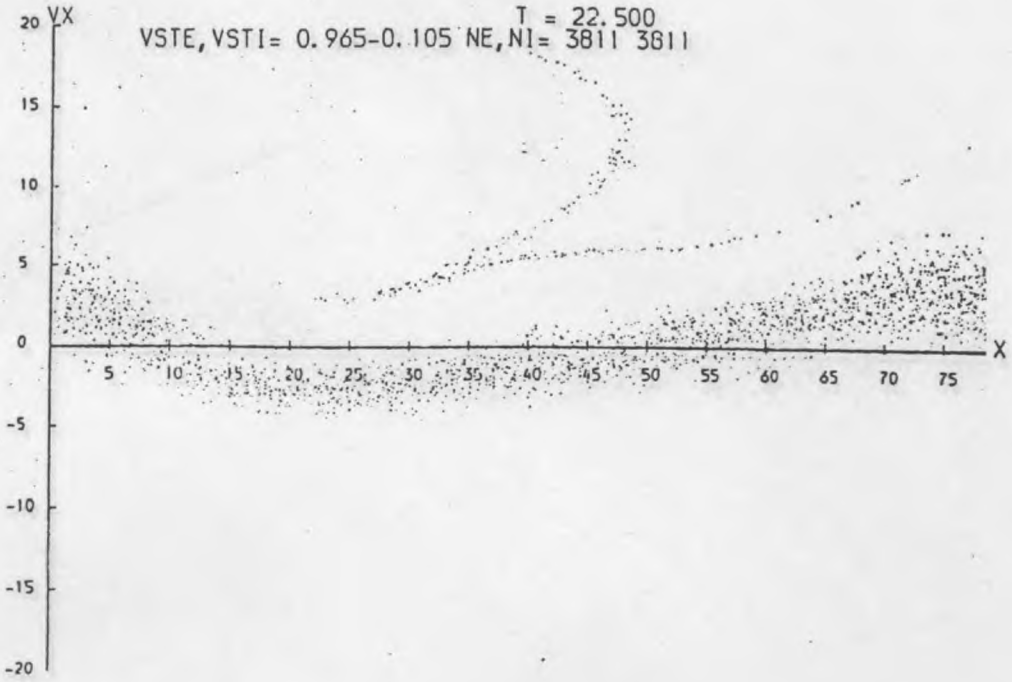
VX
T = 22.500
VSTE, VSTI= 0.965-0.105 NE, NI= 3811 3811
20
15
10
5
0
-5
-10
-15
-20
X
5 10 15 20 25 30 35 40 45 50 55 60 65 70 75

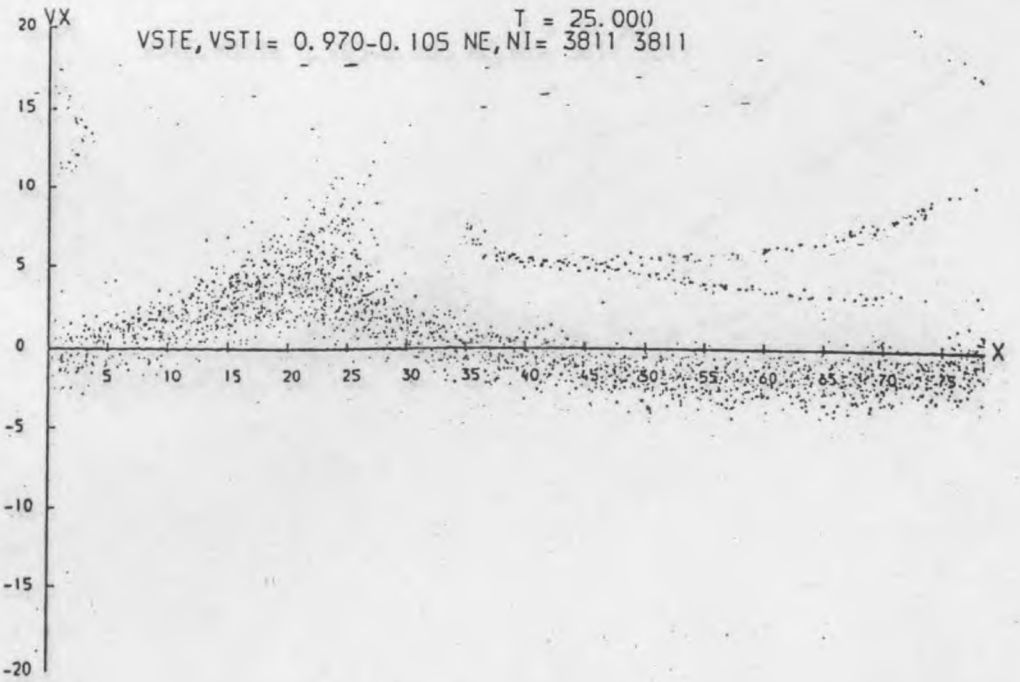
VX
T = 25.000
VSTE, VSTI= 0.970-0.105 NE, NI= 3811 3811
20
15
10
5
0
-5
-10
-15
-20
X
5 10 15 20 25 30 35 40 45 50 55 60 65 70 75

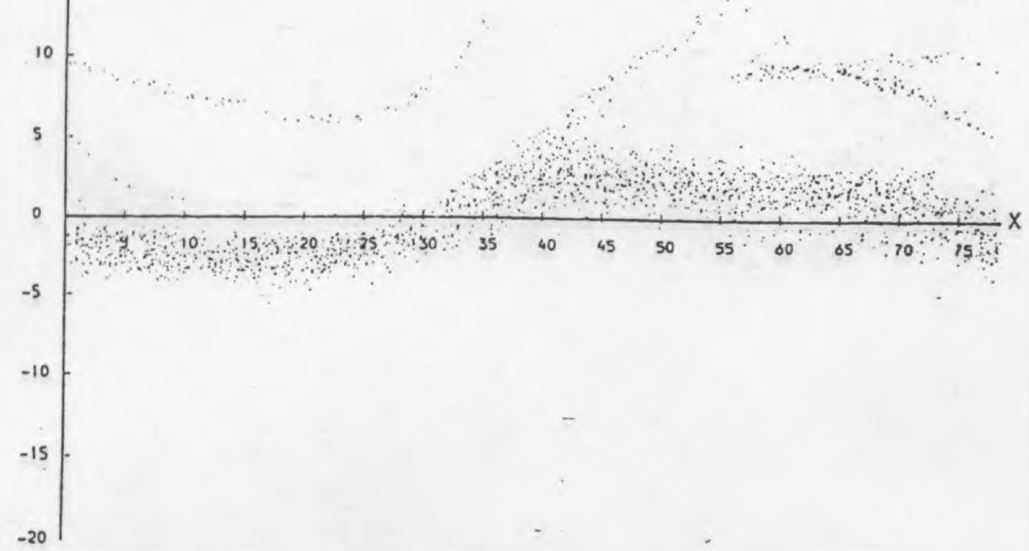
10
5
0
-5
-10
-15
-20
5 10 15 20 25 30 35 40 45 50 55 60 65 70 75
X

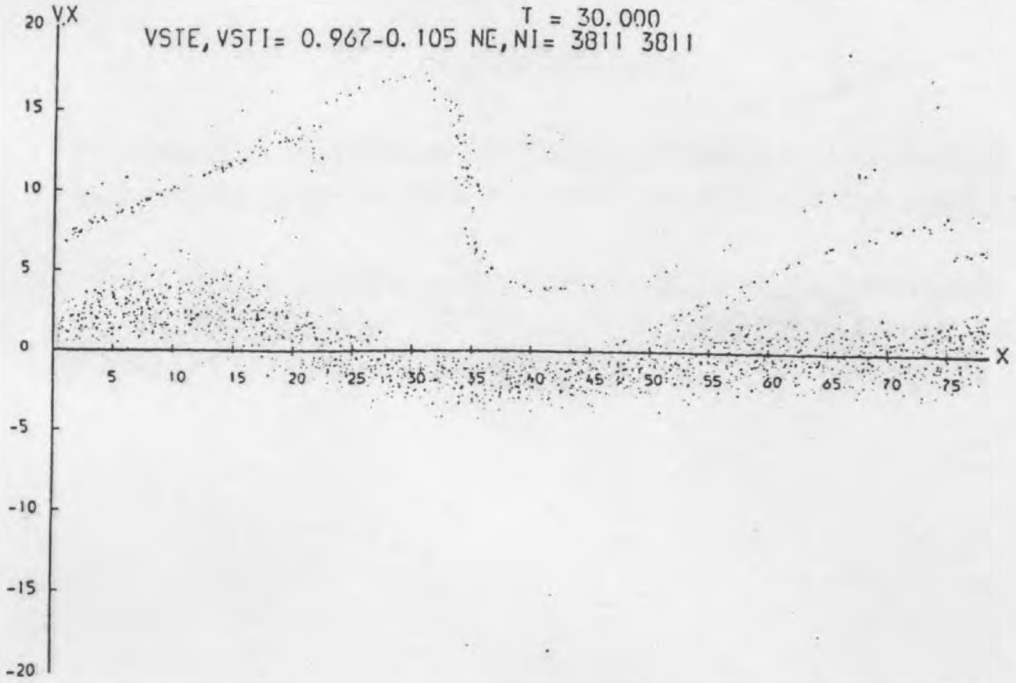
VX
T = 30.000
VSTE, VSTI= 0.967-0.105 NE, NI= 3811 3811
20
15
10
5
0
-5
-10
-15
-20
5 10 15 20 25 30 35 40 45 50 55 60 65 70 75
X

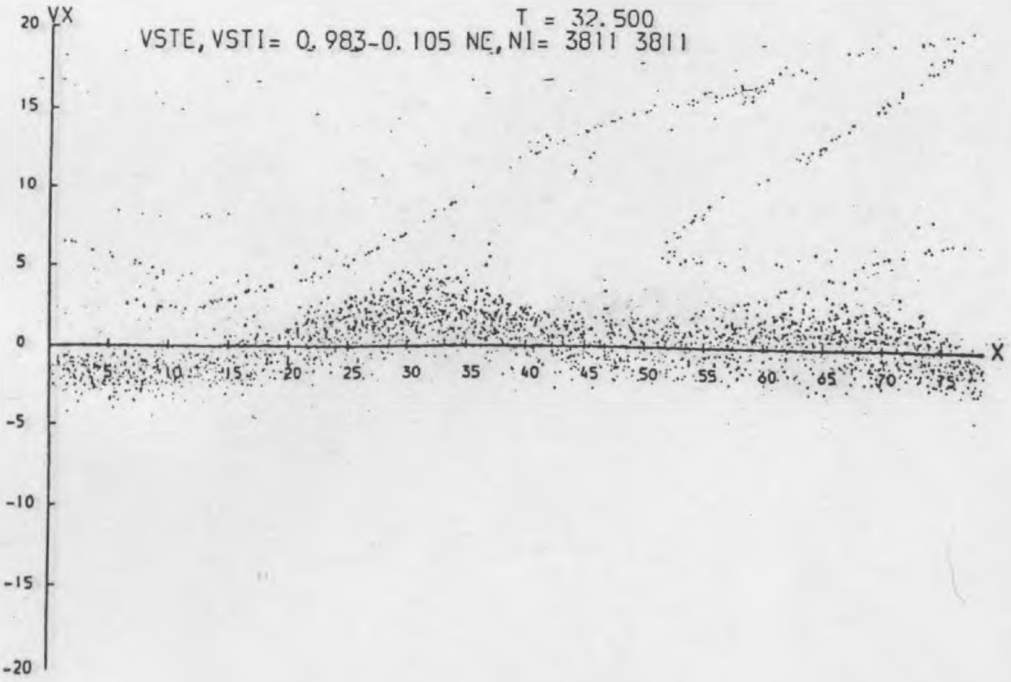
VX
T = 32.500
VSTE, VSTI= 0.983-0.105 NE, NI= 3811 3811
20
15
10
5
0
-5
-10
-15
-20
5 10 15 20 25 30 35 40 45 50 55 60 65 70 75
X


10
5
0
-5
-10
-15
-20
5 10 15 20 25 30 35 40 45 50 55 60 65 70 75
X

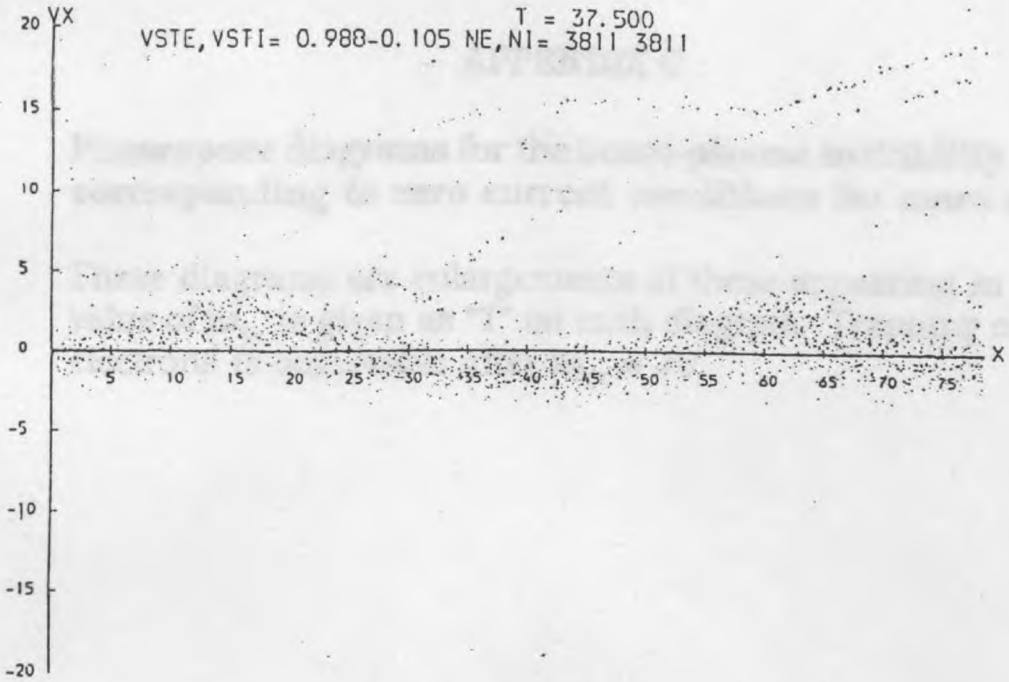
VX
T = 37.500
VSTE, VSTI= 0.988-0.105 NE, NI= 3811 3811
20
15
10
5
0
-5
-10
-15
-20
5 10 15 20 25 30 35 40 45 50 55 60 65 70 75
X

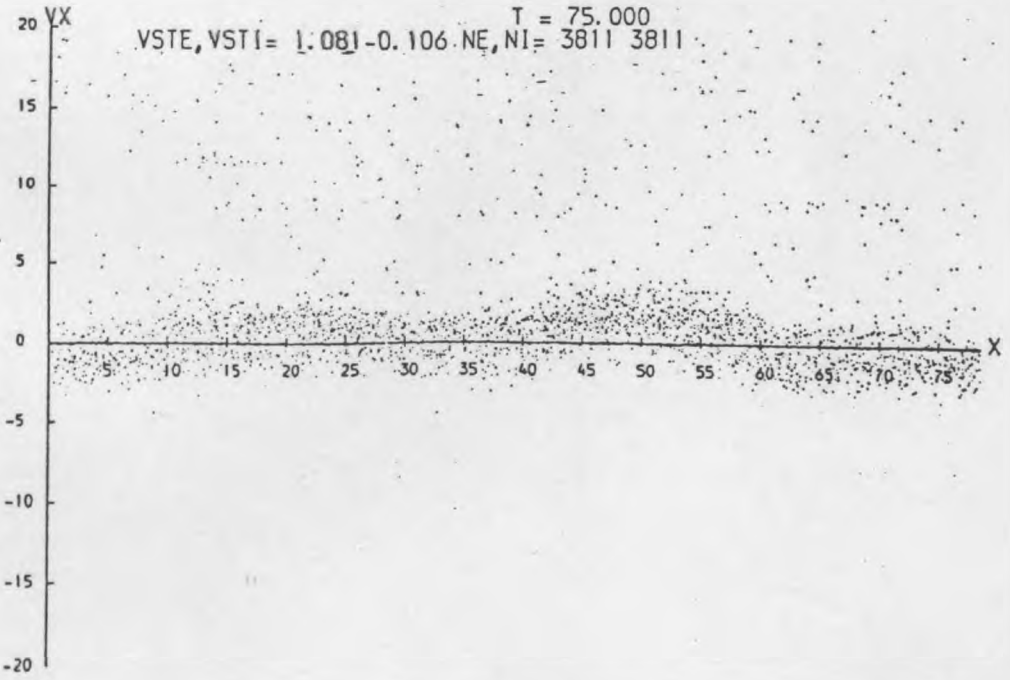
VX
T = 75.000
VSTE, VSTI= 1.081-0.106 NE, NI= 3811 3811
20
15
10
5
0
-5
-10
-15
-20
5 10 15 20 25 30 35 40 45 50 55 60 65 70 75
X

APPENDIX C

Phasespace diagrams for the beam-plasma instability corresponding to zero current conditions for mass ratio 4590.

These diagrams are enlargements of those appearing in Fig. 6.13. The value of $t\omega_{pe}$ is given as "T" on each diagram. Trapping of the beam electrons is observable after $t\omega_{pe} = 70$.

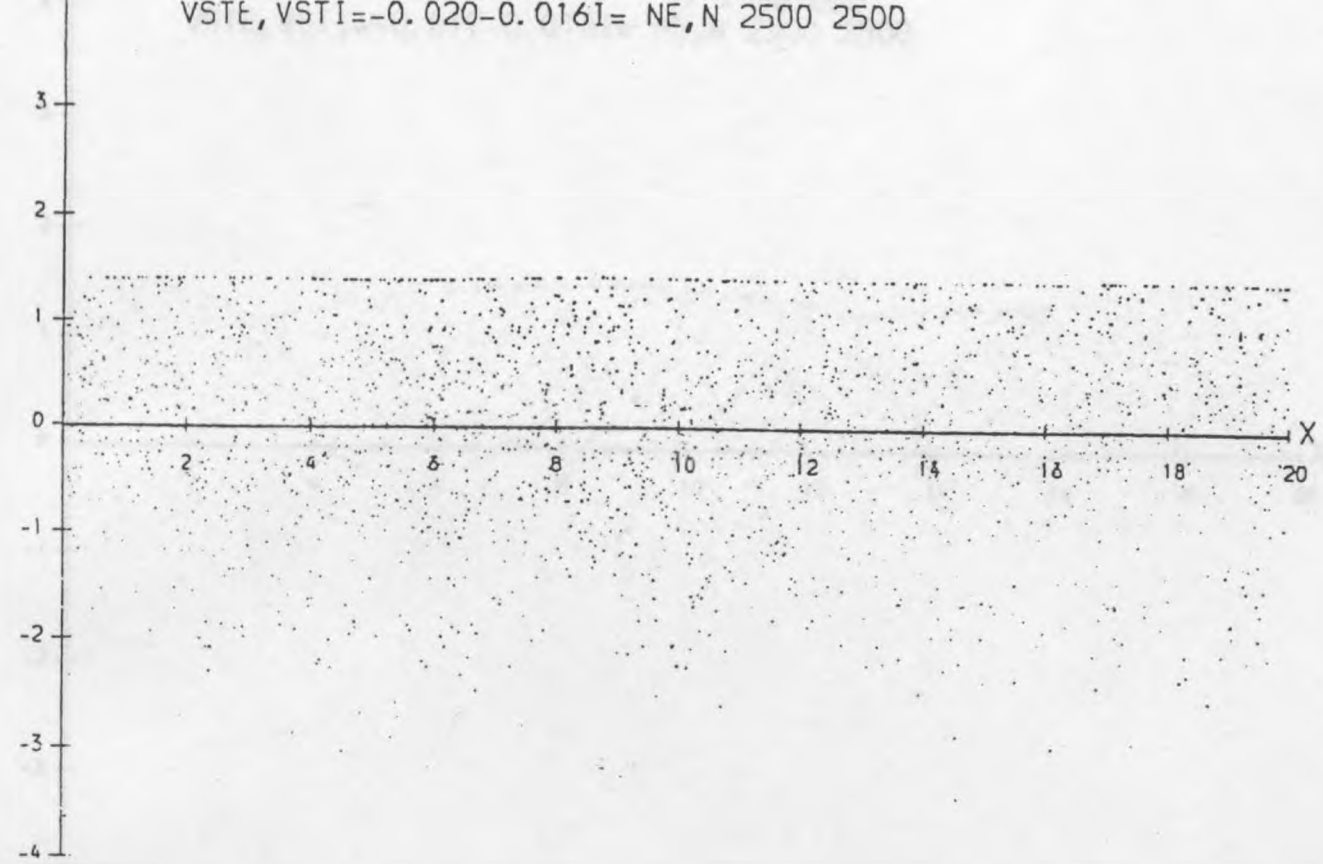
VSTE, VSTI=-0.020-0.016I= NE, N 2500 2500
4
3
2
1
0
-1
-2
-3
-4
2
4
6
8
10
12
14
16
18
20
X

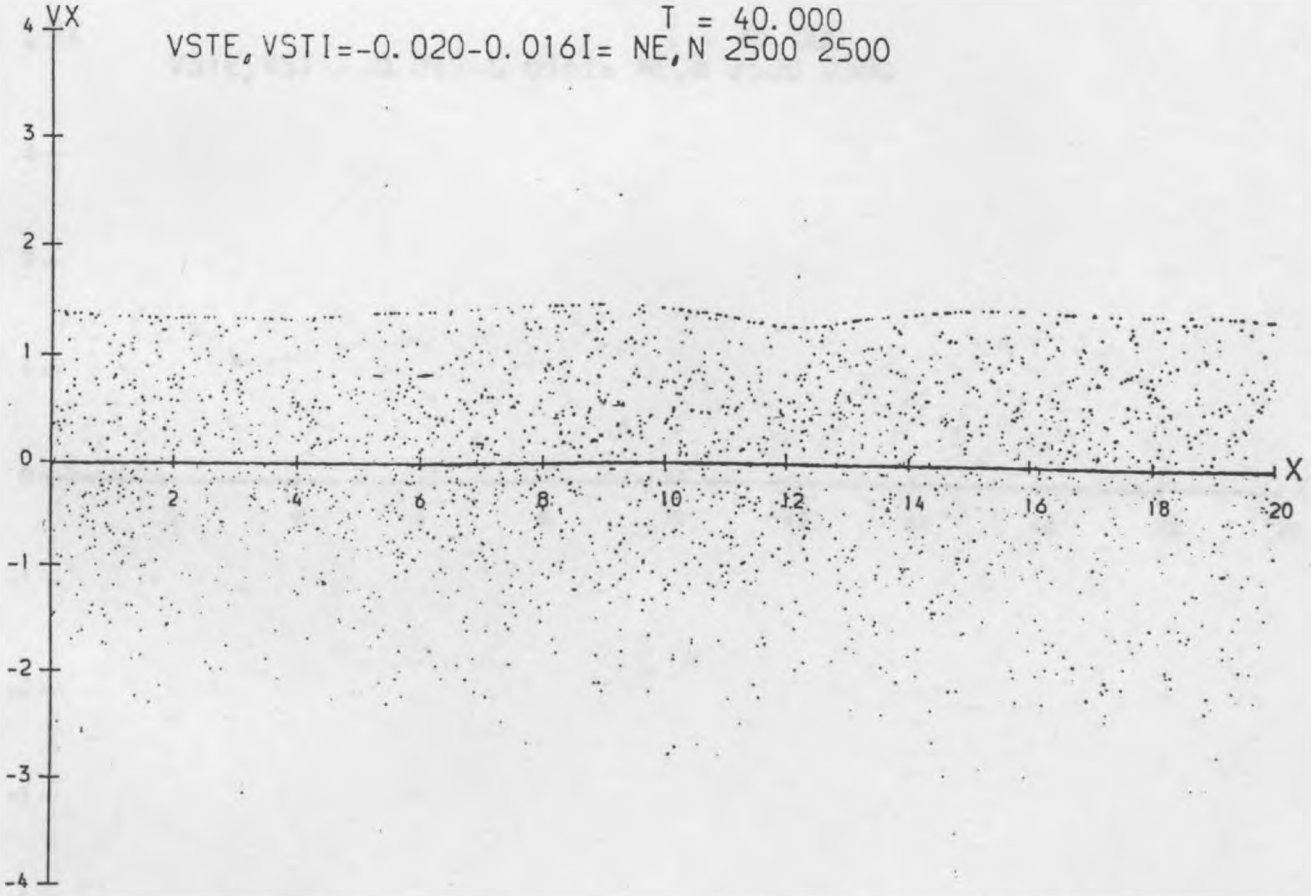
VX
T = 40.000
VSTE, VSTI=-0.020-0.016I= NE, N 2500 2500
4
3
2
1
0
-1
-2
-3
-4
2
4
6
8
10
12
14
16
18
20
X

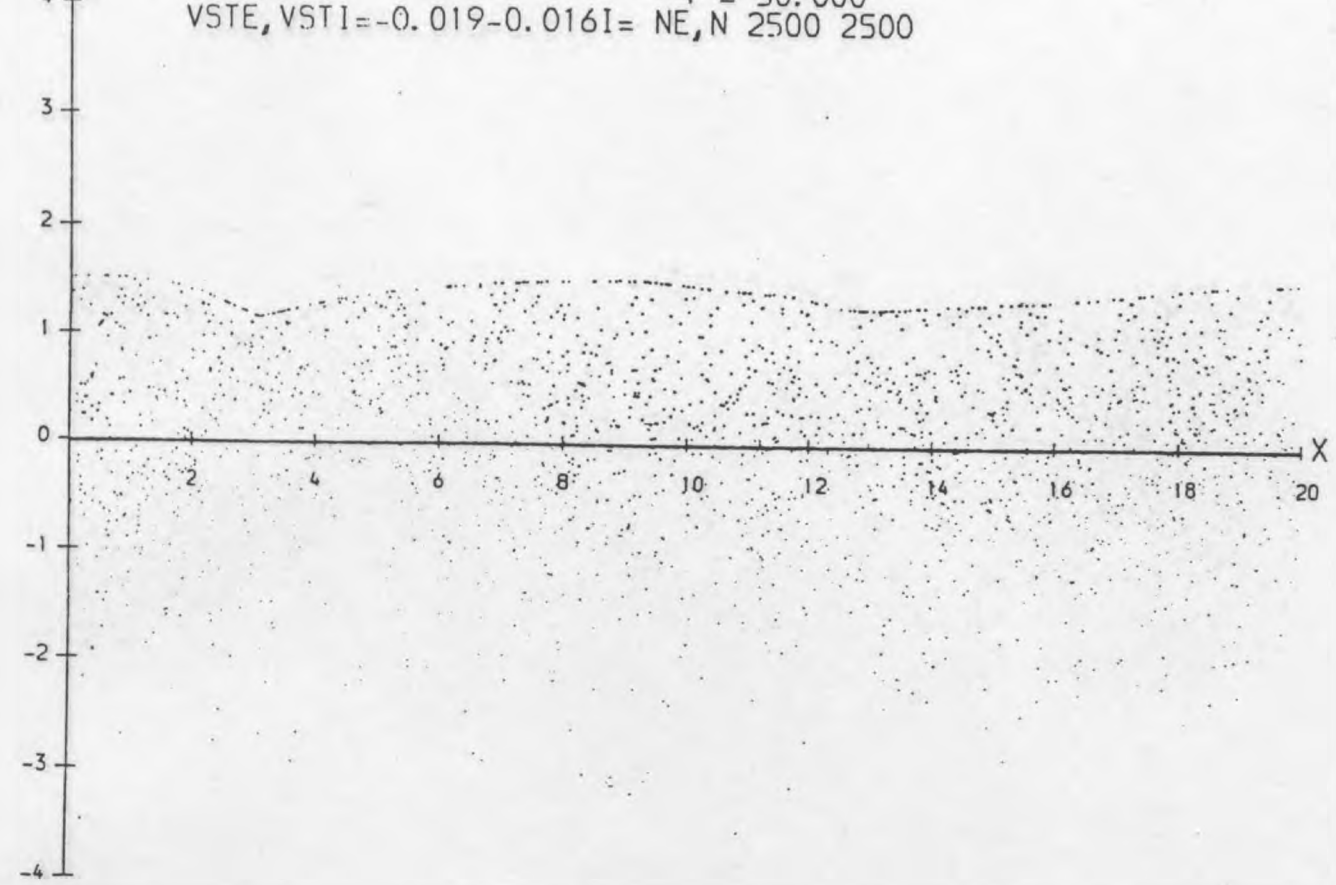
T = 30.000
VSTE, VSTI=-0.019-0.016I= NE, N 2500 2500
4
3
2
1
0
-1
-2
-3
-4
2
4
6
8
10
12
14
16
18
20
X

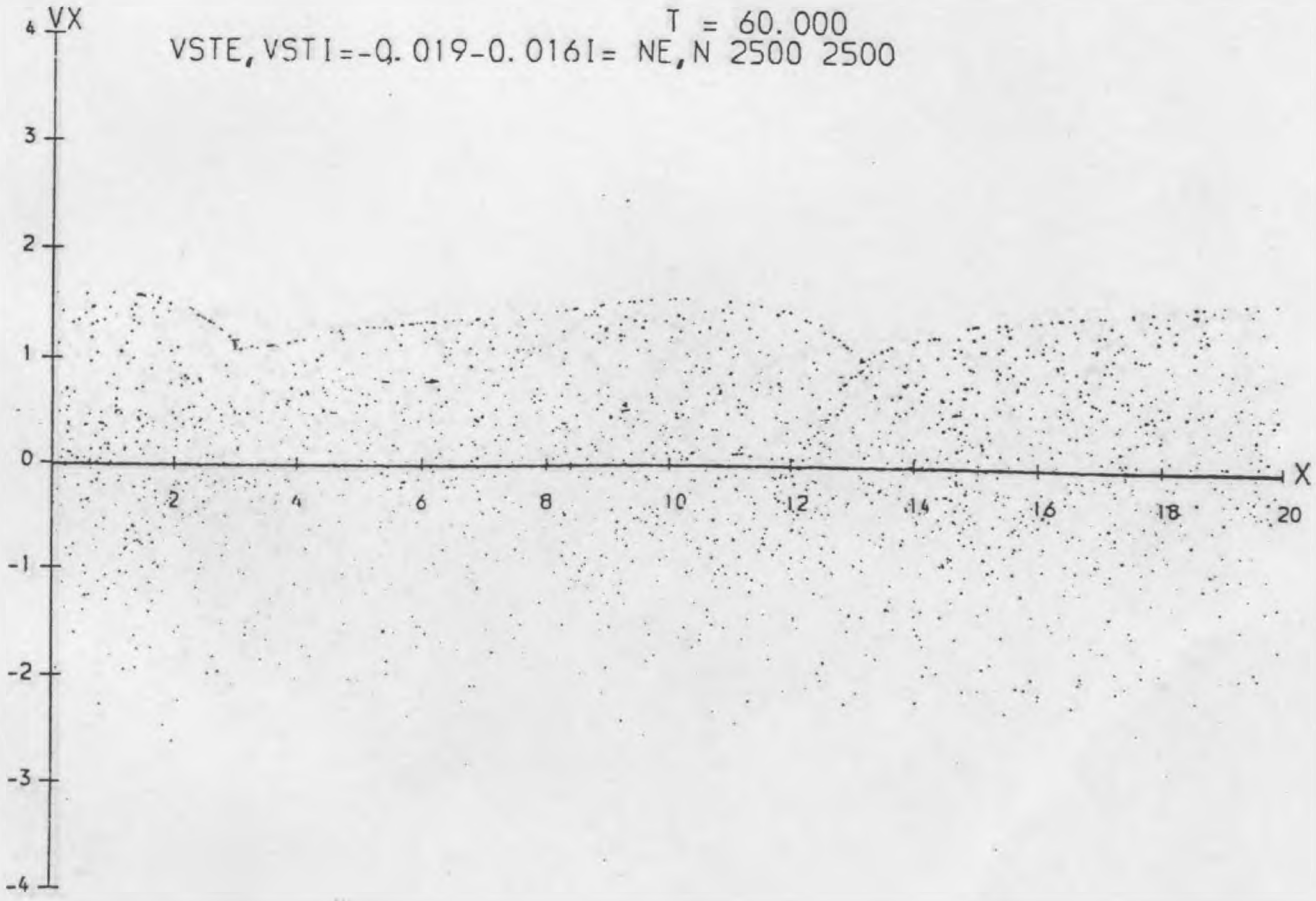
VX
T = 60.000
VSTE, VSTI=-0.019-0.016I= NE, N 2500 2500
4
3
2
1
0
-1
-2
-3
-4
2
4
6
8
10
12
14
16
18
20
X

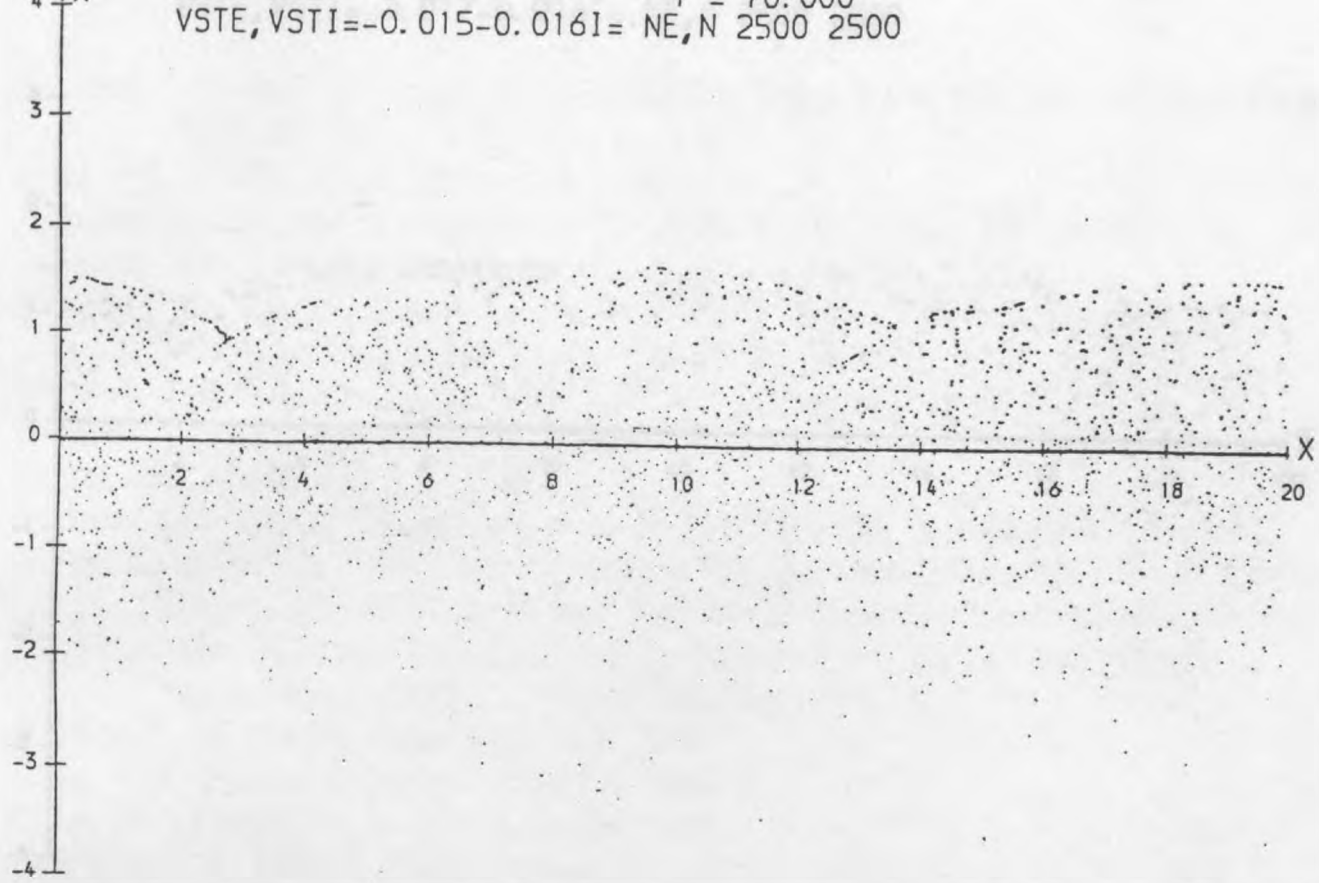
T = 70.000
VSTE, VSTI=-0.015-0.016I= NE, N 2500 2500
4
3
2
1
0
-1
-2
-3
-4
2
4
6
8
10
12
14
16
18
20
X

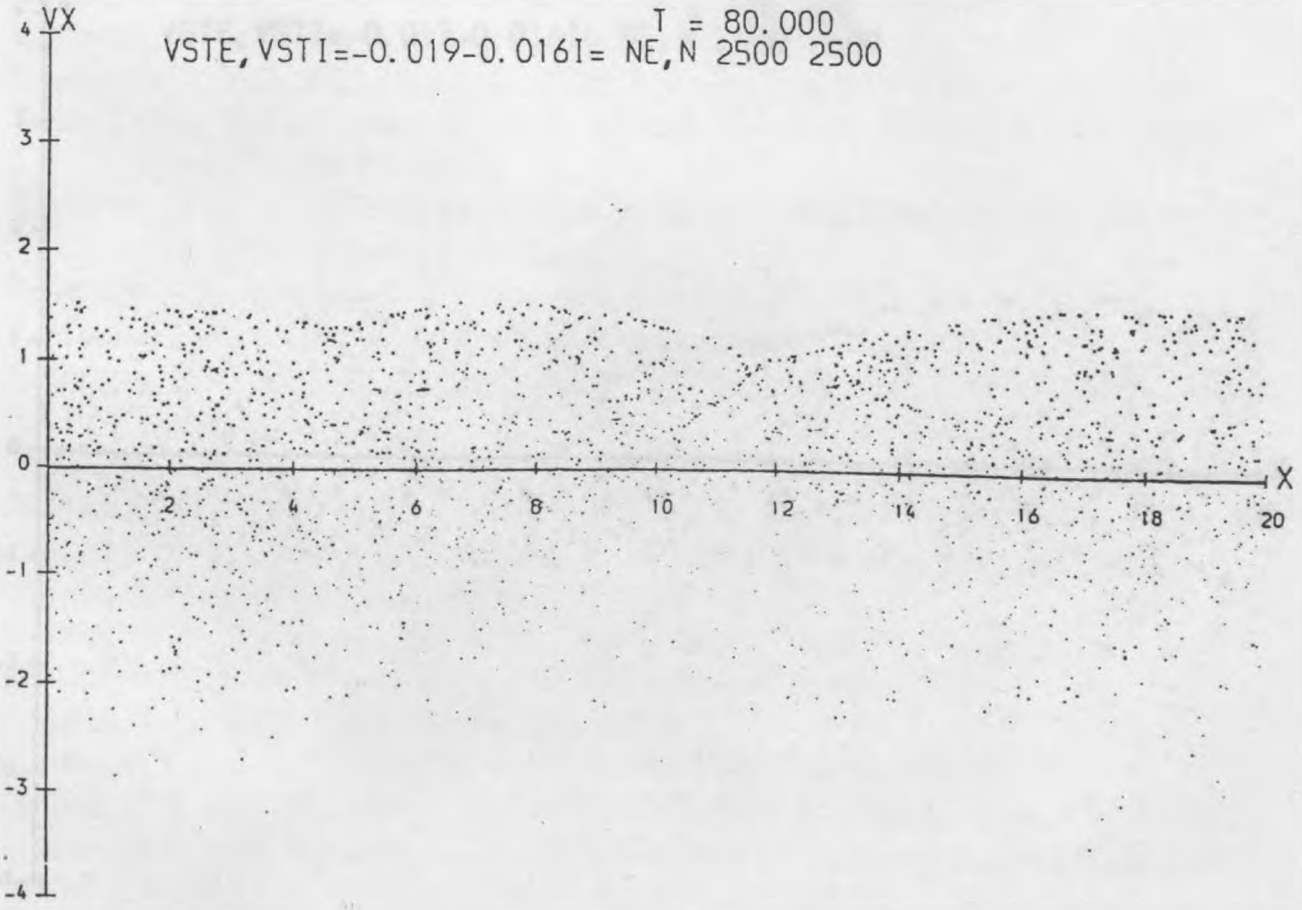
VX
T = 80.000
VSTE, VSTI=-0.019-0.016I= NE, N 2500 2500
4
3
2
1
0
-1
-2
-3
-4
2
4
6
8
10
12
14
16
18
20
X

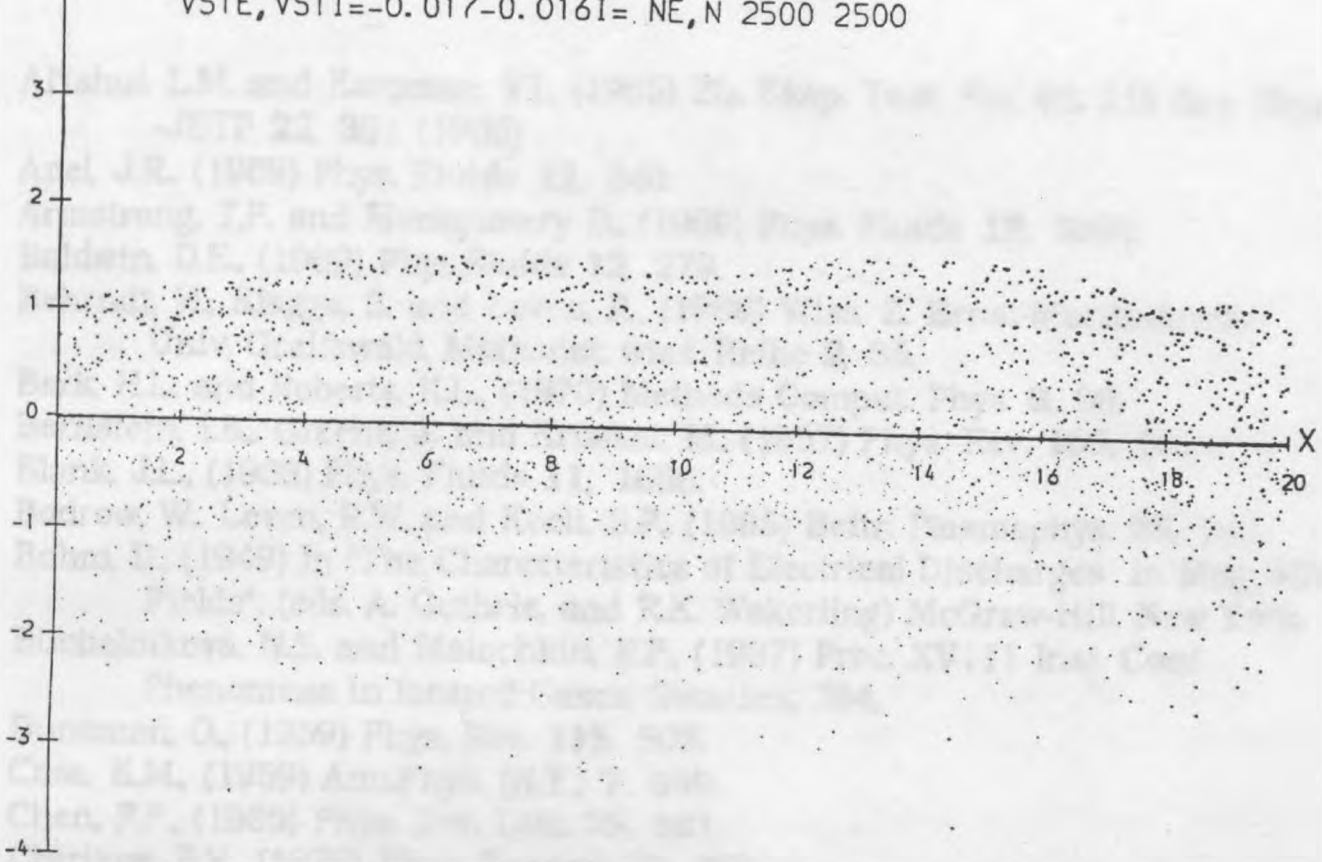
VSTE, VSTI=-0.017-0.016I= NE, N 2500 2500
3
2
1
0
-1
-2
-3
-4
2
4
6
8
10
12
14
16
18
20
X

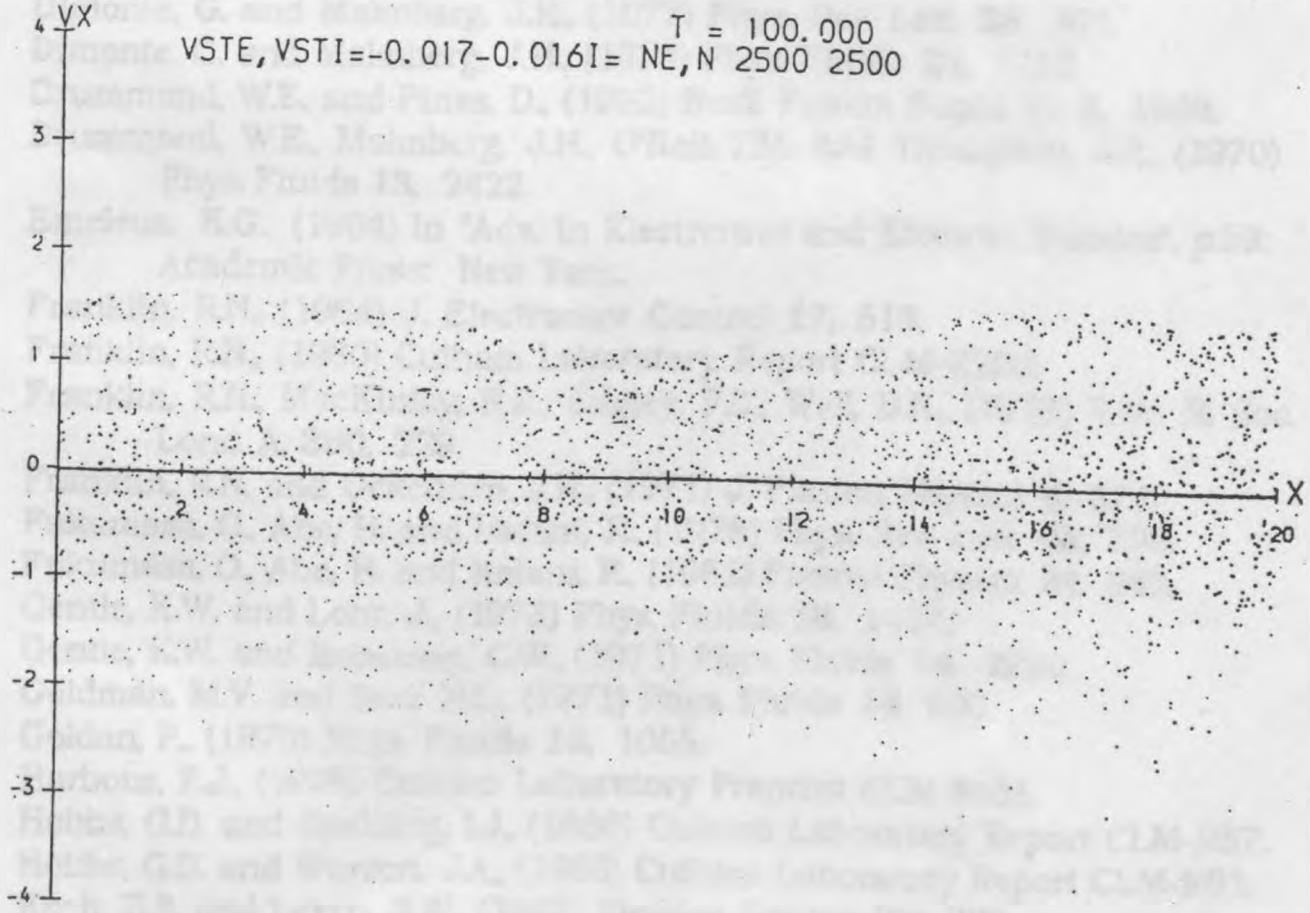
VX
T = 100.000
VSTE, VSTI=-0.017-0.016I= NE, N 2500 2500
4
3
2
1
0
-1
-2
-3
-4
2
4
6
8
10
12
14
16
18
20
X

Al'tshul, L.M. and Karpman, V.I., (1965) Zh. Eksp. Teor. Fiz. **49**, 515 Sov. Phys. -JETP **22**, 361 (1966) .
Apel, J.R., (1969) Phys. Fluids **12**, 640.
Armstrong, T.P. and Montgomery D., (1969) Phys. Fluids **12**, 2094.
Baldwin, D.E., (1969) Phys.Fluids **12**, 279.
Behrndt, H., Klagge, S. and Leven, R., (1986) Wiss. Z. Ernst-Moritz-Arndt-Univ. Greifswald, Math.-nat. wiss. Reihe **2**, 35.
Berk, H.L. and Roberts, K.L., (1970) Methods Comput. Phys. **9**, 88.
Bernstein, I.B., Greene, J. and Kruskal, M., (1957) Phys. Rev. **108**, 56. ▯
Blank, J.L., (1968) Phys. Fluids **11**, 1686.
Bodrow, W., Leven, R.W. and Koch, B.P., (1985) Beitr. Plasmaphys. **25**, 241.
Bohm, D., (1949) In "The Characteristics of Electrical Discharges in Magnetic Fields", (eds. A. Guthrie, and R.K. Wakerling) McGraw-Hill, New York.
Buchelnikova, N.S. and Matochkin, E.P., (1987) Proc. XV111 Inst. Conf. Phenomena in Ionised Gases, Swansea, 284.
Buneman, O., (1959) Phys. Rev. **115**, 503.
Case, K.M., (1959) Ann.Phys. (N.Y.) **7**, 349.
Chen, F.F., (1965) Phys. Rev. Lett. **15**, 381.
Chirikov, B.V., (1979) Phys. Reports **52**, 263.
Chirikov, B.V., Keil, E. and Sessler, A.M., (1971) J. Statist. Phys. **3**, 307.
Crawford, F.W. and Cannara, A.B., (1965) J. Appl. Phys. **36**, 3135.
Dawson, J.M. and Shanny, R., (1968) Phys. Fluids **11**, 1506.
Dimonte, G., (1982) Phys. Fluids, **25**, 604.
Dimonte, G. and Malmberg, J.H., (1977) Phys. Rev. Lett. **38**, 401.
Dimonte, G. and Malmberg, J.H., (1978) Phys. Fluids **21**, 1188.
Drummond, W.E. and Pines, D., (1962) Nucl. Fusion Suppl. Pt. **3**, 1049.
Drummond, W.E., Malmberg, J.H., O'Neil T.M. and Thompson, J.R., (1970) Phys. Fluids **13**, 2422.
Emeleus, K.G., (1964) In "Adv. in Electronics and Electron Physics", p.59; Academic Press: New York.
Franklin, R.N., (1964) J. Electronics Control **17**, 513.
Franklin, R.N., (1980) Culham Laboratory Report CLM-R200.
Franklin, R.N., MacKinlay, R.R., Edgley, P.D., Wall, D.N., (1978) Proc. R. Soc. Lond. A. **360**, 229.
Franklin, R.N. and Ockenden, J.R., (1971) J. Plasma Physics **4**, 371.
Fukumasa, O., Abe, H. and Itatani, R., (1978) Phys. Rev. Lett. **40**, 393.
Fukumasa, O., Abe, H. and Itatani, R., (1982) Plasma Physics **24**, 843.
Gentle, K.W. and Lohr, J., (1973) Phys. Fluids **16**, 1464.
Gentle, K.W. and Roberson, C.W., (1971) Phys. Fluids **14**, 2780.
Goldman, M.V. and Berk H.L., (1971) Phys. Fluids **14**, 801.
Goldan, P., (1970) Phys. Fluids **13**, 1055.
Harbour, P.J., (1978) Culham Laboratory Preprint CLM-P535.
Hobbs, G.D. and Spalding, I.J., (1966) Culham Laboratory Report CLM-R57.
Hobbs, G.D. and Wesson, J.A., (1966) Culham Laboratory Report CLM-R61.
Koch, B.P. and Leven, R.W., (1983) Physica Scripta **27**, 220.
Krall, N.A. and Trivelpiece, A.W., (1973a) "Principles of Plasma Physics", McGraw-Hill, London, p.517.

Landau, L.D., (1946) J. Physics.(U.S.S.R.) **10**, 25.
Langmuir, I., (1925) Phys. Rev. **26**, 585.
Langmuir, I., (1929) Phys. Rev. **33**, 954.
Mahaffey, D. W., (1959) J. Electronics and Control **6**, 193.
Malmberg, J.H. and Wharton C.B., (1969) Phys. Fluids **12**, 2600.
Mizuno, K. and Tanaka S., (1972) Phys. Rev. Lett. **29**, 45.
Morales, G. J. and Malmberg J. H., (1974) Phys. Fluids **17**, 609.
Morse, R.L. and Nielson C.W., (1969) Phys. Fluids **12**, 2418.
Murakami, A., Nomura, Y. and Momota, H., (1982) J. Physical Soc. Japan, **51**, 4053.
O'Neil, T.M., (1965) Phys. Fluids **8**, 2255.
O'Neil, T.M. and Malmberg, J.H., (1968) Phys. Fluids **11**, 1754.
O'Neil, T.M. and Winfrey J.H., (1972) Phys. Fluids **15**, 1514.
O'Neil, T.M., Winfrey J.H. and Malmberg J. H., (1971) Phys. Fluids **14**, 1204.
Peratt, A.L., (1973) Phys. Fluids **16**, 1032.
Prewett, P.D. and Allen, J.E., (1976) Proc. Royl. Soc., **A348**, 3132.
Richtmyer, R.D. and Morton, K.W., (1967) "Difference Methods for Initial-Value Problems", Interscience Publishers, John Wiley and Sons, Inc., New York.
Rosenbluth, M.N., MacDonald, W.M. and Judd, D., (1957) Phys. Rev. **120**, 1.
Sagdeev, R.Z. and Galeev, A.A., (1966) "Lectures on the Nonlinear Theory of Plasma", Trieste, I.A.E.A. Report No. 1C/66/64.
Self, S.A., Shoucri, M.M. and Crawford, F.W., (1971) J. Appl. Phys. **42**, 2, 704.
Shapiro, V.D. and Shevchenko, V.I., (1976) Izw. VUZov Radiofiz. **19**, 767
Strang, G. and Fix, G., (1973) "An Analysis of the Finite Element Method", Prentice-Hall, Inc., Englewood Cliffs, NJ.
Thompson, J.R., (1971) Phys. Fluids **14**, 1532.
Tonks, L. and Langmuir, I., (1929a) Phys. Rev. **33**, 1070.
Tonks, L. and Langmuir, I., (1929b) Phys. Rev. **34**, 876.
Van Kampen, N.G., (1955) Physica **21**, 949.
Wakeren, J.H. van, and Hopman, H.J., (1972) Phys. Rev. Lett. **28**, 295.
Wesson, J.A., (1974) In "Plasma Physics", p.93.
Weynants, R.R., Messaien, A.M. and Vandenplas, P.E., (1973) Phys. Fluids **16**, 1962.
Wharton, C.B., Malmberg, J.H. and O'Neil, T.M., (1968) Phys. Fluids **11**, 1761.
Williamson, J.H., (1971) J. Comp. Physics **8**, 258.
Winfrey, J.H. and Dunlop, M.L., (1977) Plasma Physics **19**, 901.
Wong, H. V., (1972) Phys. Fluids **15**, 632.
Zakharov, V.E. and Karpman, V.I., (1963) Sov. Phys. -JETP **16**, 351.
Zaslavskii, G.M. and Chirikov, B.V., (1972) Sov. Phys.-Uspekhi **14**, 549.